



PhD-FSTM-2023-113  
The Faculty of Science, Technology and Medicine

## DISSERTATION

Defence held on 03/11/2023 in Esch-sur-Alzette

to obtain the degree of

DOCTEUR DE L'UNIVERSITÉ DU LUXEMBOURG

EN *BIOLOGIE*

by

**Kyriaki BARMPIA**

Born on 04 February 1994 in Athens, (Greece)

ENHANCING THE COMPLEXITY OF 3D IN VITRO  
MODELS FOR PARKINSON'S DISEASE RESEARCH

### Dissertation defence committee

Dr Jens C. Schwamborn, dissertation supervisor  
*Professor, Université du Luxembourg*

Dr Alexander Skupin, Chairman  
*Professor, Université du Luxembourg*

Dr Nektarios Tavernarakis  
*Professor, Univeristy of Crete*

Dr Mario Bortolozzi  
*Associate Professor, Univeristy of Padova*

Dr Erasmia Taoufik  
*Principal Investigator, Hellenic Pasteur Institute*







---

# Affidavit

I declare that the PhD Thesis “Enhancing the Complexity of 3D In Vitro Models for Parkinson's Disease Research” has been written independently and without any other sources than cited.

Kyriaki Barmpa

Luxembourg, 03.10.2023



---

*"All we have to decide  
is what to do with  
the time that is given to us."*

*Gandalf, LOTR*





---

# Acknowledgements

My PhD journey started December 2020, in an environment that I had already known for two years, as a technician. In both cases I was doing research using similar techniques and on similar topics. But nothing can be compared to the adventure called PhD! You can never really know if you never experience it. I started with confidence and ambition, somewhere in the middle I crushed in the depths of anxiety and self-doubt, but the amazing thing is that there is this small window of fresh air that if you manage to open it, it lifts you up and you keep moving. And here I am, acknowledging everything and everyone that helped me achieve this big milestone in my career. Which definitely I could not do solely on my own!

Firstly, I would like to express my gratitude to my supervisor Prof. Jens C. Schwamborn, who although I had no significant experience after my master's degree, he gave me the opportunity to learn and grow in his lab. Apart from that though, he further encouraged my personal and professional development by offering me the PhD position. I couldn't wish for a better environment to pursue this journey. I thank him deeply for his trust and guidance. They say first choose your supervisor and then your research topic. I couldn't agree more!

Another quality that Prof. Schwamborn has, is his ability to build a harmonious and well-functioning work environment. I was very lucky to be part of a team full of caring and respectful individuals, and importantly excellent scientists. I never felt alone in this journey, and I was always able to discuss my problems with people eager to help and make you feel better. I specially appreciate all the help and guidance I received from Dr. Cláudia Saraiva, my postdoc supervisor! Apart from Jens, she was the one dealing with my day to day struggles and successes. Although she doesn't recognize it, she really has a talent in science communication and writing. She was always helping me refining my presentations into a better version, and I couldn't learn writing scientific texts without her! Apart from a supervisor, I am also lucky to call her my friend. And even more lucky to call many other people from the DVB group friends! Sònia, I will never forget her funny facial expression staring at me at my desk, it was always cheering me up. Isabel, she was a real inspiration with her hard-working attitude and resilience, and always passionate for a good lunch break discussion! Alise, my desk neighbor, so efficient and focused that pushed me to be efficient and focused too, discussing every little (or not) thing coming up in our minds, at any moment. I wish everyone having a desk neighbor like Alise! Nathasia, with her relaxing spirit and confident personality, but also our valuable skincare advisor. Gemma, with her sweet and joyful personality. Catarina, who really changed my

---

attitude towards western blots, my forever western blot buddy, can't wait to explore and photograph with you! Elisa, always with a contagious smile on her face and endless energy.

I want to express my appreciation to all the DVB group, past and present members. It was an amazing experience working with all of you. I will never forget all the help you provided me, in periods full of cell culture when I had to attend courses and conferences. For this I specifically thank Claudia, Catarina, Daniela, Michele, Henry, Sonia, Isabel, Alise and Elisa.

Special thanks also to Matthieu, who revised my thesis and gave me really helpful feedback and to Javi and Thea, who were my first mentors in the lab, before even starting the PhD journey and I learned a lot from them.

Outside of the DVB group, it is important to recognize the invaluable help from Dr. Paul Antony, who consistently helped me with my image analysis issues.

I would also like to thank Prof. Alexander Skupin and Prof. Nektario Tavernaraki for their contribution in my annual PhD progresses and for their time in evaluating my thesis. Additionally, I appreciate Dr. Erasmia Taoufik and Prof. Mario Bortolozzi for accepting the invitation as members to my defense committee and for their time in evaluating my thesis.

Throughout my PhD journey, I was also a member of the Greek Women in Stem team. This incredible team of inspiring women scientists gave me the opportunity to make new meaningful connections and learn so many new things. I am obliged to their priceless constant support and cheer up!

It would be a shame to not mention the biggest contributor to my mental health and burnout rescuer...my crossfit community. As the ancient Greeks say, Νους υγιής εν σώματι υγιεί! I can't imagine going through this experience without exercising. I believe it needs to be mandatory! Nothing could clear up my mind as crossfit did!

Additionally, I was lucky to have a social circle that helped me create memories and lift me up in the difficult moments. I am specifically thankful for my friends Chrysovalantou, Dimitri, Eddie (the dog), Myrto and Vyron (and their pets Ginger and Yugi), my Greek group of friends (and pets) here in Luxembourg, that without them the journey would have been much different.

Finally, I would like to thank my family in Greece, my parents and my brother. My parents with their endless love and support, have always believed in me and helped me achieve all my dreams so far and my brother, who is completely opposite to me, and reminds me that life needs to be also fun! Part of my family now are also my life-long best friends, οι κουμπάρες μου Μαρία και Νικολέτα, that they were always like sisters to me, and they are a constant support throughout my life.

---

Last but not least, I would like to thank my family, my best friend, my husband! Despite all the suffering, he is still here with me. There are not enough words to express my appreciation for this person. He never complaint about my endless working days and weekends and he tolerated my broken nerves and my mood swings. He was always willing to help me in any way possible. His constant support means everything to me. Σ' ευχαριστώ από τα βάθη της καρδιάς μου!



---

# Abbreviations

**2D** Two-dimensional

**3D** Three-dimensional

**6-OHDA** 6-hydroxydopamine

**AA** Ascorbic acid

**ActA** Activin A

**ASC** Adult stem cells

**ASCL1** Achaete-scute homolog 1

**ASD** Autism spectrum disorder

**ATP** Adenosine triphosphatase

**BDNF** Brain-derived neurotrophic factor

**BMP** Bone Morphogenetic Protein

**BSA** Bovine serum albumin

**CHIR** CHIR-99021

**CNS** Central nervous system

**CRISPR/Cas9** Clustered regularly interspaced short palindromic repeats and CRISPR-associated protein 9

**COs** Cortical organoids

**CTIP2** COUP-TF-interacting protein 2

**DA** Dopamine

**DAN** Dopaminergic neuron

**DAPT** N-(N-(3, 5-difluorophenacetyl-L-alanyl))-S-phenylglycine-butyl ester

**DAT** Dopamine transporter

**dbcAMP** Dibutyryladenosine cyclic monophosphate

**DEGs** Differentially expressed genes

**DJ-1** Parkinsonism Associated Deglycase

**DM** Dorsomorphin xvii

**DMEM** Dulbecco Modified Eagle Medium

**DMSO** Dimethylsulfoxide

**DNA** Deoxyribonucleic acid

**Drop-Seq** Droplet-sequencing

**EBs** Embryoid bodies

**EC** Embryonic cortex

---

**ECM** Extracellular matrix  
**EM** Embryonic midbrain  
**EN1** Homeobox protein engrailed-1  
**EN2** Homeobox protein engrailed-2  
**ERM** Ezrin-Radixin-Moesin proteins  
**FACS** Fluorescence-activated cell sorting  
**FGFs** Fibroblast Growth Factors  
**FOXA2** Forkhead box protein A2  
**GABAergic**  $\gamma$ -aminobutyric acid producing neurons  
**GDNF** Glial cell-derived neurotrophic factor  
**GFAP** Glial fibrillary acidic protein  
**GIRK2** G protein-activated inward rectifier potassium channel 2  
**H<sub>2</sub>O<sub>2</sub>** Hydrogen peroxide  
**hiPSC** Human induced pluripotent stem cell  
**hNESc** Human neuroepithelial stem cell  
**IBA1** Ionized calcium binding adaptor molecule 1  
**IL-34** Interleukin 34  
**iDANs** induced dopaminergic neurons  
**iNS** induced neurons  
**iPD** idiopathic Parkinson's disease  
**iPSCs** induced pluripotent stem cells  
**KOSR** Knockout serum replacement  
**LB** Lewy bodies  
**LDH** Lactate dehydrogenase  
**LDN** LDN-193189  
**LGE** Lateral Ganglionic Eminence  
**LMX1A** LIM Homeobox Transcription Factor 1 Alpha  
**LN** Lewy neurites  
**LRRK2** Leucine Rich Repeat Kinase 2  
**LPS** Lipopolysaccharide  
**MAP2** Microtubule-associated protein 2  
**mDNs** mature dopaminergic neurons  
**MEA** Multielectrode array  
**MGL** Microglia

---

**MHC-II** Major histocompatibility complex  
**MPTP** 1-methyl-4-phenyl-1,2,3,6-tetrahydropyridine  
**MO** Midbrain organoids  
**MUT** Mutant  
**NBs** Neuroblasts  
**NEAA** Non-essential amino acids  
**NURR1** Nuclear receptor related 1  
**OCT4** Octamer-binding transcription factor 4  
**PAX6** Paired box protein 6  
**PBS** Phosphate-buffered saline  
**PD** Parkinson's disease  
**PDGF-BB** Platelet-derived growth factor-BB  
**PDGFR $\beta$**  Platelet derived growth factor receptor beta  
**PDO** Patient derived organoids  
**Pen/Strep** Penicillin/Streptomycin  
**PINK1** PTEN-induced kinase 1  
**PRKN** Parkin RBR E3 Ubiquitin Protein Ligase  
**PITX3** Paired Like Homeodomain 3  
**PMA** Purmorphamine  
**RA** Retinoic acid  
**RGL** Radial glia  
**RGCs** Radial glia cells  
**RIPA** Radioimmunoprecipitation  
**RNA** Ribonucleic acid  
**ROS** Reactive oxygen species  
**RT** Room temperature  
**SAG** Smoothened agonist  
**SB** SB-431542  
**ScRNAseq** Single cell RNA sequencing  
**SDS-PAGE** Sodium dodecyl sulfate-polyacrylamide gel electrophoresis  
**SSEA-4** Stage-specific embryonic antigen-4  
**SHH** Sonic hedgehog  
**SNCA** Synuclein Alpha  
**SNpc** Substantia nigra pars compacta

---

**SnRNAseq** Single nuclei RNA sequencing

**SOX1/2** Sex determining region Y-box 1/2

**StrO** Striatum organoid

**TGF $\beta$**  Transforming growth factor beta

**TH** Tyrosine hydroxylase

**ULA** Ultra-low attachment

**VSP32**

**VPS35** Vacuolar protein sorting 35

**WNT** Wingless-related integration site

**WT** Wild type

**yNEURs** Young neurons



---

# Table of contents

Affidavit .....	ii
Acknowledgements .....	vi
Abbreviations .....	x
Table of contents.....	1
List of publications.....	3
List of Figures and Tables in Synopsis chapter .....	5
Abstract.....	6
Aim and Objectives .....	8
Chapter 1: Synopsis.....	15
1.1 Introduction.....	15
1.1.1 Neurodegeneration and Aging.....	15
1.1.1.1 Parkinson's disease .....	15
1.1.1.1.1 LRRK2 p.Gly2019Ser in Parkinson's disease .....	18
1.1.1.1.2 Neurodevelopmental aspect of Parkinson's disease.....	19
1.1.2 Modeling of Parkinson's disease .....	20
1.1.2.1 Animal Models .....	21
1.1.2.2 In vitro human brain models .....	22
1.1.2.2.1 2D iPSC-based cell culture.....	24
1.1.2.2.2 Advanced 3D brain organoid models.....	25
1.1.2.2.3 Aged <i>in vitro</i> models .....	27
1.2 Summary and discussion of the research covered in the thesis .....	30
Chapter 2: Material and Methods .....	40
Chapter 3: Results.....	42
Manuscript I .....	42

---

Manuscript II .....	74
Manuscript III .....	112
Conclusions and Perspectives.....	210
References.....	216

---

# List of publications

## Publications that are part of the thesis

### Published:

Zagare A\*, **Barmpa K\***, Smajic S, Smits LM, Grzyb K, Grünewald A, Skupin A, Nickels SL, Schwamborn JC. Midbrain organoids mimic early embryonic neurodevelopment and recapitulate LRRK2-p.Gly2019Ser-associated gene expression. *Am J Hum Genet.* 2022 Feb 3;109(2):311-327. doi: 10.1016/j.ajhg.2021.12.009. Epub 2022 Jan 24. PMID: 35077669; PMCID: PMC8874228. \*Shared 1<sup>st</sup> authorship

Sabate-Soler S, Nickels SL, Saraiva C, Berger E, Dubonyte U, **Barmpa K**, Lan YJ, Kouno T, Jarazo J, Robertson G, Sharif J, Koseki H, Thome C, Shin JW, Cowley SA, Schwamborn JC. Microglia integration into human midbrain organoids leads to increased neuronal maturation and functionality. *Glia.* 2022 Jul;70(7):1267-1288. doi: 10.1002/glia.24167. Epub 2022 Mar 9. PMID: 35262217; PMCID: PMC9314680.

### In Preparation:

**Barmpa K**, Saraiva C, Gomez-Giro G, Gabassi E, Spitz S, Brandauer K, Rodriguez-Gatica J.E, Antony P, Robertson G, Papastefanaki F, Kubitscheck U, Salti A, Ertl P, Matsas R, Edenhofer F, Schwamborn J.C. Age-induced midbrain-striatum assembloids model early phenotypes of Parkinson's disease. *bioRxiv.* 10.28.564305; doi: <https://doi.org/10.1101/2023.10.28.564305>.

## Publications that are not part of the thesis

### Published:

Jarazo J, **Barmpa K**, Modamio J, Saraiva C, Sabaté-Soler S, Rosety I, Griesbeck A, Skwirblies F, Zaffaroni G, Smits LM, Su J, Arias-Fuenzalida J, Walter J, Gomez-Giro G, Monzel AS, Qing X, Vitali A, Cruciani G, Boussaad I, Brunelli F, Jäger C, Rakovic A, Li W, Yuan L, Berger E, Arena G, Bolognin S, Schmidt R, Schröder C, Antony PMA, Klein C, Krüger R, Seibler P, Schwamborn JC. Parkinson's Disease Phenotypes in Patient Neuronal Cultures and Brain Organoids Improved by 2-Hydroxypropyl- $\beta$ -Cyclodextrin Treatment. *Mov Disord.* 2022

---

Jan;37(1):80-94. doi: 10.1002/mds.28810. Epub 2021 Oct 12. PMID: 34637165; PMCID: PMC9291890.

Garcia Santa Cruz B, Slter J, Gomez-Giro G, Saraiva C, Sabate-Soler S, Modamio J, **Barmpa K**, Schwamborn JC, Hertel F, Jarazo J, Husch A. Generalising from conventional pipelines using deep learning in high-throughput screening workflows. *Sci Rep.* 2022 Jul 6;12(1):11465. doi: 10.1038/s41598-022-15623-7. PMID: 35794231; PMCID: PMC9259641.

In preparation:

**Barmpa K**, Saraiva C, Longworth J, Hufnagel K, Skwirblies F, Schmidt R, Brenner D, Schröder C, Schwamborn J.C. Dysregulated functionality of the medium spiny GABAergic neurons in LRRK2-G2019S striatum organoids. In Preparation.

Sabate-Soler S, Zimmermann A.S, Zagare A, **Barmpa K**, Haendler K, Spielman M, Saraiva C, Schwamborn J.C. Vascularization of human midbrain organoids leads to reduced hypoxia and a complex microglia morphology. In Preparation.

Axel Chemla<sup>1</sup>, Giuseppe Arena<sup>1</sup>, Ginevra Sacripanti<sup>1</sup>, **Kyriaki Barmpa**<sup>1</sup>, Alise Zagare<sup>1</sup>, Paul Antony<sup>1</sup>, Jochen Ohnmacht<sup>2</sup>, Pierre Garcia<sup>1,3</sup>, Jaqueline Jung<sup>4</sup>, Anne Marie Marzesko<sup>1,§</sup>, Manuel Buttini<sup>1,3</sup>, Thorsten Schmidt<sup>4</sup>, Anne Grünewald<sup>1,5</sup>, Jens C.Schwamborn<sup>1,6,\*</sup>, Rejko Krüger<sup>1,2,7,\*</sup>, Claudia Saraiva<sup>1,\*</sup>. Parkinson's disease-related Miro1 mutation induces mitochondrial dysfunction and loss of dopaminergic neurons in vitro and in vivo. In Preparation.

Gemma Gomez-Giro<sup>1</sup>, Daniela Frangenberg<sup>1</sup>, Daniela Vega<sup>2</sup>, Alise Zagare<sup>1</sup>, **Kyriaki Barmpa**<sup>1</sup>, Paul M.A. Antony<sup>3</sup>, Graham Robertson<sup>1</sup>, Rahman Sabahi<sup>4</sup>, Yagmur Demircan<sup>4</sup>, Gülден Akçay<sup>4</sup>, Kristian Haendler<sup>5</sup>, Nathalie Kruse<sup>5</sup>, Florentia Papastefanaki<sup>6</sup>, Rebecca Matsas<sup>6</sup>, Malte Spielman<sup>5</sup>, Regina Luttge<sup>4</sup>, and Jens C. Schwamborn<sup>1\*</sup>. Alpha-synuclein pathology transfer in a midbrain-hindbrain assembloid model. In Preparation.

---

# List of Figures and Tables in Synopsis chapter

**Figure 1:** Illustration of PD hallmarks. (Page 16)

**Figure 2:** Aging as a risk factor for PD development. (Page 17)

**Table 1:** Key differences in human PD and animal PD models. (Page 22)

**Figure 3:** Patterning of neuroepithelial cells towards specific identity of neural progenitors.  
(Page 23)

**Figure 4:** Increasing the complexity of *in vitro* 3D brain models. (Page 26)

**Table 2:** Generation of iNs. (Page 28)

---

# Abstract

Parkinson's disease (PD) is one of the most prevalent neurodegenerative disorders primarily impacting dopaminergic neurons (DANs) within the substantia nigra pars compacta (SNpc) in the midbrain, which innervate the dorsal striatum. As conventional animal models inadequately capture disease phenotypes, the advent of induced pluripotent stem cell (iPSC) technology has revolutionized PD modeling through the development of 2D and 3D patient-derived *in vitro* models. Notably, 3D brain organoids have demonstrated exceptional capacity to replicate the cellular composition and connectivity of the human brain. In the context of PD, midbrain organoids (MOs) enriched in DANs, derived from patient cell lines, can manifest relevant neurodegenerative phenotypes, and unveil previously unexplored dysfunctional mechanisms. To further delineate the physiological relevance of MOs, we performed a single cell RNA sequencing (scRNAseq) comparative analysis with data from the human embryonic midbrain. Our results validate the high transcriptomic correlation of MOs with the human counterpart and the development of similar cellular composition. In parallel, our investigation reveals that MOs generated from a cell line carrying the PD-relevant LRRK2 p.Gly2019Ser mutation demonstrate an altered genetic profile compared to the healthy isogenic MOs, featuring disrupted neurodevelopment and dysregulated pathways relevant to PD pathogenesis.

While our findings underscore the significant relevance of MOs to the human embryonic midbrain, their physiological complexity can still be improved. The neuroectodermal origin of this model doesn't permit the development of microglia cells that are a crucial component in the homeostasis of the brain. To address this limitation, we developed a protocol for the successful integration of microglia into MOs. Single nuclei RNA sequencing (snRNAseq) and electrophysiological data reveal reduction of cellular stress and promotion of neuronal maturation. This model holds great potential for studying the impact of neuroinflammation on PD.

We further aimed to increase the complexity of the MO model by generating an assembloid model that resembles the nigrostriatal pathway connectivity, predominantly affected in PD. The assembloid combines midbrain and striatum-specific organoids, accurately replicating the nigrostriatal pathway connectivity and functionality, through the formation of active synapses and the release of catecholamines from the midbrain into the striatum. Finally, considering that aging is the major risk factor in PD, we induced aging in the midbrain-striatum assembloid by the overexpression of progerin. This method, led to the successful development of aging-

---

related characteristics and early neurodegeneration phenotypes in the assembloid. Overall, each one of the models presented here constitute a significant tool for elucidating the mechanisms of neurodegeneration and paving the way towards preventive therapies. Answering complex questions involves combining different elements to make *in vitro* models more intricate, which will bridge the gap towards the complex pathophysiology of the human brain.

---

## Aim and Objectives

Constraints on accessing and studying the human brain limit scientific efforts to the use of 2D neuronal cultures and animal models (Shadrina & Slominsky, 2021; Simmnacher et al., 2020). The brain is the most complex organ in the human body and this complexity cannot be fully recapitulated in 2D cultures. In this instance animal models can be useful to understand several functional processes of the brain, however they cannot fully mimic the human neurodegenerative process rendering them inadequate for preclinical studies. Therefore, 3D *in vitro* human based models that can emulate the complexity of the human brain, are essential for understanding and treating neurodegenerative diseases.

In the case of PD, MOs have shown a great potential in recapitulating disease phenotypes and elucidating processes that were not previously observed (Jarazo et al., 2021; Smits et al., 2019; Walter et al., 2021). While studies have demonstrated the differentiation capacity and cellular composition within MOs, no direct comparison to the physiological human midbrain has been made. This comparison is crucial for gaining deeper insights into the model's complexity and physiological significance.

The multifactorial nature of PD poses the need for further increasing the complexity of MOs with the integration of characteristics that are not innately present. MOs are region specific brain models derived from neuroectodermal patterning. Therefore, they lack the ability of developing cells coming from different lineages, such as microglia. The integration of microglia in MOs could contribute to improving the model's homeostasis and functionality.

Apart from the lack of microglia, one important characteristic missing from the MOs is the striatal input in the functionality of DANs, through the nigrostriatal pathway. Recent studies have demonstrated the generation of assembloid models by merging two or more region specific brain organoids (Miura et al., 2020; Sloan et al., 2018; Xiang et al., 2019). These models can be valuable when interregional connectivity must be considered. This is the case for PD, where nigrostriatal pathway connectivity is highly affected.

In line with the aforementioned improvements that need to be considered, aging is another limiting factor when using iPSC-derived 3D brain models. Cells are rejuvenated during the iPSCs generation processing, erasing their aging characteristics (Simpson et al., 2021). Several aging induction methods have been illustrated *in vitro* but none of them have been investigated on 3D brain specific organoids. Inducing aging in the complex 3D *in vitro* brain models will be pioneering in neurodegenerative research, where aging is the major risk factor.



---

Hence, considering all these challenges, the objectives of the thesis are:

- Validate the physiological and developmental relevance of MOs by comparing it to the human embryonic midbrain using single cell RNA sequencing data analysis.
- Evaluate the PD-related transcriptomic changes on MOs carrying the LRRK2 p.Gly2019Ser mutation.
- Advance the complexity and biological significance of MOs via the integration of microglia cells, the major immunological component of the human brain.
- Develop and characterise an assembloid model that will recapitulate the nigrostriatal pathway connectivity *in vitro*.
- Investigate the impact of aging on the development of neurodegeneration-relevant phenotypes in the assembloid model, through progerin overexpression.

---

# **Chapter 1: Synopsis**

## **1.1 Introduction**

### **1.1.1 Neurodegeneration and Aging**

Neurodegeneration is a pathophysiological process occurring in the brain, mainly characterized by the progressive loss of neuronal functionality, which ultimately leads to neuronal death (Lamprey et al., 2022). There are different hallmarks that characterize neurodegenerative diseases such as synaptic dysfunction and loss of neuronal networks, protein aggregation, abnormalities in the cytoskeleton, genetic mutations, inflammation and dysregulated metabolism (Wilson et al., 2023). While environmental and genetic factors can determine the progression and severity of neurodegenerative diseases, the aging process is crucial for the disease onset. Tissues such as the brain that are mainly composed of non-proliferating post-mitotic cells, such as neurons, are more susceptible to aging due to accumulated levels of DNA damage (Hou et al., 2019). Most of the aging hallmarks correlate with the hallmarks of neurodegenerative diseases. More specifically, during healthy brain aging there are several dysregulated processes, such as loss of proteostasis and protein aggregation, decreased mitochondria turnover, epigenetic alterations, DNA damage, neuroinflammation, stem cell exhaustion and abnormal cellular communication (López-Otín et al., 2013). The dysregulation of these processes is further enhanced in the disease state (Hou et al., 2019), such as PD.

#### **1.1.1.1 Parkinson's disease**

One of the most common age-related neurodegenerative disorders globally is PD which is mainly characterized by the progressive loss of the A9 group of DANs in the SNpc in the midbrain (Braak et al., 2003; Kouli et al., 2018). The DANs from the SNpc project their axons to the dorsal striatum, consisting of the putamen and caudate nucleus. These dopaminergic projections form the nigrostriatal pathway, which is essential for the functionality of the basal ganglia, an important component of the modulation of movement and the control of behavioral aspects such as motivation (Prensa et al., 2009). In PD, the loss of DANs and the degeneration

of their axonal projections, leads to dopamine (DA) depletion within the striatum and disturbances in the balance of neurotransmitters GABA, DA and glutamate that are important for the regulation of the locomotor activity (Dovonou et al., 2023; Raffa et al., 2013). Ultimately, this leads to the development of several motor symptoms such as rigidity, tremor, instability and bradykinesia (Kouli et al., 2018). These symptoms typically arise at the late stage of the disease. However there are also some non-motor symptoms that have been observed in early stages of PD development, such as constipation, depression, sleep disturbances and olfactory dysfunction (Gupta & Shukla, 2021; Kouli et al., 2018). The appearance of these symptoms has been considered as the pre-diagnostic phase of PD, where loss of DANs in the SNpc is progressing steadily but without the initiation of motor symptoms (Dommershuijsen et al., 2021) (Figure 1).

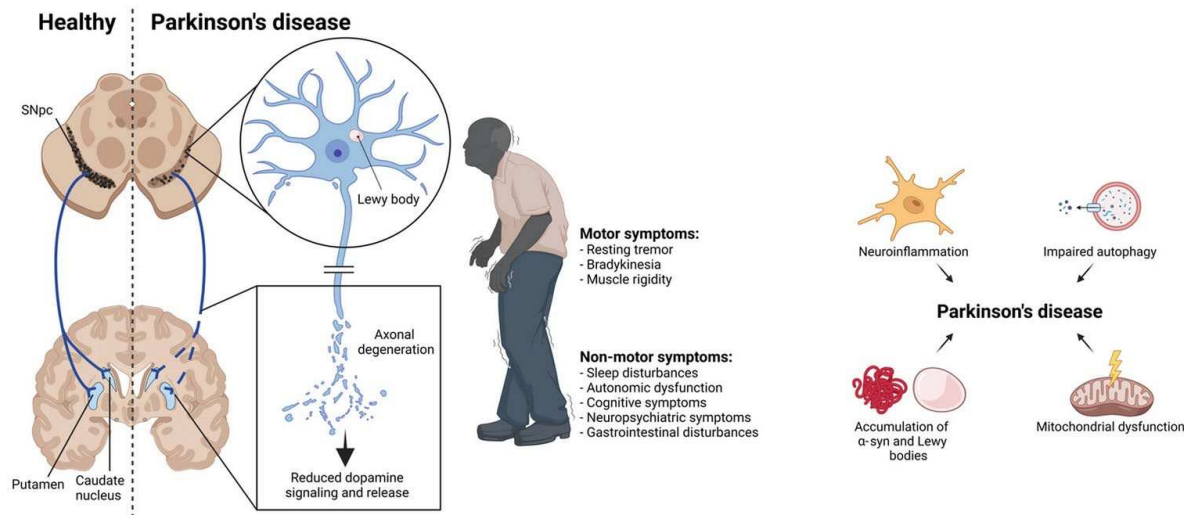


**Figure 1: Illustration of PD hallmarks.** PD non-motor symptoms arise due to the loss of dopaminergic terminals and DA depletion in the striatum, while motor symptoms appear later in the disease due to the DANs' death. Neuroinflammation, impaired autophagy, accumulation of  $\alpha$ -synuclein and mitochondrial dysfunction are some of the dysregulated processes that contribute to the degeneration and loss of DANs (Dovonou et al., 2023).

Aging is the most crucial risk factor for the development of PD, as epidemiological studies have shown a significant increase in the disease manifestation after the age of 60 (Hindle, 2010). Studies in non-human primates, have shown specifically decreased levels of DANs with aging, indicating their increased vulnerability to the dysregulated biological process that occur during aging (Figure 2) (Pang et al., 2019).

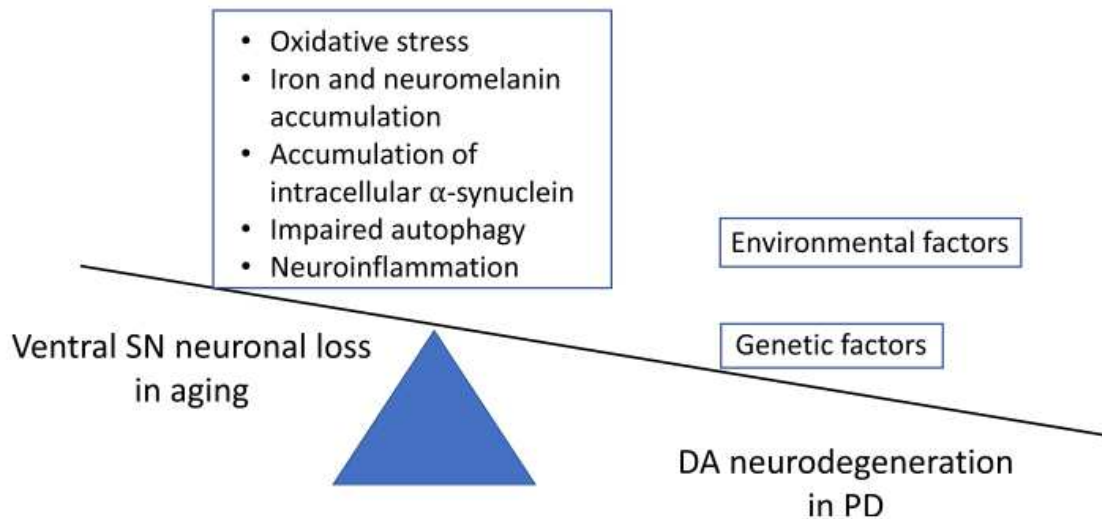


**Figure 2: Aging as a risk factor for PD development.** Several dysregulated processes contribute to the gradual loss of DANs during aging. However, the influence of environmental and genetic factors lead to more severe neurodegeneration phenotypes in PD (Pang et al., 2019).

Age-related changes overlap with many of the phenotypes observed in PD patients. One of the leading reasons for the dopaminergic neuronal loss is the aggregation of misfolded  $\alpha$ -synuclein. With aging, there is a decline in the efficiency of the proteasome activity and protein ubiquitination, which further contributes to the deposition of abnormal aggregated proteins such as  $\alpha$ -synuclein (Hindle, 2010). Although in healthy aged controls some levels of  $\alpha$ -synuclein aggregation have been identified, it is significantly lower than in the brain affected by PD, as observed in post-mortem tissue. Moreover,  $\alpha$ -synuclein aggregates form intracellular inclusions called Lewy bodies (LB) and Lewy neurites (LN). These inclusions affect the functionality of neurons by contributing to the dysregulation of multiple mechanisms, such as mitochondria and synaptic dysfunction, lysosomal defects, endoplasmic reticulum stress and membrane disruption (George et al., 2013; Gómez-Benito et al., 2020). Despite the presence of LB and LN, aging itself has been associated with mitochondrial dysfunction with the increased release of reactive oxygen species (ROS) that further induce cellular stress and DNA damage. Additionally, aging causes impairments in the autophagic machinery and induces neuroinflammation with increased activation of microglia, all phenotypes that are commonly detected in PD patients (Hindle, 2010; Pang et al., 2019).

Most PD cases are idiopathic (iPD), meaning that aging and environmental factors such as exposure to pesticides have been determined as the main contributors to disease development. However, there is approximately 10% of cases that are linked to genetic mutations and can be

---

inherited. Some of the most important PD-related genes are *SNCA*, *LRRK2*, *VSP32*, *PRKN*, *PINK1* and *DJ-1* (Kouli et al., 2018). These genes are responsible for either autosomal dominant (*SNCA*, *LRRK2* and *VSP32*) or autosomal recessive (*PRKN*, *PINK1* and *DJ-1*) forms of PD, with the former shown to be more closely associated to the phenotypes seen in iPD (Correia Guedes et al., 2020). From these genes, *LRRK2* specifically has been linked to familial and sporadic PD, and therefore extensive research has been prompted on PD cases exhibiting mutations in this particular gene (Ren et al., 2019).

#### **1.1.1.1.1 LRRK2 p.Gly2019Ser in Parkinson's disease**

Leucine-rich repeat kinase 2 (*LRRK2*) is one of the genes that has been associated with Mendelian form of PD and increased vulnerability to the disease. The *LRRK2* gene encodes for a large multidomain protein with a catalytic core composed of a kinase and a Roc GTPase domain, followed by a C-terminal domain named COR (Hur & Lee, 2021). The most common mutation in PD cases is p.Gly2019Ser, with 4% of occurrence in familial PD cases and 1% in sporadic (Hur & Lee, 2021; Jia et al., 2022). The p.Gly2019Ser mutation is a result of a G > A substitution at position 6055 of exon 41, leading to an amino acid change at codon 2019 from glycine to serine. This mutation takes place on the kinase domain of the protein thus causing increased kinase activity (Tolosa et al., 2020). PD patients with *LRRK2* p.Gly2019Ser mutation exhibit multiple dysregulated phenotypes that lead to the degeneration of DANs, with enhanced levels of  $\alpha$ -synuclein and LB formation, dysfunctional mitochondria, hyper-autophagy, reduced outgrowth of neurites and synaptic dysfunction (Ren et al., 2019). More interestingly, studies have shown that this *LRRK2* variant and others, interfere with the proper function of the canonical Wnt/ $\beta$ -catenin signalling pathway, which is essential for neurogenesis in the developing brain. The *LRRK2* role in neurogenesis can also stem from its role in cytoskeleton regulation. Specifically, *LRRK2* regulates the phosphorylation of ERM (ezrin-radixin-moesin) proteins that are important for the morphology and motion of the growth cone in neuronal axons (Berwick et al., 2013). The association of the *LRRK2* p.Gly2019Ser mutation with a broad spectrum of phenotypes, along with its clinical resemblance to cases of iPD, makes it appealing for disease modeling. This mutation holds great potential in unraveling the crucial molecular alterations and mechanisms that underlie neurodegeneration.

---

### 1.1.1.1.2 Neurodevelopmental aspect of Parkinson's disease

Although PD is an age-associated disorder, the disease is initiated many years prior to the neurodegeneration phenotypes. It has been reported that motor symptoms usually arise when there is approximately 50% loss of DANs, considering this as the clinical diagnostic phase of PD (Harris et al., 2020). Many of the non-motor symptoms linked to PD development have also been reported in the case of hippocampal dysregulated neurogenesis (Jones et al., 2022), illustrating the involvement of neurodevelopmental dysfunction in the susceptibility to several neuropsychiatric and neurodegenerative conditions. The fact that PD patients acquire pre-diagnostic symptoms relevant to neurogenesis dysfunction, has led the scientific community to the hypothesis that neurodevelopmental defects can promote neurodegeneration later in life (Schwamborn, 2018).

This hypothesis is further strengthened by the fact that PD relevant genes, such as *SNCA*, *NURR1*, *PITX3*, *PINK1*, *LRRK2* and *VSP35*, are implicated in several neurodevelopmental processes, including the regulation of DANs development and differentiation (Le Grand et al., 2015). *NURR1* is a transcription factor with an important role in DANs development and maintenance (Le et al., 1999). Mutations in this gene have been associated with PD development (Grimes et al., 2006). Along with *NURR1*, *PITX3* is another transcription factor that contributes to the differentiation of DANs. In the SNpc, *PITX3* regulates the expression of tyrosine hydroxylase (TH) (J. Li et al., 2009). Specifically, *PITX3* knockout mice develop PD phenotypes and display significant loss of DANs in the SNpc (Nunes et al., 2003). Although multiplications of the *SNCA* gene are responsible for increased levels of  $\alpha$ -synuclein aggregation in PD patients (Book et al., 2018), mice that lack the *SNCA* gene have shown impaired development of DANs in the SNpc (Garcia-Reitboeck et al., 2013). Moreover, deletion of *SNCA* has been related with clinical developmental delay and the manifestation of autism spectrum disorder (ASD), where it is mainly linked to synaptic dysfunction (Alejandra Morato Torres et al., 2020). *VSP35* and *LRRK2* have a role in the regulation of the Wnt/ $\beta$ -catenin pathway, which is essential for the development and maintenance of DANs in the SNpc. PD-related mutations in these two genes, such as p.D620N in *VSP35* and p.Gly2019Ser in *LRRK2*, have shown to cause disturbances in the Wnt/ $\beta$ -catenin signaling (Berwick & Harvey, 2012; Chiu et al., 2020). On the same line, loss of *PINK1* function caused by many PD-relevant mutations (Vizziello et al., 2021), could be linked to neurodevelopmental defects, as *PINK1* downregulation in a zebrafish model has been associated with neurodevelopmental impairment (Anichtchik et al., 2008).

---

Finally, another evidence that further supports the developmental hypothesis in PD, is the abnormally elevated levels of DANs in the olfactory bulb of PD patients. In normal human development, neurogenesis in the olfactory bulb occurs during the first 18 months of life. The observed increase in neurogenesis that occurs later in life in PD patients, further supports the appearance of early life developmental impairments (Schwamborn, 2018).

### **1.1.2 Modeling of Parkinson's disease**

Due to the complexity of the human brain, research on neurodegenerative diseases such as PD, requires the use of diverse models that provide insights on the development and progression of the disease. In 1960, two important studies from Ehringer and Hornykiewicz, and Sano et al. (1960, 2000) reported reduced DA and noradrenaline levels in post-mortem brain sections of PD patients. This finding led to further studies that enabled the development of treatments, such as L-DOPA supplementation, a precursor of DA, for compensating the DA deficiency induced by DANs degeneration, leading to alleviation of motor symptoms (Nagatsu & Sawada, 2007). Therefore, studies using post-mortem human brain tissue has played a pivotal role not only in understanding the phenotypes and main dysfunctions occurring in patients, but also in developing treatments that can alleviate symptoms. However, the use of post-mortem brain tissue possesses certain limitations for its use in validation experiments, after certain hypothesis has been formed. Considering that post-mortem tissue only reflects the end stage of the disease, it therefore cannot contribute fully to deciphering the causes of disease progression (Hartmann, 2004). Another important limitation is the quality of the post-mortem tissue and preservation. Although in recent years brain banks have advanced their quality control measures, it is still not clear if post-mortem brain tissue can be used in certain biochemical studies such as promoters methylation, histone modifications and microRNA conservation, due to the post-mortem delay effect (Ferrer et al., 2008). Therefore, the use of *in vivo* and *in vitro* models has been essential for studying molecular and cellular processes that contribute to the development and progression of PD.

---

### 1.1.2.1 Animal Models

Mammalian and non-mammalian animal models have played an important role in the efforts of understanding the neurodegenerative phenotypes in PD. With the use of these models, scientists can assess various biological dysfunctions, such as mitochondria dysfunction, lysosomal impairment, neuroinflammation and synaptic alterations, that are crucial for the development of the disease. Simple animal models such as *Drosophila melanogaster* (fruit fly), *Caenorhabditis elegans* (roundworm nematode) and the fish models *Danio rerio* (Zebrafish) and *Oryzias latipes* (Medaka) have provided key insights into the pathological processes of PD. The simplicity of these organisms with the short life span makes it easier to create genetic models which can be used to study the disease progression in the different stages of their development. However, these models cannot fully recapitulate the pathophysiology of PD due to their distant genetic makeup compared to humans and the fundamentally different organisation of their nervous system (Lim, 2010; Shadrina & Slominsky, 2021).

On the other hand, mammalian models such as non-human primates and rodents are genetically closer to humans, with a more human-like organisation of their central nervous system. Rodent models, particularly due to their small size and reduced costs, are widely used in neurodegenerative research. There are two main categories of rodent models in PD research, namely the toxin and genetic models (Blesa & Przedborski, 2014). The most prevalent neurotoxin-induced models are the MPTP (1-methyl-4-phenyl-1,2,3,6-tetrahydropyridine) and 6-hydroxydopamine (6-OHDA) models, which both recapitulate the degeneration phenotype of the DANs within the SNpc and exhibit locomotion related symptoms. However, these phenotypes are quickly exacerbated with the fast death of DANs, making these models incompatible to study the progression of the disease (Kin et al., 2019; Zeng et al., 2018) (Table 1). Genetic models on the other hand are generated by introducing, overexpressing or knocking out PD-related mutations in genes such as *SNCA*, *LRRK2*, *GBA*, *PINK1*, among others (Behl et al., 2021; Cabin et al., 2005; Deng & Yuan, 2014; Moiso et al., 2014; Seegobin et al., 2020). These models can recapitulate several dysregulated biological processes such as dysfunctional mitochondria, oxidative stress and neuroinflammation and are more suitable for unravelling mechanisms related to the progression of neurodegeneration, as they exhibit a steady development of neurodegenerative-related phenotypes over time. However, a big drawback of the genetic models is that most of them fail to recapitulate key disease phenotypes such as the loss of DANs in the SNpc or the loss of TH and DA in the striatum (Kin et al., 2019; Lama et al., 2021; Terzioglu & Galter, 2008) (Table 1).



**Table 1: Key differences in human PD and animal PD models (Kin et al., 2019).**

Animal Model	The Main Difference Between Human PD and Animal PD Model	
Neurotoxin model	6-OHDA	<ul style="list-style-type: none"> <li>• Rapid progression.</li> <li>• No lewy related pathology.</li> <li>• The pathology is completely different.</li> </ul>
	MPTP	<ul style="list-style-type: none"> <li>• Movement disorder is not obvious.</li> <li>• The pathology is completely different.</li> </ul>
	Pesticides	<ul style="list-style-type: none"> <li>• Rapid progression.</li> <li>• The pathology is completely different.</li> </ul>
Genetic model	<ul style="list-style-type: none"> <li>• Movement disorder is relatively rare.</li> <li>• Lewy related pathology can be identified in a few models.</li> <li>• Dopaminergic neuronal damage is relatively rare.</li> </ul>	

Apart from the aforementioned limitations of the toxin and genetically engineered animal models, there are also several physiological concerns for their use in PD research. It has been reported that toxins are metabolised differently in humans and rodents, therefore the phenotypes induced in toxin animal models must be taken with caution. Moreover, there are substantial differences in the blood brain barrier composition between humans and rodents than can induce further discrepancies in neuroinflammation responses, due to the distinct transport of metabolites and nutrients in the brain (Potashkin et al., 2011). This also poses an important limitation for the use of rodent models in drug testing. Additionally, substantial functional differences between non-neuronal human and rodent cell types such as astrocytes and microglia, raise further concerns on the use of these animal models in PD research (Hasselmann et al., 2019; J. Li et al., 2021).

### 1.1.2.2 *In vitro* human brain models

The complexity of the human brain with its unique neuronal organisation and gene expression profile, has generated an unmet need for the development of human-based models. With the breakthrough of Takahashi and Yamanaka in 2006, it is now possible to convert the identity of terminally differentiated cell types, such as fibroblasts, into iPSCs that possess embryonic stem

cell-like characteristics with the ability to differentiate into any cell type of the human body (Takahashi et al., 2007; Takahashi & Yamanaka, 2006). Since then, many studies have focused on the use of iPSC-derived neuronal culture models obtained from human fibroblasts or blood, from patients and healthy individuals, to recapitulate the human neuronal complexity and comprehend the underlying disease-related molecular mechanisms (Bitar & Barry, 2020). Additionally, with the use of CRISPR/Cas9 and other gene editing tools it is possible to create iPSC lines with the desired disease-related mutations or isogenic gene-corrected lines from patient cells that carry specific genetic alterations (De Masi et al., 2020). Neuronal models generated from these lines provide the means to study the specific effect of genetic mutations on different biological processes.

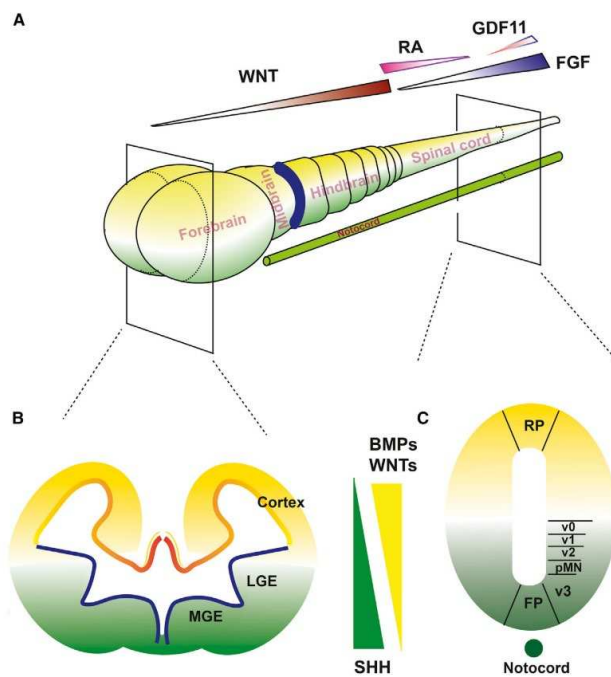


**Figure 3: Patterning of neuroepithelial cells towards specific identity of neural progenitors.** A) Shows the anterior-posterior neural tube patterning, regulated by the gradient of WNTs for the specification of forebrain, midbrain, and hindbrain neuronal populations, while RA and FGFs regulate the neural specification of the spinal cord. B-C) Dorsal-ventral specification of the forebrain and spinal cord is regulated by the gradient of WNTs, BMPs and SHH (Tao & Zhang, 2016).

For the successful differentiation of iPSCs into brain specific cell types, researchers have used small molecules and factors for the modulation of important developmental signaling pathways such as bone morphogenic protein (BMP), transforming growth factor beta (TGF $\beta$ ), wingless-related integration site (WNT) and sonic hedgehog (SHH). Specifically, cellular ectodermal,

---

neuroepithelial identity induction can be achieved by inhibition of BMP and TGF $\beta$  pathways, and stimulation of the canonical WNT and SHH pathways (Patthey & Gunhaga, 2014). Fibroblast growth factors (FGFs) and retinoic acid (RA) concentrations are also important for the patterning of neuroepithelium. Specification of the neuroepithelial cells into different subtypes of neural progenitors can be achieved by precise concentration of the morphogens mentioned above in the culture media (Figure 3). In this way, neural progenitors are patterned towards the anterior-posterior and dorsal-ventral axes of the neural tube and give rise to brain region specific neuronal and glia populations (Tao & Zhang, 2016).

With the regulated concentration of morphogens, cells acquire a distinct expression profile, with differential regulation of genes that control their differentiation process (Straccia et al., 2015). Identifying the key transcription factors that regulate gene expression in the different subtypes of neuronal and glia cells, is crucial for their characterisation and further optimisation of the cell culture protocols. The continuous advancements in the understanding of cell lines specification, lead to the generation of accurate and personalised human cellular models.

#### **1.1.2.2.1 2D iPSC-based cell culture**

2-dimensional (2D) culture is the monolayer cell culture system, where different cell types are cultured on a flat surface in the presence of specific molecules and supplements that assist their differentiation and maturation. In PD research, several studies have worked on the differentiation of iPSCs into DANs (Cooper et al., 2010; Lebedeva et al., 2023; Mahajani et al., 2019) using cell lines from healthy individuals and PD patients. This is particularly important for examining the effect of the patients' genetic background on DANs functionality and understand the specific mechanisms that are dysregulated in these neurons.

Although, DANs are crucially affected in PD, it is also important to investigate the functionality of other cell types. There are several published protocols for generation of other neuronal and glia cell populations from iPSCs in the 2D neuronal culture system, such as striatal GABAergic neurons (Grigor'eva et al., 2020), astrocytes (Juopperi et al., 2012; Leventoux et al., 2020), oligodendrocytes (Chanoumidou et al., 2020; Ehrlich et al., 2017) and microglia (Lanfer et al., 2022; Speicher et al., 2019).

The use of these models in research has helped the scientific community to answer specific questions related to the functionality of individual cell types. However, the complexity of neurodegenerative diseases, such as PD, stems from the dysregulated interactions between the different cells in the human brain. Hence, more complex *in vitro* models are needed to

---

recapitulate interactions between different neuronal types but also between neurons and glia. Researchers have created co-culture models of iPSC-derived neurons and astrocytes from PD and healthy individuals, where they could investigate how neurons are affected by the presence of diseased or healthy astrocytes (di Domenico et al., 2019). On the same line, co-culture of DANs with microglia has shown the importance of microglia cells for the maturation and functionality of DANs (Schmidt et al., 2021). Additionally, tri-culture systems of neurons, astrocytes and microglia have also been used for studying the neuroinflammation component in neurodegenerative diseases (Ryan et al., 2020).

Despite the efforts to increase the complexity of cultures in the 2D system, these models still fail to recapitulate the 3-dimensional (3D) environment and spatial organization of the human brain tissue (Jalink & Caiazzo, 2021; Moysidou et al., 2021).

### **1.1.2.2 Advanced 3D brain organoid models**

3D brain organoids represent the next step into generating more accurate human-based models that recapitulate the cellular diversity and connectivity of the human brain. Advancements in this model started with the generation of whole brain, or cerebral organoids (Lancaster et al., 2013). These organoids can develop into self-organised structures, consisting of multiple central nervous system (CNS) specific cell types. They are created following an unguided differentiation approach, leading to the development of varying proportions of cell types specific to different brain regions. Whilst enabling the study of cellular interactions from different brain regions, this model lacks a defined spatial organization of the brain regions. Additionally, this method introduces considerable variability between organoids. Therefore, scientists have focused on the development of region-specific organoids, with guided differentiation approaches, for the generation of models that resemble the structure and cellular diversity of specific brain regions (Qian et al., 2019). During this differentiation process certain small molecules and factors are used to guide the identity of stem cells towards cells of specific brain regions such as the midbrain (Jo et al., 2016a; S. W. Kim et al., 2021; Monzel et al., 2017; Smits et al., 2019), cortex (Pasca et al., 2015), striatum (Miura et al., 2020) and hindbrain (Valiulahi et al., 2021).

In the context of PD, midbrain organoids have shown a great potential of recapitulating the disease phenotypes. They are rich in DANs and they also develop glia cells such as astrocytes and oligodendrocytes, in later time points of culture (Monzel et al., 2017; Nickels et al., 2020). Electrophysiological activity assays have shown that neurons in the midbrain organoids are

capable of creating active neuronal networks (Smits et al., 2019). Additionally, midbrain organoids carrying PD-related mutations, such as the LRRK2 p.Gly2019Ser (H. Kim et al., 2019), triplication of *SNCA* (Mohamed et al., 2021) and mutations in *PINK1* (Jarazo et al., 2021), were able to recapitulate many PD-relevant phenotypes, with loss of DANs, developmental and synaptic disturbances and protein aggregation.

Although midbrain organoids have proven their utility in PD research, they are not suitable for addressing all the questions regarding the development of the disease. The dynamic nature of the brain, with neurons that project long axons into different brain regions, creates the need for the generation of models that better recapitulate this connectivity. One way to overcome this limitation is the generation of assembloid models (Figure 4) (Makrygianni & Chrousos, 2021; Paşca, 2018).

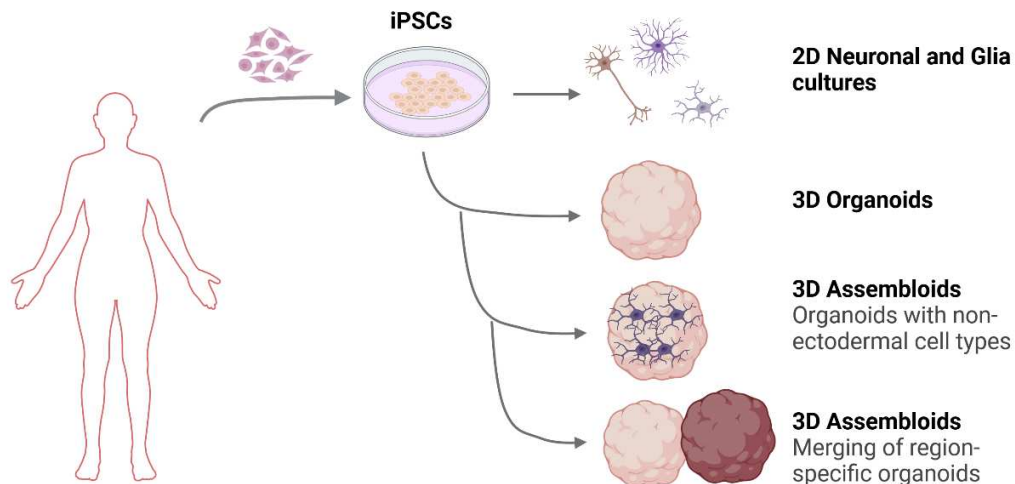


**Figure 4: Increasing the complexity of in vitro 3D brain models.** Human-derived somatic cells, such as fibroblasts, can be differentiated into iPSCs for generating 2D neuronal and glial cell culture models, as well as more complex models like 3D brain region-specific organoids and assembloids. Assembloid models can be derived either through the integration of non-ectodermal cell types, such as microglia, or by fusing different region-specific organoids. The image was created using Biorender.

Assembloid models can be created by the integration of cell types into brain organoids that cannot be differentiated from the ectodermal lineage, such as microglia, and by the fusion of different region-specific organoids (Figure 4). Microglia are the immune resident cells of the brain and their presence is extremely important for the development, maintenance and functionality of the neuronal network (Colonna & Butovsky, 2017). Microglia cells have been successfully integrated into cerebral organoids (Xu et al., 2021; W. Zhang, Jiang, et al., 2023) and have contributed to studies in Alzheimer’s disease (T. Lin et al., 2018). In parallel, brain

---

assembloids created by the direct fusion of region-specific organoids resemble physiological relevant axonal projections and establish active synapses (Andersen et al., 2020; Bagley et al., 2017; Miura et al., 2020; Sloan et al., 2018).

Advanced 3D brain models have paved the way towards more complete and physiologically relevant human-based models for studying brain-related disorders. It is possible now to develop models by merging brain region-specific organoids and integrating cell types originated from different lineages. Despite the contribution of midbrain organoids in PD research, it is important to consider that due to their embryonic-like nature, research using these models is more likely to represent an early stage of PD development. Consequently, given the relevance of age in the progression of the pathology, the incorporation of aging characteristics into the model becomes indispensable for comprehending PD's underlying mechanisms.

### **1.1.2.2.3 Aged *in vitro* models**

For deciphering the age-related dysregulated mechanisms in the process of neurodegeneration, we need to optimise our *in vitro* models in a way that aging characteristics will be retained or included in their generation process. The most common approach for the generation of neuronal cultures that retain the aged characteristics of the donor cells is the conversion of human somatic cells into induced neurons (iNs), with the forced expression of neurogenic transcription factors, specific for the different types of neurons (Table 2). In this approach, neurons retain the epigenetic information of the donor cells and therefore the aged-related phenotypes (Y. Zhang et al., 2020).

In the context of PD, several studies have succeeded in transdifferentiating induced dopaminergic neurons (iDANs), that could be used for modelling PD (De Gregorio et al., 2018; J. Kim et al., 2011; Park et al., 2015). As presented, iDANs can be an alternative model to iPSC-derived DANs for assessing the aging-related impact in the degenerative processes of DANs. Although the generation process of iDANs from somatic cells is easier and faster than the generation of iPSCs and from there the differentiation towards DANs, their inability of self-renewal poses a big constraint, as higher amount of donor cells is needed for the generation and stocking of iDANs, due to their higher sensitivity to cryopreservation (Yamatoya et al., 2022; Y. Zhang et al., 2020).

On the other hand, efforts have also been made towards the development of 3D organoids with retained aging signatures. Patient-derived organoids (PDOs) can be generated with the use of adult stem cells (ASCs). ASCs are obtained from tissue biopsies and cultured together with

niche factors that promote the stem cells differentiation but also maintain the stem cell pools. PDOs derived from old donors, maintain the aged characteristics, making an ideal model for studying age-related dysfunctions *in vitro*. Although this method is used to generate organoids from tissues with epithelial lining, it is still not possible to generate organoids from organs that are mainly consisted of non-epithelial elements, such as the brain (Fujii & Sato, 2021; J. Kim et al., 2020; Papaspyropoulos et al., 2020; Sun et al., 2023). To date the generation of brain organoids is solely based on the use of iPSCs.

**Table 2: Generation of iNs (Y. Zhang et al., 2020).**

Transcription factors	Cell type	Techniques	Neurons type	<i>In vitro/ in vivo</i>	Efficiency	Functional or not	References
ASCL1, NGN2, SOX2, NURR1 and PITX3	human fibroblasts	lentivirus	iN (mostly dopaminergic neurons)	<i>in vivo</i>	~80%	functional electrophysiology	Liu et al., 2011
Ascl1, Brn2, Myt11	mouse hepatocytes	lentivirus	iN	<i>in vivo</i>	>90%	functional electrophysiology	Marro et al., 2011
Sox2 and Mash1	pericyte-derived cells of the adult human cerebral cortex	retrovirus	GABAergic neurons	<i>in vitro</i>	~50%	these iN acquire the ability of repetitive action potential firing and serve as synaptic targets for other neurons	Karow et al., 2012
Brn2, Myt11, Zic1, Olig2, and Ascl1	Mouse Embryonic fibroblasts	lentivirus	iN (mostly GABAergic and glutamatergic neurons)	<i>in vitro</i>	~50%	functional electrophysiology Synaptic maturation	Vierbuchen et al., 2010
Ascl1, Brn2 and Myt11	mouse embryonic and postnatal fibroblasts	lentivirus	iN (mostly excitatory neurons)	<i>in vitro</i>	19.5%	functional electrophysiology Synaptic maturation	Vierbuchen et al., 2010
Ascl1, Brn2 and Myt11	mouse and human cells	viral delivery	neurons	<i>in vivo</i>	20%	functional	Torper et al., 2013
NeuroD1, Ascl1, Brn2, and Myt11	human fibroblasts	lentivirus	iN	<i>in vitro</i>	~60%	functional neurons	Pang et al., 2011
Ascl1, Lmx1a, FoxA2, and FEV	human fibroblasts	Dox-inducible lentivirus	serotonergic (5HT) neurons	<i>in vitro</i>	~25%	exhibited spontaneous electrophysiological activity and had active serotonergic synaptic transmission	Xu Z. et al., 2015
Mash1, Nurr1 and Lmx1a	mouse and human fibroblasts	lentivirus	iN (mostly dopaminergic neurons)	<i>in vitro</i>	high	functional electrophysiology	Caiazzo et al., 2011
NGN2 with (Forskolin and dorsomorphin)	human fetal lung fibroblasts	retrovirus	cholinergic neurons	<i>in vitro</i>	>90%	characteristic electrophysiological properties	Liu et al., 2013
LDN193189, SB431542, TTNPB, Tzv, CHIR99021, VPA, DAPT, SAG, Purmo	Human astrocytes	with medium	Functional neurons (mainly glutamatergic neurons)	<i>in vitro</i>	>90%	functional	Zhang et al., 2015
Forskolin, ISX9, CHIR99021 and SB431542	mouse fibroblasts	with medium	iN	<i>in vitro</i>	>90%	functional electrophysiology	Li et al., 2015

Importantly, different strategies have been used to induce aging phenotypes on iPSCs. One way is stress induced cellular senescence, where iPSCs are exposed to hydrogen peroxide (H<sub>2</sub>O<sub>2</sub>), ROS or small molecules that will induce aging related phenotypes, such as DNA damage (Fathi et al., 2022; Zhu et al., 2019).

Another approach is the induction of telomeres shortening. Telomeres are shortened progressively with aging, and it is one of the main aging hallmarks. The reason of telomeres shortening is due to the ineffective replication of the 3' end of the lagging DNA strand from

---

DNA-polymerase, leading to the progressive telomeres shortening in each cell division (Rossiello et al., 2022; Vaiserman & Krasnienkov, 2021). Studies have tested the telomerase inhibitor BIBR1532 on iPSCs and although it induces aging phenotypes in iPSC-derived neurons (Vera et al., 2016), it showed to be cytotoxic in feeder-free iPSCs cultures (Rossiello et al., 2022), therefore making it not suitable for all culture conditions.

Finally, inducible aging has also been tested via overexpression of Progerin, a truncated form of lamin A, a nuclear envelope protein essential for the organisation and regulation of nuclear function, in iPSCs. Progerin is produced by a mutated form of the *LMNA* gene (c.1824 C>T), and it is associated with the development of the Hutchinson–Gilford progeria syndrome (Bidault et al., 2020; Brennand, 2013). Transient expression of progerin using synthetic mRNA in iPSC-derived fibroblasts and iPSC-derived DANs, induced aging and neurodegeneration related phenotypes (Miller et al., 2013). However, another study, where progerin was overexpressed in the mouse brain, demonstrated that neurons are not significantly affected (Baek et al., 2015). These contradictory results could arise either from differences in susceptibility to aging stimuli between mouse and human neurons, or from the heightened sensitivity of 2D iPSC-derived neurons. 2D *in vitro* neuronal models lack most of the homeostatic mechanisms present in the brain of a whole organism, rendering them more vulnerable to agents that induce aging.

So far, none of these methods have been tested for inducing aging in brain organoids. This could provide further insights into the effectiveness of these methods in simulating aging in human-based models and determining their utility in neurodegenerative studies.



---

## 1.2 Summary and discussion of the research covered in the thesis

The complexity of neurodegenerative diseases urges the need for developing advanced human based models that can recapitulate the disease phenotypes *in vitro*. Although 2D neuronal cultures and co-cultures with other brain cells such as astrocytes and microglia have proven their relevance in assessing the vulnerability of specific cell types and their response to different treatments in the scope of drug development (Cetin et al., 2022), they still lack the complex interactions that are present in the actual human brain. Even though specific types of neurons, such as the DANs in PD, are more vulnerable in the disease state, this vulnerability can stem from ineffective or detrimental interactions with other cell types that further contribute to the disease development. Moreover, 2D monolayer cultures fail to recapitulate the 3D arrangement of cells in the human brain, leading to alterations in their morphology, spatial organisation and differentiation capacity (Centeno et al., 2018).

To overcome the limitations of 2D models, the generation of 3D organoids has paved the way towards *in vitro* systems with higher complexity and physiological relevance. In the recent years, several protocols have been published for the generation of different types of human brain organoids, such as whole brain cerebral organoids (Lancaster et al., 2013), cortical (Eigenhuis et al., 2023), hindbrain (Valiulahi et al., 2021), striatal (Miura et al., 2020) and midbrain organoids (Jo et al., 2016b; H. Kim et al., 2019; Kwak et al., 2020; Monzel et al., 2017).

For the use of these models in disease research, extensive characterisation and phenotyping is necessary for proper validation of their physiological relevance. With the advancements in single cell sequencing technologies, the transcriptome of organoid tissues can be deciphered on the single cell level, granting the ability to define cellular populations through the identification of specific genetic signature. Several studies have shown through scRNAseq analysis that organoids patterned towards specific brain regions can indeed acquire regional specification with the development of a diverse cellular composition (Fiorenzano et al., 2021a; Miura et al., 2020; Smits et al., 2020). Additionally, the accessibility of scRNAseq data from post-mortem and embryonic human brain tissues enables their juxtaposition with brain organoid transcriptomic profiles. This comparison can provide additional insights into how closely the transcriptomic identity of organoids aligns with that of their physiological counterparts (Camp et al., 2015; Tanaka et al., 2020).

---

During my thesis, we focused on the comparison of scRNAseq data from MOs at 35 (MO\_WT35) and 70 (MO\_WT70) days of differentiation, with scRNAseq data of the human embryonic midbrain (EM) from weeks 6-11 of embryo development (La Manno et al., 2016) (**Manuscript I**). To further validate the identity specificity of the MOs, we also compared them with data from human embryonic prefrontal cortex (EC) (Zhong et al., 2018). Hierarchical clustering of the four datasets for the average expression of the common top 500 variable genes, illustrates the transcriptional similarity between MOs and the EM. This is further supported by the high expression of midbrain specific markers, such as *FOXA2*, *TH*, *EN1* and *EN2* in the EM and MO datasets but not in the EC dataset (**Figure 1, Manuscript I**). Additionally, correlation analysis based on the expression of common genes between the EM and MOs has shown the developmental association of MOs at day 35 (D35) of differentiation with the gestational week 9 of EM, while MOs at day 70 (D70) of differentiation correlated better with week 10. These results indicate that MOs not only exhibit a transcriptomic profile closer to EM but also manifest a developmental pattern that aligns with the progressive development of the human embryo. The same correlation analysis with EM was also applied on data from cortical organoids (COs) (Winner, Kohl, et al., 2011), where the not significant correlation further illustrates that organoid models are capable of developing identities towards specific brain regions (**Supplementary Figure 3, Manuscript I**).

Moreover, MOs can develop a cellular composition relevant to the EM (**Figure 2, Manuscript I**), with higher abundance of more mature populations such as glia and pericytes, in the later time point of differentiation (MO\_WT70). However, key differences such as the presence of *in vitro* specific Neuroblasts (NBs *in vitro*) in MOs and endothelial cells in EM, reveal the *in vitro* nature of the organoids, with their induced differentiation from the neuroepithelium towards midbrain identity restricting them from developing mesodermal-specific cells, such as endothelial cells (Vasudevan & Bhide, 2008). These findings support the identity specificity of MOs towards the equivalent midbrain region in the developing human brain and their ability to develop a variety of physiologically relevant cell types.

The transcriptional similarity of MOs with the EM further validates the robustness of this model for elucidating the developmental component of PD. MOs derived from PD patient cell lines, or cell lines carrying PD-relevant mutations have shown the capacity to recapitulate disease phenotypes, and reveal therapeutic targets (Becerra-Calixto et al., 2023; Jarazo et al., 2021; H. Kim et al., 2019; S. W. Kim et al., 2021; Mohamed et al., 2021; Smits et al., 2019). In our study, MOs derived from an isogenic cell line carrying the LRRK2 p.Gly2019Ser mutation

---

demonstrated a PD-related phenotype, with dysregulated neurodevelopment, altered cellular composition and PD-related dysregulated pathways (**Manuscript I**).

More specifically, differential expression analysis of the MOs ScRNAseq data from the two time points of culture (day 35 and 70) generated from the LRRK2 p.Gly2019Ser mutated cell line (MUT) and the WT isogenic line, revealed differentially expressed genes (DEGs) in MUT MOs that are associated with the PD phenotype (**Figure 3 Manuscript I**). Interestingly, enrichment analysis of the DEGs between MUT and WT MOs, demonstrated the dysregulation of pathways related to the role of LRRK2 in PD and the development of the nervous system, along with cytoskeleton remodelling and cell adhesion pathways. LRRK2 plays an important role in the cytoskeleton remodelling (Parisiadou & Cai, 2010), by interacting with several cytoskeleton proteins for the regulation of neurite outgrowth (Häbig et al., 2013). Additionally, studies have shown the important role of LRRK2 in synapses regulation and cell adhesion, where mutated LRRK2 can lead to altered synaptic activity, impairments in synaptic vesicle endocytosis (Arranz et al., 2015; Plowey et al., 2014), but also dysregulation of motility and adhesion of cells such as microglia (Choi et al., 2015). Altered expression of genes responsible for the regulation of these processes was evident in the MUT MO dataset (**Figure 3 Manuscript I**).

Comparison of the DEGs between the two conditions and time points, showed the significantly higher amount of DEGs between WT and MUT MOs at D70 of culture, indicating a progressive dysregulated phenotype in the oldest organoids. Moreover, the majority of the DEGs between the two conditions are originating from NBs, mature dopaminergic neurons (mDNs) and young neurons (yNEURs) clusters in both time points. Since mDNs are the main neuronal population that is affected in PD, a closer look into the DEGs of this cluster, exhibited dysregulated pathways related to  $\gamma$ -secretase role and several developmental processes. Previous studies have illustrated the role of mutated LRRK2 in neurodevelopment, with specific impact on the DANs differentiation capacity (Smits et al., 2019; Walter et al., 2021). Similarly, although WT MOs showed a normal developmental phenotype from D35 to D70 of differentiation, with a more variable and mature cellular population in the latest time point, MUT MOs in our study demonstrated an altered developmental pattern, with an accelerated differentiation phenotype at D35 which stagnated until D70 (**Figure 4 and 5 Manuscript I**).

In parallel, in the observed enrichment in the  $\gamma$ -secretase pathway, altered expression of *APP* was evident in both time points of MUT MOs. The implication of this gene in neurodegeneration (K. V. Nguyen, 2019; X. Wang et al., 2017; Xia et al., 2022) and its important role in neurogenesis and brain development (Arnaud et al., 2021; Coronel et al., 2018; B. Wang et al.,

---

2014; Zhou et al., 2011), further signifies the potential role of mutated *LRRK2* in neurodevelopmental defects that could ultimately lead to neurodegeneration.

Apart from the dysregulation of the *APP* expression, another evidence of the *LRRK2* p.Gly2019Ser mutant role in neurodevelopmental impairment is the differences in *DNAJC12*, *GATA3* and *PTN* genes expression between MUT and WT MOs (**Figure 3 and Figure 6 Manuscript I**). The important role of these genes in neurodevelopment has been previously reported, with mutations in *DNAJC12* to be responsible for neurodevelopmental delay and hyperphenylalaninemia (Straniero et al., 2017; Wong et al., 2023), *GATA3* knock-out leading to impaired neurodevelopment in mice (Tsarovina et al., 2010; van Doorninck et al., 1999) and *PTN* to be essential in the development of the nigrostriatal DA system (Marchionini et al., 2007) and the specification of neurons and glia cells during development (Asai et al., 2011; González-Castillo et al., 2015; Skelton et al., 2019). *DNAJC12* and *GATA3* genes showed a progressive decreased expression in EM, while *APP* and *PTN* genes expression is increased throughout EM development. Although this expression pattern was followed by the WT MOs, the opposite expression pattern was found in MUT MOs, with upregulation of *DNAJC12* and *GATA3*, and downregulation of *APP* and *PTN* genes (**Figure 6 Manuscript I**).

The results of this study, demonstrate the physiological robustness of the MO model, which closely resembles the human embryonic midbrain in its development. Additionally, it illustrates the utility and relevance of MOs in PD research, by recapitulating disease relevant phenotypes and highlighting key candidates that may contribute to the neurodevelopmental component of PD.

However, other factors, such as neuroinflammation and aging related dysregulations, that contribute to PD development are not considered in the aforementioned MO model. In neurodegenerative diseases, a characteristic phenotype is the chronic inflammation of the CNS which may be responsible for the development of a neurotoxic environment that further aggravates the disease (W. Zhang, Xiao, et al., 2023). Neuroinflammation is linked to microglia activity, which are the immune cells native to the CNS and account for approximately 10% of the cells in the brain. These so called resident macrophages of the brain have a mesodermal origin being originated from myeloid progenitors of the yolk sac that migrate into the developing neural tube in early stages of the embryonic development (Colonna & Butovsky, 2017). As mentioned, the generation of MOs is achieved through a guided differentiation approach towards the neuroectodermal lineage. A general population of glia cells was identified in MOs, without the presence of microglia (**Manuscript I**). Therefore, the innate development of microglia is infeasible in this model.

---

Microglia are very important for the homeostasis of the brain. They have a role in neurodevelopment, assisting in the neuronal survival with the release of neurotrophic factors and in the refinement of neuronal networks, by the constant surveillance of synapses formation, with the pruning of inactive, unnecessary synapses (Fujita & Yamashita, 2021; Weinhard et al., 2018). Additionally, their phagocytic activity is important for the removal of dead cells, debris, protein aggregates and other danger antigens for the CNS (Fu et al., 2014). Therefore, the presence of these cells in our MO is crucial not only for the ability to study the neuroinflammatory component in PD, but also for the extended improvement of the model's complexity and physiological relevance.

Previous studies have shown that microglia (MGL) can be either innately derived in the iPSCs-derived 3D brain models (Hong et al., 2023; Ormel et al., 2018) or separately integrated into cerebral organoids (Abud et al., 2017; Song, Yuan, et al., 2019). However, there is no study showing the integration of MGL into MOs and their impact on the homeostasis of this particular model. In **Manuscript II** we show the successful integration of MGL into our MO model. For achieving this, we developed a co-culture system where macrophage precursors, capable of differentiating into MGL with phagocytic activity (**Figure 1 Manuscript II**), are added into the MOs, where they differentiate into MGL.

To characterise the presence of MGL in MOs we evaluated the expression of the MGL and macrophage specific marker Ionized calcium-binding adaptor molecule 1 (IBA1) (Hopperton et al., 2018). After 20 days of MO and MGL in the optimised co-culture conditions, 6.4% of microglia cells (IBA1-positive) were quantified in MO-MGL assembloids (**Figure 2 Manuscript II**). Considering that approximately 10% MGL was observed in post-mortem human SNpc tissue (Mittelbronn et al., 2001), the 6.4% of MGL in MOs is a good indication that microglia cells can sustain physiological densities in organoids.

MGL specific identity in MOs was further validated through its distinctive transcriptomic profile in snRNAseq data (**Figure 2 Manuscript II**). Hierarchical clustering and correlation analysis demonstrated the MGL specific genetic signature in MOs (**Figure 2 Manuscript II**), as expected due to the MGL mesodermal origin and MOs neuroectodermal origin.

In parallel, MGL do not only acquire phagocytic activity in 2D microglia but also in MOs. In line with the MGLs' high expression of phagocytic genes in MOs (**Supplementary Figure 4 Manuscript II**), their phagocytic activity is further demonstrated by the significant reduction of MOs size due to the clearing of the dead cells (**Figure 3 Manuscript II**). Moreover, the high expression of cytokine and chemokine genes along with their increased levels in the MO-MGL media further underlines the functionality of MGL in MOs. Cytokines and chemokines are

---

important molecules for cellular communication and they are necessary for triggering the phagocytic ability of MGL (Fu et al., 2014; Noda & Suzumura, 2012). Although cytokines and chemokines are mostly released from microglia and astrocytes, there is evidence that they can also be released by neurons (De Haas et al., 2007; Prieto & Cotman, 2017), which is also shown here by the expression of *IL6*, *IL7* and *CX3CL1* in neuronal clusters (**Figure 3 Manuscript II**). Additionally, the fact that chemokines and cytokines release is exacerbated in the presence of MGL in assembloids compared to MOs, suggests a potential MGL-dependent stimuli in the chemokine and cytokine signalling between neurons and glia cells.

Apart from the fact that MGL integrated in MOs acquire a physiologically relevant identity and functionality, they also contribute to the general homeostasis of the model, by remodelling the synaptic network and leading to higher neuronal excitability (**Figure 4 and Figure 5 Manuscript II**). Additionally, the downregulation of genes related to oxidative and cellular stress, but also inflammatory response, is another indication of the contribution of MGL to the homeostasis and neuroprotection of MOs (**Figure 5 Manuscript II**).

Overall, it is evident that the presence of MGL in MOs is beneficial for the functionality of the model. Increasing the complexity of *in vitro* systems is important for their physiological improvement and for addressing specific research questions, which is not feasible when using more simple cellular models. As illustrated in **Manuscript II**, a diverse cellular communication in the MO model is important for achieving homeostasis and physiological relevance with the human brain. However, neurons and glia cells from one brain region also receive signals from other brain regions that are important for the definition of their functionality (Mišić et al., 2014; Yeh, 2022). Particularly in PD, the vulnerable DANs in the SNpc of the midbrain, form the nigrostriatal pathway through their axonal projections to the dorsal striatum. The inhibitory GABAergic medium spiny neurons (MSNs) in the dorsal striatum control the activity of DANs which are responsible for the release of DA and the control of behavioural and motor responses (Aarts et al., 2011; Sulzer et al., 2016). In the case of PD, severe phenotypes are developed when there is already a substantial loss of DANs and crucial depletion of DA levels in the striatum. Research findings indicate that there is a noteworthy decline in dopaminergic axons within the striatum prior to the occurrence of perikaryal neuronal loss. This decline in dopaminergic axons is approximately twice as much pronounced in the striatum when compared to the reduction in dopaminergic neuronal bodies within the SNpc. (Heng et al., 2023; L. H. Li et al., 2009; Tagliaferro & Burke, 2016). Hence, directing our efforts towards comprehending the underlying mechanisms and processes driving the degeneration of

---

dopaminergic axons in the striatum could be the key to developing early intervention therapies and prevent the ultimate loss of DANs in the SNpc.

To be able to study the human nigrostriatal pathway connectivity, with the use of human derived iPSCs, we developed an *in vitro* assembloid model of midbrain and striatum (StrO) organoids (**Manuscript III**). In contrast to **Manuscript II**, where microglia are derived from the mesodermal lineage, here the two components of the assembloid are both developed from the neuroectoderm. However, for achieving the regional specificity of each organoid we followed a similar approach, where each organoid is differentiated independently before merging them in the optimised co-culture assembloid system. With this approach, we achieved to maintain the identity specificity of MOs and StrOs after 30 days of co-culture, which was checked via the expression of progenitor and mature dopaminergic markers in the MO side of the assembloid, and striatum specific markers in the StrO side (**Figure 1 Manuscript III**). It is also important that our optimised protocol for StrOs generation leads to high abundance of DARPP32 protein, a specific marker for MSNs, the main GABAergic neuronal population in the striatum (Reinius et al., 2015). The identity specificity of both parts of the assembloid model was further confirmed by snRNAseq analysis which showed a cellular composition relevant to the midbrain and striatum brain regions, respectively (**Supplementary Figure 8 and 9 Manuscript III**). These data are consistent with the findings of **Manuscript I**, demonstrating the close identity of MOs to the actual embryonic midbrain.

The cellular composition in the assembloid model demonstrates the preservation of the midbrain and striatum cellular identities (**Figure 2 Manuscript III**). Additionally, we were able to identify more defined dopaminergic subclusters, with an identity close to A9 DANs of the SNpc and A10 DANs of the ventral tegmental area (VTA) of the midbrain. The identification of these two subclusters is determined by the expression of *KCNJ6* and *OTX2*, respectively (**Supplementary Figure 7 Manuscript III**). Although many studies have regarded different markers to be specific for VTA and SNpc DANs, it is important to consider that each of these midbrain regions is divided into subregions with mixed markers expression, found in both SNpc and VTA neurons (Anderegg et al., 2015). Important to note, *OTX2* is one of the few specific markers for the VTA DANs (C. Y. Chung et al., 2010; Di Salvio et al., 2010; Poulin et al., 2014). On the other hand, although *KCNJ6* is still expressed in lower number of DANs in VTA (Anderegg et al., 2015), it is widely acceptable for specifying the A9 DANs (Birtele et al., 2022; Fiorenzano et al., 2021b; Lebedeva et al., 2023). Its expression is also observable in DANs2 cluster in MOs, implying the potential of neuronal refinement from a broader expression profile

---

of dopaminergic markers (DANs clusters) into more specific A9 DANs (**Supplementary Figure 8 Manuscript II**).

In addition to enhancing the specification of the dopaminergic clusters in the assembloid model, we also identified MSNs co-expressing the specific markers *DARPP32* (or *PPP1R1B*) and *ARPP21*. The expression of these two genes specifically defines the mature MSNs in the striatum (Ivkovic & Ehrlich, 1999; Nair et al., 2016). The fact that MSNs in StrOs were identified solely by the expression of *ARPP21*, and that the majority of DANs in MOs have a broader genetic signature, suggests that the interaction between the two organoids in the assembloid model further enhances their identity specification and maturation. In line with our observation of the distinct cellular composition, DEG analysis between the assembloid and MO or StrO models, revealed the upregulation of neuronal maturity genes and genes related to neurogenesis and axonal guidance in the assembloid (**Figure 2 Manuscript III**). This observation agrees with another study on assembloids of thalamic and cortical organoids where an improved neuronal maturity due to higher frequency firing was observed in patch-clamp recordings in the assembloid model compared to the thalamic organoids alone (Xiang et al., 2019).

Similar to the observations in **Manuscript II**, oxidative and cellular stress related genes were downregulated in the assembloid model compared to MO and StrO (**Supplementary Figure 10 Manuscript III**). These results further support the influence of the intercellular and interregional communication system on the homeostasis of the brain, as higher levels of stress can negatively impact the normal CNS function (P. Li & Elowitz, 2019; Qin et al., 2015).

An important aspect of our midbrain-striatum assembloid model is the recapitulation of the nigrostriatal pathway connectivity. As mentioned before, physiologically this pathway is formed by dopaminergic projections from the midbrain to the dorsal striatum, where DA is released. In our model, TH-positive axons are visibly projected from the MO towards the StrO part of the assembloid. Additionally, using the Rabies monosynaptic tracing methodology, we confirmed that TH-positive neurons from MO can form active synapses with neurons in the StrO. Finally, electrochemical measurements in StrOs alone and in the assembloid model, revealed significantly higher catecholamine levels in the StrO side of the assembloid. As previously shown, although these electrochemical measurements cannot directly detect DA, they can provide important information regarding the presence of DA, due to the neglectable interference of the cationic catecholamines norepinephrine and epinephrine (Zanetti et al., 2021). This outcome underscores the model's ability to progress toward the functional establishment of the nigrostriatal pathway (**Figure 3 and Supplementary Figure 11 Manuscript III**). Our results



---

align with other studies on assembloid models, showing the generation of physiologically relevant active neuronal circuits between the two organoids (Bagley et al., 2017; Birey et al., 2017; Miura et al., 2020), underlying the capacity of brain assembloids to resemble the interregional connectivity of the human brain.

Having comprehensively characterized the assembloid model, we are confident that its application in PD studies will provide new insights for the mechanisms involved in synaptic dysregulation and axonal degeneration of dopaminergic terminals within the striatum.

One common characteristic of the models mentioned so far, is their developmental identity. The reprogramming of human cells into iPSCs leads to cellular rejuvenation. The reset of the cellular biological age is mainly due to reorganisation of the epigenome, which converts somatic cells back to a pluripotent state (Simpson et al., 2021). Therefore, the use of iPSCs in the generation of our 3D models is a great way to mimic the embryonic development and differentiation of brain cells and study the developmental aspects of PD (see section 1.1.1.1.2). Although developmental dysregulations are crucial for the onset of neurodegenerative diseases, many of the processes that lead to the disease state are triggered later in life. The exposure into certain environmental stimuli and the epigenetic and genetic alterations accumulating over time, are influencing the onset and severity of the disease (Lardenoije et al., 2015).

Several studies have focused on inducing neuronal aging *in vitro* (see section 1.1.2.2.3), but without any efforts on brain 3D models. Here, we utilised a line engineered with a progerin transgene to trigger aging in our midbrain-striatum assembloid model (**Figure 4 Manuscript III**). In contrast to the transient expression used by Miller and colleagues (Miller et al., 2013), here the progerin transgene is introduced into the cells' genome under the control of the Tet-On system, where its expression is induced only in the presence of doxycycline (Das et al., 2016). This approach provides a more stable system for longer cultures and better optimisation of aging induction. Overexpression of progerin resulted in the generation of a mosaic assembloid model where approximately 50% of the cells overexpress progerin. Progerin-overexpressing cells acquire aging characteristics with the accumulation of p53, p21 and p16 proteins in neuronal cells, which are indicative markers of cellular aging (López-Otín et al., 2023). Additionally, evidence of DNA damage with the double positive H2AX-53BP1 foci (Shibata & Jeggo, 2020) were evident in progerin expressing cells in assembloids at D60 of culture (**Figure 5 Manuscript III**).

The aging phenotype in progerin-overexpressing assembloids was further validated by their distinct transcriptomic profile. Noteworthy dysregulated genes, common between progerin

---

assembloids and human post-mortem brain tissue data, were all linked to aging and neurodegeneration. Moreover, significantly lower levels of Lamin B1 protein (Bedrosian et al., 2021; bin Imtiaz et al., 2021) and higher  $\beta$ -galactosidase (Geng et al., 2010) positive areas in progerin expressing assembloids further support the acquisition of an aged phenotype (**Figure 6 Manuscript III**).

Aging is directly associated with neurodegeneration, and even in the absence of severe disorders such as PD, there is still gradual neuronal network disturbances and neuronal loss during the healthy aging process (Azam et al., 2021). Synaptic deterioration is one of the crucial characteristics of the aging brain that can promote cognitive decline and neurodegeneration (Buss et al., 2021; Talyansky & Brinkman, 2021). In line with this, enrichment analysis of the transcriptomic data from the progerin-overexpressing assembloids, revealed dysregulated pathways related to synapses and neurotransmission. Significantly lower levels of the post-synaptic protein Gephyrin and the pre-synaptic proteins VAMP2 and Synaptotagmin1, further validated the dysregulated synaptic system in progerin-overexpressing assembloids (**Figure 7 Manuscript III**).

DANs are specifically vulnerable to aging-related dysregulations (Bohnen, 2020). In our model, we found significantly lower TH protein levels in progerin-overexpressing assembloids, indicating a dysregulation in the DA synthesis system. Additionally, we saw a higher neurite fragmentation index in DANs of progerin-overexpressing assembloids, a clear sign of neurodegeneration that precedes neuronal death (L. Lin et al., 2016). This result is further supported by the significantly reduced catecholamine levels in the striatum of assembloids overexpressing progerin, signifying a broader dysregulation in the nigrostriatal pathway functionality (**Figure 7 Manuscript III**). Overall, these results support that aging induction in the midbrain-striatum assembloid model via progerin overexpression, promotes the development of early neurodegeneration phenotypes. Therefore, this model could be used for unraveling important insights into the early stages of neurodegeneration in PD.

---

## **Chapter 2: Material and Methods**

All comprehensive information concerning the material and methods that were used in this thesis can be found in the original articles listed in Chapter 3 - Results. The following section lists the experimental procedures I performed in each study.

- Cell culture (hiPSCs, NESCs, vNESCs)
  - See Manuscript II and III
- Generation of MOs
  - See Manuscript II and III
- Generation of StrOs
  - See Manuscript III
- Generation of Midbrain-Striatum Assembloids
  - See Manuscript III
- Co-culture of MOs with macrophage precursors
  - See Manuscript II
- Immunofluorescence staining
  - See Manuscript I and III
- Western blotting and analysis
  - See Manuscript II and III
- Confocal microscopy
  - See Manuscript I and III
- High-Content Imaging and image analysis with MATLAB
  - See Manuscript III
- Multi-electrode array (MEA)
  - See Manuscript III
- LDH and ATP assays
  - See Manuscript III
- RT-PCR
  - See Manuscript I and III
- Flow Cytometry
  - See Manuscript III
- $\beta$ -galactosidase assay

- 
- See Manuscript III
  - Rabies monosynaptic tracing experiment
    - See Manuscript III
  - Single cell/nuclei RNA sequencing analysis
    - See Manuscript I and III

---

# **Chapter 3: Results**

## **Manuscript I**

### **Midbrain organoids mimic early embryonic neurodevelopment and recapitulate LRRK2-p.Gly2019Ser-associated gene expression**

Alise Zagare<sup>1,\*</sup>, **Kyriaki Barmpa**<sup>1,\*</sup>, Semra Smajic<sup>1</sup>, Lisa M. Smits<sup>1</sup>, Kamil Grzyb<sup>1</sup>, Anne Grünewald<sup>1</sup>, Alexander Skupin<sup>1</sup>, Sarah L. Nickels<sup>1,°</sup> and Jens C. Schwamborn<sup>1,°</sup>

<sup>1</sup>Luxembourg Centre for Systems Biomedicine, University of Luxembourg, Esch-sur-Alzette, Luxembourg

\* These authors share first authorship

° Shared corresponding authors: Sarah L. Nickels - sarah.nickel@uni.lu, Jens C. Schwamborn - jens.schwamborn@uni.lu

The article has been published in the American Journal of Human Genetics (AJHG).

---

## **Preface**

LRRK2 p.Gly2019Ser is one of the most common mutations associated with autosomal dominant PD. LRRK2 is a multidomain protein that is involved in the regulation of several biological processes, such as neurogenesis, synaptic function and axonal guidance (Ren et al., 2019). Patients carrying this alteration, develop similar symptoms with the idiopathic PD patients. The fact that LRRK2 has an important role in neurodevelopment and the association of the G2019S mutation with late on set PD, further strengthens the hypothesis of neurodevelopmental defects that contribute to the manifestation of the disease (Schwamborn, 2018).

With the advancement of *in vitro* disease modeling using human iPSCs, we are now able to generate 3D brain organoids that recapitulate the cellular diversity and connectivity of the human brain. Specifically in PD research, MOs have been a great tool for unravelling disease related neurodevelopmental phenotypes (Jarazo et al., 2021; H. Kim et al., 2019; Smits et al., 2019). Additionally, with the use of CRISPR/Cas9, mutated and gene corrected isogenic cell lines can be created from both patient and healthy individuals, to evaluate the effect of the specific mutation to the disease phenotype (Arias-Fuenzalida et al., 2017). Similarly, here we used single cell RNA sequencing data from MOs derived from healthy control iPSCs and their isogenic pair with the LRRK2 p.Gly2019Ser introduced by CRISPR/Cas9.

The complexity and *in vitro* nature of the MOs compel the study of their cellular variability and their physiological similarity to the human counterparts. Using single cell RNA sequencing transcriptomic data, we evaluated the developmental comparison of the healthy (WT) MOs with the embryonic midbrain and cortex. Moreover, based on the cellular diversity in the embryonic midbrain data from La Manno and colleagues (La Manno et al., 2016), we identified specific cell populations in MOs derived from WT and LRRK2 p.Gly2019Ser (MUT) lines, from 35 and 70 days of culture. Interestingly MUT MOs showed a different cellular composition compared to the WT, and they had no clear cell type evolution over time when compared with the embryonic midbrain. Additional comparison of pseudotime trajectories of the WT and MUT MOs, revealed an impaired maturation phenotype of dopaminergic neurons (mDNs) and an arrest in the developmental process of more mature cell types, such as glia, in the MUT MOs. Finally, differential expression analysis between WT and MUT organoids revealed PD related phenotypes in the MUT organoids and candidate genes that could contribute to their neurodevelopmental defects.

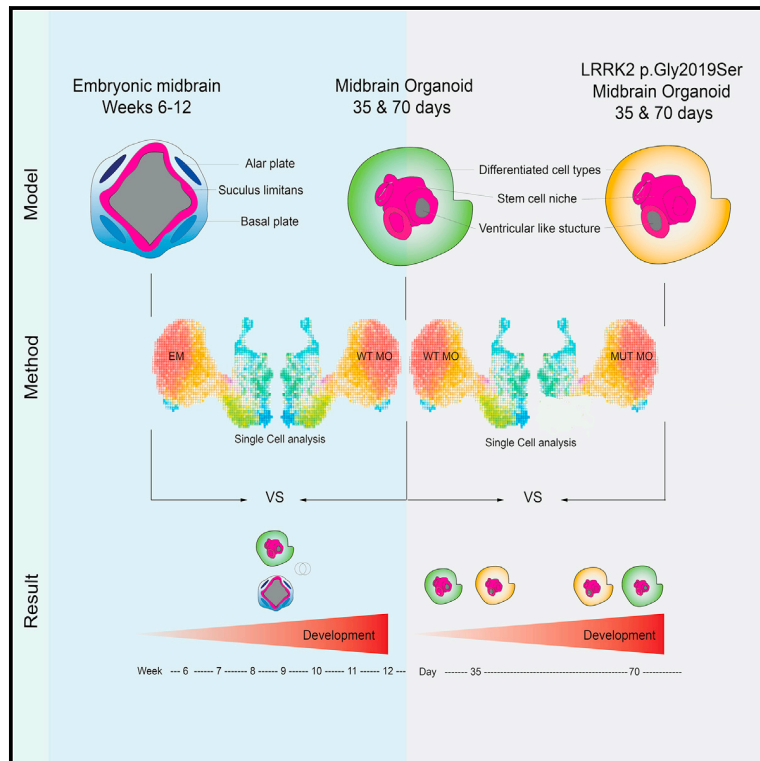
---

## **Contribution statement**

In this study, I share the first authorship with Alise Zagare. We both contributed equally to the development of the scripts, the data analysis, and the writing of the manuscript.

# Midbrain organoids mimic early embryonic neurodevelopment and recapitulate LRRK2-p.Gly2019Ser-associated gene expression

## Graphical Abstract



## Authors

Alise Zagare, Kyriaki Barmpa, Semra Smajic, ..., Alexander Skupin, Sarah L. Nickels, Jens C. Schwamborn

## Correspondence

sarah.nickels@uni.lu (S.L.N.), jens.schwamborn@uni.lu (J.C.S.)





# Midbrain organoids mimic early embryonic neurodevelopment and recapitulate LRRK2-p.Gly2019Ser-associated gene expression

Alise Zagare,<sup>1,2</sup> Kyriaki Barmpa,<sup>1,2</sup> Semra Smajic,<sup>1</sup> Lisa M. Smits,<sup>1</sup> Kamil Grzyb,<sup>1</sup> Anne Grünewald,<sup>1</sup> Alexander Skupin,<sup>1</sup> Sarah L. Nickels,<sup>1,\*</sup> and Jens C. Schwamborn<sup>1,\*</sup>

## Summary

Human brain organoid models that recapitulate the physiology and complexity of the human brain have a great potential for *in vitro* disease modeling, in particular for neurodegenerative diseases, such as Parkinson disease. In the present study, we compare single-cell RNA-sequencing data of human midbrain organoids to the developing human embryonic midbrain. We demonstrate that the *in vitro* model is comparable to its *in vivo* equivalents in terms of developmental path and cellular composition. Moreover, we investigate the potential of midbrain organoids for modeling early developmental changes in Parkinson disease. Therefore, we compare the single-cell RNA-sequencing data of healthy-individual-derived midbrain organoids to their isogenic LRRK2-p.Gly2019Ser-mutant counterparts. We show that the LRRK2 p.Gly2019Ser variant alters neurodevelopment, resulting in an untimely and incomplete differentiation with reduced cellular variability. Finally, we present four candidate genes, *APP*, *DNAJC6*, *GATA3*, and *PTN*, that might contribute to the LRRK2-p.Gly2019Ser-associated transcriptome changes that occur during early neurodevelopment.

## Introduction

Parkinson disease (PD) is a multifactorial neurodegenerative disorder with varying motor and non-motor symptoms, characterized by the loss of dopaminergic neurons (DNs) in the substantia nigra pars compacta (SNpc) of the midbrain.<sup>1</sup> The most common mutation associated with PD is c.6055G>A (p.Gly2019Ser) in leucine-rich repeat kinase 2 (*LRRK2*) (GenBank: NM\_198578.4).<sup>2–4</sup> *LRRK2* is a multidomain protein involved in many cellular functions, including cell proliferation, survival regulation of neural stem cells (NSCs), and neurogenesis.<sup>5,6</sup> Altered neurogenesis and neurodevelopment have been suggested to have major implications in the development of neurodegenerative diseases, including PD.<sup>7</sup> Accordingly, various studies show an accelerated neuronal differentiation in *LRRK2*-mutant human cellular models, with a simultaneous impairment specifically of DN development.<sup>8–10</sup> In particular, the interaction of *LRRK2* with the canonical Wnt/b-catenin signaling pathway has been linked to the development of DNs through the regulation of axonal guidance, dendritic morphogenesis, and synapse formation.<sup>11–14</sup>

Taking into consideration the complexity of the etiology of PD related to age, genetics, and environmental causes and the possibility of a neurodevelopmental component in PD, it is essential to have an adequate model, which can represent the human brain development and the manifestation of the disease. Studies on human postmortem brain tissue provided precious understanding of PD-associated alterations.<sup>15</sup> However, postmortem tissues are

generally available at the end stage of the disease and display a late stage in the disease progression. In order to overcome the limitation of understanding the disease development throughout life, we rely on various experimental models. Our understanding of pathological mechanisms underlying the disease largely depends on models that do not fully portray the complexity of the disease pathology or the cellular composition of the human brain. Genetic and toxin-based animal models often are not able to adequately capture the critical aspects of human PD, resulting in incomplete disease phenotypes.<sup>16</sup> The discovery of induced pluripotent stem cells (iPSCs) and CRISPR-Cas9 technology surpassed this obstacle and enabled the access to human-derived cells for isogenic disease modeling.<sup>17–19</sup> Although such 2D cultures capture the specific effect of mutation-induced PD and its molecular mechanisms, they still lack the cellular diversity of the human brain. To overcome these limitations, the recent developments in self-organizing 3D human-derived midbrain organoids represent a promising advancement in modeling neurodegenerative diseases.<sup>9,20–24</sup>

In order to study the role of human *LRRK2* p.Gly2019Ser in a physiological context of early human development, we used previously published single-cell RNA-sequencing (scRNA-seq) datasets of human embryonic midbrain between developmental week 6 and week 11<sup>25</sup> as well as healthy-individual-derived isogenic wild-type (WT) and *LRRK2* p.Gly2019Ser midbrain organoids of 35 and 70 days of differentiation.<sup>26</sup> We have previously demonstrated that the respective midbrain organoids comprise different neuronal types, including dopaminergic, GABAergic,

<sup>1</sup>University of Luxembourg, Luxembourg Centre for Systems Biomedicine, 6, Avenue du Swing, L-4367 Belvaux, Luxembourg

<sup>2</sup>These authors contributed equally

\*Correspondence: sarah.nickels@uni.lu (S.L.N.), jens.schwamborn@uni.lu (J.C.S.)

<https://doi.org/10.1016/j.ajhg.2021.12.009>

© 2021 The Author(s). This is an open access article under the CC BY license (<http://creativecommons.org/licenses/by/4.0/>).



glutamatergic, and serotonergic neurons as well as glia cells.<sup>26</sup> First, we sought to use the single-cell transcriptomes of healthy midbrain organoids and the human embryonic midbrain to analyze the shared cellular identities and correlation between the *in vitro* and *in vivo* systems. Further, we exploit the transcriptome of the healthy and isogenic (in which LRRK2 p.Gly2019Ser has been inserted) midbrain organoids to investigate the LRRK2-p.Gly2019Ser-dependent changes in gene expression. We report that the midbrain organoids share proportionately similar transcriptomic profile and cell-type diversity with the developing human midbrain. Additionally, our analysis shows that midbrain organoids accurately adopt human midbrain development and are able to capture a LRRK2-p.Gly2019Ser-associated gene expression profile that might underlie LRRK2-mutation-related phenotypes.

## Material and methods

### Midbrain organoid generation from midbrain floorplate neural progenitor cells

Neural progenitor cells (NPCs) were derived from iPSCs of a healthy individual and isogenic LRRK2-p.Gly2019Ser-inserted cell line. Gene-editing of the iPSCs was done with CRISPR-Cas9 and piggyBac systems, and it has been described in Qing et al., 2017.<sup>27</sup> The derivation of NPCs from iPSCs and further organoid generation have been described in detail previously<sup>9,26</sup> (Table S1). In brief, NPCs were cultured in N2B27 base medium supplemented with 2.5  $\mu$ M SB-431542 (SB, Ascent Scientific), 100 nM LDN-193189 (LDN, Sigma), 3  $\mu$ M CHIR99021 (CHIR, Axon Medchem), 200  $\mu$ M ascorbic acid (AA, Sigma), and 0.5  $\mu$ M SAG (Merck). For the derivation of midbrain, 3,000 NPCs were seeded per well in an ultra-low-attachment 96-well plate. For 7 days, cells were kept under maintenance conditions, following 3 days of pre-patterning where LDN and SB were withdrawn, and CHIR concentration was reduced to 0.7  $\mu$ M. On day 9 of organoid culture, the differentiation was induced by changing the medium to N2B27 with 10 ng/mL brain-derived neurotrophic factor (BDNF, Peprotech), 10 ng/mL glial-cell-derived neurotrophic factor (GDNF, Peprotech), 200  $\mu$ M AA, 500  $\mu$ M dibutyl cAMP (Sigma), 1 ng/mL TGF- $\beta$ 3 (Peprotech), 10  $\mu$ M dual antiplatelet therapy (DAPT) (Cayman), and 2.5 ng/mL ActivinA (Peprotech). The organoids were cultured under static conditions with media changes every third day for 35 or 70 days. 30 midbrain organoids of each condition (WT35, WT70, MUT35, and MUT70) were pulled for Drop-seq analysis as described in Smits et al., 2020.<sup>26</sup>

### Immunofluorescence staining

Midbrain organoids were fixed with 4% paraformaldehyde (PFA) overnight at 4°C followed by three washes with PBS for 15 min. The washed organoids were embedded in 3%–4% low-melting point agarose in PBS. Embedded organoids were sectioned into 50  $\mu$ m sections with vibratome (Leica VT1000s). Organoid sections were blocked with 0.5% Triton X-100, 0.1% sodium azide, 0.1% sodium citrate, 2% BSA, and 5% normal donkey serum in PBS for 90 min at room temperature (RT) on a shaker. We diluted the primary antibodies in the same solution but with 0.1% Triton X-100 instead. The sections were incubated with the primary antibodies for 48 h at 4°C. Next, they were washed three times with

PBS and subsequently blocked for 30 min at RT on a shaker. Next, sections were incubated with the secondary antibodies diluted in 0.05% Tween-20 in PBS for 2 h at RT and subsequently washed twice with 0.05% Tween-20 in PBS and once with Milli-Q water before mounting them in Fluoromount-G mounting medium (Southern Biotech). The primary antibodies used were TH rabbit Abcam ab112, FOXA2 mouse Santa Cruz sc-101060, and EN1 goat Santa Cruz sc-46101. The secondary antibodies used were Hoechst 33342 solution (20 mM) Invitrogen 62249, anti-rabbit secondary 488 Thermo Fisher a21206, anti-mouse secondary 568 Invitrogen A10037, and anti-goat secondary 647 Invitrogen A21447.

### Data pre-processing

In this study, we used already published scRNA-seq datasets. The midbrain organoids dataset was published from our lab,<sup>26</sup> while the other three datasets (embryonic midbrain, embryonic prefrontal cortex, and cortical organoids) are external<sup>25,28,29</sup> (Figure S1). scRNA-seq data from 30 pooled midbrain organoids per cell line and time point were generated following the Drop-seq pipeline.<sup>30</sup> Reads were mapped to human reference genome hg38 (GRCh38.87). From midbrain organoids datasets, cells having unique feature counts over 2,500 were removed as probable doublets or multiplets. Similarly, low-quality cells or empty droplets were further filtered out with unique feature counts below 100 (for day 35 data) and 200 (for day 70 data) and mitochondrial transcripts above 30% (Figure S2). Embryonic midbrain scRNA-seq data did not include any mitochondrial (MT) genes, thus to make midbrain organoid data more comparable to the embryonic midbrain data, we removed all MT genes from midbrain organoid datasets after quality control (QC). After QC, WT35 midbrain organoids included 2,864 cells, WT70 included 2,005 cells, MUT35 included 2,946 cells, and MUT70 included 2,660 cells.

The external datasets of embryonic midbrain, prefrontal cortex, and cortex organoid did not show any outliers in terms of doublets or empty droplets. Therefore, no additional QC was applied to these datasets.

Embryonic midbrain data of developmental week 6 to 11 included in total 1,977 cells, embryonic prefrontal cortex data at developmental stages between gestational weeks 8 and 26 included 2,309 cells, and cortex organoid data from 1 month old organoid comprised 4,832 cells.

### Data integration and normalization

To better transmit the biological information between *in vivo* and *in vitro* ventral midbrain datasets, midbrain organoid data (WT35, WT70, MUT35, and MUT70) and embryonic midbrain data were integrated with the Seurat integration analysis workflow.<sup>31</sup> Integration was performed on the basis of the top 20 dimensions. RNA assay data of integrated object were log normalized and scaled to 10,000 transcripts per cell.

### Cell type identification

After the integration of embryonic midbrain and midbrain organoid datasets, integrated object was scaled and principal-component analysis (PCA) was applied. Cell clustering was performed on the basis of the top 20 principal components via Louvain algorithm modularity optimization with a resolution of 0.5. Uniform manifold approximation and projection (UMAP) was used for cell cluster visualization.<sup>32</sup> Nine distinct cell clusters were identified in the UMAP plot. Clusters 0 and 7 were present only in

midbrain organoids and located in a close proximity to each other in the UMAP plot, indicating their high similarity and *in vitro* specificity. Because of this overclustering both clusters were pulled, resulting in eight distinct cellular identities labeled 1–8. For cell type identification, a binarized gene list across cell types from La Manno et al., 2016<sup>25</sup> was used. This list of genes comprises information about the marker genes in a binarized manner, where 1 means that gene is marking a specific cell population and 0 means that it cannot be considered as a marker gene. For more details on how this list is generated, please refer to La Manno et al., 2016.<sup>25</sup> Expression of each cluster-defining gene was overlapped with the marker gene (1) in the marker matrix from La Manno et al., 2016.<sup>25</sup> The total number of marker genes of a particular cell type of La Manno et al., 2016<sup>25</sup> that was present in each cluster of embryonic-midbrain- and midbrain-organoid-integrated dataset is visualized in Figure S4A. Cellular subtypes described by La Manno et al., 2016<sup>25</sup> were grouped in five major neuronal identity clusters—neurons subdivided in dopaminergic neurons (DNs) and non-dopaminergic neurons (non-DNs), then neuroblasts (NBs), progenitors (PROGs), and radial glia cells (RGLs). In addition, we identified non-neuronal identity cell populations—pericytes and endothelial cells. Cell types were assigned on the basis of the highest number of major cluster marker genes being expressed in the respective clusters of integrated embryonic midbrain and midbrain organoid dataset.

### Differential gene expression analysis

Differentially expressed genes (DEGs) were detected with the FindMarkers function of the Seurat pipeline with the default thresholds. In all comparisons, we used the MUT midbrain organoids as ident.1 and the WT midbrain organoids as ident.2.

### Pathway analysis

Pathway enrichment analysis was performed with MetaCore version 21.1 build 70400 on the basis of DEGs detected with the FindMarkers function from Seurat. DEGs were filtered for fold change (FC) > 0.25 and *p* adj. value < 0.05. From the analysis, we obtained the most significant enriched pathways, GO processes, network processes, and related diseases lists. The most significantly enriched pathways were illustrated in GraphPad Prism 9.

### Cytoscape

Cell-cluster-specific genes were identified with the FindAllMarkers function from Seurat. The top 100 marker genes of each cell cluster were visualized in the network created with the Cytoscape software version 3.8.0.

### Pseudotime analysis

Pseudotime analysis was performed with the Monocle package version 3. Merged Seurat object was uploaded in the Monocle workflow. Cell clustering was performed on the basis of 150 principal components with default settings. UMAP was used for visualization. Because Monocle does not allow a full metadata integration from Seurat object, we assigned cell identities manually to correspond to the ones previously defined. For the comparison between developmental stages of embryonic midbrain and midbrain organoid, we used the align\_cds function to remove the batch effect between *in vivo* and *in vitro* midbrain systems. As a starting point for cell ordering along the pseudotime trajectory, the NB *in vitro* cluster of WT35 was chosen. For the compar-

ison between developmental stages of WT midbrain organoids and MUT midbrain organoids, the same starting point of the NB *in vitro* cluster of WT35 was chosen. Genes that vary the most over the pseudotime were computed with the fit\_models function. Midbrain-organoid- and embryonic-midbrain-integrated Seurat object was subset by pseudotime genes for the visualization of their expression in midbrain organoids.

### Statistical analysis

If not stated otherwise, statistical analysis of scRNA-seq data was performed with RStudio R version 3.6.2 with the ggplot2 package. For all comparison, non-parametric Kruskal-Wallis test was performed. Statistical significance between comparisons are represented with asterisks: *p* < 0.05\*, *p* < 0.01\*\*, *p* < 0.001\*\*\*, *p* < 0.00001\*\*\*\*.

### *In vitro* and *in vivo* midbrain data comparison to the cortex

WT midbrain organoids and embryonic midbrain were merged with embryonic prefrontal cortex and integrated on the basis of the top 20 dimensions. SCTransform normalization was applied to reduce the technical variation in the data and stabilize gene abundance levels, which can be highly variable between *in vitro* and *in vivo* tissues, especially between different tissue types—midbrain and cortex.<sup>33</sup> We determined mutual genes between midbrain organoids, embryonic midbrain, and embryonic prefrontal cortex by intersecting row names of respective datasets. Integrated object was subset by mutual genes. The top 2,000 variable genes in this subset of complete integrated dataset were detected with the FindVariableFeature function.

For the comparison of embryonic midbrain to cortical organoid, datasets were merged, SCTransformed, and subset by the mutual genes for the correlation analysis.

### Ethical approval

The responsible national ethical commission has approved the study under the CNER report no. 201901/01. Written informed consent was obtained from all individuals who donated samples to this study (Smits et al., 2020).<sup>26</sup> The cell lines used in this study are summarized in Table S1.

## Results

### Midbrain organoids show a gene expression signature comparable to the human embryonic midbrain

To assess the similarity between the *in vitro* and *in vivo* midbrain systems, we compared scRNA-seq data of midbrain organoids cultured for 35 days (WT35) and 70 days (WT70)<sup>26</sup> to the human embryonic midbrain of developmental weeks 6–11.<sup>25</sup> In addition, to investigate possible transcriptome similarities between midbrain organoids and other brain regions during early development, we compared the scRNA-seq data of midbrain organoids to scRNA-seq data of the human embryonic prefrontal cortex.<sup>28</sup>

The transcriptome datasets of midbrain organoids, embryonic midbrain, and embryonic prefrontal cortex were embedded into a single Seurat object (Figure S3A). The average expression of the top 500 variable mutual genes

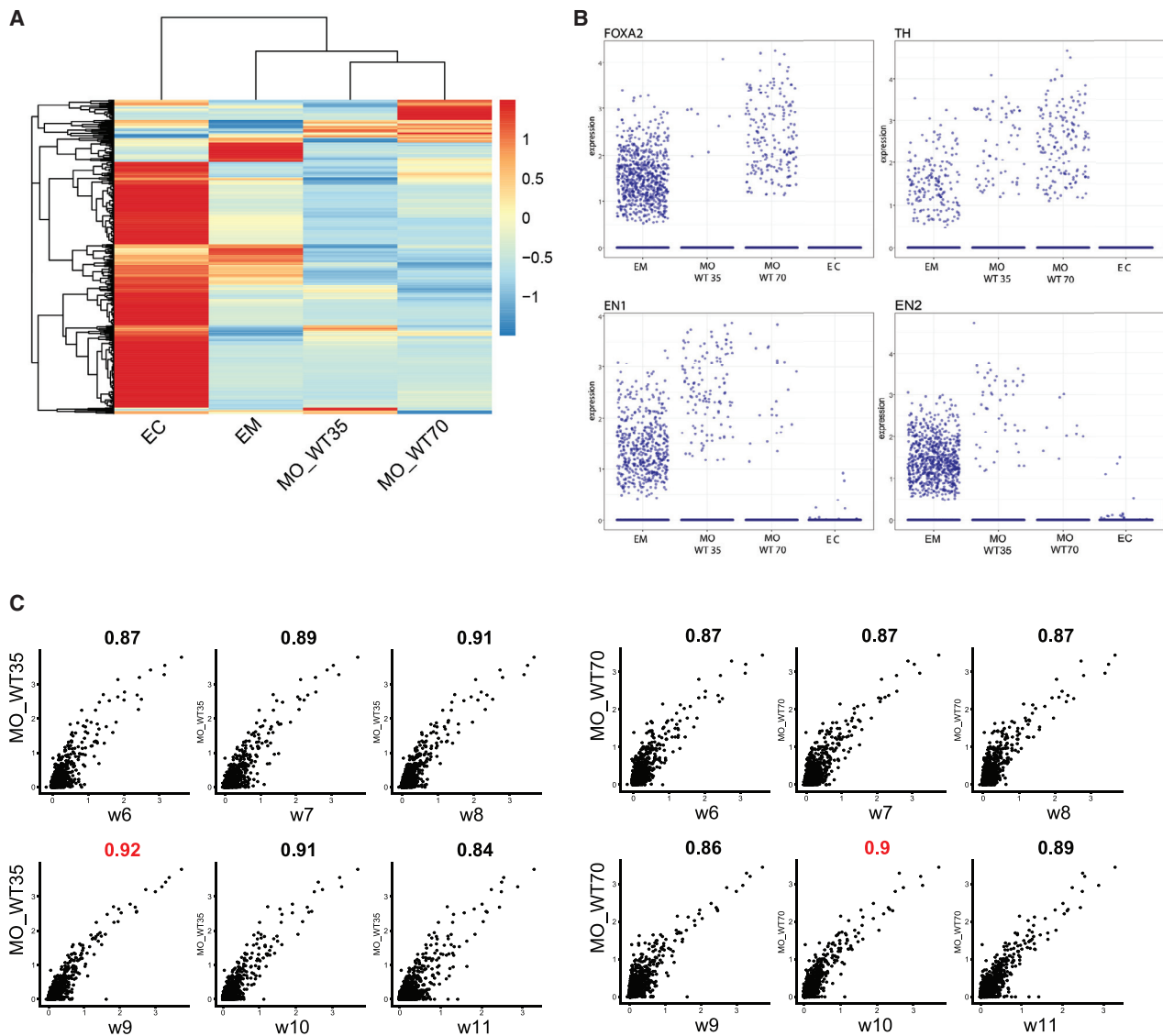


**Figure 1. Midbrain organoids show a genetic signature comparable to the embryonic midbrain**

(A) The top 1,000 most variable genes of Seurat integrated object of merged scRNA-seq datasets of embryonic cortex (EC), embryonic midbrain (EM), midbrain organoids 35 days of differentiation (MO\_WT35), and midbrain organoids 70 days of differentiation (MO\_WT70). The average gene expression visualized after Z score normalization.

(B) Expression of midbrain markers *FOXA2*, *TH*, *EN1*, and *EN2* in Seurat integrated object of merged scRNA-seq datasets of embryonic cortex (EC), embryonic midbrain (EM), midbrain organoids 35 days of differentiation (MO\_WT35), and midbrain organoids 70 days of differentiation (MO\_WT70). Each dot represents a single cell.

(C) The average common gene expression correlation between midbrain organoids 35 days of differentiation (MO\_WT35) and midbrain organoids 70 days of differentiation (MO\_WT70) and embryonic midbrain (EM) developmental weeks (w6–w11). The Pearson correlation coefficient is displayed above each comparison. The highest correlation between midbrain organoids and embryonic developmental time point is highlighted in red. Each dot represents a single cell.

showed a clear separation of the embryonic prefrontal cortex from midbrain organoids and the embryonic midbrain (Figure 1A). This separation indicates the expected greater similarity between midbrain organoids and the embryonic midbrain than the embryonic prefrontal cortex. The following correlation analysis of the average expression of all common genes confirmed that the transcriptome of midbrain organoids is more similar to the embryonic midbrain ( $\rho > 0.7$ ) than to the embryonic prefrontal cortex ( $\rho < 0.7$ ) (Figure S3B). Moreover, the embryonic midbrain

and midbrain organoids express typical midbrain markers, such as *TH*, *FOXA2*, *EN1*, and *EN2*, which were absent or expressed at low levels in the embryonic prefrontal cortex (Figure 1B). The expression of *TH*, *FOXA2*, and *EN1* in midbrain organoids was also validated by immunofluorescence staining (Figure S3C). In addition, we aimed to associate midbrain organoids to different time points in embryonic midbrain development by comparing the expression of the common genes between both datasets. The WT35 midbrain organoids highly correlated with embryonic

week 9 ( $R = 0.92$ ), while the midbrain organoids WT70 highly correlated with the week 10 ( $R = 0.90$ ) (Figure 1C). These findings not only suggest that *in-vitro*-derived midbrain organoids show high gene expression similarities with the human embryonic midbrain but also manifest a developmental pattern comparable to their *in vivo* counterpart. In order to further validate the brain regional specificity of the organoids, we compared the scRNA-seq data of the embryonic midbrain to a cortex organoid<sup>29</sup> in the same manner (Figure S3D). The Pearson correlation coefficient of 0.05 showed insignificant correlation between the embryonic midbrain and the cortex organoid, providing evidence that organoids derived from different brain regions exhibit no close transcriptome similarities with the developing embryonic midbrain *in vivo*.

### Midbrain organoids inherit physiological-relevant cellular populations that are shared with the developing embryonic midbrain

After confirming that midbrain organoids present a gene expression signature comparable to embryonic midbrain *in vivo*, we used the integration workflow from Seurat<sup>31</sup> to identify shared cellular populations across the *in vivo* and *in vitro* midbrain systems. We integrated the scRNA-seq data of the embryonic midbrain with healthy control and LRRK2-p.Gly2019Ser-mutant midbrain organoids of both differentiation time points 35 and 70 days (WT35, WT70, MUT35, and MUT70, respectively). We identified eight different cell types and visualized them by using UMAP (Figure 2A). To define cellular identities, we used the cell type marker gene list proposed by La Manno and colleagues<sup>25</sup> and compared it to the marker gene list per cluster of the integrated object (Figure S4). We verified each marker expression in every cell cluster identified in the integrated Seurat object. The number of marker genes that were present in the cell populations (corresponding to the cell types defined in La Manno et al., 2016<sup>25</sup>) are shown in Figure S5A. La Manno and colleagues<sup>25</sup> reported the presence of 25 cellular identities in the embryonic midbrain, including several sub-clusters of radial glia, progenitors, and dopaminergic neurons. To simplify cell identification, we grouped all 25 cell identities in more generic cell type clusters, such as neurons (NEURs), neuroblasts (NBs), progenitors, glia, pericytes, and endothelial cells. Neurons were further separated in non-dopaminergic neurons (non-DNs) and dopaminergic neurons (DNs). Cell identities were assigned to cell populations within the integrated Seurat object on the basis of the highest number of marker genes defining each generic cell type (Figure S5A). Once these clusters were broadly defined, using the embryonic midbrain data,<sup>25</sup> we verified and refined the assigned cell identities on the basis of additional cell type and maturity-specific marker expression (Figure 2B, Figure S5B). We confirmed the particularly high expression of neuronal maturity markers<sup>34</sup> and dopaminergic markers<sup>9</sup> in DNs. Therefore, we defined DNs as mature DNs (mDNs). The neuronal cluster presenting lower

expression of maturity and neuronal-type-specific marker expression, we defined as young neurons (yNEURs) (Figure S5B). The vast majority of cells in the yNEUR cluster showed a stable expression of young neuronal markers such as *NCAM1*, *STMN1*, and *DCX* (Figure 2B). The mature neuronal marker *MAP2* as well as synaptic genes such as *SYP* and *SYT1* were expressed in the mDN and non-DN clusters. Lastly, expression of the DN markers *TH*, *KCNJ6*, and *NR4A2* as well as of the DN-specific synaptic markers *ROBO1* and *DCC* were confirmed in yNEURs and mDNs. Importantly, midbrain identity markers *FOXA2* and *LMX1A* were expressed in most of the cell types (glia, progenitors, yNEURs, and mDNs). The radial glia marker *SLC1A3* and neural progenitor markers *SOX2* and *MSI1* showed high expression in the glia and progenitor clusters, suggesting that glia cells are rather immature at this stage of embryonic midbrain development and, thus, display a genetic signature of early development in midbrain organoids. However, also more specific glial markers such as *GFAP* and *S100B* were already detectable in some of the cells. Endothelial cell identity was confirmed by the positive expression of the *CDH5*, while pericyte cells showed robust expression of the blood vessel development regulator *CSPG4*. Cells belonging to the NB cluster were positive for neural stem cell marker (*SOX2*) as well as immature (*DCX*) and mature neural (*SYT1*) and DN markers (*TH* and *KCNJ6*). However, none of these markers showed a constantly high expression among all cells in the NB cluster. This suggests that the identity of NBs is rather yet undefined and might be a specific feature of *in vitro* cultures, with the potential to develop into more mature neural cell types over time.

Further, we visualized UMAP embeddings of cell types and split them by datasets to reveal common and distinct cell types across embryonic midbrain and midbrain organoids (Figure 2C). Clusters of progenitors, yNEURs, mDNs, non-DNs, and glia were present in the embryonic midbrain as well as midbrain organoids, demonstrating that most cell types are common between the *in vitro* and *in vivo* midbrain systems. We observed that the NB cluster was present mainly in midbrain organoids and not in the embryonic midbrain and therefore was called NBs *in vitro*. Pericytes were found in midbrain organoids and the embryonic midbrain, however more mature endothelial cells were only present in the embryonic midbrain.

Next, we investigated the most variable gene expression pattern between the defined cell types (Figure 2D). The top 100 most variable genes led to a clustering of yNEURs, mDNs, non-DNs, and NBs together, confirming the common neuronal expression profile of these cell types. Pericytes and endothelial cells showed rather distinct genetic signature, consistent with the fact that these cells have non-neuronal identity. Glia and progenitors formed another separate cluster with a similar transcriptomic profile, implying again an early developmental stage of the glial cells.

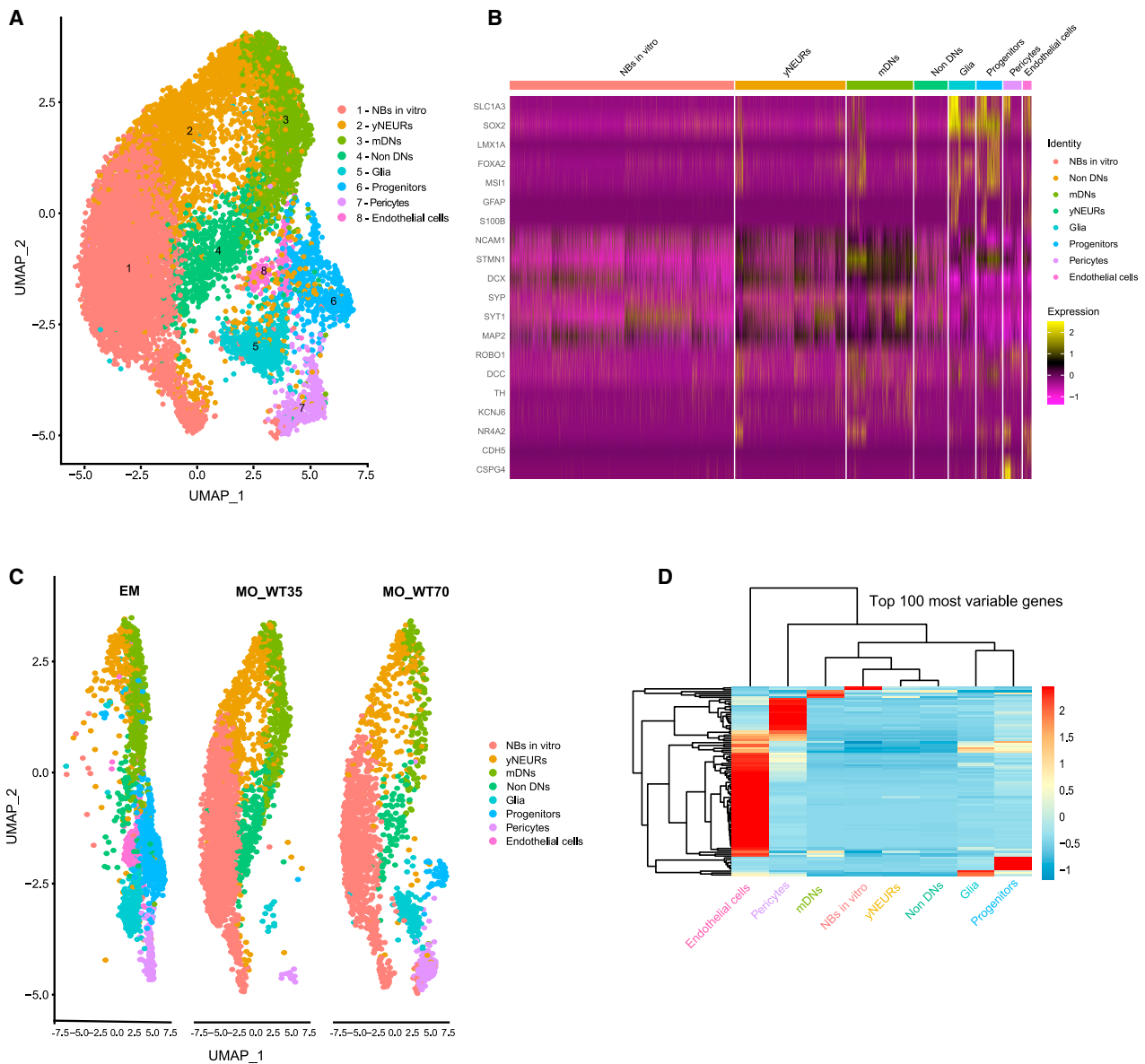


**Figure 2. Midbrain organoids inherit physiological-relevant cellular populations that are shared with the developing embryonic midbrain**

(A) UMAP of integrated Seurat object of merged scRNA-seq datasets of embryonic midbrain, and WT and MUT midbrain organoids 35 and 70 days of differentiation, showing cell clusters 1–8, after manual correction of oversampling. Each dot represents a single cell and is colored according to the cell identity.

(B) Identity heatmap showing cell-type-specific marker expression in identified cell clusters.

(C) UMAP of cell clusters in embryonic midbrain (EM), WT midbrain organoids of 35 days of differentiation (MO\_WT35), and 70 days of differentiation (MO\_WT70). Each dot represents a single cell and is colored according to the cell identity.

(D) Unsupervised hierarchical clustering of cell types, using the average expression of the top 100 most variable genes, visualized after Z score normalization.

### Differential gene expression analysis reveals a *LRRK2*-related PD phenotype in the mutant midbrain organoids

Further, we assessed the potential of midbrain organoids in disease modeling by comparing the transcriptomic signature of the midbrain organoids derived from the healthy control where the *LRRK2* p.Gly2019Ser variant was inserted with the isogenic WT counterpart.<sup>27</sup> As with the WT midbrain scRNA-seq data, we analyzed MUT midbrain organoid scRNA-seq data from organoids sampled at day 35 and

day 70 of differentiation. We verified *LRRK2* expression in midbrain organoids and observed that it is expressed in a larger proportion of cells at later time points in both WT and MUT midbrain organoids (Figure S6A). In order to identify the key differences in the transcriptomic signature between MUT midbrain organoids and WT midbrain organoids, we computed the DEGs across both time points and all cell types with subsequent pathway enrichment analysis. The combined enrichment analysis of DEGs of both time

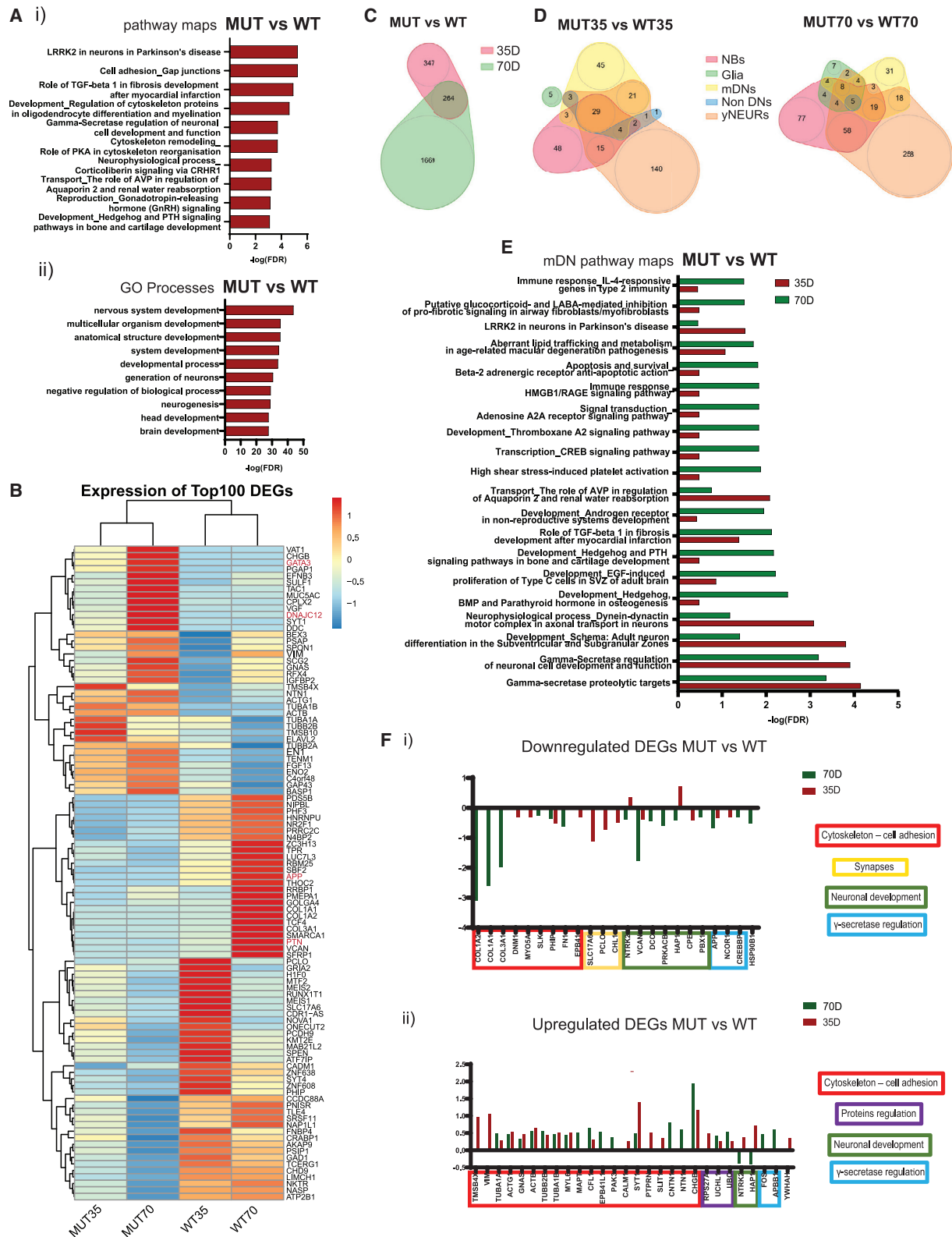


**Figure 3. LRRK2-p.Gly2019Ser-mutant midbrain organoids recapitulate PD-associated pathways**

(A) Pathway maps (i) and GO processes (ii) of the enrichment analysis of 294 DEG (p adj. value < 0.05) between MUT and WT midbrain organoids.

(B) Heatmap of to 100 DEG (p adj. value < 0.05) between MUT and WT midbrain organoids. Genes highlighted in red are the potential LRRK2 p.Gly2019Ser target genes involved in the neurodevelopment (see also Figure 6)

(legend continued on next page)

points showed the most significant enrichment in the pathway of LRRK2 role in neurons in PD (Figure 3Ai). Moreover, other pathways associated with *LRRK2*, such as cytoskeleton regulation and cell adhesion, were also enriched in the MUT midbrain organoids. In addition, we found a significant DEG enrichment in protein kinase cAMP-dependent signaling and the  $\gamma$ -secretase regulation pathway. We identified that the most significant Gene Ontology (GO) and network processes were related to the neuronal development and axonal guidance (Figure 3Aii, Figure S6Bi). Furthermore, the most enriched diseases were linked to the brain and nervous system, confirming a diseased state of MUT midbrain organoids (Figure S6Bii). Last, the top 100 DEGs (adj. p value < 0.05) clustered MUT midbrain organoids separately from the WT midbrain organoids for both time points, confirming that LRRK2 p.Gly2019Ser induced changes in gene expression (Figure 3B). Interestingly, in the WT midbrain organoids, the expression levels of the DEGs differ between the two time points of differentiation, while in the MUT35 and MUT70 midbrain organoids, DEGs showed very similar expression patterns, indicating a potential developmental impairment of MUT organoids. Similarly, the top 100 DEGs separated the majority of different cell types of the MUT midbrain organoids from the WT midbrain organoids for both time points (Figure S5C), indicating that the presence of the *LRRK2* variant is responsible for gene expression changes in all cell types in at least one of the time points. However, the pathway enrichment analysis combined for all cell types showed a higher significance in the enrichment of cytoskeleton remodeling,  $\gamma$ -secretase regulation, and LRRK2-related pathways for day 70, suggesting a stronger manifestation of the LRRK2-p.Gly2019Ser-associated changes overtime (Figure S6D). In support of that, we identified in total 347 DEGs (adj. p value < 0.05) at day 35 and 1,669 DEGs (adj. p value < 0.05) at day 70 between the MUT and WT midbrain organoids. 264 DEGs were common between both time points (Figure 3C). Next, we overlapped all DEGs (adj. p value < 0.05) between cell types and saw that the highest number of DEGs at both time points were present in NBs *in vitro*, yNEURs, and mDNs (Figure 3D, Figure S7A). Pathway enrichment analysis identified that the cytoskeleton-regulation-related pathways were significant in the MUT35 and MUT70 midbrain organoids in all three respective cell types, while LRRK2-PD-related pathway occurred to be highly significant in NBs *in vitro*. (Figure 3E, Figure S7Bi). In mDNs and yNEURs, the  $\gamma$ -secretase and neurodevelopmental regulation pathways were identified as the most enriched for both time points (Figure 3E, Figure S6Bii), additionally indicating a

possible link between LRRK2 p.Gly2019Ser and  $\gamma$ -secretase function.

In order to investigate the gene expression profiles between the MUT and WT midbrain organoids in more detail, we visualized the fold changes of the genes involved in the most significantly enriched pathways (Figures 3Fi and 3Fii). Genes related to cytoskeleton dysregulations, such as *COL1A2*, *COL1A1*, *COL3A1*, *DNM1*, *MYO5A*, *PHIP*, *SLK*, *FN1*, and *EPB41*, were found to be downregulated with a log<sub>2</sub>FC between -0.26 and -3, while others, such as *TMSB4X*, *VIM*, *TUBA1A*, *ACTG1*, *GNAS*, *TUBB2B*, *TUBA1B*, *MYL6*, *MAPT*, *CFL1*, *EPB41L1*, *PAK3*, *CALM1*, *SYT1*, *PTPRN*, *SLIT1*, *CNTN1*, *NTN1*, and *CHGB*, were found upregulated (log<sub>2</sub>FC between 0.26 and 1.93) in MUT midbrain organoids at the majority of both time points. Synapses-related genes, such as *SLC17A6*, *PCLO*, and *CHL1*, were particularly downregulated (log<sub>2</sub>FC between -0.5 and -1.12) in MUT35 midbrain organoids, but they were not differentially expressed in MUT70 midbrain organoids. Genes that are associated with neuronal development, such as *NTRK2*, *VCAN*, *DCC*, *PRKACB*, *HAP1*, *CPE*, and *PBX1*, were also dysregulated in MUT midbrain organoids. The majority of them were downregulated (log<sub>2</sub>FC between -0.38 and -1.77) in MUT70 midbrain organoids, while *NTRK2* and *HAP1* were upregulated (log<sub>2</sub>FC 0.36 and 0.72, respectively) in MUT35 midbrain organoids. Protein regulation-associated genes, such as *RPS27A*, *UCHL1*, and *UBC*, were upregulated (log<sub>2</sub>FC between 0.25 and 0.52) at both time points. Additionally, genes that are related to the  $\gamma$ -secretase regulation pathway, such as *APP*, *NCOR1*, and *CREBBP*, were downregulated (log<sub>2</sub>FC between -0.31 and -0.68) in MUT35 and MUT70 midbrain organoids, but *FOS* and *APBB1* were upregulated (log<sub>2</sub>FC 0.47 and 0.59, respectively), particularly in MUT70 midbrain organoids. We also observed a dysregulation of *HSP90B1*, which was downregulated (log<sub>2</sub>FC -0.51) at MUT70 midbrain organoids and *YWHAH* showing upregulation (log<sub>2</sub>FC 0.36) in MUT35 midbrain organoids. These genes encode HSP90B1 and 14-3-3 family proteins, respectively, known as direct interacting partners with LRRK2.

### Mutant midbrain organoids have a distinct cellular composition and correlate differently with the stages of embryonic development

We observed that MUT midbrain organoids differ from WT midbrain organoids in their cellular composition. In the UMAP embedding plot split by models and colored by cell types (Figure S8A), we saw that progenitors and pericytes, which are shared cellular populations between WT midbrain organoids and embryonic midbrain, are not present in MUT

(C) Venn diagram, showing the number of DEGs between MUT and WT midbrain organoids found at 35 days and 70 days of differentiation (p adj. value < 0.05).

(D) Venn diagrams, showing the number of DEGs found in each cell type between MUT and WT midbrain organoids fat 35 days and 70 days (p adj. value < 0.05).

(E) Mature DN pathway processes enrichment based on the DEGs identified in mDNs between MUT and WT midbrain organoids (p adj. value < 0.05).

(F) Fold changes of genes selected from the top enriched pathways dysregulated in mDNs.



midbrain organoids at any time point. On the contrary, we observed that the glia population is more enriched in MUT35 than in WT35 midbrain organoids. To confirm our observations, we subset the integrated Seurat object by the respective cell clusters and plotted them separately in the embryonic midbrain and in the WT as well as in the MUT midbrain organoids for both time points (Figure 4A). We saw that pericytes positive for the endothelial lineage marker *MCAM* and for the major regulator of angiogenic events, *SPARC*, are highly represented in WT70 midbrain organoids and in the embryonic midbrain but not in MUT midbrain organoids. Similarly, progenitors positive for the G2-proliferation-associated *CENPF* marker were only detected in the embryonic midbrain and WT70 midbrain organoids. A higher number of glia cells expressing *VIM* were already detected in MUT35 midbrain organoids compared to WT35 midbrain organoids. However, an increase of glia over time is more evident in WT than in MUT midbrain organoids.

Next, we calculated the proportion of each cell type present in WT and MUT midbrain organoids at both time points (Figure 4B). We saw a reduction of NBs *in vitro* (62%→51%) and yNEURs (17%→12%) from WT35 to the WT70. This reduction of less mature cells in WT35 midbrain organoids resulted in an increased variety of cell types present in WT70 midbrain organoids. Moreover, the cellular profile of WT70 midbrain organoids was quite similar to the cellular diversity observed in embryonic midbrain (Figure S8B). The major difference here was a high percentage of progenitors in the embryonic midbrain that seemed to be replaced by the presence of NBs *in vitro* in WT70 midbrain organoids.

Contrary to the WT midbrain organoids, in the MUT midbrain organoids, there was no evident difference in cell-type evolution over time. The same cell types were present in the MUT35 and MUT70 midbrain organoids, besides the fact that NBs *in vitro* almost doubled over time. Furthermore, the average gene expression correlation between MUT midbrain organoids and embryonic midbrain developmental time points showed that MUT35 midbrain organoids correlated better with embryonic development for all time points, compared to WT35 midbrain organoids (Figure 1C, Figure 4C). On the other hand, MUT70 midbrain organoids had a weaker correlation with the embryonic midbrain than the WT70 midbrain organoids, especially for week 11, which is also the latest and therefore most mature time point ( $R_{WT} = 0.89$  versus  $R_{MUT} = 0.83$ ). All together, these findings suggest that MUT midbrain organoids have a different developmental path compared to WT midbrain organoids and embryonic midbrain.

To further investigate the developmental differences between the MUT and WT midbrain organoids, we computed pseudotime trajectories to explore pseudotemporal ordering of midbrain organoid cell populations compared to the embryonic midbrain developmental time points. As the root, we chose WT35 NBs *in vitro* and we visualized the trajectories in UMAP plots colored by cell types and developmental time points of midbrain organoids and embryonic midbrain (Figures 4Di and 4Dii). We observed that

mDNs of WT35 midbrain organoids are placed closer to embryonic developmental week 9 (branch point 2 and red circle 1 in Figure 4Dii), while mDNs of WT70 midbrain organoids were closer to embryonic developmental week 10 (branch point 2 and red circle 2 in Figure 4Dii), which is consistent with the gene average expression correlation analysis between WT midbrain organoids and embryonic midbrain. In clear contrast to this, we observed that mDNs of MUT35 and MUT70 midbrain organoids are placed closely to each other and formed a separate branch (branch point 3 to the endpoint 3 in Figure 4Di), which did not align with the embryonic midbrain trajectory. Further, we observed that glia cells of MUT70 and WT70 midbrain organoids (endpoint 2 and endpoint 8 in Figure 4Di) were arranged in close proximity to embryonic week 11 (endpoint 2 in Figure 4Dii), presenting appropriate developmental pattern, where gliogenesis follows neurogenesis. The similar distribution of MUT and WT glia within the pseudotemporal space indicates that the previously observed stagnation in glial development is linked to its number and not its quality. In general, the cells of MUT70 midbrain organoids were placed further from the embryonic developmental trajectory in the UMAP plot than the cells of WT70 midbrain organoids. This indicates that MUT midbrain organoids manifest a developmental deviation, while the development of WT midbrain organoids is more similar to embryonic midbrain *in vivo*. Moreover, MUT70 midbrain organoids demonstrated a more cyclic trajectory, confirming a limited cellular developmental path that is resulting in less variable cellular identities.

#### **Mutant midbrain organoids compared to wild-type midbrain organoids show impaired pseudotemporal development that manifests in an untimely and incomplete differentiation**

In order to further explore the developmental deviation of the MUT midbrain organoids from WT midbrain organoids, we computed a developmental pseudotime trajectory only across midbrain organoids (WT35, WT70, MUT35, and MUT70), excluding the embryonic midbrain. The cell distribution along the trajectory starting from NBs *in vitro* of WT35, demonstrated accelerated differentiation of MUT35 midbrain organoids with subsequent developmental with-hold (Figure 5A). We observed that mDNs might be the most affected cellular population. We saw that mDNs of WT midbrain organoids follow a differentiation path along the pseudotime trajectory from WT35 to the edge of WT70 midbrain organoids (endpoint 4 to 9). Contrary, mDNs of MUT35 midbrain organoids were located in close proximity to mDNs of MUT70 midbrain organoids (between endpoints 1 and 6), implying the impaired mDN maturation. In addition, glia cells of MUT35 midbrain organoids were located close to the WT70 midbrain organoids on the pseudotime trajectory (between branch points 7 and 8), confirming forward glia differentiation of MUT35 midbrain organoids.

Next, we computed genes with a clear expression switch across the developmental trajectory between WT35 and

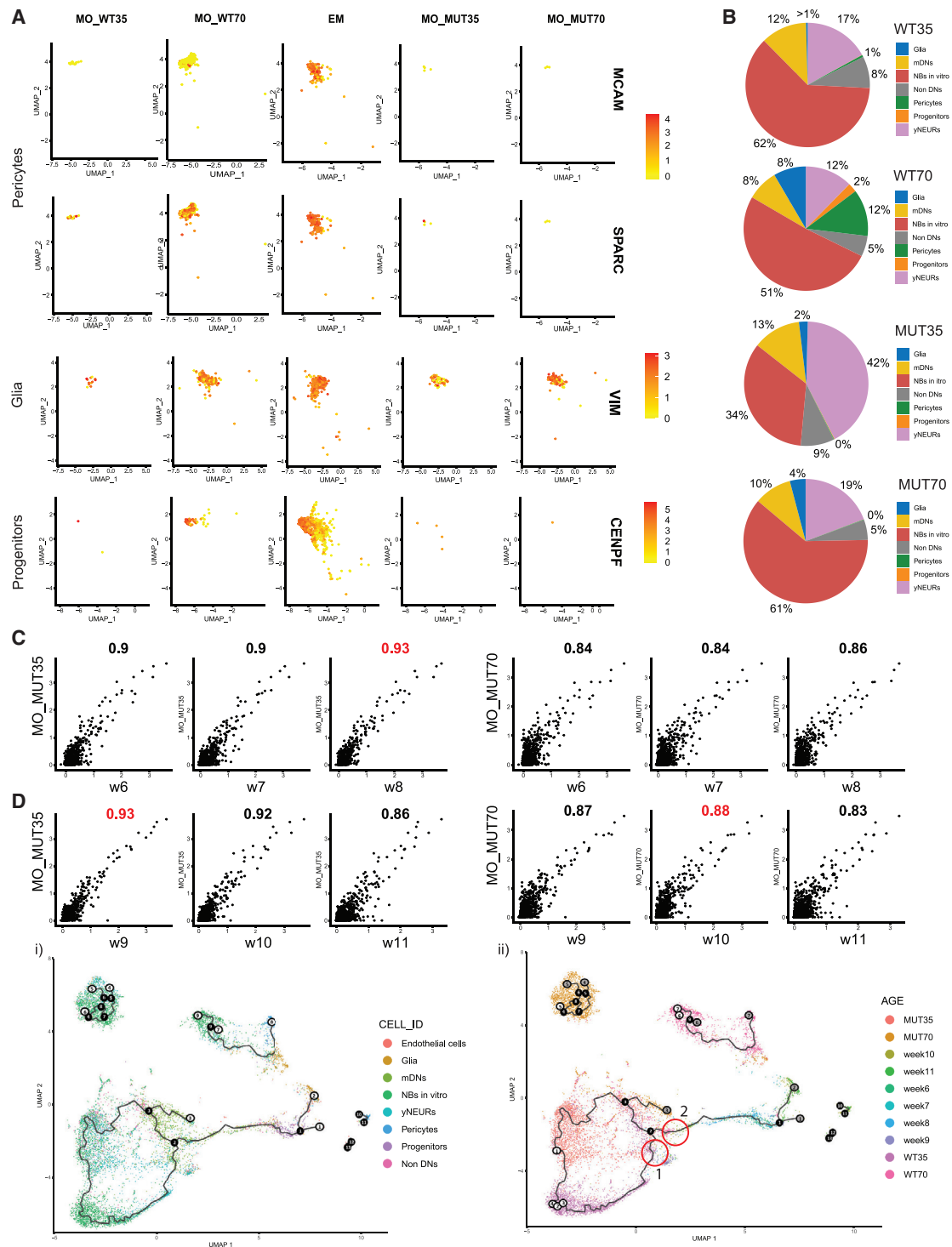


**Figure 4. LRRK2-p.Gly2019Ser-mutant midbrain organoids have a different cellular composition and correlate differently with the stages of embryonic midbrain development**

(A) Cell cluster identities defined by typical marker expression between WT and MUT midbrain organoids for pericytes, glia, and progenitor cells. Each dot represents a single cell and is colored according to the expression level.

(B) Percentage of cell identities in WT35, WT70, MUT35, and MUT70 midbrain organoids.

(C) The average gene expression correlation between MUT midbrain organoids 35 days of differentiation (MO\_MUT35) and 70 days of differentiation (MO\_MUT70) compared to the embryonic midbrain (EM) developmental weeks (w6–w11). The Pearson correlation coefficient is displayed above each comparison. Each dot represents a single cell.

(D) Batch-corrected pseudotime analysis based on the 150 dimensions. Each dot represents a single cell. The starting point is WT35 NBs *in vitro*. Cell distribution along the trajectory colored by cell identities (i) and by datasets (ii). Black nodes define branchpoints of the trajectory, white nodes define trajectory graph nodes, and gray nodes define endpoints of the certain trajectory leaf. Red circles indicate the position of mDNs of WT35 and WT70 midbrain organoids.

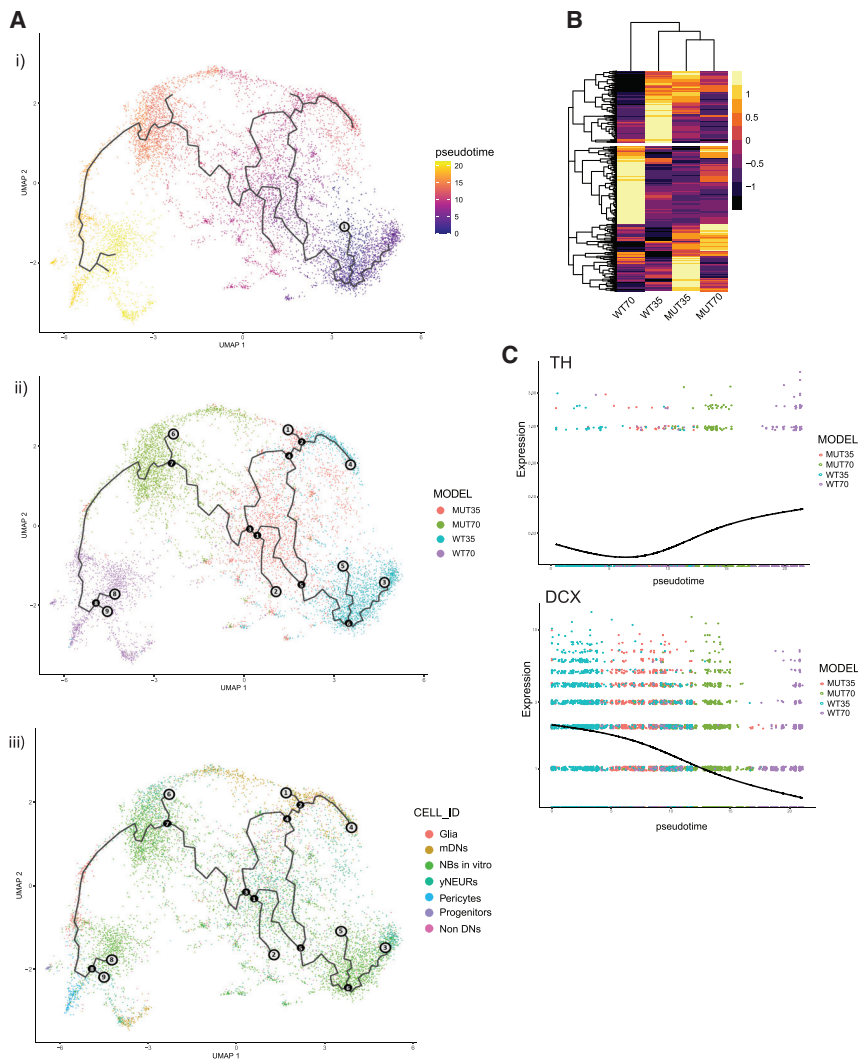


**Figure 5. Transcriptome signatures over time reveal impaired development of LRRK2-p.Gly2019Ser-mutant midbrain organoids**

(A) Pseudotime analysis of midbrain organoids with the root node WT35 NBs *in vitro* (i). Pseudotime trajectory, cells colored by the model: WT35, WT70, MUT35, and MUT70 (ii). Pseudotime trajectory, cells colored by cell identity (iii). Black nodes define branchpoints of the trajectory and gray nodes define endpoints/outcomes of the certain trajectory leaf.

(B) Genes with fitted expression pattern along the trajectory between WT35 and WT70 midbrain organoids, visualized in heatmap after Z score normalization in WT and MUT organoids.

(C) Pseudotemporal expression of *TH* and *DCX* across the cells in WT and MUT midbrain organoids. Each dot represents a single cell.

These results imply that mutant midbrain organoids reach a deadlock at some point during development.

#### Identification of potential LRRK2 p.Gly2019Ser target genes that could underlie impaired neurodevelopment and contribute to explain the PD-associated genetic signature

On the basis of the DEG analysis and after pseudotime trajectory examination, we distinguished four potentially promising candidate genes that have already been associated with

WT70 midbrain organoids (Figure 5B, Figure S8C). We investigated whether the same genes that have a temporal dynamic expression pattern in WT midbrain organoids show similar expression tendency in MUT midbrain organoids (Figure 5B). We observed that MUT midbrain organoids presented a completely different expression of the same genes, suggesting that MUT midbrain organoids do not follow the same developmental process as WT midbrain organoids. Furthermore, we highlighted the temporal expression of the rate-limiting enzyme of dopamine synthesis, tyrosine hydroxylase (*TH*), and the developing neuronal marker doublecortin (*DCX*). *TH* expression showed an increase over time in WT midbrain organoids but was impaired in the MUT midbrain organoids at both time points. *DCX* showed a clear decrease in the expression between WT35 and WT70 midbrain organoids. While in MUT35 midbrain organoids its expression was already further declined, it was still expressed at MUT70 midbrain organoids, further supporting an accelerated differentiation in MUT midbrain organoids at early time points of development accompanied by an incomplete differentiation at later developmental stages.

PD<sup>35–40</sup>—*DNAJC12*, *GATA3*, *PTN*, and *APP* (Figure 3B). These genes showed a temporal dynamic expression in the developing embryo and were significantly differentially expressed in MUT midbrain organoids compared to WT midbrain organoids. Their considerable change in expression during embryonic development indicates an active role in neurodevelopment (Figure 6A). Moreover, differential expression between MUT and WT midbrain organoids further supports altered MUT midbrain organoid neurodevelopment. *DNAJC12* and *GATA3* showed a significant upregulation in every neuronal cell type and glia in MUT midbrain organoids compared to WT midbrain organoids in both time points (Figures 6B and 6C). In addition, in MUT organoids, *DNAJC12* and *GATA3* expression increased over time in contrast to the embryonic midbrain where the expression decreased after peaking at week 9. In the neuronal clusters of WT midbrain organoids, the expression pattern of these two genes was comparable to embryonic development, showing highest expression levels at 35 days (corresponding to week 9). In contrast, *PTN* and *APP* were found to be significantly downregulated

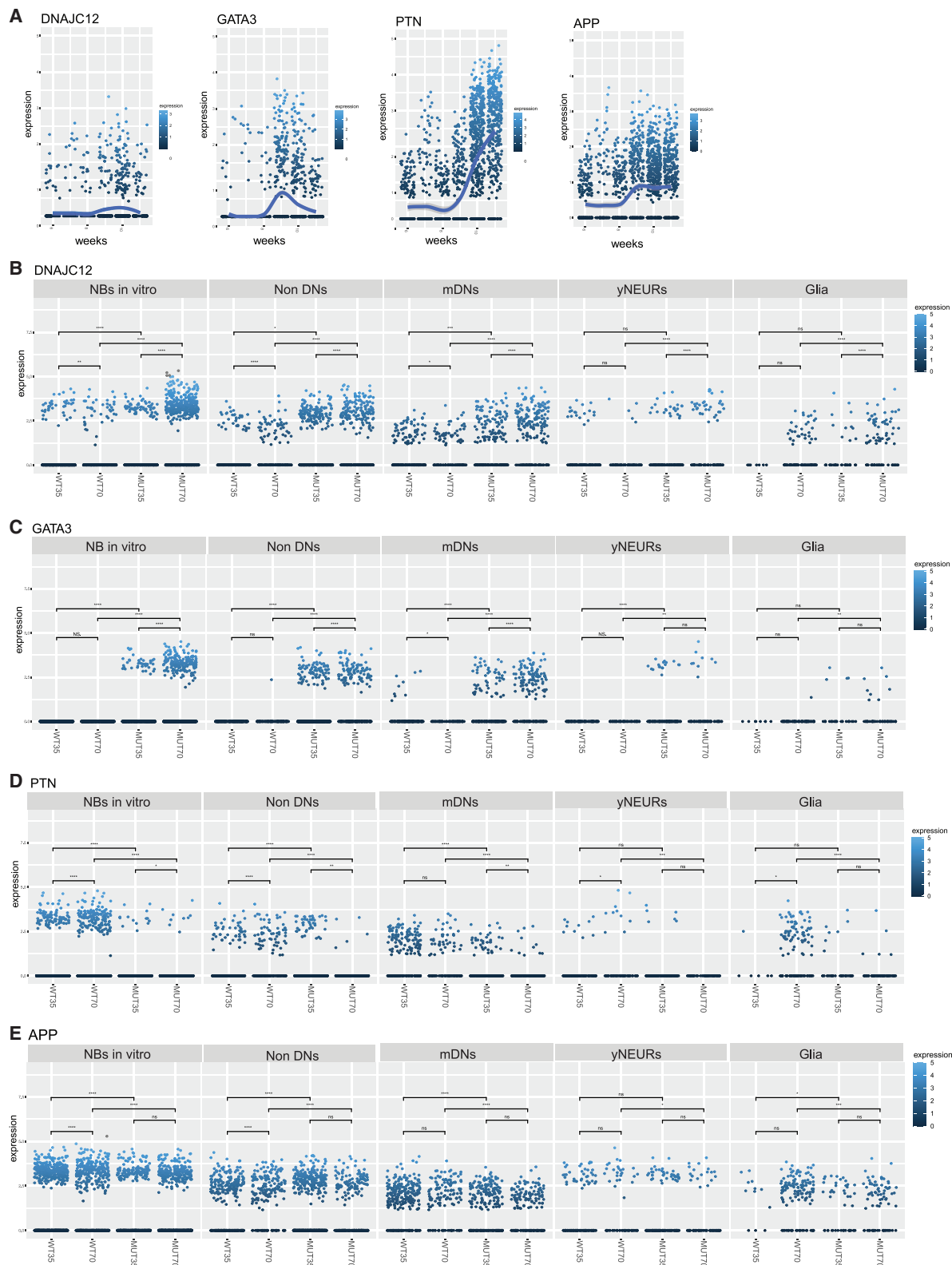


**Figure 6.** Discovery of potential LRRK2 p.Gly2019Ser target genes that might be involved in impaired neurodevelopment of mutant midbrain organoids

(A) *DNAJC12*, *GATA3*, *PTN*, and *APP* expression profile over the embryonic development time points (w6–w11). Each dot represents a single cell of embryonic midbrain and is colored according to the expression level.

(legend continued on next page)

in MUT midbrain organoid neuronal cell types and glia compared to WT midbrain organoids (Figures 6D and 6E). We observed that both *PTN* and *APP* expression tended to increase over time in embryonic midbrain development. A similar expression pattern was observed in NBs *in vitro*, yNEURs, and glia of WT midbrain organoid but not in MUT midbrain organoids. These results highlight a dysregulation of genes with essential roles in neuronal development and neuroprotection that might be directly associated with the LRRK2 p.Gly2019Ser variant, linking *LRRK2* to the regulation of nigrostriatal system development.

## Discussion

Our analysis of scRNA-seq data of human midbrain organoids and embryonic midbrain highlights the physiological relevance of midbrain organoids and their potential in disease modeling. Over the recent years, midbrain organoids have become a widely used model in PD studies, as the midbrain is the most affected region in the brain of PD patients.<sup>9,20,23,41,42</sup> In the present study, we were able to show the developmental correlation of healthy control-derived midbrain organoids from 35 and 70 days of culture<sup>9</sup> with human embryonic midbrain.<sup>25</sup> Importantly, midbrain organoids showed a higher degree of correlation with embryonic midbrain development than with the embryonic prefrontal cortex, validating the midbrain identity of the organoids. In support of this, we did not find a significant correlation between the cortex organoids<sup>29</sup> and embryonic midbrain, which further validates the specificity of the brain regional organoids. In addition, our analysis implicates developmental maturation of midbrain organoids after long time culture (e.g., 70 days), which showed a better correlation with the later stages of embryonic midbrain development.

Previous studies have demonstrated the cellular heterogeneity of human brain organoids and their similarities with their fetal counterparts.<sup>43,44</sup> Similarly, our analysis showed that midbrain organoids exhibit a shared cellular composition with the developing embryonic midbrain. One interesting finding is the identification of pericytes in midbrain organoids. It has been reported that pericytes can originate from the neuroectoderm and contribute to the formation of vasculature in the CNS.<sup>45–47</sup> The presence of mesenchymal cells was also originally reported by Smits et al., 2020.<sup>26</sup> Moreover, recent studies showed that a mesenchymal-like cell population appears in the early development of the cortex, even before the beginning of neurogenesis.<sup>48</sup> Nevertheless, because the cells in midbrain organoids are guided toward midbrain identity by the expansion of the neuroepithelium, the presence of more mature endothelial

cells is not expected. Accordingly, the endothelial cell cluster was found only in the embryonic midbrain and not in midbrain organoids. In contrast, the NB *in vitro* cluster was almost uniquely present in the midbrain organoids. Although these cells did not show a significant variable gene expression profile and clustered with neuronal cell types, there was no expression of reliable marker genes. Due to their unclear gene expression profile, NBs *in vitro* seemed to be less comparable to the physiological cell types shared between midbrain organoids and embryonic midbrain. We speculate that this NB cluster represents mfNPCs, which is the starting cell population for midbrain organoid generation. Although these cells are artificially patterned toward midbrain identity<sup>49</sup> and show unspecific genetic identity,<sup>50</sup> they can give rise to multiple physiologically relevant neuronal cell types and glia, similar to their *in vivo* neural progenitor counterpart.

When comparing MUT to WT midbrain organoids, clear differences become visible regarding their cellular composition, revealing PD-associated phenotypic differences. The MUT midbrain organoids reveal a faster differentiation profile that limits the development of a more variable and mature cellular composition. The accelerated differentiation phenotype at 35 days that we observed with pseudotime analysis has been described before in *LRRK2*-related PD.<sup>8–10</sup> In addition, the MUT midbrain organoids have no evident differences in the cell type populations at both time points and pseudotime analysis revealed that besides the untimely differentiation, the MUT70 midbrain organoids face a premature arrest or slowdown of the differentiation capacity. Importantly, the mDNs were the most affected population of cells. They showed no indication of maturation along the trajectory in the MUT70 compared to the MUT35 midbrain organoids and had a reduced expression of TH in MUT midbrain organoids. The doubling of the number of NBs *in vitro* in MUT70 midbrain organoids might be a compensation strategy linked to the incapacity of terminal differentiation or an increase in mature cell death. Moreover, we observed that the MUT midbrain organoids contain a higher number of glial cells than WT midbrain organoids at early time points. A situation that is inverted in longer cultures (MUT70 and WT70). The pseudotime trajectory confirmed that glial cells of MUT35 midbrain organoids were located closer to the WT70 midbrain organoids, indicating a faster gliogenesis. Finally, and most importantly, in contrast to MUT midbrain organoids, WT midbrain organoids from longer cultures are capable of capturing the cellular diversity found in human embryonic midbrain development *in vivo*.

Regarding the developmental pattern of organoids and embryonal tissue, MUT midbrain organoids showed a different developmental path compared to WT midbrain

---

(B–E) *DNAJC12*, *GATA3*, *PTN*, and *APP* expression across major cell types in WT and MUT midbrain organoids at 35 days and 70 days of differentiation. Each dot represents a single cell of midbrain organoid and is colored according to the expression level. Kruskal-Wallis test  $p < 0.05^*$ ,  $p < 0.01^{**}$ ,  $p < 0.001^{***}$ ,  $p < 0.00001^{****}$ .

organoids. From the correlation analysis, we saw that the MUT70 midbrain organoids have lower correlation than MUT35 midbrain organoids with the different time points of embryonic midbrain development. Furthermore, cells of MUT70 midbrain organoids were positioned further away from the embryonic pseudotemporal developmental trajectory in the UMAP plot, while cells of WT70 midbrain organoids have a development trail closer to embryonic development.

On the basis of the here-presented data, we propose that LRRK2 p.Gly2019Ser could be responsible for the observed developmental defects and the impaired cellular composition. Our *LRRK2* midbrain organoid model was able to capture the dysregulation of gene expression linked to *LRRK2*-induced PD. The analysis of DEGs between MUT and WT midbrain organoids showed the significance of *LRRK2*-related pathway in PD and highlighted GO processes related to nervous system development. In addition to individual gene dysregulation of *LRRK2*-associated pathways, the overall DEG analysis showed a clear separation of the MUT and WT midbrain organoid clusters, confirming the presence of disease-associated phenotypes.

The major dysregulated pathways were cytoskeleton remodeling and cell adhesion. It is well known that *LRRK2* plays an important role in actin and microtubule dynamics. *LRRK2* p.Gly2019Ser has been reported to disturb the cytoskeleton processes through increased kinase activity.<sup>51,52</sup> The dysregulation of actin and microtubule genes, which are key components of cytoskeleton dynamics, may lead to failure of the proper cellular differentiation process.<sup>26</sup> Cytoskeleton-related proteins, such as MYO5A, DNM1, EPB41, ACTB, MAPT, and VIM, are direct interacting partners of *LRRK2*.<sup>53</sup> We found that the corresponding genes have a dysregulated expression in the MUT midbrain organoids, indicating that altered *LRRK2* function is able to impair the gene expression profile of its interactome. Altered *LRRK2* function has also been described to have a role in impaired synaptogenesis.<sup>51,54,55</sup> Here, we identified significant downregulation of the synapse-related genes *SLC17A6*, *PCLO*, and *CHL1* specifically in MUT35 but not in MUT70 midbrain organoids. This observation suggests an impaired synaptogenesis occurring in early neurodevelopment of MUT midbrain organoids.

Further, direct *LRRK2*-interacting partners such as HSP90B1 and YWHAH have also been altered upon presence of the *LRRK2* p.Gly2019Ser. HSP90B1 along with the other heat-shock proteins is involved in protein folding and has been linked to PD.<sup>56</sup> HSP90B1 is a chaperone protein from the HSP90 family that interacts with *LRRK2*. This interaction is important for the proteasomal degradation of *LRRK2*.<sup>57</sup> Thus, the downregulation of *HSP90B1* in MUT70 midbrain organoids could be linked to the toxic aggregation of mutant *LRRK2*. *YWHAH* encodes the 14-3-3 eta, known to regulate the activity of kinases, including *LRRK2*.<sup>58</sup>

Additionally, we identified dysregulation of genes related to the  $\gamma$ -secretase pathway. *APP* belongs to this

pathway and shows a severe dysregulation in MUT midbrain organoid. *APP* encodes the  $\beta$ -amyloid precursor protein that has an important role in the development of neurodegenerative pathologies such as Alzheimer disease because of the accumulation of its derivative amyloid-beta ( $A\beta$ ) peptide, which is induced by cleavage from secretases including the  $\gamma$ -secretase.<sup>59,60</sup> A link between  $A\beta$  accumulation and *LRRK2* p.Gly2019Ser PD cases has also been made. *LRRK2* phosphorylates the intracellular domain (AICD) of *APP*, which regulates the transcription of cytoskeleton-related genes and has a role in the loss of dopaminergic neurons in the midbrain of PD cases by induced neurotoxicity.<sup>61</sup> *APP* has also an important role in neurogenesis, gliogenesis, and neuroprotection in the developing brain.<sup>35,60,62</sup> Therefore, dysregulation of *APP* can be associated not only with the neurodegeneration but also with the aberrations of neuronal development. Indeed, during embryonic midbrain development, we observed a strong increase of *APP* expression over time, whereas in MUT midbrain organoids, we observed a significant reduction compared to WT midbrain organoids, especially in mDNs and glia cells.

Further evidence of altered cellular development of MUT midbrain organoids comes also from the changed expression of three PD-associated DEG candidates, *DNAJC12*, *GATA3*, and *PTN*. The expression pattern of these genes in the embryonic midbrain suggests their important role in development and differentiation of the cells, although these findings would benefit from further experimental validation. *DNAJC12* is described to have a role in protein folding and export. Bi-allelic mutations of *DNAJC12* have been associated with hyperphenylalaninemia and neurodevelopmental delay in children. However, recent findings link mutation in *DNAJC12* to early-onset PD because of its interaction with aromatic amino-acid hydroxylases, including TH.<sup>37,63</sup> *GATA3* has been described as an important regulator of CNS development and neuronal fate.<sup>36</sup> An association with PD has been reported via *GATA* family transcriptional regulation of *TRPM2* and *SNCA*.<sup>38,64</sup> Until now, there is no reported interaction of *GATA3* and *DNAJC12* with *LRRK2*. However, the notable upregulation of *GATA3* and *DNAJC12* in MUT midbrain organoids suggests their possible dysregulation due to *LRRK2* p.Gly2019Ser and might explain the accelerated differentiation phenotype, subsequent maturation decline, and decreased expression of *TH*. In contrast, we observed that *PTN* is expressed significantly higher in WT midbrain organoids. *PTN* is a neurotrophic factor, highly expressed during development of nigrostriatal dopamine system, and later plays a role in cellular recovery and repair.<sup>39,40</sup> It has been shown to restore neuronal survival and functionality in a 6-OHDA mouse model.<sup>39</sup> The high expression of *PTN* in NBs *in vitro* of WT midbrain organoids may explain their better developmental trail compared to MUT midbrain organoids.

In summary, we demonstrated a high degree of transcriptome similarity between human midbrain organoids and embryonic midbrain, supporting the potential of midbrain

organoids to recapitulate human brain physiology. Moreover, our study showed the ability of midbrain organoids to capture LRRK2-p.Gly2019Ser-dependent alterations in gene expression, which highlights cellular processes related to cytoskeleton regulation, cell adhesion, and  $\gamma$ -secretase regulation during neuronal development. Finally, we observed developmental aberrations in MUT midbrain organoids and altered gene expression patterns along pseudotemporal trajectories, supporting a neurodevelopmental component in LRRK2-p.Gly2019Ser-associated PD.

### Data and code availability

WT midbrain organoid scRNA-seq datasets are available at the following doi: <https://doi.org/10.17881/lcsb.20190326.01>. LRRK2-G2019S MUT midbrain organoid scRNA-seq datasets are available at the following doi: <https://doi.org/10.17881/rc4f-nk07>. The accession number for the raw data for WT and MUT midbrain organoids is GEO: GSE133894. The accession number for the raw data for the human embryo ventral midbrain between 6 and 11 weeks is GEO: GSE76381. The accession number for the raw data for scRNA-seq data of prefrontal cortex at developmental stages between gestational weeks 8 and 26 is GEO: GSE104276. The accession number for the raw data for scRNA-seq data of human cortical organoids is GEO: GSE130238. We used data only of 1-month-old cortical organoid, which better corresponds to the developmental stage of midbrain organoids. Data were analyzed with R version 3.6.2 with single-cell analysis toolkit Seurat version 3.2.0<sup>31,65,66</sup> and Monocle 3.<sup>67</sup> All scripts used for the analysis are available via GitHub: <https://github.com/LCSB-DVB>.

### Supplemental information

Supplemental information can be found online at <https://doi.org/10.1016/j.ajhg.2021.12.009>.

### Acknowledgments

This work was supported by the National Centre of Excellence in Research on Parkinson Disease (NCER-PD), which is funded by the Luxembourg National Research Fund (FNR/NCER13/BM/11264123). S.S. is supported by the FNR-funded doctoral training program PARK-QC (PRIDE17/12244779/PARK-QC). L.M.S. was supported by a fellowship from the FNR (AFR, Aides à la Formation-Recherche). A.G. received funding from the FNR within the framework of the ATTRACT (FNR9631103) and INTER (INTER/DFG/19/14429377) programs. Additionally, we would like to acknowledge support by an LCSB flagship project.

### Declaration of interests

J.C.S. is co-inventor on a patent covering the generation of the here-described midbrain organoids (WO2017060884A1). Furthermore, J.C.S. is co-founder and shareholder of the company OrganoTherapeutics, which makes use of the midbrain organoid technology. The other authors declare no competing interests.

Received: June 14, 2021

Accepted: December 13, 2021

Published: January 24, 2022

### Web resources

Metacore, <https://portal.genego.com/>

nVenn, <http://degradome.uniiovi.es/cgi-bin/nVenn/nVenn.cgi>

### References

1. Inamdar, N.N., Arulmozhi, D.K., Tandon, A., and Bodhankar, S.L. (2007). Parkinson's disease: genetics and beyond. *Curr. Neuropharmacol.* 5, 99–113.
2. Paisán-Ruiz, C., Jain, S., Evans, E.W., Gilks, W.P., Simón, J., van der Brug, M., López de Munain, A., Aparicio, S., Gil, A.M., Khan, N., et al. (2004). Cloning of the gene containing mutations that cause PARK8-linked Parkinson's disease. *Neuron* 44, 595–600.
3. Zimprich, A., Biskup, S., Leitner, P., Lichtner, P., Farrer, M., Lincoln, S., Kachergus, J., Hulihan, M., Uitti, R.J., Calne, D.B., et al. (2004). Mutations in LRRK2 cause autosomal-dominant parkinsonism with pleomorphic pathology. *Neuron* 44, 601–607.
4. Ren, C., Ding, Y., Wei, S., Guan, L., Zhang, C., Ji, Y., Wang, F., Yin, S., and Yin, P. (2019). G2019S Variation in LRRK2: An Ideal Model for the Study of Parkinson's Disease? *Front. Hum. Neurosci.* 13, 306.
5. Nickels, S.L., Walter, J., Bolognin, S., Gérard, D., Jaeger, C., Qing, X., Tisserand, J., Jarazo, J., Hemmer, K., Harms, A., et al. (2019). Impaired serine metabolism complements LRRK2-G2019S pathogenicity in PD patients. *Parkinsonism Relat. Disord.* 67, 48–55.
6. Liu, G.H., Qu, J., Suzuki, K., Nivet, E., Li, M., Montserrat, N., Yi, F., Xu, X., Ruiz, S., Zhang, W., et al. (2012). Progressive degeneration of human neural stem cells caused by pathogenic LRRK2. *Nature* 491, 603–607.
7. Winner, B., Kohl, Z., and Gage, F.H. (2011). Neurodegenerative disease and adult neurogenesis. *Eur. J. Neurosci.* 33, 1139–1151.
8. Milosevic, J., Schwarz, S.C., Ogunlade, V., Meyer, A.K., Storch, A., and Schwarz, J. (2009). Emerging role of LRRK2 in human neural progenitor cell cycle progression, survival and differentiation. *Mol. Neurodegener.* 4, 25.
9. Smits, L.M., Reinhardt, L., Reinhardt, P., Glatza, M., Monzel, A.S., Stanslowsky, N., Rosato-Siri, M.D., Zanon, A., Antony, P.M., Bellmann, J., et al. (2019). Modeling Parkinson's disease in midbrain-like organoids. *NPJ Parkinsons Dis.* 5, 5.
10. Schulz, C., Paus, M., Frey, K., Schmid, R., Kohl, Z., Mennerich, D., Winkler, J., and Gillardon, F. (2011). Leucine-rich repeat kinase 2 modulates retinoic acid-induced neuronal differentiation of murine embryonic stem cells. *PLoS ONE* 6, e20820.
11. Le Grand, J.N., Gonzalez-Cano, L., Pavlou, M.A., and Schwamborn, J.C. (2015). Neural stem cells in Parkinson's disease: a role for neurogenesis defects in onset and progression. *Cell. Mol. Life Sci.* 72, 773–797.
12. Sancho, R.M., Law, B.M.H., and Harvey, K. (2009). Mutations in the LRRK2 Roc-COR tandem domain link Parkinson's disease to Wnt signalling pathways. *Hum. Mol. Genet.* 18, 3955–3968.
13. Winner, B., Melrose, H.L., Zhao, C., Hinkle, K.M., Yue, M., Kent, C., Braithwaite, A.T., Ogholikhan, S., Aigner, R., Winkler, J., et al. (2011). Adult neurogenesis and neurite outgrowth are impaired in LRRK2 G2019S mice. *Neurobiol. Dis.* 41, 706–716.
14. Berwick, D.C., and Harvey, K. (2012). LRRK2 functions as a Wnt signaling scaffold, bridging cytosolic proteins and membrane-localized LRP6. *Hum. Mol. Genet.* 21, 4966–4979.

15. Hartmann, A. (2004). Postmortem studies in Parkinson's disease. *Dialogues Clin. Neurosci.* 6, 281–293.
16. Blesa, J., and Przedborski, S. (2014). Parkinson's disease: animal models and dopaminergic cell vulnerability. *Front. Neuroanat.* 8, 155.
17. Takahashi, K., and Yamanaka, S. (2006). Induction of pluripotent stem cells from mouse embryonic and adult fibroblast cultures by defined factors. *Cell* 126, 663–676.
18. Arias-Fuenzalida, J., Jarazo, J., Qing, X., Walter, J., Gomez-Giro, G., Nickels, S.L., Zaehres, H., Schöler, H.R., and Schwamborn, J.C. (2017). FACS-Assisted CRISPR-Cas9 Genome Editing Facilitates Parkinson's Disease Modeling. *Stem Cell Reports* 9, 1423–1431.
19. Vermilyea, S.C., Babinski, A., Tran, N., To, S., Guthrie, S., Kluss, J.H., Schmidt, J.K., Wiep, G.J., Meyer, M.G., Murphy, M.E., et al. (2020). In Vitro CRISPR/Cas9-Directed Gene Editing to Model LRRK2 G2019S Parkinson's Disease in Common Marmosets. *Sci. Rep.* 10, 3447.
20. Monzel, A.S., Smits, L.M., Hemmer, K., Hachi, S., Moreno, E.L., van Wuellen, T., Jarazo, J., Walter, J., Brüggemann, I., Boussaad, I., et al. (2017). Derivation of Human Midbrain-Specific Organoids from Neuroepithelial Stem Cells. *Stem Cell Reports* 8, 1144–1154.
21. Schwamborn, J.C. (2018). Is Parkinson's disease a neurodevelopmental disorder and will brain organoids help us to understand it? *Stem Cells Dev.* 27, 968–975.
22. Chlebanowska, P., Tejchman, A., Sułkowski, M., Skrzypek, K., and Majka, M. (2020). Use of 3D organoids as a model to study idiopathic form of parkinson's disease. *Int. J. Mol. Sci.* 21, 694.
23. Kim, H., Park, H.J., Choi, H., Chang, Y., Park, H., Shin, J., Kim, J., Lengner, C.J., Lee, Y.K., and Kim, J. (2019). Modeling G2019S-LRRK2 Sporadic Parkinson's Disease in 3D Midbrain Organoids. *Stem Cell Reports* 12, 518–531.
24. Kwak, T.H., Kang, J.H., Hali, S., Kim, J., Kim, K.P., Park, C., Lee, J.H., Ryu, H.K., Na, J.E., Jo, J., et al. (2020). Generation of homogeneous midbrain organoids with in vivo-like cellular composition facilitates neurotoxin-based Parkinson's disease modeling. *Stem Cells* 38, 727–740.
25. La Manno, G., Gyllborg, D., Codrussi, S., Nishimura, K., Salto, C., Zeisel, A., Borm, L.E., Stott, S.R.W., Toledo, E.M., Villaescusa, J.C., et al. (2016). Molecular Diversity of Midbrain Development in Mouse, Human, and Stem Cells. *Cell* 167, 566–580.e19.
26. Smits, L.M., Magni, S., Kinugawa, K., Grzyb, K., Luginbühl, J., Sabate-Soler, S., Bolognin, S., Shin, J.W., Mori, E., Skupin, A., and Schwamborn, J.C. (2020). Single-cell transcriptomics reveals multiple neuronal cell types in human midbrain-specific organoids. *Cell Tissue Res.* 382, 463–476.
27. Qing, X., Walter, J., Jarazo, J., Arias-Fuenzalida, J., Hillje, A.L., and Schwamborn, J.C. (2017). CRISPR/Cas9 and piggyBac-mediated footprint-free LRRK2-G2019S knock-in reveals neuronal complexity phenotypes and  $\alpha$ -Synuclein modulation in dopaminergic neurons. *Stem Cell Res. (Amst.)* 24, 44–50.
28. Zhong, S., Zhang, S., Fan, X., Wu, Q., Yan, L., Dong, J., Zhang, H., Li, L., Sun, L., Pan, N., et al. (2018). A single-cell RNA-seq survey of the developmental landscape of the human prefrontal cortex. *Nature* 555, 524–528.
29. Trujillo, C.A., Gao, R., Negraes, P.D., Gu, J., Buchanan, J., Preissl, S., Wang, A., Wu, W., Haddad, G.G., Chaim, I.A., et al. (2019). Complex Oscillatory Waves Emerging from Cortical Organoids Model Early Human Brain Network Development. *Cell Stem Cell* 25, 558–569.e7.
30. Macosko, E.Z., Basu, A., Satija, R., Nemes, J., Shekhar, K., Goldman, M., Tirosh, I., Bialas, A.R., Kamitaki, N., Martersteck, E.M., et al. (2015). Highly parallel genome-wide expression profiling of individual cells using nanoliter droplets. *Cell* 161, 1202–1214.
31. Stuart, T., Butler, A., Hoffman, P., Hafemeister, C., Papalexi, E., Mauck, W.M., 3rd, Hao, Y., Stoeckius, M., Smibert, P., and Satija, R. (2019). Comprehensive Integration of Single-Cell Data. *Cell* 177, 1888–1902.e21.
32. Becht, E., McInnes, L., Healy, J., Dutertre, C.A., Kwok, I.W.H., Ng, L.G., Ginhoux, F., and Newell, E.W. (2018). Dimensionality reduction for visualizing single-cell data using UMAP. *Nat. Biotechnol.* 37, 38–47.
33. Hafemeister, C., and Satija, R. (2019). Normalization and variance stabilization of single-cell RNA-seq data using regularized negative binomial regression. *Genome Biol.* 20, 296.
34. Chen, X., Zhang, K., Zhou, L., Gao, X., Wang, J., Yao, Y., He, F., Luo, Y., Yu, Y., Li, S., et al. (2016). Coupled electrophysiological recording and single cell transcriptome analyses revealed molecular mechanisms underlying neuronal maturation. *Protein Cell* 7, 175–186.
35. Zhou, Z.D., Chan, C.H.S., Ma, Q.H., Xu, X.H., Xiao, Z.C., and Tan, E.K. (2011). The roles of amyloid precursor protein (APP) in neurogenesis, implications to pathogenesis and therapy of Alzheimer Disease (AD). *Cell Adh. Migr.* 5, 280–292.
36. Tsarovina, K., Reiff, T., Stubbusch, J., Kurek, D., Grosveld, F.G., Parlato, R., Schütz, G., and Rohrer, H. (2010). The Gata3 transcription factor is required for the survival of embryonic and adult sympathetic neurons. *J. Neurosci.* 30, 10833–10843.
37. Cortès-Saladelafont, E., Lipstein, N., and García-Cazorla, À. (2018). Presynaptic disorders: a clinical and pathophysiological approach focused on the synaptic vesicle. *J. Inher. Metab. Dis.* 41, 1131–1145.
38. Scherzer, C.R., Grass, J.A., Liao, Z., Pepivani, I., Zheng, B., Eklund, A.C., Ney, P.A., Ng, J., McGoldrick, M., Mollenhauer, B., et al. (2008). GATA transcription factors directly regulate the Parkinson's disease-linked gene  $\alpha$ -synuclein. *Proc. Natl. Acad. Sci. USA* 105, 10907–10912.
39. Gombash, S.E., Lipton, J.W., Collier, T.J., Madhavan, L., Steece-Collier, K., Cole-Strauss, A., Terpstra, B.T., Spieles-Engemann, A.L., Daley, B.F., Wohlgenant, S.L., et al. (2012). Striatal pleiotrophin overexpression provides functional and morphological neuroprotection in the 6-hydroxydopamine model. *Mol. Ther.* 20, 544–554.
40. Marchionini, D.M., Lehmann, E., Chu, Y., He, B., Sortwell, C.E., Becker, K.G., Freed, W.J., Kordower, J.H., and Collier, T.J. (2007). Role of heparin binding growth factors in nigrostriatal dopamine system development and Parkinson's disease. *Brain Res.* 1147, 77–88.
41. Galet, B., Cheval, H., and Ravassard, P. (2020). Patient-Derived Midbrain Organoids to Explore the Molecular Basis of Parkinson's Disease. *Front. Neurol.* 11, 1005.
42. Nickels, S.L., Modamio, J., Mendes-Pinheiro, B., Monzel, A.S., Betsou, F., and Schwamborn, J.C. (2020). Reproducible generation of human midbrain organoids for in vitro modeling of Parkinson's disease. *Stem Cell Res. (Amst.)* 46, 101870.
43. Quadrato, G., Nguyen, T., Macosko, E.Z., Sherwood, J.L., Min Yang, S., Berger, D.R., Maria, N., Scholvin, J., Goldman, M., Kinney, J.P., et al. (2017). Cell diversity and network dynamics in photosensitive human brain organoids. *Nature* 545, 48–53.
44. Camp, J.G., Badsha, F., Florio, M., Kanton, S., Gerber, T., Wilsch-Bräuninger, M., Lewitus, E., Sykes, A., Hevers, W.,



- Lancaster, M., et al. (2015). Human cerebral organoids recapitulate gene expression programs of fetal neocortex development. *Proc. Natl. Acad. Sci. USA* *112*, 15672–15677.
45. Payne, L.B., Hoque, M., Houk, C., Darden, J., and Chappell, J.C. (2020). Pericytes in Vascular Development. *Curr. Tissue Microenviron. Rep.* *1*, 143–154.
  46. Korn, J., Christ, B., and Kurz, H. (2002). Neuroectodermal origin of brain pericytes and vascular smooth muscle cells. *J. Comp. Neurol.* *442*, 78–88.
  47. Yamazaki, T., and Mukoyama, Y.S. (2018). Tissue Specific Origin, Development, and Pathological Perspectives of Pericytes. *Front. Cardiovasc. Med.* *5*, 78.
  48. Eze, U., Bhaduri, A., Haeussler, M., Nowakowski, T., and Kriegstein, A. (2020). Single-Cell Atlas of Early Human Brain Development Highlights Heterogeneity of Human Neuroepithelial Cells and Early Radial Glia. *Nat. Neurosci.* *1*, 143–154.
  49. Reinhardt, P., Glatza, M., Hemmer, K., Tsytsyura, Y., Thiel, C.S., Höing, S., Moritz, S., Parga, J.A., Wagner, L., Bruder, J.M., et al. (2013). Derivation and expansion using only small molecules of human neural progenitors for neurodegenerative disease modeling. *PLoS ONE* *8*, e59252.
  50. van den Hurk, M., and Bardy, C. (2019). Single-cell multimodal transcriptomics to study neuronal diversity in human stem cell-derived brain tissue and organoid models. *J. Neurosci. Methods* *325*, 108350.
  51. Jeong, G.R., and Lee, B.D. (2020). Pathological Functions of LRRK2 in Parkinson's Disease. *Cells* *9*, 1–19.
  52. Häbig, K., Gellhaar, S., Heim, B., Djuric, V., Giesert, F., Wurst, W., Walter, C., Hentrich, T., Riess, O., and Bonin, M. (2013). LRRK2 guides the actin cytoskeleton at growth cones together with ARHGEF7 and Tropomyosin 4. *Biochim. Biophys. Acta* *1832*, 2352–2367.
  53. Manzoni, C., Denny, P., Lovering, R.C., and Lewis, P.A. (2015). Computational analysis of the LRRK2 interactome. *PeerJ* *3*, e778.
  54. Matikainen-Ankney, B.A., Kezunovic, N., Mesias, R.E., Tian, Y., Williams, F.M., Huntley, G.W., and Benson, D.L. (2016). Altered development of synapse structure and function in striatum caused by Parkinson's disease-linked LRRK2-G2019S mutation. *J. Neurosci.* *36*, 7128–7141.
  55. Lamonaca, G., and Volta, M. (2020). Alpha-Synuclein and LRRK2 in Synaptic Autophagy: Linking Early Dysfunction to Late-Stage Pathology in Parkinson's Disease. *Cells* *9*, 1115.
  56. Vergara, D., Gaballo, A., Signorile, A., Ferretta, A., Tanzarella, P., Pacelli, C., Di Paola, M., Cocco, T., and Maffia, M. (2017). Resveratrol Modulation of Protein Expression in *parkin*-Mutant Human Skin Fibroblasts: A Proteomic Approach. *Oxid. Med. Cell. Longev.* *2017*, 2198243.
  57. Ko, H.S., Bailey, R., Smith, W.W., Liu, Z., Shin, J.H., Lee, Y.I., Zhang, Y.J., Jiang, H., Ross, C.A., Moore, D.J., et al. (2009). CHIP regulates leucine-rich repeat kinase-2 ubiquitination, degradation, and toxicity. *Proc. Natl. Acad. Sci. USA* *106*, 2897–2902.
  58. Obsilova, V., and Obsil, T. (2020). The 14-3-3 proteins as important allosteric regulators of protein kinases. *Int. J. Mol. Sci.* *21*, 1–16.
  59. Zhang, X., Li, Y., Xu, H., and Zhang, Y.W. (2014). The  $\gamma$ -secretase complex: from structure to function. *Front. Cell. Neurosci.* *8*, 427.
  60. O'Brien, R.J., and Wong, P.C. (2011). Amyloid precursor protein processing and Alzheimer's disease. *Annu. Rev. Neurosci.* *34*, 185–204.
  61. Chen, Z.C., Zhang, W., Chua, L.L., Chai, C., Li, R., Lin, L., Cao, Z., Angeles, D.C., Stanton, L.W., Peng, J.H., et al. (2017). Phosphorylation of amyloid precursor protein by mutant LRRK2 promotes AICD activity and neurotoxicity in Parkinson's disease. *Sci. Signal.* *10*, 1–12.
  62. Bergström, P., Agholme, L., Nazir, F.H., Satir, T.M., Toombs, J., Wellington, H., Strandberg, J., Bontell, T.O., Kvartsberg, H., Holmström, M., et al. (2016). Amyloid precursor protein expression and processing are differentially regulated during cortical neuron differentiation. *Sci. Rep.* *6*, 29200.
  63. Straniero, L., Guella, I., Cilia, R., Parkkinen, L., Rimoldi, V., Young, A., Asselta, R., Soldà, G., Sossi, V., Stoessl, A.J., et al. (2017). DNAJC12 and dopa-responsive nonprogressive parkinsonism. *Ann. Neurol.* *82*, 640–646.
  64. Zhou, Y., and Han, D. (2017). GATA3 modulates neuronal survival through regulating TRPM2 in Parkinson's disease. *Int. J. Clin. Exp. Med.* *10*, 15178–15186.
  65. Hao, Y., Hao, S., Andersen-nissen, E., Iii, W.M.M., Zheng, S., Lee, M.J., Wilk, A.J., Darby, C., Zagar, M., Hoffman, P., et al. (2020). Integrated analysis of multimodal single-cell data. *bioRxiv*. <https://doi.org/10.1101/2020.10.12.335331>.
  66. Butler, A., Hoffman, P., Smibert, P., Papalexi, E., and Satija, R. (2018). Integrating single-cell transcriptomic data across different conditions, technologies, and species. *Nat. Biotechnol.* *36*, 411–420.
  67. Cao, J., Spielmann, M., Qiu, X., Huang, X., Ibrahim, D.M., Hill, A.J., Zhang, F., Mundlos, S., Christiansen, L., Steemers, F.J., et al. (2019). The single-cell transcriptional landscape of mammalian organogenesis. *Nature* *566*, 496–502.

**The American Journal of Human Genetics, Volume 109**

**Supplemental information**

**Midbrain organoids mimic early embryonic  
neurodevelopment and recapitulate**

**LRRK2-p.Gly2019Ser-associated gene expression**

**Alise Zagare, Kyriaki Bampa, Semra Smajic, Lisa M. Smits, Kamil Grzyb, Anne  
Grünewald, Alexander Skupin, Sarah L. Nickels, and Jens C. Schwamborn**

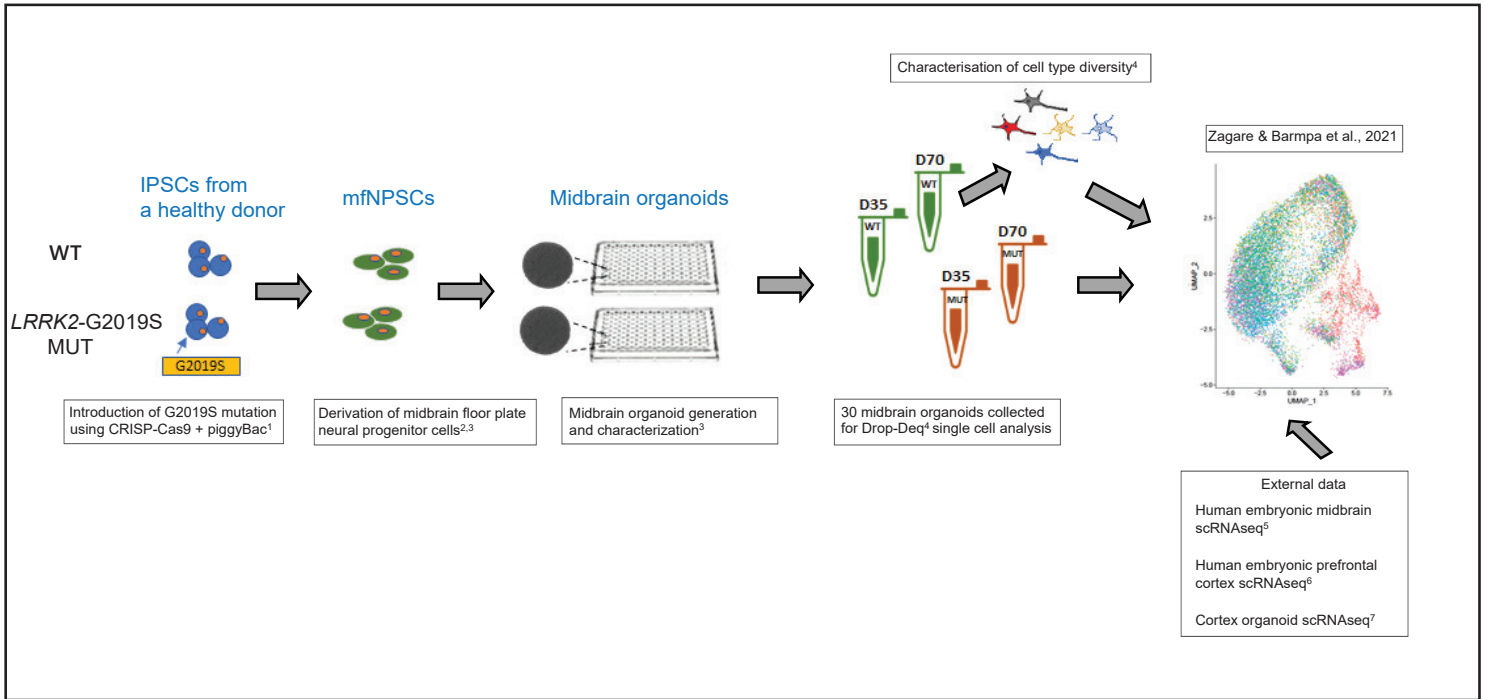


Figure S1. Graphical representation showing the origin of the data used in this study. WT and LRRK2 MUT midbrain organoids were generated in parallel in our lab. WT midbrain organoids were characterized in previous studies of Smits et al.<sup>3,4</sup> The present study comprises analysis of internal scRNAseq data from the respective midbrain organoids and comparison to external datasets<sup>5,6,7</sup>.

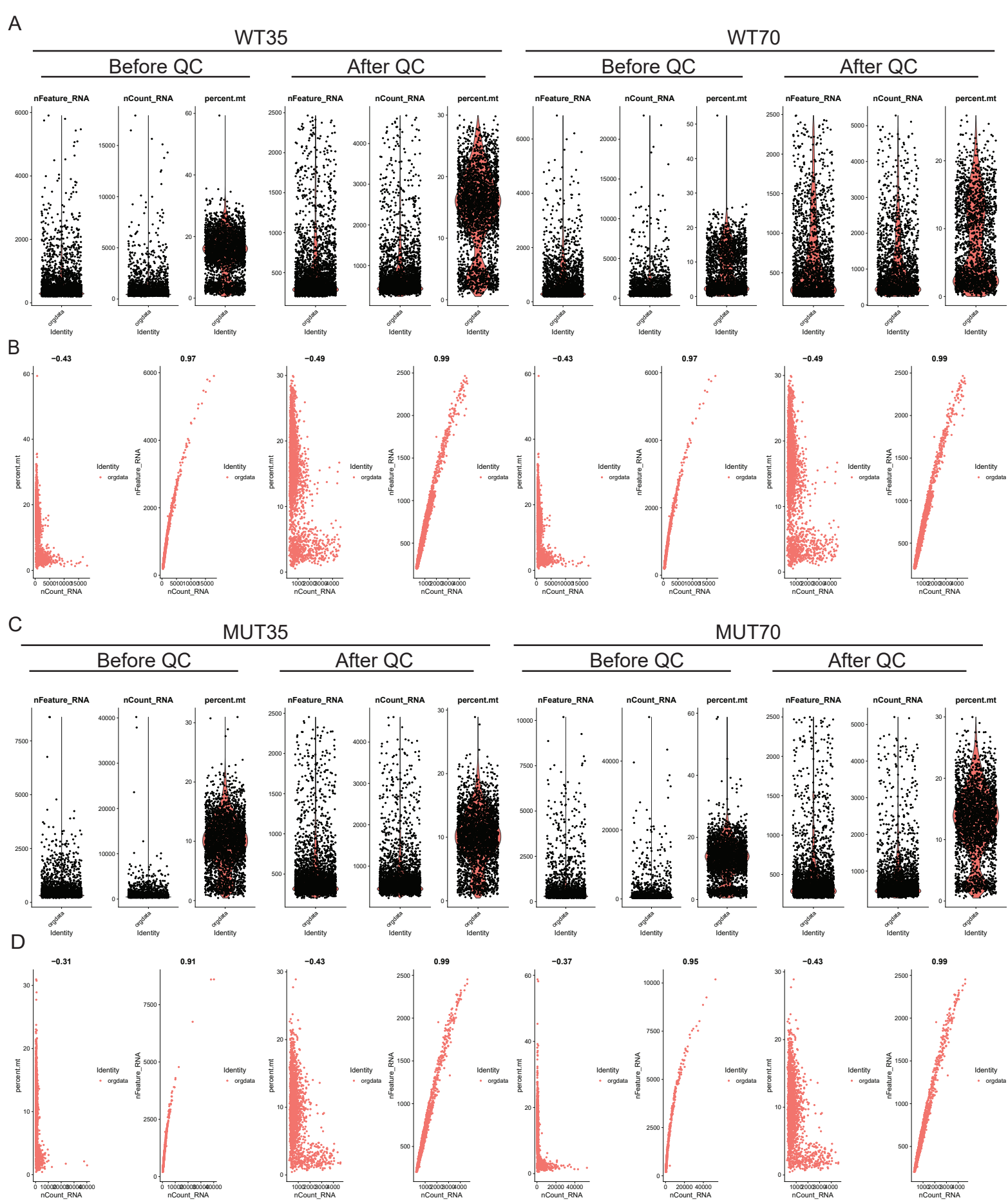


Figure S2. Quality control of midbrain organoid scRNAseq datasets. **A**) Number of genes (nFeature\_RNA), total number of molecules (nCount), percent of mitochondrial genes, detected in each cell for WT35 and WT70 midbrain organoids, before and after quality control. **B**) Correlations between percentage of mitochondrial genes, the number of genes and the total number of molecules for WT35 and WT70 midbrain organoids, before and after quality control. **C**) Same as (A), for MUT35 and MUT70 midbrain organoids. **D**) Same as (B), for MUT35 and MUT70 midbrain organoids.

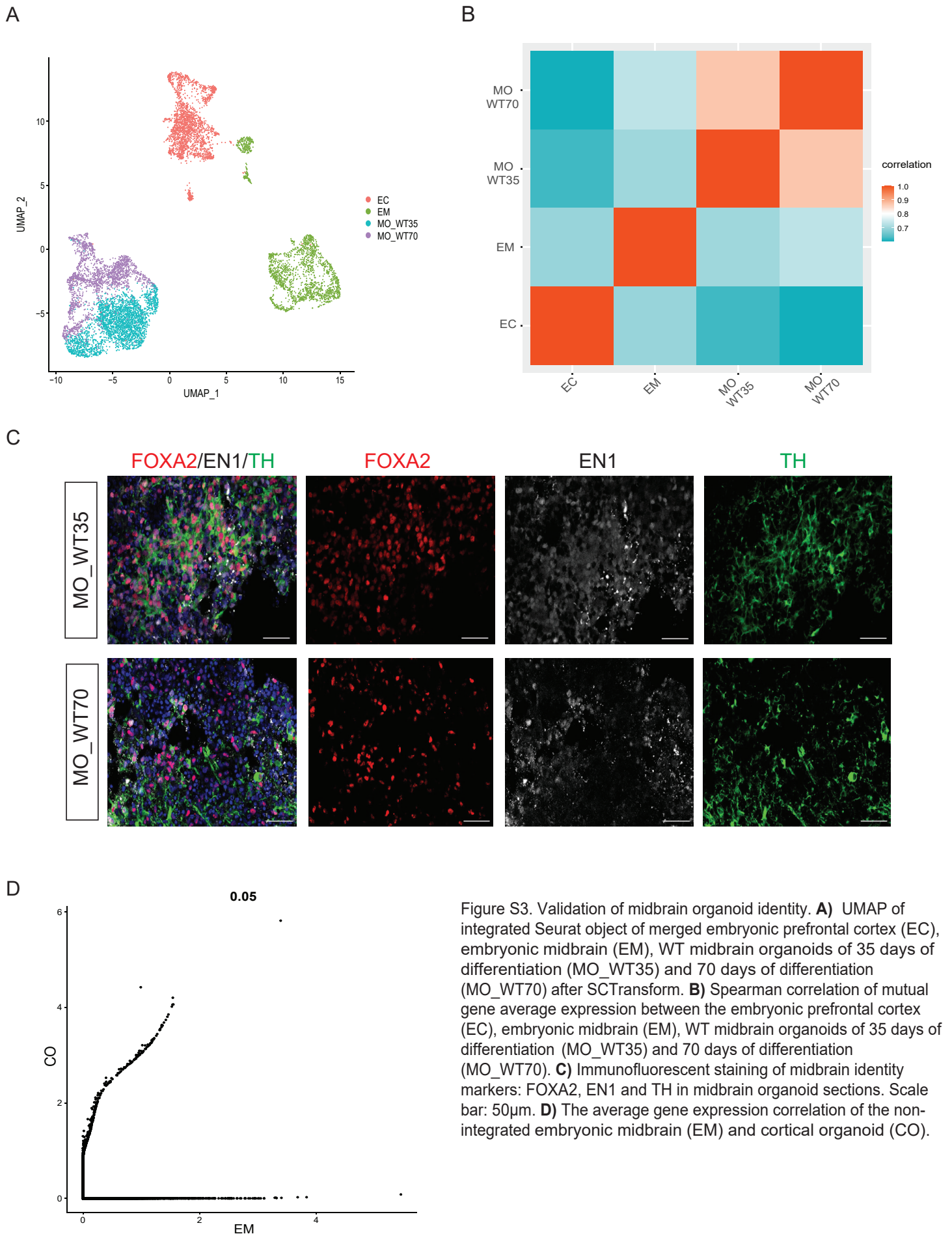


Figure S3. Validation of midbrain organoid identity. **A**) UMAP of integrated Seurat object of merged embryonic prefrontal cortex (EC), embryonic midbrain (EM), WT midbrain organoids of 35 days of differentiation (MO\_WT35) and 70 days of differentiation (MO\_WT70) after SCTransform. **B**) Spearman correlation of mutual gene average expression between the embryonic prefrontal cortex (EC), embryonic midbrain (EM), WT midbrain organoids of 35 days of differentiation (MO\_WT35) and 70 days of differentiation (MO\_WT70). **C**) Immunofluorescent staining of midbrain identity markers: FOXA2, EN1 and TH in midbrain organoid sections. Scale bar: 50µm. **D**) The average gene expression correlation of the non-integrated embryonic midbrain (EM) and cortical organoid (CO).

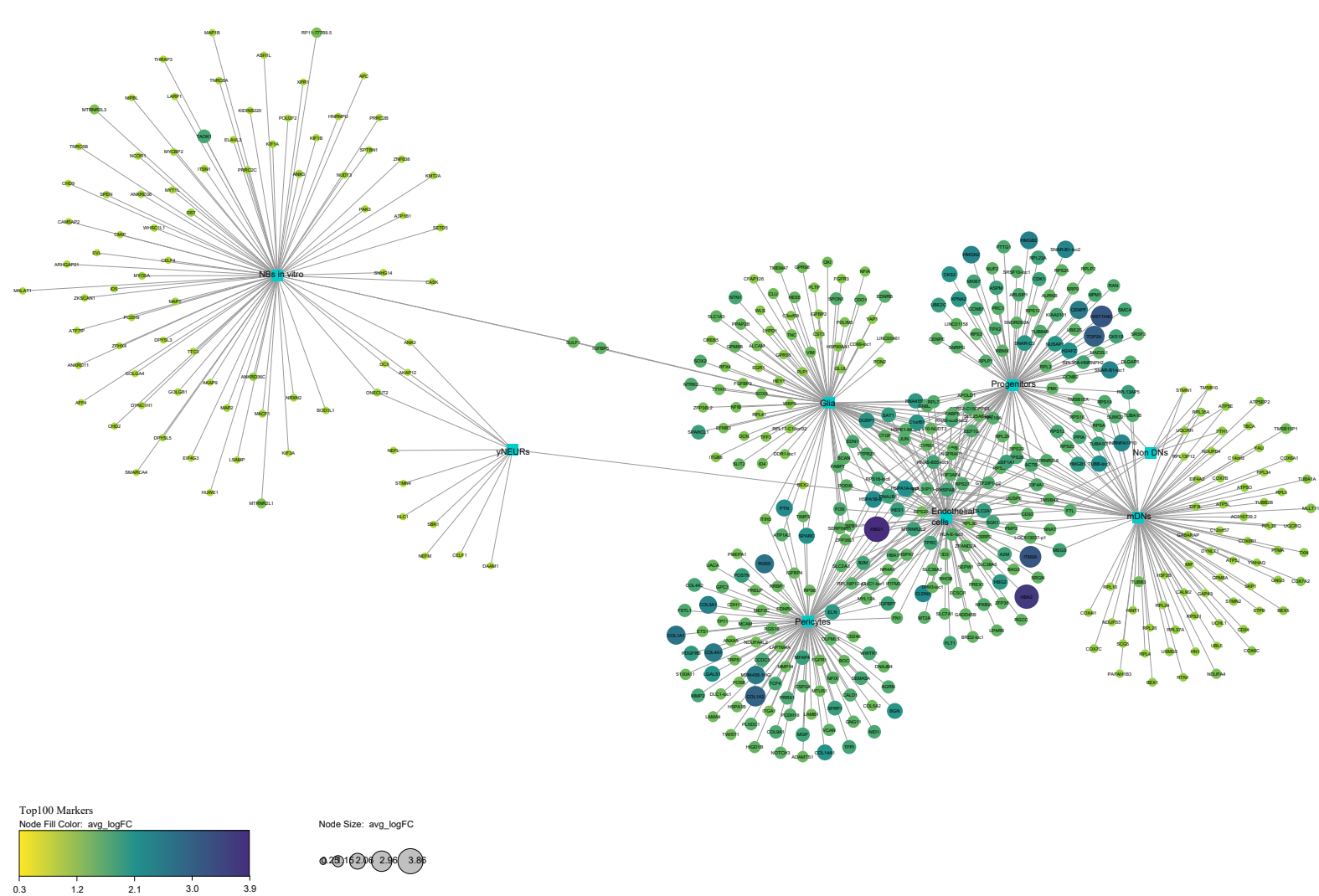
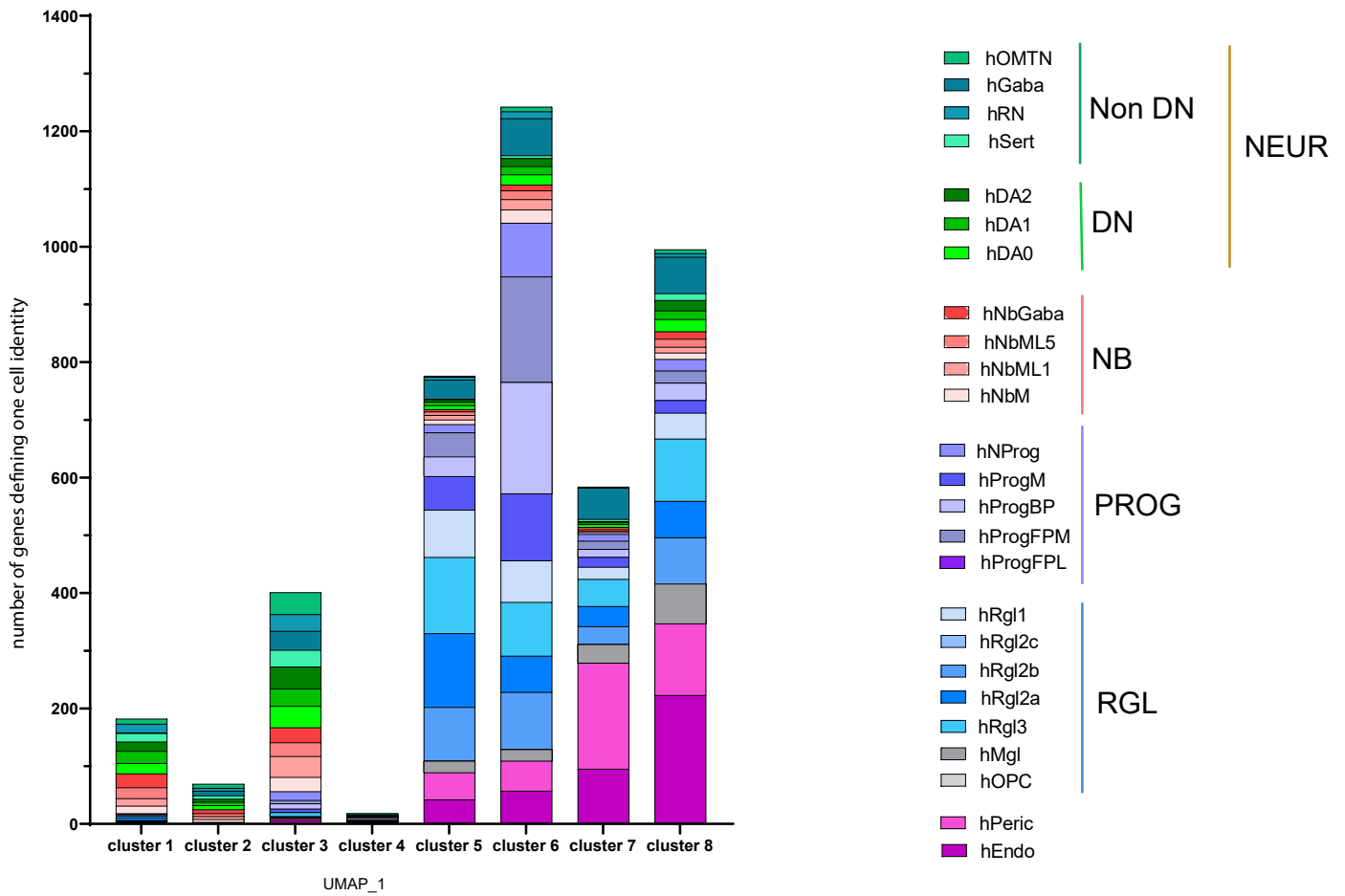


Figure S4. Network representing top marker genes for each cell cluster. The top 100 cell type markers identified by the FindAllMarkers function. The size and color of nodes represent logarithmic fold change (avg\_logFC) of each marker expression in the particular cell type compared to its expression in other cell clusters.

A



B

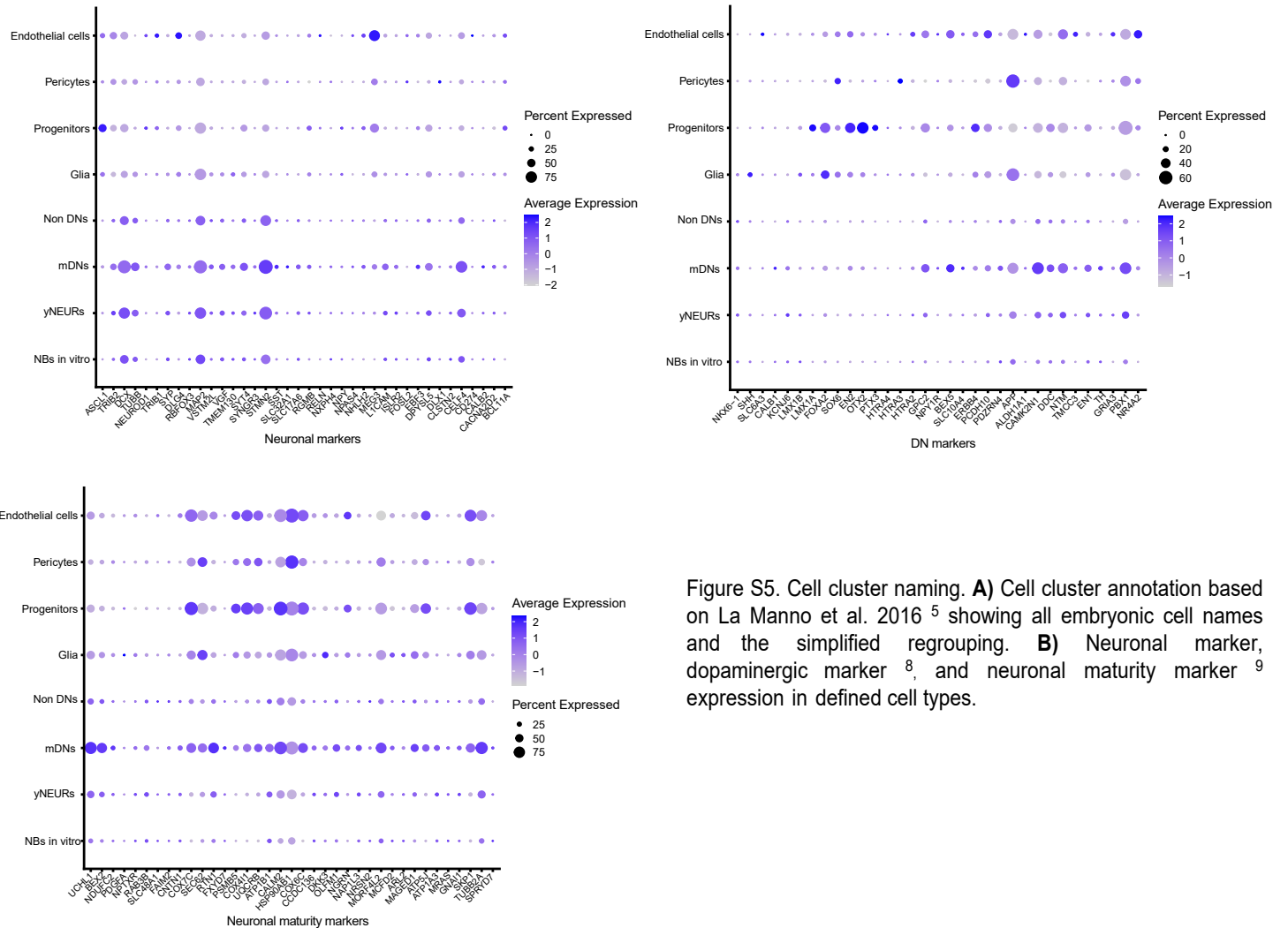


Figure S5. Cell cluster naming. **A)** Cell cluster annotation based on La Manno et al. 2016<sup>5</sup> showing all embryonic cell names and the simplified regrouping. **B)** Neuronal marker, dopaminergic marker<sup>8</sup>, and neuronal maturity marker<sup>9</sup> expression in defined cell types.

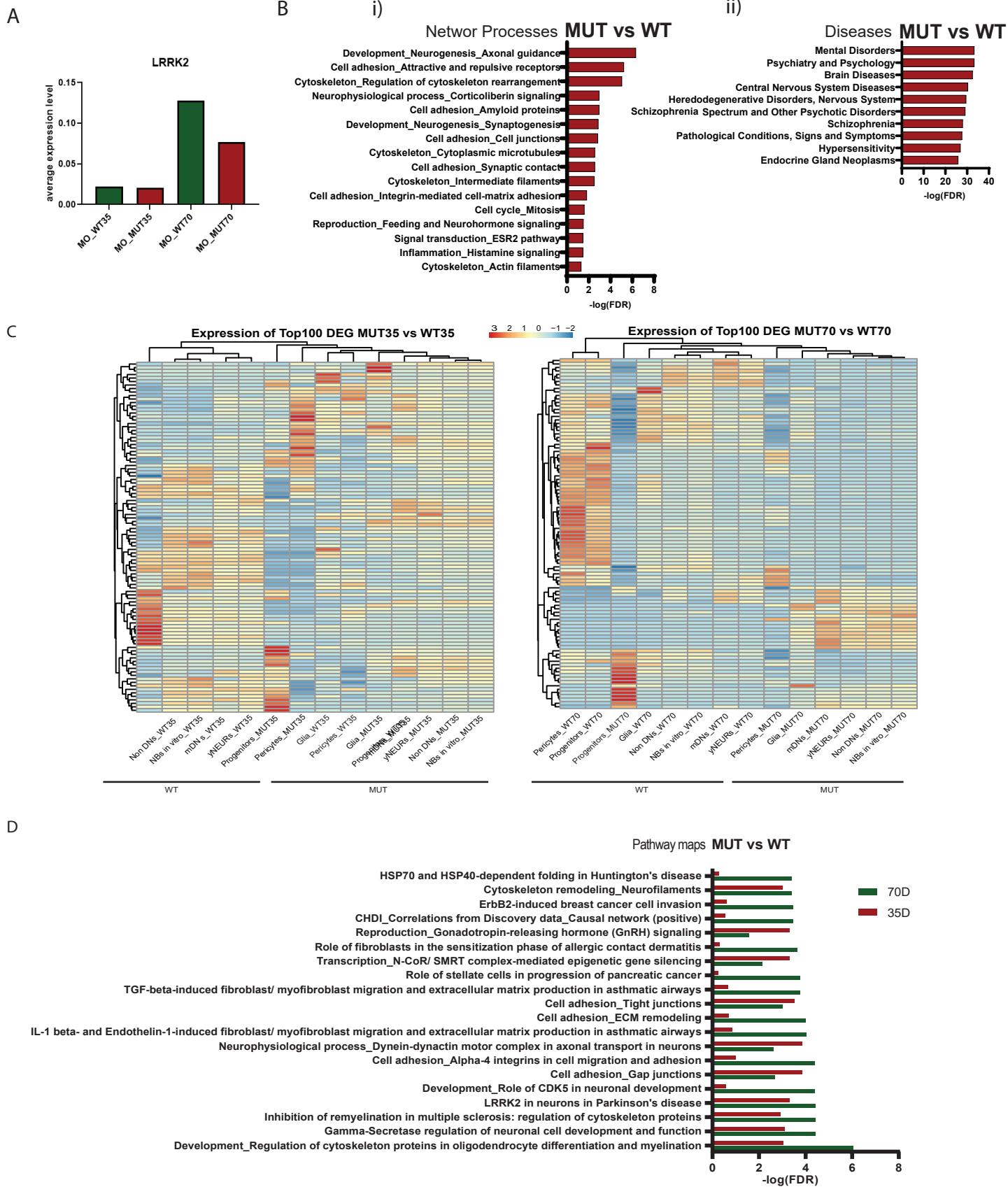
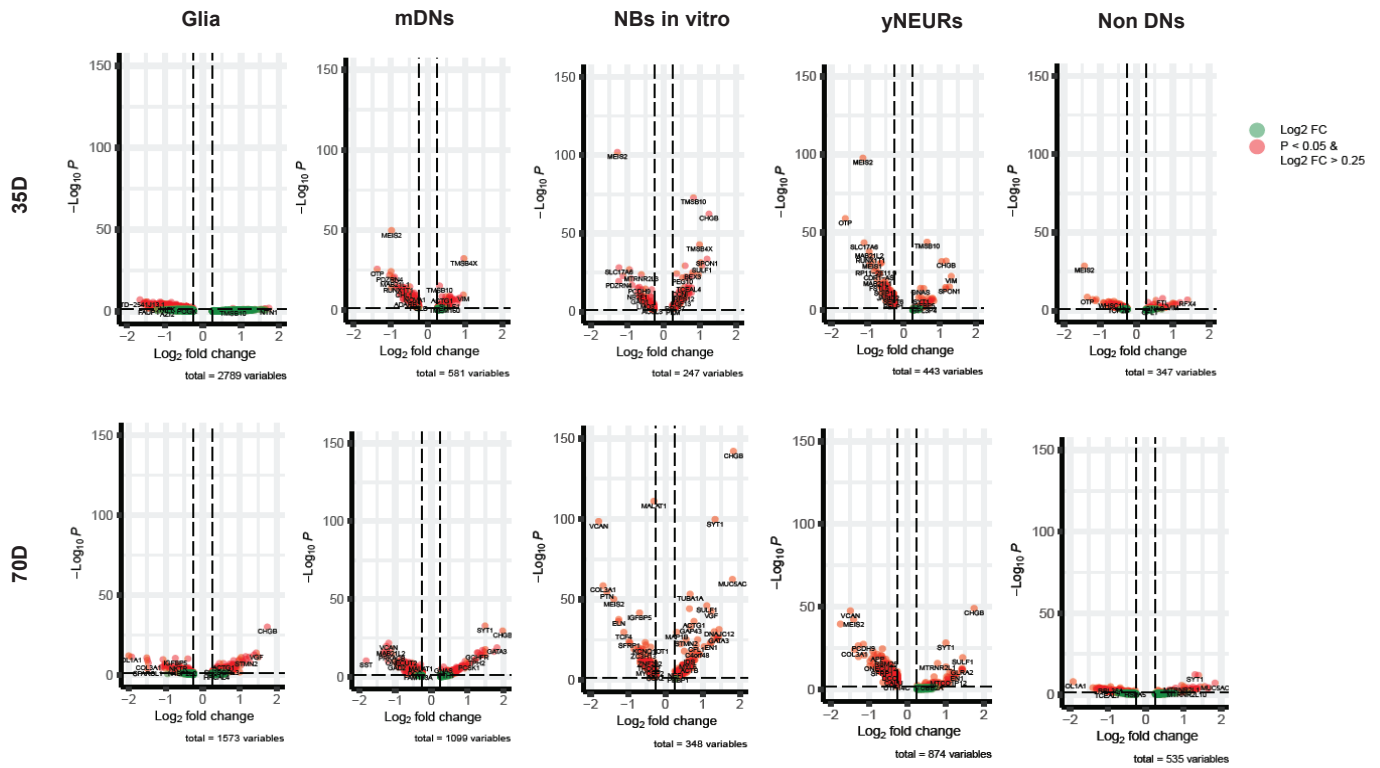


Figure S6. Differentially expressed gene analysis I. **A**) The bulk average *LRRK2* expression in midbrain organoids. **B**) i) Network processes and ii) diseases from the enrichment analysis of 294 DEGs (adjusted p-value < 0.05) between MUT and WT midbrain organoids. **C**) Heatmaps of top 100 DEGs (adjusted p-value < 0.05) at day 35 and day 70 respectively, showing the cell type unsupervised clustering between MUT and WT organoids. **D**) Pathway processes based on MUT vs WT midbrain organoid DEGs (adjusted p-value < 0.05).



A



B

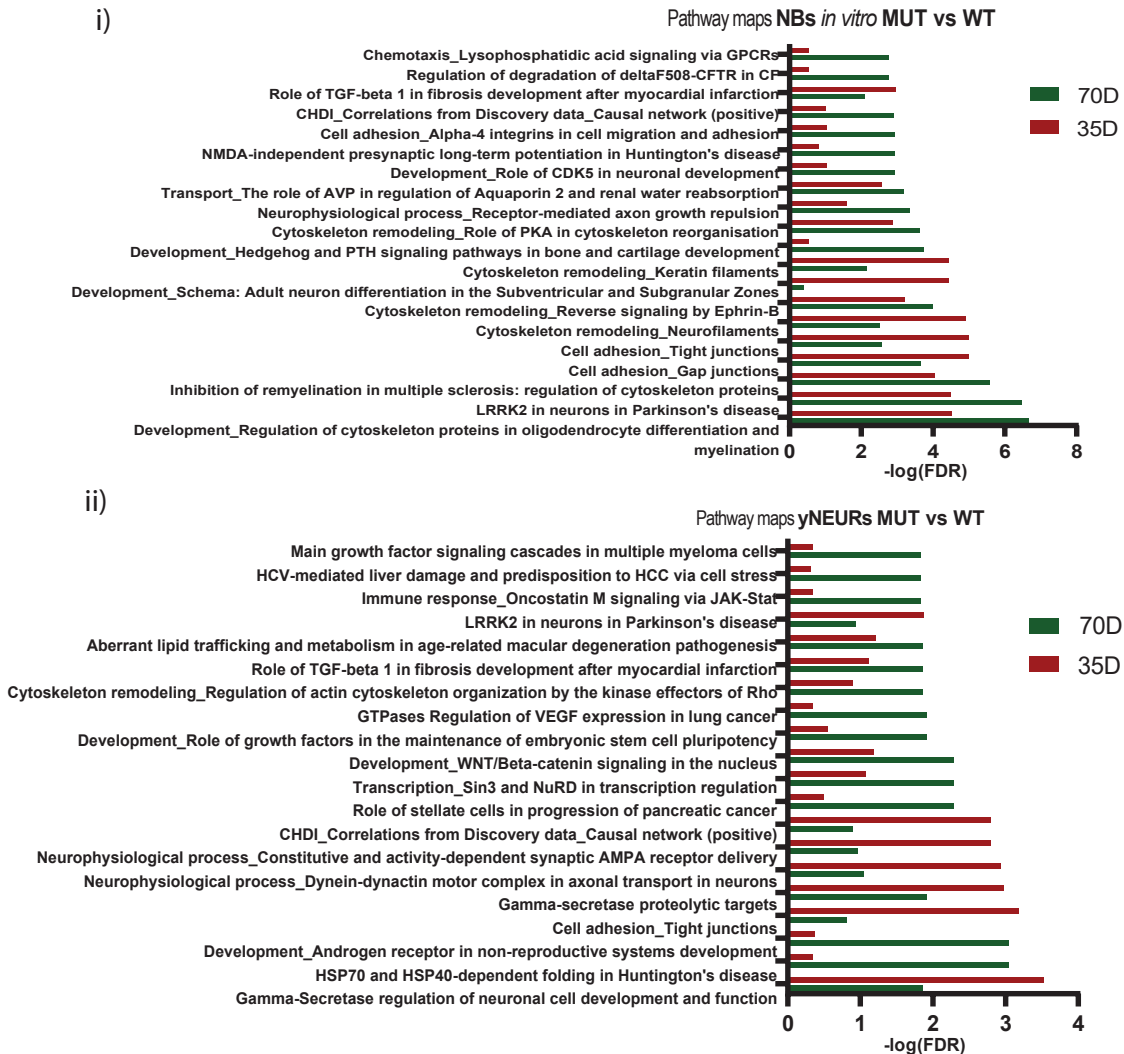


Figure S7. Differentially expressed gene analysis II. **A)** Volcano plots showing DEG fold changes in cell clusters between MUT and WT midbrain organoids. **B)** Pathway enrichment analysis in i) yNEURs and ii) NBs *in vitro* based on the DEGs in the respective cell clusters (adjusted p-value < 0.05).

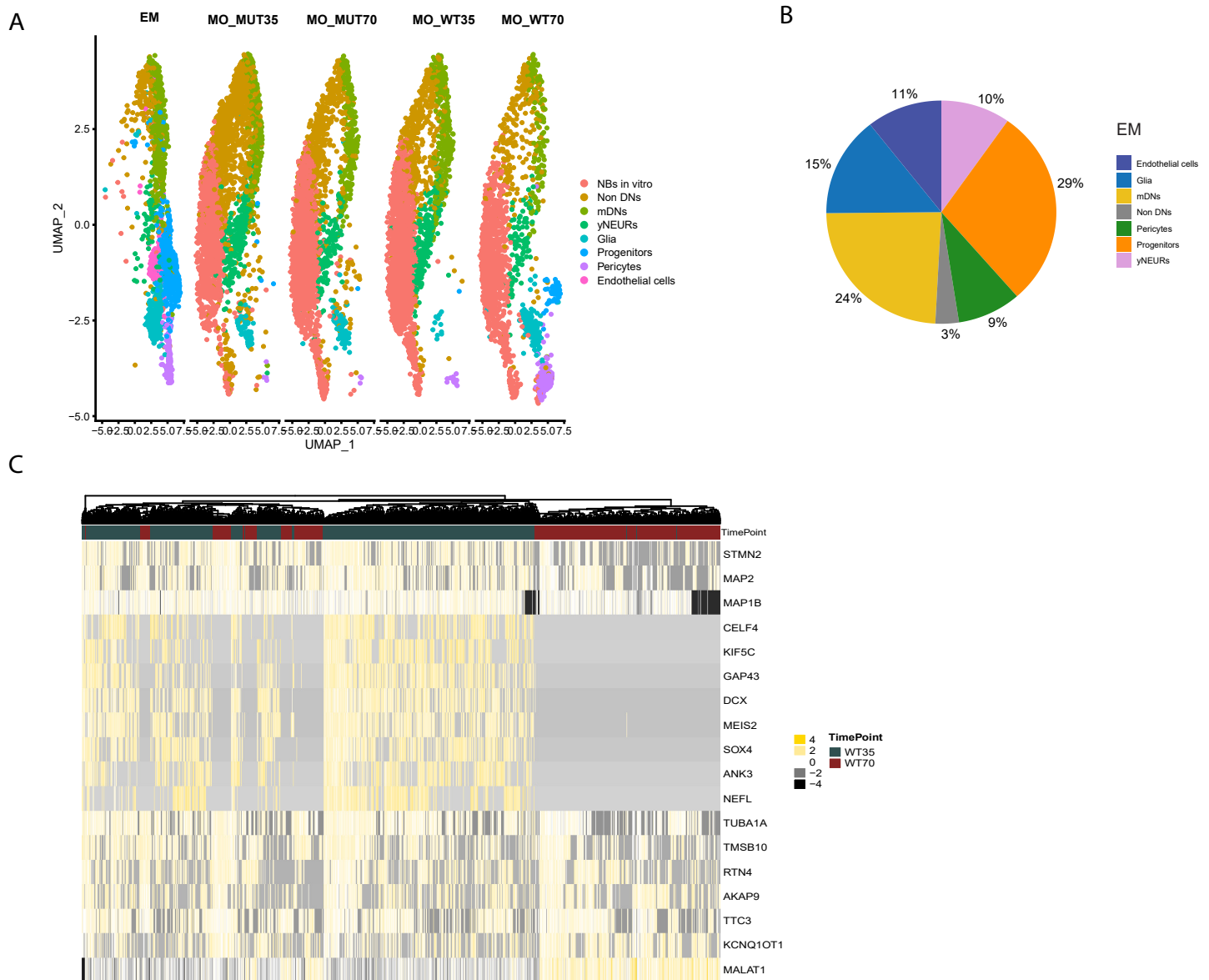


Figure S8. *LRRK2-G2019S* mutant midbrain organoids have a different cellular composition and altered developmental path. **A)** UMAP of integrated Seurat object of merged scRNAseq datasets of embryonic midbrain, and WT and MUT midbrain organoids 35 and 70 days of differentiation, colored by cell clusters and split by the dataset. **B)** Percentage of cell identities present in the embryonic midbrain (EM). **C)** Heatmap of genes with changed expression pattern in at least 50% of cells between WT35 and WT70 midbrain organoids.

<b>Source of iPSCs</b>	<b>Mutation</b>	<b>Age at sampling</b>	<b>Sex</b>	<b>Corresponding midbrain organoid culture</b>
The Wellcome Trust Sanger Institute, Cambridge, UK	-	55	Male	MO_WT35 MO_WT70
The Wellcome Trust Sanger Institute, Cambridge, UK	Introduced LRRK2 G2019S <sup>1</sup>	55	Male	MO_MUT35 MO_MUT70

Table S1. Cell lines used to generate midbrain floor plate neural progenitor cells and further the midbrain organoids for scRNAseq.

## References of Supplemental Data

1. Qing, X., Walter, J., Jarazo, J., Arias-Fuenzalida, J., Hillje, A.L., and Schwamborn, J.C. (2017). CRISPR/Cas9 and piggyBac-mediated footprint-free LRRK2-G2019S knock-in reveals neuronal complexity phenotypes and  $\alpha$ -Synuclein modulation in dopaminergic neurons. *Stem Cell Res.* 24, 44–50.
2. Smits, L.M., Reinhardt, L., Reinhardt, P., Glatza, M., Monzel, A.S., Stanslowsky, N., Rosato-Siri, M.D., Zanon, A., Antony, P.M., Bellmann, J., et al. (2019). Modeling Parkinson's disease in midbrain-like organoids. *Npj Park. Dis.* 5,.
3. Reinhardt, P., Glatza, M., Hemmer, K., Tsytsyura, Y., Thiel, C.S., Höing, S., Moritz, S., Parga, J.A., Wagner, L., Bruder, J.M., et al. (2013). Derivation and Expansion Using Only Small Molecules of Human Neural Progenitors for Neurodegenerative Disease Modeling. *PLoS One* 8,.
4. Smits, L.M., Magni, S., Kinugawa, K., Grzyb, K., Luginbühl, J., Sabate-Soler, S., Bolognin, S., Shin, J.W., Mori, E., Skupin, A., et al. (2020). Single-cell transcriptomics reveals multiple neuronal cell types in human midbrain-specific organoids. *Cell Tissue Res.* 382, 463–476.
5. La Manno, G., Gyllborg, D., Codeluppi, S., Nishimura, K., Salto, C., Zeisel, A., Borm, L.E., Stott, S.R.W., Toledo, E.M., Villaescusa, J.C., et al. (2016). Molecular Diversity of Midbrain Development in Mouse, Human, and Stem Cells. *Cell* 167, 566-580.e19.
6. Zhong, S., Zhang, S., Fan, X., Wu, Q., Yan, L., Dong, J., Zhang, H., Li, L., Sun, L., Pan, N., et al. (2018). A single-cell RNA-seq survey of the developmental landscape of the human prefrontal cortex. *Nature* 555, 524–528.
7. Trujillo, C.A., Gao, R., Negraes, P.D., Gu, J., Buchanan, J., Preissl, S., Wang, A., Wu, W., Haddad, G.G., Chaim, I.A., et al. (2019). Complex Oscillatory Waves Emerging from Cortical Organoids Model Early Human Brain Network Development. *Cell Stem Cell* 25, 558-569.e7.
8. Paisán-Ruiz, C., Jain, S., Evans, E.W., Gilks, W.P., Simón, J., Van Der Brug, M., De Munain, A.L., Aparicio, S., Gil, A.M., Khan, N., et al. (2004). Cloning of the gene containing mutations that cause PARK8-linked Parkinson's disease. *Neuron* 44, 595–600.
9. Ren, C., Ding, Y., Wei, S., Guan, L., Zhang, C., Ji, Y., Wang, F., Yin, S., and Yin, P. (2019). G2019S Variation in LRRK2: An Ideal Model for the Study of Parkinson's Disease? *Front. Hum. Neurosci.* 13, 1–6.

---

# **Manuscript II**

## **Microglia integration into human midbrain organoids leads to increased neuronal maturation and functionality**

Sonia Sabate-Soler<sup>1</sup>, Sarah Louise Nickels<sup>1</sup>, Cláudia Saraiva<sup>1</sup>, Emanuel Berger<sup>1</sup>, Ugne Dubonyte<sup>1</sup>, **Kyriaki Barmpa**<sup>1</sup>, Yan Jun Lan<sup>3,4</sup>, Tsukasa Kouno<sup>3</sup>, Javier Jarazo<sup>1,2</sup>, Graham Robertson<sup>1</sup>, Jafar Sharif<sup>3</sup>, Haruhiko Koseki<sup>3</sup>, Christian Thome<sup>5</sup>, Jay W. Shin<sup>3</sup>, Sally A. Cowley<sup>6</sup>, Jens C. Schwamborn\*<sup>1</sup>

<sup>1</sup> Luxembourg Centre for Systems Biomedicine (LCSB), Developmental and Cellular Biology, University of Luxembourg, Belvaux, Luxembourg.

<sup>2</sup> OrganoTherapeutics SARL-S, Esch-sur-Alzette, Luxembourg

<sup>3</sup> RIKEN Center for Integrative Medical Sciences, Yokohama, Kanagawa 230-0045, Japan.

<sup>4</sup> ETH Zurich, Institute of Pharmaceutical Sciences, Zurich 8057 Switzerland

<sup>5</sup> Institute of Physiology and Pathophysiology, Heidelberg University, Heidelberg, Germany.

<sup>6</sup> Oxford Parkinson's Disease Centre, James Martin Stem Cell Facility, Sir William Dunn School of Pathology, University of Oxford, Oxford, UK.

Contact information: jens.schwamborn@uni.lu

The article has been published in *Glia*.

---

## **Preface**

The proper functionality and development of the human brain depends on the homeostasis of intercellular interactions of neurons, microglia, astrocytes, oligodendrocytes and vasculature (Song, Yan, et al., 2019). Although neurons are the main cell population in the brain, their viability and functionality are highly dependent on the other cell types. Microglia on the other hand constitute approximately 10% of the cellular population in the human brain and they are crucial for the maintenance and functionality of the neuronal networks. Apart from their synaptic support, microglia along with astrocytes are the immune cells of the brain (Q. Li & Barres, 2018). Activation of microglia is necessary for the removal of debris and for fighting pathogens in the brain. However, in neurodegenerative processes microglia can adapt an activated state that leads to chronic neuroinflammation and contributes to disease progression (Muzio et al., 2021). Therefore, it is very important to consider the biological processes that could be affected by microglia in neurodegenerative research.

Midbrain organoids are used extensively in PD research, due to their cellular diversity and better representation of the cellular interactions in the human brain. However, these models are developed through a guided differentiation approach patterned to the neuroectoderm (Nickels et al., 2020; Smits et al., 2019), and they are incapable of developing microglia cells that originate from the mesoderm (Ginhoux et al., 2013).









In this study, we successfully integrated iPSC-derived microglia into midbrain organoids. Extensive characterization of the model with single nuclei RNA sequencing transcriptomic analysis, immunoassays, and electrophysiological assessment, demonstrated that the microglia presence in midbrain organoids is beneficial for the overall functionality of the model. The results of this research facilitate progress towards more physiological relevant models, where the neuroinflammation component in PD could be also considered.

## **Contribution statement**

In this article, I supported the first author by generating and maintaining cultures. At the end of the culture period, I collected samples, and performed protein extraction, Western blots and analysis for the evaluation of the synaptic protein VAMP2 (Figure 6c). I also contributed to the writing of the methodology description of Western blot in the manuscript.

## RESEARCH ARTICLE

# Microglia integration into human midbrain organoids leads to increased neuronal maturation and functionality

Sonia Sabate-Soler<sup>1</sup>  | Sarah Louise Nickels<sup>1</sup>  | Cláudia Saraiva<sup>1</sup>  | Emanuel Berger<sup>1</sup>  | Ugne Dubonyte<sup>1,4</sup>  | Kyriaki Barmpa<sup>1</sup> | Yan Jun Lan<sup>2,3</sup> | Tsukasa Kouno<sup>2</sup> | Javier Jarazo<sup>1,4</sup>  | Graham Robertson<sup>1</sup> | Jafar Sharif<sup>2</sup> | Haruhiko Koseki<sup>2</sup> | Christian Thome<sup>5</sup> | Jay W. Shin<sup>2</sup> | Sally A. Cowley<sup>6</sup>  | Jens C. Schwamborn<sup>1</sup> 

<sup>1</sup>Luxembourg Centre for Systems Biomedicine (LCSB), Developmental and Cellular Biology, University of Luxembourg, Belvaux, Luxembourg

<sup>2</sup>Center for Integrative Medical Sciences, RIKEN, Yokohama, Kanagawa, Japan

<sup>3</sup>ETH Zurich, Institute of Pharmaceutical Sciences, Zurich, Switzerland

<sup>4</sup>OrganoTherapeutics SARM-S, Esch-sur-Alzette, Luxembourg

<sup>5</sup>Institute of Physiology and Pathophysiology, Heidelberg University, Heidelberg, Germany

<sup>6</sup>Oxford Parkinson's Disease Centre, James Martin Stem Cell Facility, Sir William Dunn School of Pathology, University of Oxford, Oxford, UK

**Correspondence**

Jens C. Schwamborn, Luxembourg Centre for Systems Biomedicine (LCSB), Developmental and Cellular Biology, University of Luxembourg, Belvaux, Luxembourg.  
Email: [jens.schwamborn@uni.lu](mailto:jens.schwamborn@uni.lu)

**Funding information**

Fondation du Pelican de Mie et Pierre Hippert-Faber; Fonds National de la Recherche Luxembourg, Grant/Award Numbers: FNR/NCER13/BM/11264123, FNR/PoC16/11559169, INTER/JPND/15/11092422, NCER13/BM/11264123, PRIDE17/12244779/PARK-QC; International Program Associate (IPA); Japanese Ministry of Education, Culture, Sports, Science and Technology (MEXT); RIKEN Integrative Medical Sciences (IMS)

**Abstract**

The human brain is a complex, three-dimensional structure. To better recapitulate brain complexity, recent efforts have focused on the development of human-specific midbrain organoids. Human iPSC-derived midbrain organoids consist of differentiated and functional neurons, which contain active synapses, as well as astrocytes and oligodendrocytes. However, the absence of microglia, with their ability to remodel neuronal networks and phagocytose apoptotic cells and debris, represents a major disadvantage for the current midbrain organoid systems. Additionally, neuroinflammation-related disease modeling is not possible in the absence of microglia. So far, no studies about the effects of human iPSC-derived microglia on midbrain organoid neural cells have been published. Here we describe an approach to derive microglia from human iPSCs and integrate them into iPSC-derived midbrain organoids. Using single nuclear RNA Sequencing, we provide a detailed characterization of microglia in midbrain organoids as well as the influence of their presence on the other cells of the organoids. Furthermore, we describe the effects that microglia have on cell death and oxidative stress-related gene expression. Finally, we show that microglia in midbrain organoids affect synaptic remodeling and increase neuronal excitability. Altogether, we show a more suitable system to further investigate brain development, as well as neurodegenerative diseases and neuroinflammation.

**KEYWORDS**

3D models, brain organoids, inflammation, iPSC, microglia

This is an open access article under the terms of the [Creative Commons Attribution](https://creativecommons.org/licenses/by/4.0/) License, which permits use, distribution and reproduction in any medium, provided the original work is properly cited.

© 2022 The Authors. *GLIA* published by Wiley Periodicals LLC.



## 1 | INTRODUCTION

The human brain is a highly complex organ in terms of structure, molecular and cellular composition, making it a challenging target for research. Three-dimensional (3D) brain models have been recently developed to better mimic the spatial and functional complexity of the human brain. Over the last decade, different protocols were developed to generate either whole-brain organoids (Lancaster et al., 2013; Lindborg et al., 2016) or discrete regions of the brain (Birey et al., 2017; Jo et al., 2016; Monzel et al., 2017; Qian et al., 2016; Shi et al., 2012). These models have proven to be suitable to model neurological disorders, including microcephaly (Lancaster et al., 2013), Batten disease (Gomez-Giro et al., 2019), Parkinson's disease (PD) (Smits et al., 2019), and others (Choi et al., 2014; Qian et al., 2016). In fact, to better model PD recent efforts have focused on the development of PD patient-specific midbrain organoids (Kim et al., 2019; Smits et al., 2019). Mid-brain organoids contain spatially patterned groups of dopaminergic neurons, making them a suitable model to study PD. They consist of differentiated and functional neurons, which contain active synapses, as well as astrocytes and oligodendrocytes (Monzel et al., 2017; Smits et al., 2019). Moreover, they are able to recapitulate cardinal features of PD, including loss of dopaminergic neurons (Smits et al., 2019), and protein aggregation (Kim et al., 2019).

A major feature of neurological disorders is chronic inflammation (Bradburn et al., 2019; Tu et al., 2019). Previous studies have shown integration of iPSC-derived microglia in cerebral organoids (Abud et al., 2017; Muffat et al., 2016). Furthermore, innate differentiation of microglia within whole-brain organoids has also been achieved (Ormel et al., 2018; Ramani et al., 2020). Those systems used iPSCs to generate their cerebral organoids, instead of a neuro-epithelial stem cell population, used normally to generate midbrain region-specific brain organoids. The current midbrain organoid system derived from neuro-epithelial stem cells—with ectodermal origin—lacks microglia, due to their mesodermal origin. The absence of microglia, with their ability to prune neuronal synapses as well as phagocytose apoptotic cells and debris represents a major disadvantage for the understanding of the physiological brain. Additionally, neuro-inflammation-related disease modeling is not possible in a system that lacks microglia.

Microglia, the largest population of immune cells in the brain, are tissue-resident macrophages. In the adult brain they represent 5% to 15% of the adult brain cells, depending on the brain region (Thion et al., 2018). Microglia have a unique ontogeny; they are derived from Yolk sac progenitors in a very early embryonic age (Ginhoux et al., 2010; Li & Barres, 2017; Schulz et al., 2012). Microglia have particular functions during brain development. Among others, they establish contacts with neural progenitors to support neurogenesis and proliferation (Choi et al., 2008; Ueno et al., 2013). In the adult brain, they interact with neurons, astrocytes, and oligodendrocytes, and their major functions are maintenance of brain homeostasis and immune defense. They also interact with synapses, modulating neuronal activity, and perform synaptic pruning (Tremblay et al., 2011; Wake et al., 2009). They phagocytose apoptotic neurons, induce programmed cell death (Witting et al., 2000), guide sprouting blood

vessels, and participate in neuronal maturation (Rymo et al., 2011). Chronic neuroinflammation is one of the neuropathological characteristics of neurodegenerative disorders, including PD (Shabab et al., 2017).

Recent advances have been made to increase the complexity of organoid systems and better recapitulate the complexity of the human brain. This has been achieved with the development of multi-lineage assembloids, which can be generated via region-specific organoid fusion or coculture with cells from different developmental layers (Marton & Pasca, 2020; Pasca, 2019). Here, we describe the stable integration of functional human iPSC-derived microglia into midbrain organoids, which represents a significant advancement of the mid-brain model, increasing its complexity. Moreover, microglia within assembloids express phagocytosis-related genes and release cytokines and chemokines, demonstrating relevant cellular communication abilities. Moreover, we demonstrate that assembloids display a reduction of cell death and oxidative stress-related genes in the system, compared with midbrain organoids without microglia. Furthermore, microglia seem to affect synapse remodeling, and lead to increased electrophysiology properties in neurons. Overall, we have established a stable and reproducible way to integrate functional microglia into midbrain organoids, leading to the next generation of midbrain organoid modeling. Our technology represents a step forward for the understanding and modulation of the complexity of the healthy and diseased human brain, with especial relevance for neuro-inflammatory conditions.

## 2 | MATERIALS AND METHODS

### 2.1 | 2D cell culture

#### 2.1.1 | iPSCs

Generation of iPSCs was performed as described in (Reinhardt et al., 2013). iPSCs (Table S1) were cultured in Matrigel® (Corning, 354277) coated 6-well plates (Thermo Scientific, 140675), using Essential 8 Basal medium (Thermo Scientific, A1517001) supplemented with ROCK Inhibitor (Y-27632, Millipore, SCM075) for the first 24 h after plating. The medium was exchanged on a daily basis. Confluence iPSCs (~70%–90%) split using Accutase® (Sigma, A6964) and plated at around 300,000 cells per well. Neural progenitor cells needed to generate organoids were derived from iPSCs and maintained in culture as described previously (Nickels et al., 2020; Smits et al., 2019). iPSCs were also used to generate Macrophage precursors (van Wilgenburg et al., 2013) and further differentiate them into microglia as described previously (Haenseler, Sansom, et al., 2017).

### 2.2 | Microglia

The 50 K macrophage precursors were plated per well in a glass-bottom 96-glass bottom well plate (IBL Baustoff, 220.230.042). Cells



were cultured with microglia differentiation medium (Advanced DMEM/F12 [Thermo Fisher, 12634010], 1× N2 [Thermo Fisher, 17502001], 1× Pen/Strep [Invitrogen, 15140122], 1× GlutaMax [Thermo Fisher, 35050061], 50 μM 2-mercaptoethanol [Thermo Fisher, 31350-010], 100 ng/ml IL-34 [Peprotech, 200-34], 10 ng/ml GM-CSF [Peprotech, 300-03]). Cells were kept in culture for 10 days, with a medium change every 3–4 days, and then fixed with 4% formaldehyde (Millipore, 1.00496.5000) for immunostaining or used for a phagocytosis or MTT assay.

## 2.3 | 3D cell culture

### 2.3.1 | Midbrain organoid generation and culture

Midbrain organoids generation is described in (Nickels et al., 2020; Smits et al., 2019). Shortly, 6000 cells per well were seeded in an Ultra-Low Attachment 96-well Well plate (Merck, CLS3474) and kept under maintenance conditions (N2B27 medium supplemented with 0.2 mM Ascorbic acid [Sigma, A4544-100G], 3 μM CHIR 99021 [Axon, CT 99021], 0.5 μM Smoothed Agonist [SAG, Stem cell technologies, 73412], 2.5 μM SB-431542 [Abcam, ab120163], 0.1 μM LDN-193189 [Sigma, SML0559]) for 2 days. After that, we started the pre-patterning (day 0 of dopaminergic differentiation) by removing SB and LDN from the medium. Two days after, CHIR concentration was reduced to 0.7 μM. On day 6 of dopaminergic differentiation, the medium was changed into maturation medium (N2B27 plus 0.2 mM Ascorbic acid, 10 ng/ml Brain Derived Neurotrophic Factor, BDNF (Peprotech, 450-02), 10 ng/ml Glial-Derived Neurotrophic Factor, GDNF (Peprotech, 450-10), 1 pg/ml TGF-β3 (Peprotech, 100-36E), 0.5 mM db cAMP (Sigma, D0627-5X1G), 10 μM DAPT (R&D Systems, 2634/10) and 2.5 ng/ml Activin A (Thermo Scientific, PHC9564). Organoids were kept under static culture conditions with media changes every third day until day 15 of dopaminergic differentiation.

## 2.4 | Medium optimization for coculture with macrophage precursors

Two batches of organoids and assembloids were used for the media optimization. Midbrain organoids from line K7 were used as controls. Midbrain organoids from line K7 were cocultured with macrophage precursors, either from line K7, 163, or EPI. Therefore, graphs indicating “Midbrain organoids” refer to K7 midbrain organoids, and “Assembloids” refer to pooled results from K7 organoids cocultured with K7, 163, and EPI microglia separately. For the media test, midbrain organoids and assembloids were cultured in the previously described maturation medium until day 15 of dopaminergic differentiation. Then, independently of the addition or not of macrophage precursors, the medium was kept the same, exchanged by microglia differentiation medium or coculture medium (Table S2; Advanced DMEM/F12, 1× N2 supplement, 1× GlutaMAX™, 50 μM 2-mercaptoethanol, 100 U/ml Penicillin-Streptomycin, 100 ng/ml IL-34, 10 ng/ml GM-CSF,

10 ng/ml BDNF, 10 ng/ml GDNF, 10 μM DAPT and 2.5 ng/ml Activin A). We kept the culture until day 35 of differentiation, fixed with 4% formaldehyde (Millipore, 1.00496.5000) and proceeded to immunofluorescence staining.

## 2.5 | Coculture of midbrain organoids with macrophage precursors

From day 15 of dopaminergic differentiation—when the coculture started—the culture medium of midbrain organoids and assembloids was replaced by coculture medium containing 186,000 freshly harvested macrophage precursor cells per organoid. As described in the previous Methods and Results sections, K7 midbrain organoids were used as controls, and K7 organoids were separately cocultured with macrophage precursors from lines K7, 163, or EPI. The “Assembloids” group on graphs represent the pooled results from organoids cocultured with the K7, 163, and EPI microglia lines. After, the plate was centrifuged at 100g for 3 min to promote the attachment of the cells to the surface of the organoids. Medium was changed every 2–3 days and the system was kept for 20 or 70 days (until day 35 or 85 of dopaminergic differentiation, respectively). Then, organoids and assembloids were snap-frozen for sequencing and protein extraction or fixed with 4% formaldehyde (Millipore, 1.00496.5000) for immunofluorescence staining.

## 2.6 | Phagocytosis assay

For immunofluorescence staining, macrophage precursors were harvested and 30,000 cells per well were plated in 96-glass bottom well plates (IBL Baustoff, 220.230.042) and differentiated into microglia. On day 10, two Zymosan A (*S. cerevisiae*) BioParticles™ (Thermo Fisher, Z23373) per cell were added (60,000 particles/well). Then, cells were incubated for 30 min at 37°C, washed with 1× PBS and fixed with 4% formaldehyde (Millipore, 1.00496.5000). Then fixed samples were used for immunofluorescence staining. For live imaging (Video S1, S2, and S3), 100,000 cells per well were seeded in 8-well Nunc™ Lab-Tek™ Chamber Slides (Thermo Fisher, 177402PK) and immediately imaged.

## 2.7 | Viability assay (MTT)

The 50 K macrophage precursors were plated per well in a 96-glass bottom well plate (IBL Baustoff, 220.230.042). After 10 days of microglia differentiation induction, 10 μl of 5 mg/ml MTT (3-[4,5-dimethylthiazol-2-yl]-2,5-diphenyltetrazolium bromide (Sigma, M2128)) were added to each well. Cells were incubated for 4 h at 37°C. Then, the medium was aspirated and 100 μl of DMSO were added to each well, pipetting vigorously in order to detach and disrupt the cells. Absorbance was measured at 570 nm. Results were compared with midbrain organoid medium (MOm).



## 2.8 | Immunofluorescence staining in 2D

Cells cultured in glass coverslips (150 K cells/well) or 96-well imaging plates were fixed for 15 min with 4% formaldehyde (Sigma, 100496) and washed 3× with PBS. Permeabilization was done by using 0.3% Triton X-100 in 1× PBS for 15 min. The cells were washed three times with PBS and blocked the cells with 3% BSA (Carl Roth, 80,764) in PBS at room temperature. Cells were then incubated in a wet chamber, overnight (16 h) at 4°C with the primary antibodies (diluted in 3% BSA + 0.3% Triton X-100 in 1× PBS). Cells were rinsed three times with PBS and further incubated with secondary antibodies diluted in 3% BSA + 0.3% Triton X-100 in 1× PBS for 1 h at room temperature. After three more PBS washes, the plates were directly imaged and the coverslips were mounted in a glass slide with Fluoromount-G® (Southern Biotech, Cat. No. 0100-01). The antibodies used are listed in Table S3.

## 2.9 | Immunofluorescence staining in 3D

Midbrain organoids and assembloids were fixed with 4% Formaldehyde overnight at 4°C and washed three times with PBS for 15 min. Organoids were embedded in 4% low-melting point agarose (Biozym, Cat. No. 840100) in PBS; 70 μm sections were obtained using a vibratome (Leica VT1000 S). We selected sections coming from the center of the organoids and assembloids, rather than border sections. The sections were blocked with 0.5% Triton X-100, 0.1% sodium azide, 0.1% sodium citrate, 2% BSA and 5% donkey serum in PBS for 90 min at room temperature. Primary antibodies were diluted in 0.1% Triton X-100, 0.1% sodium azide, 0.1% sodium citrate, 2% BSA, and 5% donkey serum and were incubated for 48 h at 4°C in a shaker. After incubation with the primary antibodies (Table S3), sections were washed 3× with PBS and subsequently incubated with secondary antibodies (Table S3) in 0.05% Tween-20 in PBS for 2 h at RT and washed with 0.05% Tween-20 in PBS. Sections were mounted in Fluoromount-G mounting medium on a glass slide.

## 2.10 | Imaging

Qualitative images were acquired with a confocal laser-scanning microscope (Zeiss LSM 710). For quantitative image analysis, the Operetta CLS High-Content Analysis System (Perkin Elmer) was used to automatically acquire 25 planes per organoid section, with a spacing between planes of 1 μm. Images were modified with the ZEN blue Software. For live imaging (supporting videos), the Cell Observer SD and the CSU-X1 Spinning Disc Unit (ZEISS) were used. One hundred frames were acquired in each video using the ZEN blue software, during 3054.06 s (163 line), 3053.27 s (EPI line), and 3053.66 s (K7 line). The videos were processed and modified with Adobe Premiere and Screenpresso softwares in order to obtain a representative time-line of the phagocytosis process. The shown videos represent 29.97 frames per second, resulting in a total

number of 659.34 frames (163 line), 689.31 frames (EPI line), and 449.55 frames (K7 line).

## 2.11 | Image analysis

To measure the area of organoids and assembloids, we used ImageJ. We delimited the perimeter of the organoids and assembloids and used the “Measure” tool to obtain a pixel surface. Surfaces were then compared using Graphpad Prism and displayed as “fold change” in graphs.

For immunofluorescence staining analysis, 3D images of mid-brain organoids and assembloids were analyzed in Matlab (Version 2017b, Mathworks) following (Bolognin et al., 2019; Smits et al., 2019). The in-house developed image analysis algorithms facilitate the segmentation of Nuclei, neurons, and microglia, obtaining as a result the positive pixel surface for a selected marker. To estimate the Iba1 positive cell number, we used the *regionprops* Matlab function in eight sections coming from four assembloids from two different batches. This function detected different a total number of 310 IBA1<sup>+</sup> events. We separated the Hoechst<sup>+</sup> detection by “live nuclei” (bigger and less intense) and “pyknotic nuclei” (smaller and more intense due to the chromatin condensation). A total number of 776 live nuclei and 4178 pyknotic nuclei were detected. After that, we averaged the volume results for IBA1, live nuclei, and pyknotic nuclei, and we added a new line in the main image analysis function to automatically divide the IBA1 Mask (pixel volume) by the averaged IBA1 volume number previously calculated. We did the same for the live nuclei, obtaining then an approximate IBA1<sup>+</sup> cell number, and live nuclei number. We obtained the percentage of IBA1<sup>+</sup> cells following this formula: (IBA1<sup>+</sup> cell number /live nuclei number) × 100. The reason why we used the live nuclei number is that dead cells may lose the IBA1 expression.

## 2.12 | Western blot

Protein was extracted from midbrain organoids from three batches, and from assembloids with microglia from line K7, 163, and EPI from three batches. Protein extraction was done from 5 or 4 pooled organoids using the 1× RIPA buffer (Abcam, ab156034) containing 1× Phosphatase inhibitor cocktail (Merck Millipore, 524629-1ML) and 1× cOmplete™ Protease Inhibitor Cocktail (Sigma, 11697498001). The lysates were sonicated in the Bioruptor (Diagenode) for 10 cycles of 30 s on and 30 s off. The amount of protein was measured using the Pierce BCA Protein Assay Kit (ThermoFisher, 23227) and the BIOTEK Cytation 5 Imaging reader. Then, 30 μg of protein was used from each sample in the western blot; 6× loading buffer containing 0.375 M Tris (MW 121.14 g/mol), 9% SDS, 50% Glycerol, 0.2% Bromphenolblue, 0.3 M DTT was added in each sample and boiled at 95°C for 5 min. The protein samples were loaded into precast polyacrylamide gels (ThermoFisher, NW04120BOX). The iBlot2 device from Invitrogen was used for

transferring the proteins from the gel to PVDF membranes (ThermoFisher, IB24001). The membranes were blocked in 1× PBS containing 0.2% Tween-20 and 5% Milk in for 60 min at RT. Primary antibodies were incubated in 1× PBS containing 0.02% Tween-20, 5% BSA at 4°C overnight. Secondary antibodies were incubated for 60 min at RT in the same buffer as the one for primary antibodies. Enhanced fluorescent signal was detected in the LI-COR OdysseyFc imaging system. Band quantifications were performed with ImageJ and statistics were run using GraphPad Prism. A Mann–Whitney test was run to compare the midbrain organoid against the assembloid group.

### 2.13 | RT-PCR

Between one and three million microglia cells were used per RNA extraction. We used the RNeasy Mini Kit (Qiagen) as well as DNase I Amplification Grade (Sigma-Aldrich) to isolate RNA. After conducting reverse transcription by following the protocol of the High Capacity RNA to DNA Kit (Thermo Fisher Scientific), RT-PCRs were performed using GreenTaq polymerase and 50 ng of cDNA per reaction. An initial denaturing step, 5 min at 95°C, 40 cycles of denaturation for 30 s at 95°C, annealing for 45 s at 55°C (for *Iba-1*, *CD68*, and *TMEM119*) or 61°C (for *RPL37A* and *P2RY12*), extension for 30 s at 72°C and a final extension for 5 min at 72°C. The used primers are listed in Table S4.

### 2.14 | Cytokine and chemokine release assay

Cytokine and chemokine measurements were performed using the Human XL Cytokine Discovery Luminex® Performance Assay (RD Systems, #FCTSM18). We collected supernatants from three mid-brain organoid and assembloid batches and three biological replicates (microglia lines K7, 163, and EPI). When values were too low to be detected, they appeared as “out of range.” In order to consider them statistically, they were assigned the lowest measured value of the standard curve for that metabolite. The statistics were run with three batches and three cell lines for the assembloid group (midbrain organoids vs. assembloids K7, 163, and EPI).

### 2.15 | Metabolomics

For the extracellular metabolomics analysis, we used snap-frozen media from 20 days of coculture old midbrain organoids or assembloids after 48 h of culture. We also incubated coculture media, not in contact with organoids, as a control. Three organoids or assembloids were used per batch, three batches were analyzed, and the three different cell lines were used for the assembloid group. From the measured results, the control (basal medium) was subtracted in order to discriminate secreted (positive numbers) against uptaken (negative numbers) metabolites.

### 2.16 | Polar metabolite extraction, derivatization, and GC–MS measurement

Extracellular metabolites from media samples were extracted using a methanolic extraction fluid (5:1, methanol/water mixture, vol/vol). The water fraction contained two internal standards Pentanedioic acid-D6 ( $c = 10 \mu\text{g/ml}$ ; C/D/N Isotopes Inc.) and [UL-13C5]-Ribitol ( $c = 20 \mu\text{g/ml}$ ; Omicron Biochemicals). Then, 40  $\mu\text{l}$  of medium was added to 240  $\mu\text{l}$  ice-cold extraction fluid. After adding 100  $\mu\text{l}$  ice-cold chloroform, the mixture was shaken for 5 min at 4°C. For phase separation, 100  $\mu\text{l}$  chloroform and 100  $\mu\text{l}$  water were added and vortexed for 1 min. Then, the mixture was centrifuged at 21,000g for 5 min at 4°C; 250  $\mu\text{l}$  of the polar (upper) phase was transferred to GC glass vial with micro insert (5–250  $\mu\text{l}$ ) and evaporated to dry under vacuum at –4°C.

Metabolite derivatization was performed by using a multi-purpose sample preparation robot (Gerstel). Dried medium extracts were dissolved in 30  $\mu\text{l}$  pyridine, containing 20 mg/ml methoxyamine hydrochloride (Sigma-Aldrich), for 120 min at 45°C under shaking. After adding 30  $\mu\text{l}$  N-methyl-N-trimethylsilyl-trifluoroacetamide (Macherey-Nagel), samples were incubated for 30 min at 45°C under continuous shaking.

GC–MS analysis was performed by using an Agilent 7890A GC coupled to an Agilent 5975C inert XL Mass Selective Detector (Agilent Technologies). A sample volume of 1  $\mu\text{l}$  was injected into a Split/Splitless inlet, operating in split mode (10:1) at 270°C. The gas chromatograph was equipped with a 30 m (I.D. 0.25 mm, film 0.25  $\mu\text{m}$ ) DB-5 ms capillary column (Agilent J&W GC Column) with 5 m guard column in front of the analytical column. Helium was used as carrier gas with a constant flow rate of 1.2 ml/min. The GC oven temperature was held at 90°C for 1 min and increased to 220°C at 10°C/min. Then, the temperature was increased to 280°C at 20°C/min followed by 5 min post run time at 325°C. The total run time was 22 min. The transfer line temperature was set to 280°C. The MSD was operating under electron ionization at 70 eV. The MS source was held at 230°C and the quadrupole at 150°C. Mass spectra were acquired in full scan mode ( $m/z$  70 to 700).

### 2.17 | Data normalization and data processing

All GC–MS chromatograms were processed using MetaboliteDetector, v3.220190704 (REF). Compounds were annotated by retention time and mass spectrum using an in-house mass spectral library. The internal standards were added at the same concentration to every medium sample to correct for uncontrolled sample losses and analyte degradation during metabolite extraction. The data set was normalized by using the response ratio of the integrated peak area\_analyte and the integrated peak area\_internal standard. The results correspond to triplicates from three cocultured batches and three biological replicates (midbrain organoids against assembloids with microglia from lines K7, 163, and EPI).



## 2.18 | Patch clamp

Passive and active electrophysiological properties of cells in assembloids (with microglia from line 163) and midbrain organoids were characterized by whole-cell patch-clamp recordings in voltage and current clamp.

Each organoid was transferred from the incubator to a submerged type recording chamber with constant perfusion of carbogen-buffered artificial cerebrospinal fluid (ACSF) at 32°C. The ACSF contained (in mM): 124 NaCl, 3 KCl, 1.8 MgSO<sub>4</sub>, 1.6 CaCl<sub>2</sub>, 10 glucose, 1.25 NaH<sub>2</sub>PO<sub>4</sub>, 26 NaH<sub>2</sub>CO<sub>3</sub> with an osmolarity of 295 mOsm/L. The organoid was fixated between a large diameter pipette and a custom-made platinum harp. Cells were visualized using phase-contrast on an upright BX51 microscope (Olympus, Hamburg, Germany) with a ×60 water-immersion objective. Recording electrodes were pulled using borosilicate glass on a Flaming/Brown P-97 Puller (Sutter Instrument, Novato, CA) to yield a resistance of 3–6 MΩ. The electrode solution contained (in mM): 126 potassium gluconate, 4 KCl, 10 HEPES, 0.3 EGTA, 4 MgATP, 0.3 Na<sub>2</sub>GTP, and 10 phosphocreatine adjusted to pH 7.2 using KOH and to 288 mOsm/L by adding sucrose. Recordings were obtained in voltage and current-clamp mode with an ELC-03XS amplifier (NPI electronic, Tamm, Germany). Signals were low-pass filtered at 3 kHz and digitized with 20 kHz using a Micros 1401MKII AC-converter (CED, Cambridge, UK). Data were collected using the Signal 4.10 software (CED). Voltages were not corrected for the calculated liquid-junction potential of +14.5 mV. Test pulses of –50 pA and 100 ms were applied regularly to control for changes in series resistance.

Putative neurons were visually identified by their size and shape. After obtaining the whole-cell configuration, the resting membrane potential was determined in the current clamp and the cell subsequently stabilized at –70 mV by continuous current injection. To assess active and passive membrane properties, hyper- and depolarizing current steps were injected at increments of 10 pA and of 500 ms length starting from –50 pA. Passive parameters were assessed by the smallest negative current step that yielded a constant plateau potential, which varied due to the heterogeneity of input resistances. To measure maximum firing rates, cells were depolarized by voltage steps of increasing amplitudes until APs started to fail due to sodium channel inactivation (up to +500 pA depending on input resistance). Action potential waveforms characteristics were analyzed for the first action potential that fired 50 ms after the onset of current injections. The voltage threshold was defined as the potential at which the rising slope exceeded 5 mV/ms and amplitudes were measured from threshold to peak. In voltage-clamp mode, cells were held at –70 mV and positive voltage steps of 300 ms duration and 10 mV increments were applied every 5 s. Maximal voltage was +30 mV. The power of voltage-gated cation channels (predominantly sodium) was quantified at –30 mV and used for statistical comparison. Data analysis was performed using Stimfit (Guzman, 2014) and custom-written Python routines. Values were tested for Gaussian distribution by D'Agostino-Pearson omnibus normality test. Unpaired *t* tests were used to assess statistical significance in normally distributed data and

Mann-Whitney tests for non-normally distributed data (indicated as *p* in figures). Outliers deviating 2.5 *SD* were excluded from statistical analysis but indicated in the figures.

The presence of microglia in the recorded assembloids was confirmed using immunohistochemical staining and confocal imaging. Organoids were fixed in 4% formaldehyde and stained for nuclei (Fluoroshield with DAPI, Sigma-Aldrich), neuronal markers (MAP2, Sigma-Aldrich Chemie GmbH), and microglia (anti-Iba1, WAKO Chemicals). Imaging was carried out on an A1 Nikon confocal microscope at the Nikon Imaging Center Heidelberg, Germany.

## 2.19 | Statistical analyses

First, Gaussian distribution was evaluated by performing D'Agostino and Pearson omnibus normality test. According to this distribution, either a one-way analysis of variance (ANOVA) or a Kruskal-Wallis test with a Dunnett's test for multiple comparisons were used to evaluate statistical significance. For the pooled results (organoids against assembloids), gaussian distribution was also tested. Depending on the outcome, an unpaired *t* test or Mann-Whitney test was used to assess the difference between groups. Outliers deviating 2.5 *SD* were excluded from statistical analysis but indicated in the figures. Cells that showed a resting membrane potential above –40 mV and action potentials shorter than 50 mV and wider than 3 ms in half-width were excluded from analysis, assuming that these cells were either not fully matured neurons or recording conditions were poor. The presence of microglia in the recorded organoids was confirmed using immunohistochemical staining and confocal imaging. For the image analysis, a two-way ANOVA, Tukey's multiple comparisons test was performed to evaluate statistical significance. Data are presented as mean ± *SEM*. All analyses were performed with three different biological replicates (assembloids microglia from three different cell lines).

## 2.20 | Multi-electrode array

Forty-eight-well multi-electrode array (MEA) plates (Axion, M768-tMEA-48B-5) were coated as follows: 24 h incubation with 0.1 mg/ml poly-D-lysine (Sigma, P7886) followed by a 24 h incubation with 1 mg/ml laminin (Sigma, L2020). On day 20 of coculture (or 35 days of dopaminergic differentiation), midbrain organoids and assembloids were transferred to 48-well pre-coated MEA plates. Midbrain organoids and assembloids were placed in the center of the wells, and left in the incubator for 25 min to ensure the maximum media evaporation and adherence of the organoids and assembloids to the well bottom. Then, we added 25 μl of Geltrex (Invitrogen, A1413302) to the top, to avoid the detachment from the wells. Data were acquired with an Axion Maestro Multiwell 768-channel MEA System (Axion Biosystems) and using the Axis software (Axon Biosystems). Data were exported and analyzed using the available R script following a published method ([Modamio et al., 2021] see “Resource availability”).

## 2.21 | Single-nuclei RNA sequencing

Five snap-frozen organoids or assembloids from one batch per condition were used to perform single-nuclei RNA sequencing (snRNAseq).

## 2.22 | Data generation

Whole frozen organoids and assembloids (with microglia from lines K7, 163, and EPI) were dissociated for generating single-nuclei gene-expression libraries. The following steps were performed on ice using chilled and freshly prepared buffers. In brief, organoids and assembloids were gently dissociated using 500 ml of 0.1× Lysis Buffer (10 mM Tris-HCl pH 7.4, 10 mM NaCl, 3 mM MgCl<sub>2</sub>, 0.1% Tween-20, 0.1% Nonidet P40 Substitute, 0.01% digitonin, 1% BSA, nuclease-free water) by pipetting 10X with a wide-pore 1000 µl pipette, followed by a 10-min incubation period on ice. This was repeated for two cycles. To reduce batch effects and increase the number of nuclei per experiment, material from four different organoids or assembloids were pooled for each group. Cells were filtered through a 40-µm strainer using 300 µl at a time, using a new 40-µm strainer. The same procedure was done with 20-µm (Sysmex, AN777717) and 10-µm (Sysmex, AP275603) strainers, followed by centrifugation for 5 min at 500g, at 4°C. Nuclei were then stained using Hoechst 33342 (1:2000) for 5 min at room temperature and counted on the Countess II.

Using Diluted Nuclei Buffer (10x Genomics, 2,000,153) each sample was adjusted to a concentration of 4000 nuclei/µl. We generated one library for each sample, aiming for 6000 nuclei. Single-nuclei experiments were performed using the 10x Genomics Next GEM Single Cell 5' Library Kit v1.1 (1000168) to encapsulate nuclei and amplify cDNA, to generate sequencing libraries. Each library was barcoded using i7 barcodes provided by 10x Genomics. cDNA and sequencing library quality and quantity were determined using Agilent's High Sensitivity DNA Assay (5067-4626) and KAPA (KK4824). Final libraries were pooled, loaded on two lanes of the Illumina's HiSeq X, and sequenced in 150PE mode.

## 2.23 | Count matrix generation

Following steps are performed on default settings if not otherwise specified. Single-nucleus libraries were demultiplexed based on their i7 index sequences and for each library mapping to the human genome was performed using the Cell Ranger 4.0.0 software and human reference GRCh38 3.0.0, both provided by 10x Genomics. Next, count matrix files for each sample were generated using cell ranger count.

## 2.24 | Data preprocessing

Since the material coming from assembloids with the EPI microglia line was lost, count matrixes for the assembloids with K7 and

163 microglia, as well as the midbrain organoid control were uploaded and Seurat Objects were created. Data were preprocessed as described by [https://satijalab.org/seurat/v3.2/pbmc3k\\_tutorial.html](https://satijalab.org/seurat/v3.2/pbmc3k_tutorial.html). An independent data quality control was performed of all three objects, by checking levels of ribosomal genes, and by removing cells with a high mitochondrial gene fraction (Lake et al., 2019; Osorio & Cai, 2021). Moreover, cells containing less than 100 or more than 5000 (100 < RNA n Feature < 5000) genes were removed from the analysis, being considered empty droplets or doublets, respectively. After quality assessment all three objects were combined, log normalized, scaled, and a linear dimensional reduction was performed (PCA). Dimensionality was assessed (20) and cells were clustered with a resolution of 0.5. A nonlinear dimensional reduction using "umap" was performed, and cluster markers were assessed. Cluster names were defined by their characteristic marker gene expression.

## 2.25 | Cell type identification

Cell clustering was performed based on the top 20 principal components using Louvain algorithm modularity optimization with a resolution of 0.5. UMAP was used for cell cluster visualization (Becht et al., 2018). The distinct cell clusters were identified in the UMAP plot. For cell type identification, binarized gene list across cell types from La Manno et al., 2016 was used. This list of genes comprises information about the marker genes in a binarized manner, where 1 means that gene is marking a specific cell population and 0 means that it cannot be considered as a marker gene. For more details on how this list is generated please refer to La Manno et al., 2016. Expression of each cluster defining gene was overlapped with the marker gene (1) in the La Manno marker matrix. Cell types were assigned based on the highest number of major cluster marker genes being expressed in the respective clusters. Cellular subtypes were verified and grouped in neuronal identity clusters based on neuronal marker gene lists (Table S5). (Chen et al., 2016; Smits et al., 2020). Moreover manual marker verifications were done using known marker genes for each cluster. For instance, RGLs expressed *SLC1A3* (*Glast*). MidNECs expressed midbrain markers *SHH*, *LMX1A*, and *FOXA2* and stem cell markers *SOX2* and *MSI1* (*Musashi*). PROG highly expressed *VIM* (*Vimentin*) and lower levels of stem cell markers. NB were positive for young neuronal markers *DCX* (*doublecortin*) and *STMN1* (*sthaminin*) without expressing mature neuronal markers. YDN&CN still expressed *DCX* and *STMN1* but also some mature neuronal markers for synapses such as *SYP* (*synaptophysin*) and subtype specification markers such as *TH* (dopaminergic neurons) and *SLC18A3* (cholinergic neurons). Mature neurons expressed low levels of *STMN1* and *DCX* but high levels of *SYP*. Subtype specification revealed that mDN(A10) & GaN&GIN expressed high levels of genes that define neurons from the ventral tegmental area (VTA). Besides, cells expressing dopaminergic marker *TH* also expressed the marker for A10 DN *CALB1*, as well as *ADCYAP1*. Moreover, the glutamatergic *SLC18A1* and GABAergic *GAD1* transporters were highly expressed in these neurons. Last mDN(A9)&SN were qualified by high amounts of *TH* and *KCNJ6*



(*Girk2*) as well as DN defining synaptic markers *ROBO1*. Moreover, also serotonergic transporters *SLC18A2* were expressed in that cluster. Microglial cells expressed *IBA1*. Cell type proportions were calculated by counting the cells of each cluster. A spearman correlation and a heatmap clustering (pheatmap) were performed on the average expression of clusters defining genes. Because of a substantial sample loss during sample processing, that affected the microglia cell count, 26 microglial cells were detected (Table S6). The microglial cluster, 26 cells, was subsetted and an independent analysis was performed. The top 100 genes defining the microglial cluster are shown in a heatmap. Moreover, the average gene expression across all microglial cells was exported, and representative genes (Galatro et al., 2017), are presented in a violin plot. Significances were calculated based on a one sample Wilcoxon test  $*p < .05$ . The same was done for genes involved in the phagocytic pathway. Cytokines and chemokines were represented in a heatmap.

## 2.26 | Differential expressed gene and enrichment analysis

The most variable features were identified and a heatmap clustering (pheatmap) was performed on the average expression of the top 100 most variable genes. DEG were identified between assembloids and midbrain organoids. This was done for all the cell types together and each cell type independently. Data of the DEG lists are represented in heatmaps (top 100), or underwent metacore enrichment analysis. Metacore analysis was based on the following arbitrary threshold  $p < .05$ , adj  $p < .5$ . Moreover, Venn diagrams were formed using nVenn <http://degradome.uniovi.es/cgi-bin/nVenn/nVenn.cgi>. Genes involved in the enriched pathways are shown separately in box plots. Statistics were performed using a Wilcoxon test  $p < .05^*$ .

## 3 | RESULTS

### 3.1 | hiPSC-derived microglia express specific markers and are functional

The work presented here is based on the use of quality controlled hiPSC lines (lines: K7, 163, EPI, Table S1) from three different healthy individuals that express the pluripotency markers SSEA-4, OCT-4, TRA-1-60, NANOG, TRA-1-81, and SOX2 (Figure S1A). We started by deriving macrophage precursors from hiPSCs that were then differentiated into microglia for 10 days, as previously described (Haenseler, Zambon, et al., 2017). hiPSC-derived microglia in monoculture expressed macrophage-specific markers, including IBA1, PU1, and CD45, and microglia markers, notably TMEM119 and P2RY12, as detected by immunostaining (Figure 1a). Moreover, PCR confirmed that microglia also expressed the macrophage specific genes *IBA1* and *CD68*, and the microglia-specific genes *TMEM119* and *P2RY12* (Figure 1b). After confirming the microglia cell identity, we next assessed their phagocytic capacity. Incubation of microglia with

Zymosan particles showed the cells' ability in phagocytosing these particles, detectable within their cell bodies (Figure 1c, Figure S1B, Video S1, S2, and S3).

A major challenge in assembloid generation is the compatibility of cell culture conditions for different cell types. In order to assess the microglia compatibility with the organoid culture medium, we first examined the toxicity of each midbrain organoid medium supplement on microglia survival. Macrophage precursors were cultured for 10 days with organoid maturation medium (containing BDNF, GDNF, TGF $\beta$ 3, db cAMP, DAPT, and Activin A), microglia differentiation medium (containing IL-34 and GM-CSF), or microglia medium individually supplemented with each of the neurotrophic factors contained in the organoid medium. After 10 days of exposure to the different media, an MTT viability assay showed a significant decrease in cell viability in the presence of TGF $\beta$ 3 ( $69.18\% \pm 8.371$ ,  $p = .0024$ ), db cAMP ( $47.10\% \pm 8.371$ ,  $p < .0001$ ) and Activin A ( $76.01\% \pm 8.371$ ,  $p = .0292$ ) compared with microglia medium (Figure 1d,e). After only 7 days of exposure, an impairment of differentiation and a lower viability were already observed visually in the cells cultured with organoid medium as well as the microglia medium supplemented with TGF $\beta$ 3 or db cAMP (Figure 1e). These results indicate that the midbrain organoid medium, containing TGF $\beta$ 3, db cAMP, and Activin A might not be suitable for the cultivation of microglia containing midbrain organoids.

### 3.2 | The coculture medium allows an efficient integration of functional microglia and expression of midbrain specific neuronal markers in assembloids

After testing the organoid medium on microglia, we next assessed the effects of the different media compositions on the neuronal population of midbrain organoids. Taking into consideration the cytotoxic effect on 2D monoculture microglia, we combined the microglia differentiation medium with the least microglia-toxic neurotrophic factors from the organoid maturation medium. Hence, we supplemented the microglia differentiation medium with BDNF, GDNF, DAPT, and Activin A and refer to this medium combination as the "coculture medium" (Table S2). In order to study the effects of the coculture medium on the organoids, we used midbrain organoids from the line K7 as a control, and three groups of assembloids represented in Figure 1f (The "assembloids" group in graphs represents the pooled results from the three cocultured groups). We cultured those groups with midbrain organoid medium, microglia differentiation medium or coculture medium for 20 more days (Figure 1f). As expected, the IBA1 positive microglial population was significantly reduced when organoid medium was used, whereas no difference was observed when cultured with microglia or coculture medium (Figure 1g, Figure S1C). Interestingly, we observed a significant decrease in TH positive neurons in both midbrain organoids and assembloids in the presence of microglia differentiation medium (Figure 1h, Figure S1C). This decrease was not observed in the MAP2 positive pan neuronal population (Figure S1D, Figure 2c, and Figure S1I). The reduction of

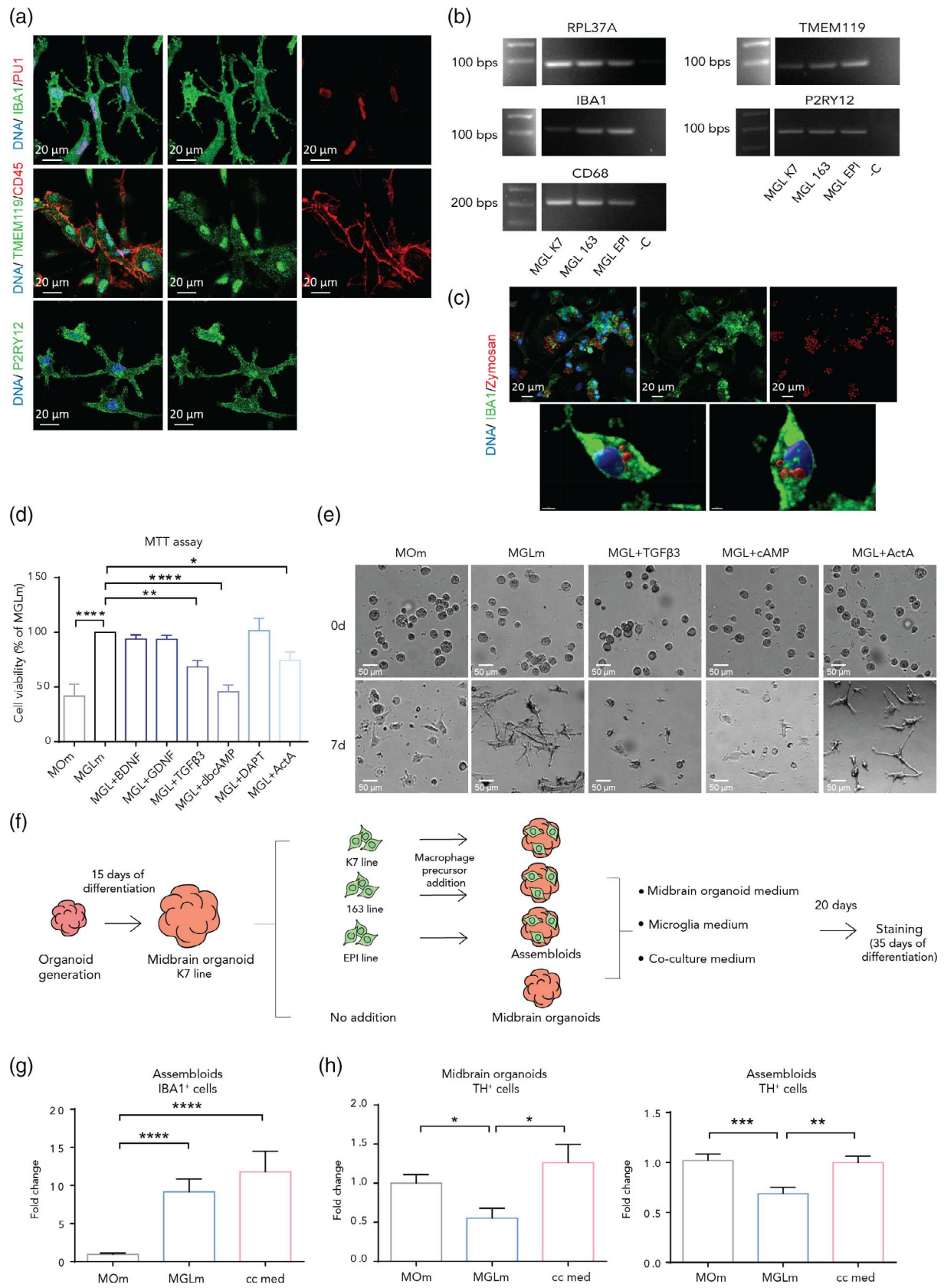


FIGURE 1 Legend on next page.

TH positive cells indicates an impairment of dopaminergic neuron differentiation under microglia medium culture conditions. Notably, in the presence of coculture medium, the levels of TH in both midbrain organoids and assembloids remained at similar levels as for the organoids cultured with midbrain organoid maturation medium (Figure 1h, Figure S1C).

After successfully optimizing the coculture conditions, midbrain organoids were generated using a pure ventral midbrain-patterned NESC population (Figure S1E) from the hiPSC line K7 (Nickels et al., 2020; Smits et al., 2019). After 2 days of maintenance, and 15 days of dopaminergic neuron differentiation induction, we proceeded to the cocultures (Figure 2a). They were performed using K7 midbrain organoids as controls, and co-culturing K7 organoids with K7 macrophage precursors, with 163 macrophage precursors or with EPI macrophage precursors (following Figure 1f excluding the media testing). During the whole study, we did not observe any major line specific differences. During the coculture, the macrophage precursors first aggregated, forming smaller round colonies that attached to the surface of the organoid and then incorporated within that same structure (Figure S1F).

After 20 days of coculture (35 days of dopaminergic differentiation), we validated the incorporation of microglia into the organoids by IBA1 immunostaining. We then assessed the percentage of IBA1 positive cells in assembloids using a previously published computer-assisted image analysis pipeline for marker identification and quantification with small modifications (Smits et al., 2019). On average, 6.4% of the assembloid cells were IBA1 positive (Figure 2b). The morphology of the incorporated microglial cells varied between round and partially ramified (Figure S1G). We confirmed the presence of a neuronal population by a Beta-tubulin III (TUJ1) staining, and assessed further neuronal differentiation by MAP2 staining. In addition, FOXA2 positive midbrain specific dopaminergic neuron precursors and TH positive differentiated dopaminergic neurons were observed in assembloids (Figure 2c, Figure S1I). After culturing the assembloids for 70 days, we further confirm the presence of a GFAP positive astrocytic population in the assembloids (Figure S1H).

### 3.3 | Single nuclear RNA-sequencing reveals eight different cell populations within midbrain-microglia assembloids

In order to further characterize the microglia within assembloids we performed single nuclear RNA-sequencing (snRNA-Seq). Separation of clusters in cells coming from midbrain organoids and assembloids clearly showed that the microglia cluster is specific for assembloids and not present in midbrain organoids (Figure 2d). Cell types were identified based on marker gene expression from la Manno et al. (2016). Moreover, the identified cell clusters were validated and neuronal subtypes were specified (Figure S2 and Table S5). Quality controlled clustering of single cells (Figure S3) showed eight different cell types: radial glia (RGL), midbrain specific neural epithelial stem cells (midNESC), neuronal progenitors (PROG), neuroblasts (NB), young dopaminergic and cholinergic neurons  $\gamma$ DN&CN, mature A10 specific dopaminergic neurons, GABAergic and glutamatergic neurons (mDN(A10)&GABA&GLUT), mature A9 specific dopaminergic neurons and serotonergic neurons (mDN(A9)&SN) as well as microglia (MGL, Figure S3).

Proportions of the different clusters in midbrain organoids and assembloids are represented in pie charts (Figure 2e). midNESC were the most prominent cell type by representing 35% of total cells. More than 60% of the organoid and assembloid cells showed neuronal identity (corresponding to the groups NB,  $\gamma$ DN&CN, mDN(A10)&GIN&Gan, and mDN(A9)&SN). Less than 5% were represented by glial cells (astrocytes, oligodendrocytes, and microglia) at this stage of differentiation. Because of a considerable sample and cell loss, we believe the proportion of microglia cells represented in the Figure 2e is not accurate. However, we proceeded with the analysis of microglial identity and functionality-related genes, as well as for the other cell clusters. Progenitors were closest to neuroblasts and young neurons, whereas radial glial cells were very similar to midNESCs. The different mature neuronal groups clustered together. Clustering of the marker genes showed the relation between different cell clusters (Figure 2f). As expected, MGL cells clustered apart from all other cell

**FIGURE 1** iPSC-derived microglia express specific markers, have phagocytosis ability and are compatible with the engineered coculture medium. (a) Immunofluorescence staining of microglia from line 163 for IBA1, PU.1 (upper panels), TMEM119 and CD45 (middle panels) and P2RY12 (bottom panels). (b) IBA1, CD68, TMEM119, and P2RY12 gene expression in microglia from the three used lines. The ribosomal protein RPL37A coding gene was used as a housekeeping gene due to its stable expression. (c) Immunofluorescence staining of microglia from the EPI line for IBA1 and Zymosan (upper panels). For lines K7 and 163 see Figure S1B). 3D reconstruction of a microglia cell from the line K7 with Zymosan particles in its cytoplasm (bottom panels, scale bar left = 4  $\mu$ m, scale bar right = 3  $\mu$ m). (d) Cell viability of 2D microglia from lines 163 and EPI (MTT assay) after 10 days of treatment with midbrain organoid media (MOM) or microglia medium (MGLm) without further supplementation or supplemented with neurotrophic factors. ( $n = 3$ , 3 batches). (e) Representative bright field images of the microglia morphology (line 163) at day 0 and 7 of culture with MOM, MGLm, MGLm supplemented with TGF $\beta$ 3 (MGL + TGF $\beta$ 3), with cAMP (MGL + cAMP), or with Activin a (MGL + ActA). (f) Schematic diagram of the steps for the media optimization in assembloids and midbrain organoids. (g) IBA1 positive (IBA1<sup>+</sup>) population in assembloids upon culture with MOM, MGLm or coculture medium (cc med). Y-axis represents the fold change with respect to the control (MOM). (h) TH positive (TH<sup>+</sup>) neuron population in midbrain organoids (left) and assembloids (right). Y-axis represents the fold change with respect to the control (MOM) ( $n$  [midbrain organoids] = 2, 2 batches,  $n$  [assembloids] = 5, 2 batches and three cell lines). Data are represented as mean  $\pm$  SEM. \* $p < .05$ , \*\* $p < .01$ , \*\*\* $p < .001$ , \*\*\*\* $p < .0001$  using a two-way ANOVA with Dunnett's multiple comparisons test. Abbreviations: BDNF, brain-derived neurotrophic factor; GDNF, glial cell-derived neurotrophic factor; TGF $\beta$ 3, transforming growth factor beta-3, cAMP, cyclic adenosine monophosphate; ActA, activin A



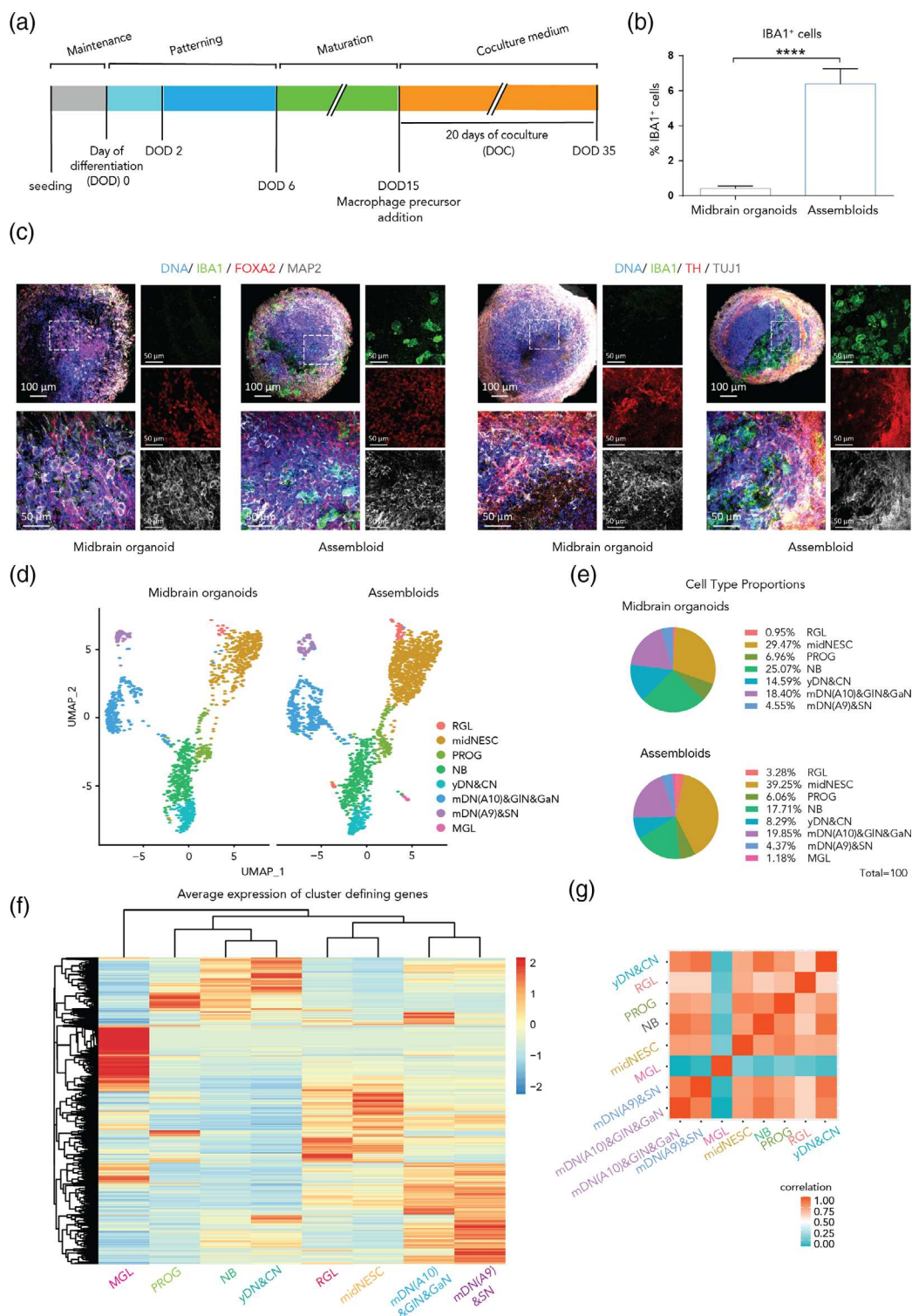


**FIGURE 2** The coculture medium allows a successful microglia integration and seven other neural cell populations in assembloids. (a) Timeline of the coculture of midbrain organoids with macrophage precursors. DOD = day of differentiation, DOC = day of coculture. (b) IBA1 positive (IBA1<sup>+</sup>) cell percentage in midbrain organoids and assembloids. Assembloids present around 6.4% of IBA1<sup>+</sup> cells ( $n$  [midbrain organoids] = 5, 5 batches,  $n$  [assembloids] = 15, 5 batches, 3 cell lines). Data are represented as mean  $\pm$  SEM. (c) Immunofluorescence staining of midbrain organoids and assembloids with microglia from the line K7 for IBA1, FOXA2 and MAP2 (left panels), and for TH and TUJ1 (right panels). For lines 163 and EPI see Figure S1H. (d) UMAP visualization of scRNA-seq data—split by microglial presence—shows eight different defined cell clusters in assembloids. RGL, radial glia; midNESC, midbrain specific neural epithelial stem cells; PROG, neuronal progenitors; NB, neuroblasts; yDN&CN, young dopaminergic and cholinergic neurons; mDN(A10)&gaN&GIN, mature A10 specific dopaminergic neurons, gabaergic and glutamatergic neurons; mDN(A9)&SN, mature A9 specific dopaminergic neurons and serotonergic neurons, MGL, microglia. (e) Proportions of different cell types in midbrain organoids and assembloids. (f) Average expression of cluster defining genes in assembloids. (g) Spearman's correlation between different cell types in assembloids. \* $p$  < .05, \*\* $p$  < .01, \*\*\* $p$  < .001, \*\*\*\* $p$  < .0001 using a Kruskal-Wallis one-way ANOVA with Dunn's multiple comparisons test (for MGLm and cc med vs. MOm), and a Mann-Whitney test (for MGLm vs. cc med) in (a) and (b), and a Mann-Whitney test in (e)

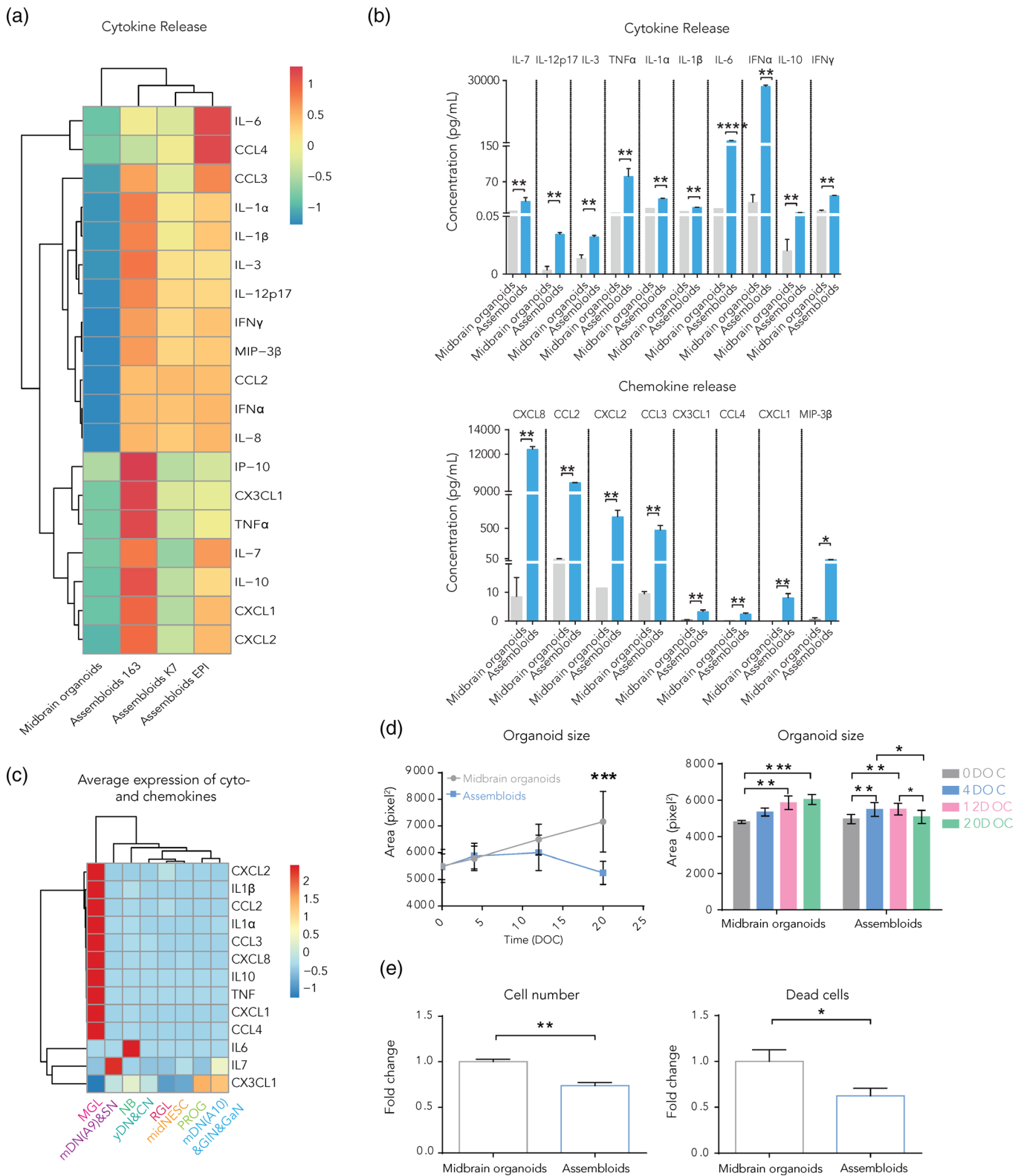


**FIGURE 3** Microglia in assembloids have phagocytic capacities and release cytokines and chemokines. (a) Heatmap representing the measured levels of cytokines and chemokines in cell culture media (pg/ml) shows two different clusters corresponding to midbrain organoids and assembloids ( $n = 9$ , 3 batches, 3 lines). (b) Cytokine (upper graph) and chemokine (bottom graph) levels in midbrain organoids and assembloids ( $n = 9$ , 3 batches, 3 lines). (c) Average expression of cytokine and chemokine genes across cell types. (d) Organoid surface area in midbrain organoids and assembloids over time (left graph,  $n = 3$ , 3 batches). Comparison of the organoid size, measuring the same organoids and assembloids, in four time points during culture (right graph,  $n = 3$ , 3 batches). (e) Cell number (total nuclei count, left panel) and dead cells (pyknotic nuclei, right panel) in midbrain organoids and assembloids after 20 days of culture ( $n$  [midbrain organoids] = 5, 5 batches,  $n$  [assembloids] = 15, 5 batches, 3 lines). Data are represented as mean  $\pm$  SEM. \* $p < .05$ , \*\* $p < .01$ , \*\*\* $p < .001$ , \*\*\*\* $p < .0001$  using a Mann-Whitney test in (a) and (b), a multiple t test with the Holm-Sidak method for (d) (left panel), a two-way ANOVA with Tukey's multiple comparisons test for (d) (right panel) and a Mann-Whitney test in (e)

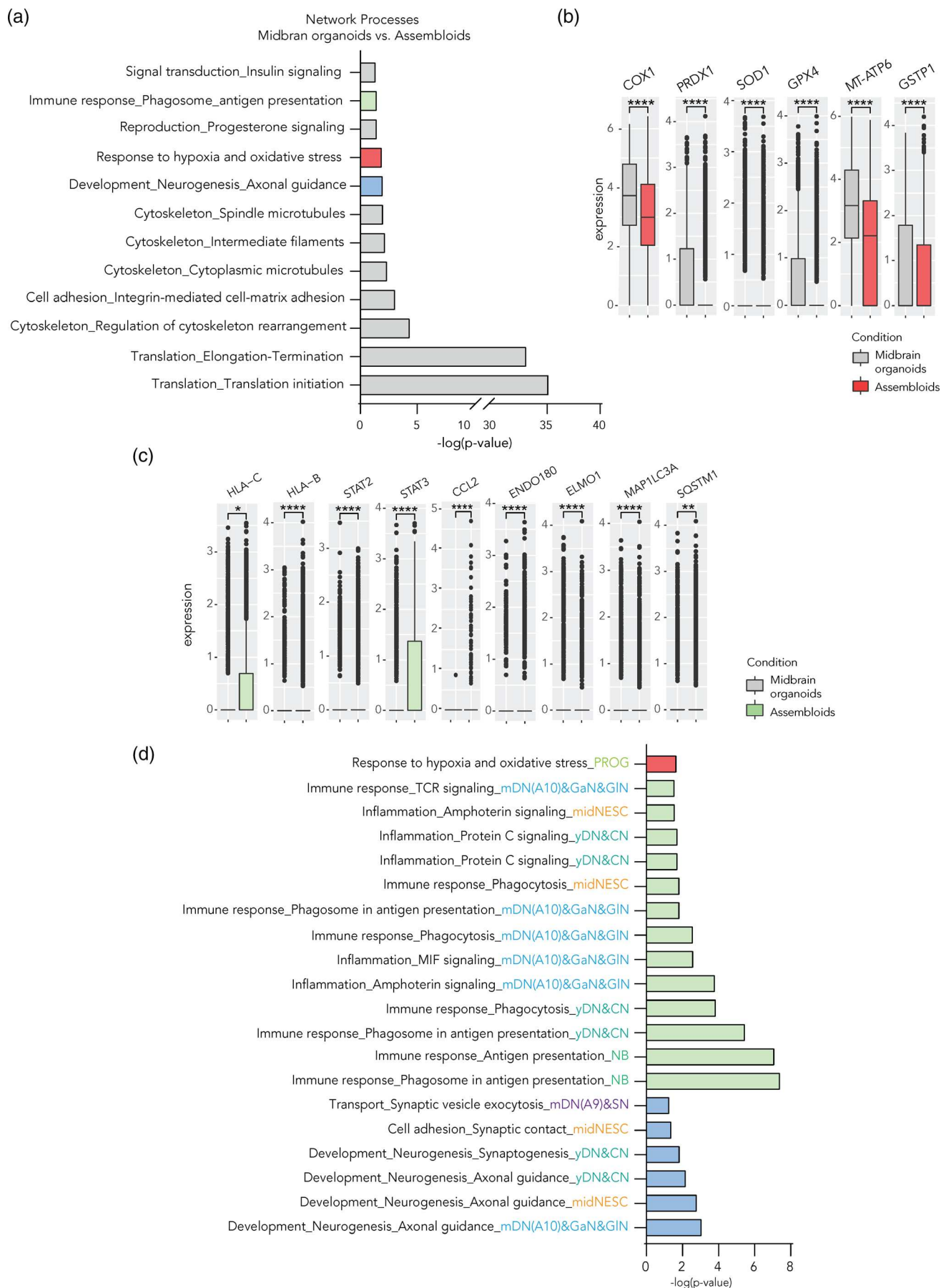


FIGURE 4 Legend on next page.



types. A distinct genetic signature of the microglia cells was further validated by a Spearman correlation analysis (Figure 2g).

### 3.4 | Microglia in assembloids show a typical immune cell signature

Next, we aimed at identifying gene signatures unique to microglia in comparison to the other cell types in assembloids. Firstly, we used the expression of the 100 most variable genes obtained from the snRNA-Seq analysis to cluster the different cell populations observed in assembloids (Figure S3A). Indeed most variability between cells clusters came from the microglia, which had a completely different genetic signature (Figure S4A). Then, we identified the top 100 markers defining microglia identity (Figure S4B). From those, several canonical marker genes were chosen in order to characterize the main functions of microglia. General microglia marker genes such as *IBA1* and *PU1* were significantly and specifically expressed in microglia. In addition, the microglia core signature revealed genes involved in antigen presentation (*HLA-DMB*), cytokine and complement signaling (*CSF1R*, *IL18*, *C1QC*) as well as pathogen and self-recognition such as toll-like receptor signaling (*TLR2*), C-type lectins (*CLEC7A*) and mannose and nod-like receptors (*MRC1*, *NAIP*). Moreover, genes involved in microglial adhesion (*ITGAM*) and motility through chemokine signaling (*CCL2*), as well as purinergic signaling (*P2RX4*) were significantly expressed in microglia (Figure S4C). Furthermore, several chemokines and cytokines were expressed predominantly in microglia (Figure S4D).

In order to address microglia functionality, we then measured chemokine and cytokine release in midbrain organoids and assembloids. For that, culture medium from midbrain organoids and assembloids at day 20 of coculture was used. The medium collected was in contact with the organoids or assembloids for 3 days. As expected, in a hierarchical clustering analysis, midbrain organoids clustered in a different group than the microglia containing assembloids (Figure 3a). For a total of 18 analyzed cytokines (IL-7, IL-12p17, IL-3, TNF $\alpha$ , IL-1 $\alpha$ , IL-1 $\beta$ , IL-6, IFN $\alpha$ , IL-10, and IFN $\gamma$ ) and chemokines (CXCL8, CCL2, CXCL2, CCL3, CXCL1, CCL4, CX3CL1, and MIP-3 $\beta$ ) we observed a significant increase in the medium from assembloids compared with midbrain organoids, suggesting that immune functionality was acquired through the microglia incorporation (Figure 3b). Interestingly, although the RNA expression levels for IL-6, IL-7 and CX3CL1 were higher in non-microglia cells (Figure 3c), the levels of

released cytokines were higher in the assembloids medium (Figure 3b). Hence, potentially the released cytokines are not necessarily produced in the microglia, but their secretion is stimulated by the presence of microglia.

### 3.5 | Microglia in assembloids are functional and affect the expression of cell survival-related genes

As we previously demonstrated, microglia have the ability to phagocytose Zymosan particles in 2D monoculture (Figure 1c). Therefore, we assessed if microglia in assembloids express genes involved in phagocytosis. Indeed, in assembloids we observed a higher expression of phagocytic genes suggesting the presence of a functional phagolysosomal pathway (Figure S4D). Genes included antigen recognition (*HLA-A*, *B*, *C*), receptor (*TLR2*, 4), and internal signaling (*ATG7*), as well as autophagic vesicle formation (*LAMP2*, *SQSTM1* [p62]) and lysosomal degradation/oxidation (*CYBB*). These results indicate these microglia should have phagocytic capacity and hence the ability to remove dead cells. Interestingly and in agreement with this hypothesis, when we measured the organoid size throughout the culture period we observed a decrease of the assembloid size over time (Figure 3d). Midbrain organoids and assembloids were stained using the DNA dye Hoechst, and using our computer-assisted image analysis pipeline for cell type segmentation (Smits et al., 2019), we quantified Hoechst signal. Levels of total cells, live cells and necrotic/late apoptotic cells were evaluated. We observed that the total amount of cells was lower in assembloids compared with midbrain organoids, correlating with the size measurements. Particularly, the amount of dead cells was significantly lower in the assembloids (Figure 3e), suggesting that microglia may eliminate dead cells in assembloids.

### 3.6 | Microglia have an effect on oxidative stress and immune response in assembloids

After establishing the successful integration of microglia into midbrain organoids and showing important aspects of microglia functionality, we investigated the potential influence of microglia on the neural cells in midbrain organoids. We performed differential gene expression analysis over the neural cells in assembloids and midbrain organoids, which revealed 423 significantly different genes ( $p < .05$ ). The top

**FIGURE 4** Microglia affect the expression of oxidative stress and immune response-related genes in assembloids. (a) Differentially expressed gene enrichment analysis in assembloids against midbrain organoids reveals 12 significant network process pathways (FDR <0.05). (b) Expression of genes related to response to oxidative stress in assembloids compared with midbrain organoids. (c) Gene expression of genes related to immune response of assembloids. The presence of microglia increases the expression of genes related to antigen presentation and immune response, and decreases the expression of those related to autophagy in non-microglia cells. Box plots show mean expression and SD. (d) Enrichment analysis of cluster specific DEG  $p < .05$  between assembloids and midbrain organoids reveals significant FDR <0.05 network processes involved in oxidative stress, immune response as well as synaptic regulation. Dots represent single cells. Data are represented as mean  $\pm$  SD. \* $p < .05$ , \*\* $p < .01$ , \*\*\* $p < .001$ , \*\*\*\* $p < .0001$  using a Wilcoxon test

100 differentially expressed genes (DEGs) across all cells are represented in a heat-map and clustered by cell type (Figure S5A). We assigned DEGs to each cell type and represented their overlap in

Venn diagrams ( $p < .05$ , Figure S5B). The left Venn diagram shows an overlap of all three neuronal clusters and the right Venn diagram overlaps NB, RGL, PROG, and midNECs. Most DEG were cell type-

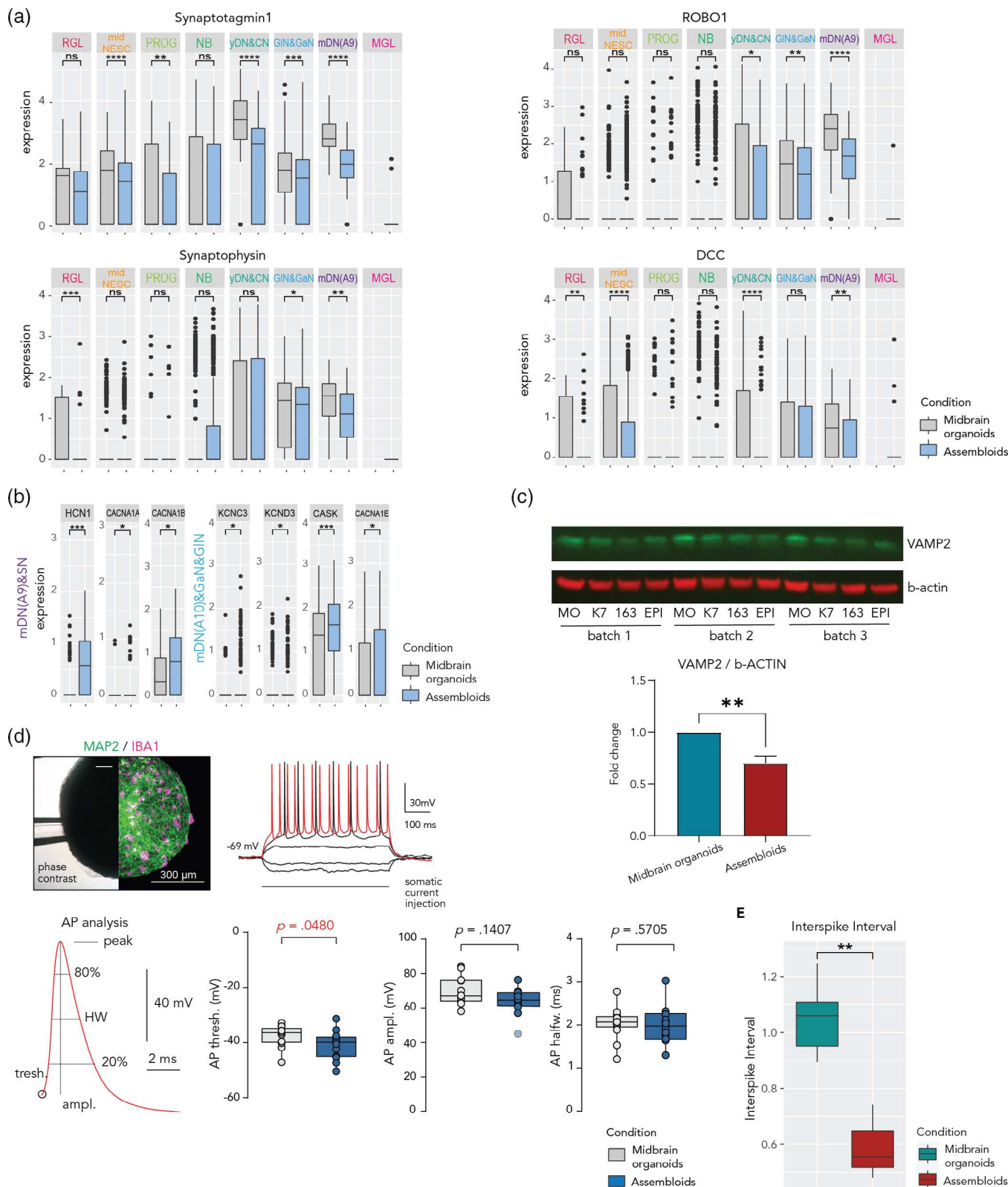


FIGURE 5 Legend on next page.

specific, although some cell types shared DEGs, which was especially the case between both mature neuronal clusters.

Next, a pathway enrichment analysis was performed MetaCore using the DEG across all cell types in midbrain organoids and assembloids (Figure 4a). The analysis revealed 12 significantly enriched biological pathways. Besides ribosomal and cytoskeletal genes, genes for oxidative stress (10/160 genes), the immune response (12/242 genes) as well as neurogenesis and axonal guidance were significantly different (13/229). Interestingly, we found 10 enriched genes involved in hypoxia and oxidative stress. Among those, six genes showed a clear downregulation of this pathway in the presence of microglial cells; the expression of mitochondrial cytochrome oxidase 1 (complex IV) (*COX1*), peroxiredoxin1 (*PRDX1*), superoxide dismutase 1 (*SOD1*), glutathione peroxidase 4 (*GPX4*), ATPase (complex V) (*MT-ATP6*), as well as glutathione S-transferase 1 (*GSTP1*) was significantly lower in assembloids (Figure 4b).

Next, we assessed the 12 genes involved in the immune response and in the antigen presentation processes (Figure 4c). Indeed, non-microglial cells expressed genes from the MHCII such as *HLA-C* and *B*. Moreover, the *STAT2* and *STAT3* genes were upregulated in the presence of microglia. The *MRC2* (*ENDO180*) receptor involved in collagen internalization and remodeling was upregulated, while genes involved in cytokine-mediated phagocytosis (*ELMO1*) and autophagy (*MAP1LC3A* (*LC3*), *SQSTM1* (*p62*)) were downregulated (Figure 4c). An enrichment analysis of the DEGs for each cell cluster showed differences in genes involved in immune response, inflammation, phagocytosis and response to hypoxia and oxidative stress, among others (Figure S5C).

Microglia are important to main brain homeostasis. However, neuroinflammation might occur when this homeostasis is compromised. Therefore, we assessed the expression of genes involved in pyroptosis—inflammation related cell death through inflammasome activation—including *CASP1*, *NLRP3*, *PYCARD* (data not shown) *PPIA*

(Figure S6A), and observed that neuroinflammation related genes were unchanged or decreased in assembloids.

### 3.7 | Microglia affect the expression of synaptic remodeling-related genes in assembloids

Enrichment analysis of the DEGs for each cell cluster showed differences in genes involved in synaptic vesicle exocytosis, synaptic contact, synaptogenesis, and axonal guidance in assembloids (Figure 4d and Figure S5C). To further investigate the microglia effects on synaptic pathways, we performed an extensive analysis of genes involved in synaptic processes. In assembloids, general synaptic markers such as *Synaptotagmin* (*SYT1*) and *Synaptophysin* (*SYP*), as well as the dopaminergic neuron circuit formation genes *ROBO1* and *DCC* were significantly downregulated across cell types (Figure 5a). Other important genes involved in synaptic vesicle exocytosis—such as *VMAT2* and *SNAP25*—were differentially expressed (Figure S6B). Moreover, we assessed axonal guidance and growth molecules, such as semaphorins (*SEMA3C*, *DPYSL2*), plexins, ephrins (*EPHA5*), neuropilins, neurofilaments, and actin cytoskeleton (*NEFM*, *ACTB*) (Figure S6C). These genes were all differentially expressed, depending on the cell type, indicating that axonal remodeling is influenced by the presence of microglia. Furthermore, we examined some cell specific genes in mature neurons involved in action potential (*CASK*, *CACNA1A*, *CACNA1E*, *CACNA1B*) and active zones (*HCN1*, *KCNC3*, *KCND3*) within synapses and observed that those genes are upregulated in assembloids (Figure 5b). Apart from assessing the synapse-related gene expression, we observed reduced protein levels of the synaptic vesicle protein *VAMP2* in assembloids compared with midbrain organoids (Figure 5c). Together these results suggest a role of microglia in synaptic remodeling and maturation within midbrain organoids.

**FIGURE 5** Microglia affect the expression of genes related to synaptic remodeling in assembloids and develop mature electrophysiological characteristics. (a) Gene expression of general synaptic markers such as *Synaptotagmin* (*SYT1*) and *Synaptophysin* (*SYP*), and the dopaminergic neuron circuit formation genes *ROBO1* and *DCC* across cell clusters in midbrain organoids and assembloids. Data are represented as mean  $\pm$  SD. \* $p < .05$  using a Wilcoxon test. Dots represent single cells. (b) Expression of genes involved in action potential (*CASK*, *CACNA1A*, *CACNA1E*, *CACNA1B*) and active zones (*HCN1*, *KCNC3*, *KCND3*) within synapses in the dopaminergic neuron cluster (mDN(A9)&SN) in midbrain organoids and assembloids. Data are represented as mean  $\pm$  SD. \* $p < .05$  using a Wilcoxon test. Dots represent single cells. (c) Western blot showing protein levels of the synaptic vesicle marker *VAMP2* and the housekeeping protein  $\beta$ -actin (upper panels). Bar graph showing the Western blot quantification from the upper panels ( $n$  [midbrain organoids] = 3, 3 batches,  $n$  [assembloids] = 9, 3 batches, 3 cell lines). \*\* $p < .01$  using a Mann-Whitney test. Data are represented as mean  $\pm$  SEM. (d) Fixation of organoid during recording and post hoc verification of microglia presence. The left half shows an infrared phase-contrast life image with the fixation pipette (upper left panel). The right half shows the same organoid after immunofluorescence staining for *MAP2* and *IBA1*. Example traces show voltage response to hyperpolarizing and depolarizing current injections of a neuron inside an assembloid measured by whole-cell patch-clamp. Voltage responses that exhibited action potential (AP) following 50 ms after stimulus onset were used for AP analysis (upper right panel). Analysis of AP waveform characteristics (bottom left panel). Voltage thresholds were significantly more depolarized in assembloid neurons (bottom middle-left panel,  $n = 14$  neurons in midbrain organoids and  $n = 13$  cells in assembloids), although analysis of AP amplitude (bottom middle-right panel) and half width (bottom right panel) shows no systematic differences between both groups. Box plots indicate median, 25th, and 75th percentiles and raw data points. Outliers deviating 2.5 SD are marked translucent and were excluded from statistical analysis for normally distributed data.  $p$ -values were determined using unpaired  $t$  tests or Mann-Whitney rank test (indicated as  $p$ ). (e) Multi-electrode array results showed a lower inter-spike interval in assembloids compared with midbrain organoids ( $n$  [midbrain organoids] = 3, 3 batches,  $n$  [assembloids] = 9, 3 batches, 3 cell lines). \*\*\* $p = .001$ , \*\* $p = .01$ , \* $p = .05$  using a Wilcoxon test. Boxes cover data from the first to the third quartile. The whiskers go from each quartile to the minimum or maximum

In order to investigate the functional impact of microglia in midbrain organoids we performed electrophysiological measurements of passive and active membrane properties as well as firing behavior. We performed patch-clamp experiments of visually identified neurons in the intact organoids from 20 to 35 days after microglia addition (Figure 5d). Neurons in midbrain organoids and assembloids exhibited similar resting membrane potentials and input resistances and reliably fired repetitive action potentials in response to somatic current injections ( $n$  midbrain organoids = 14;  $n$  assembloids = 13 cells; Figure S6D). Depolarizing steps in voltage-clamp configuration triggered strong inward currents in all tested neurons, indicative of fast voltage-activated sodium currents (Figure S6E). The amplitude of these currents was not different between both groups. Firing characteristics and action potential waveforms (Figure 5d) varied considerably, which was expected from neurons at different degrees of maturation. Importantly, the voltage threshold for the action potential generation was more negative in the group of assembloid neurons ( $-39.86$  [midbrain organoids] against  $-36.35$  [assembloids]  $\pm 3.281$ ,  $p = .0480$ , Figure 5d), which is a common and strong indicator of increased neuronal excitability in mature neurons. In sum, neurons in assembloids develop fully mature electrophysiological properties with a lower threshold for action potential generation than in midbrain organoids. Furthermore, we performed multi-electrode array (MEA) analysis with midbrain organoids and assembloids containing microglia from line K7, 163, or EPI (Figure 5e). The results showed that, after 40 days of coculture, which corresponds with the time point when the Patch clamp measurements were performed, assembloids had a lower interspike interval than midbrain organoids (Figure 5e). These results back up the observed lower action potential threshold observed in the patch-clamp experiment.

In order to support these findings and investigate further the differences between midbrain organoids and assembloids, we performed a nonpolar exo-metabolomic analysis from culture supernatants 20 days after microglia addition. The assay showed a different metabolic profile in midbrain organoids compared with assembloids (Figure S6F). A total number of 14 metabolites were significantly different. Among them, we observed a higher uptake of glucose and pyruvic acid from assembloids (Figure S7A). Regarding amino-acid metabolism, we observed a lower secretion of phenylalanine, tyrosine, methionine, lysine, putrescine, threonine, leucine, isoleucine, and valine by the assembloids compared with midbrain organoids. Furthermore, the levels of uptaken asparagine and serine from the medium were higher in assembloids. The secretion of glutamine was higher in assembloids (Figure S7B).

## 4 | DISCUSSION

### 4.1 | Microglia can be efficiently integrated into midbrain organoids

Here we described the generation of human midbrain assembloids containing microglia as well as the effect that microglia have on

midbrain organoid structure and function. Although some studies have shown a microglia-like population in brain organoids (Mansour et al., 2018; Ormel et al., 2018), integration of human iPSC-microglia cells into midbrain organoids has not previously been reported. Moreover, particularly the assessment of how microglia are affecting brain organoid physiology is heavily under-investigated.

In this study, we have shown for the first time the successful incorporation of a significant amount of microglia into midbrain organoids, obtaining an average of 6.4% of IBA1 positive cells in assembloids. Studies based on immunocytochemistry show around 10% of IBA1 positive cells in human substantia nigra (Mittelbronn et al., 2001). One of the main challenges we faced during the integration were the cytotoxic effects of the midbrain organoid medium on microglia, and the unsuitability of the microglia differentiation medium on the organoids. Interestingly, while TGF-beta 1 and 2 have been associated with microglia function and inflammatory response (Hu et al., 1995; Kim et al., 2004; Lieb et al., 2003; Taylor et al., 2017), very little is known about the relationship between TGF-beta 3 and microglia. TGF-beta 3 has been associated with dopaminergic neuron differentiation (Roussa et al., 2006), which is the reason why the dopaminergic neuron differentiation medium contains this recombinant molecule. However, no studies associating a beneficial relationship between TGF-beta3 and microglia have been found. We hypothesize that this subtype of the TGF-beta family may be acting differently than TGF-beta 1 and 2, since the 3D structure of TGF-beta 1 and 2 are considerably different than TGF-beta3, which could lead to functional differences with respect to their effect toward microglia (Bocharov et al., 2000; Grütter et al., 2008; Hinck et al., 1996). The absence of neurotrophic factors—which promote dopaminergic differentiation—in the microglia differentiation medium, led to a significantly lower amount of dopaminergic neurons in midbrain organoids and assembloids. This incompatibility might be one of the reasons why, so far, no studies have shown an efficient coculture of dopaminergic neurons with microglia. Here, we developed an optimized coculture medium, which allowed the survival of microglia within the organoids as well as an efficient dopaminergic neuron differentiation. The incorporated microglia clustered separately from the cells of ectodermal origin in the midbrain organoids, showing that both cell lines keep their cellular identity under coculture conditions. This is in line with *in vivo* development, as microglia are derived from primitive hematopoietic stem cells and as such have a completely different genetic signature (Alliot et al., 1999; Ginhoux et al., 2010; Schulz et al., 2012). Unfortunately, and as stated before, the sample loss during the pre-processing for snRNA-Seq makes the cell proportions from the sequencing inaccurate. Thus, additional runs of sequencing would allow us to obtain more reliable results concerning the cell proportions. However, the obtained data is still of good quality to proceed with gene expression analysis for cell clustering and for assessing functionality-related genes. Apart from clustering separately from the rest of the assembloid cells, microglial cells express genetic markers for all the major functions of the human microglial core signature (Galatro et al., 2017). This confirms that the population we integrated into the organoid is, indeed, microglial.



Until now, no studies analyzed which effect the integration of microglia cells have on the functionality of midbrain organoids. Our data demonstrate that the integration of microglia influence neural stress, cell death, neuronal cyto-architecture and synapse remodeling-related gene expression in the neuronal network.

## 4.2 | Microglia communicate with neurons and play a role in midbrain organoid stress response

Microglia have cell–cell communication ability through cytokine and chemokine signaling (Arnò et al., 2014; Carbonell et al., 2005; Haenseler, Sansom, et al., 2017; Siddiqui et al., 2016). They can move towards apoptotic cells in order to phagocyte and eliminate cell debris (Chan et al., 2003). Apoptotic neurons generate chemotactic signals recognized by microglial receptors, which attract them to the apoptotic area in order to phagocytose dying cells (Witting et al., 2000). Our data suggest that microglia are functional in assembloids. Phagocytic genes were significantly expressed. These gene expression data were experimentally confirmed through a 2D Zymosan phagocytosis assay. Furthermore, our gene expression analysis via snRNA-Seq showed the expression of multiple cytokines and chemokines, as well as cyto- and chemokine receptors, in microglia from assembloids. We also measured many cytokines and chemokines in culture media, and observed that their levels were significantly higher in assembloid medium compared with midbrain organoids medium. We observed a reduced size of assembloids compared with midbrain organoids, and a lower amount of dead cells in assembloids. These results lead us to hypothesize that microglia in assembloids may be attracted to apoptotic areas and phagocytose apoptotic cells and cell debris. High levels of cell death and absence of removal mechanisms for dead cells, particularly in the center of organoids, was previously a key limitation of organoid technology (Berger et al., 2018; Nickels et al., 2020).

Previous work on organoids suggested that neurons in organoids have unusual high stress levels (Bhaduri et al., 2020). Interestingly, the DEG analysis shows differences in oxidative cell stress-related genes (often linked to cell death). Moreover, the downregulation of autophagy within non-microglial cells might be linked to reduced overall stress due to starvation, which is in line with the increased metabolite uptake from the media. Additionally, the metabolomics analysis revealed a significantly lower amount of Leucine, Isoleucine, Valine, Phenylalanine, and Tyrosine in the assembloid culture medium. Increased plasma levels of those metabolites have been associated with acute hypoxic exposure in rats (Muratsubaki & Yamaki, 2011).

We also observed upregulated genes involved in the immune response in assembloids. Non-microglial cells may have reacted towards microglia by upregulating antigen presenting factors, and STAT2 and STAT3 pathways involved in the inflammatory response. Although neuronal cells respond to microglia, the expression of pyroptosis-related genes was decreased or unchanged in assembloids, indicating that there might be no inflammasome activation in the system. This, together with reduced oxidative stress and cell death in assembloids, suggests that the communication could be

neuroprotective. In addition, ER stress and UFPR remained unaffected or reduced in assembloids. Overall, these results indicates alterations in cell signaling, oxidative stress and inflammation. Further studies on cell death and oxidative stress would be of value to confirm the observed results and support our hypothesis.

## 4.3 | Microglia induce alterations in synaptic gene expression in assembloids

In the current study, the expression of synaptic marker genes is reduced in assembloids. Furthermore, protein levels of the pre-synaptic protein VAMP2 were lower in assembloids compared with midbrain organoids. Physiologically, microglia are responsible, among other functions, for remodeling the cyto-architecture and connectivity of the brain by stripping unnecessary or misguided synapses (Tremblay et al., 2011; Wake et al., 2009). Here we could show that genes in axonal guidance and cytoskeletal organization are deregulated upon microglia presence. Moreover, whereas the expression of most synaptic genes are reduced, the expression of genes involved in triggering action potential are increased. These results lead us to hypothesize that inactive synapses may be eliminated while active synapses are strengthened. This phenomenon would be in line with the previously described synaptic pruning function of microglia (Paolicelli et al., 2011; Sellgren et al., 2019). The metabolomics results may be supporting this theory; there was an increase in glucose metabolism in assembloids via a higher uptake of glucose and pyruvic acid from the medium. The higher metabolic activity in the glucose metabolism may indicate a higher need for substrates for the TCA cycle, which leads to amino-acid production and, eventually, to neurotransmitter production (Tiwari et al., 2013). Further, we observed a lower release of methionine to the medium. Methionine is related to processes of neurotransmission and neuromodulation (Kurbat & Lelevich, 2009). The secretion of glutamine to the medium was higher in assembloids. Since this amino acid is directly linked to the neurotransmitter glutamate production, this might indicate a higher production of glutamate. The uptake of the amino acids phenylalanine and tyrosine was higher in assembloids. Interestingly, tyrosine can be metabolized from phenylalanine, which can be metabolized to L-DOPA and, after that, to dopamine (Weinberg et al., 2019). Further experiments assessing synapse pruning would be of great value to confirm these observations.

Finally, the electrophysiology analysis showed that neurons in assembloids form a functional network. Interestingly, the voltage threshold for action potential generation, a common marker of neuronal excitability, was lower in assembloids compared with midbrain. Furthermore, the MEA results show a lower inter-spike interval in assembloids compared with midbrain organoids. Together with a tendency to higher membrane potentials, this indicates elevated levels of excitability in these neurons. Since the intrinsic excitability of neurons is often fine-tuned to the amount and frequency of external inputs and network activity, this change might in fact compensate for the possible degree of synaptic pruning previously discussed.



Furthermore, these results are in line with previous reports, which describe that microglia increase neuronal excitability (Klapal et al., 2016).

Thus, our results suggest that microglia in assembloids may perform synaptic pruning, leaving the system with fewer inactive synapses. Microglia could strengthen and support active synapses, and lead to a more active TCA cycle in the assembloids. Furthermore, the electrophysiological properties of assembloids suggest a higher excitability of neurons.

#### 4.4 | Midbrain-microglia assembloids as a new model for neuroinflammation in Parkinson's disease

Microglia play an important role in neurodegenerative diseases. Reactive microgliosis and neuroinflammation are known to promote neuronal cell death and the pathophysiology of those disorders (Block et al., 2007; Duffy et al., 2018). Midbrain organoids have been used to model neurodegeneration in PD in vitro (Kim et al., 2019; Smits et al., 2019). However, until now, no 3D in vitro model for studying neuroinflammation in PD was described. The new assembloid model presented here will enable to study reactive microgliosis and neuroinflammation in PD. Furthermore, a personalized approach, in which patient-specific assembloids are used, can be assessed for genetic and idiopathic cases of PD. This opens doors to studies of neuroinflammation related pathways and, to new therapeutic targets for compounds that focus on the immune system in the brain.

#### ACKNOWLEDGMENTS

The authors would like to thank Dr. Jared Sternecker for providing us with the cells from K7 line, and Dr. Christine Klein from the Institute of Neurogenetics, University of Lübeck for providing the 163 line. Javier Jarazo was supported by a Pelican award from the Fondation du Pelican de Mie et Pierre Hippert-Faber. SLN is supported by the National Centre of Excellence in Research on Parkinson's Disease (NCER-PD) which is funded by the Luxembourg National Research Fund (FNR/NCER13/BM/11264123). We thank the LCSB Metabolomics Platform, and specially Christian Jäger and Xiangyi Dong for their contribution to this manuscript. We also thank Dr. Paul Antony and Dr. Silvia Bolognin for the development of the image analysis codes used in this study. We thank Dr. Jennifer Modamio for the development of the R script used for the MEA analysis. The Jens C. Schwamborn lab is supported by the Fonds National de la Recherche (FNR) Luxembourg (PRIDE17/12244779/PARK-QC; FNR/PoC16/11559169, FNR/NCER13/BM/11264123). This is an EU Joint Program—Neurodegenerative Disease Research (JPND) project (INTER/JPND/15/11092422). We also would like to thank the private donors who support our work at the Luxembourg Centre for Systems Biomedicine. Jay W. Shin and Yan Jun Lan are supported by research grants to RIKEN Integrative Medical Sciences (IMS) from the Japanese Ministry of Education, Culture,

Sports, Science and Technology (MEXT) and Yan Jun Lan is part of the International Program Associate (IPA) program in RIKEN.

#### CONFLICT OF INTEREST

Jens C. Schwamborn and Javier Jarazo are co-founders and shareholders of the biotech company Organo Therapeutics SARL. This company uses midbrain organoids and assembloids for in vitro disease modeling and drug discovery.

#### AUTHOR CONTRIBUTIONS

Sonia Sabate-Soler designed and conducted the experiments, interpreted the data and drafted the manuscript. Sarah Louise Nickels analyzed data. Emanuel Berger, Ugne Dubonyte, Kyriaki Barmpa, Yan Jun Lan, Tsukasa Kouno, Javier Jarazo, Graham Robertson, Jafar Sharif, Haruhiko Koseki, and Christian Thome conducted specific experiments. Cláudia Saraiva contributed to the manuscript. Jay W. Shin, Sally A. Cowley, and Jens C. Schwamborn coordinated and conceptualized the study. All authors reviewed and approved the final manuscript and agreed to be accountable for their contributions.

#### ETHICS STATEMENT

Written informed consent was obtained from all individuals who donated samples to this study and all work with human stem cells was done after approval of the national ethics board, Comité National d'Ethique de Recherche (CNER), under the approval numbers 201305/04 and 201901/01.

#### DATA AVAILABILITY STATEMENT

All original and processed data as well as scripts that support the findings of this study are public available at this <https://doi.org/10.17881/cx25-ht49>.

#### ORCID

Sonia Sabate-Soler  <https://orcid.org/0000-0001-6430-6357>  
 Sarah Louise Nickels  <https://orcid.org/0000-0003-0575-156X>  
 Cláudia Saraiva  <https://orcid.org/0000-0003-4866-8790>  
 Ugne Dubonyte  <https://orcid.org/0000-0001-8681-7318>  
 Javier Jarazo  <https://orcid.org/0000-0001-9652-3620>  
 Sally A. Cowley  <https://orcid.org/0000-0003-0297-6675>  
 Jens C. Schwamborn  <https://orcid.org/0000-0003-4496-0559>

#### REFERENCES

- Abud, E. M., Ramirez, R. N., Martinez, E. S., Healy, L. M., Nguyen, C. H. H., Newnan, S. A., Yeromin, A. V., Scarfone, V. M., Marsh, S. E., Fimbres, C., Caraway, C. A., Fote, G. M., Madany, A. M., Agrawal, A., Kaye, R., Gyls, K. H., Cahalan, M. D., Cummings, B. J., Antel, J. P., ... Blurton-Jones, M. (2017). iPSC-derived human microglia-like cells to study neurological diseases. *Neuron*, 94(2), 278–293.e9. <https://doi.org/10.1016/j.neuron.2017.03.042>
- Alliot, F., Godin, I., & Pessac, B. (1999). Microglia derive from progenitors, originating from the yolk sac, and which proliferate in the brain. *Developmental Brain Research*, 117(2), 145–152. [https://doi.org/10.1016/S0165-3806\(99\)00113-3](https://doi.org/10.1016/S0165-3806(99)00113-3)
- Arnò, B., Grassivaro, F., Rossi, C., Bergamaschi, A., Castiglioni, V., Furlan, R., Greter, M., Favaro, R., Comi, G., Becher, B., Martino, G., &



- Muzio, L. (2014). Neural progenitor cells orchestrate microglia migration and positioning into the developing cortex. *Nature Communications*, 5, 5611. <https://doi.org/10.1038/ncomms6611>
- Becht, E., McInnes, L., Healy, J., Dutertre, C. A., Kwok, I. W. H., Ng, L. G., Ginhoux, F., & Newell, E. W. (2019). Dimensionality reduction for visualizing single-cell data using UMAP. *Nature Biotechnology*, 37(1), 38–44. <https://doi.org/10.1038/nbt.4314>
- Berger, E., Magliaro, C., Paczia, N., Monzel, A. S., Antony, P., Linster, C. L., Bolognin, S., Ahluwalia, A., & Schwamborn, J. C. (2018). Millifluidic culture improves human midbrain organoid vitality and differentiation. *Lab on a Chip*, 18(20), 3172–3183. <https://doi.org/10.1039/c8lc00206a>
- Bhaduri, A., Andrews, M. G., Mancía Leon, W., Jung, D., Shin, D., Allen, D., Jung, D., Schmunk, G., Haeussler, M., Salma, J., Pollen, A. A., Nowakowski, T. J., & Kriegstein, A. R. (2020). Cell stress in cortical organoids impairs molecular subtype specification. *Nature*, 578(7793), 142–148. <https://doi.org/10.1038/s41586-020-1962-0>
- Birey, F., Andersen, J., Makinson, C. D., Islam, S., Wei, W., Huber, N., Fan, H. C., Metzler, K. R. C., Panagiotakos, G., Thom, N., O'Rourke, N. A., Steinmetz, L. M., Bernstein, J. A., Hallmayer, J., Huguenard, J. R., & Paşca, S. P. (2017). Assembly of functionally integrated human forebrain spheroids. *Nature*, 545(7652), 54–59. <https://doi.org/10.1038/nature22330>
- Block, M. L., Zecca, L., & Hong, J.-S. (2007). Microglia-mediated neurotoxicity: Uncovering the molecular mechanisms. *Nature Reviews. Neuroscience*, 8(1), 57–69. <https://doi.org/10.1038/nrn2038>
- Bocharov, E. V., Blommers, M. J. J., Kuhla, J., Arvinte, T., Bürgi, R., & Arseniev, A. S. (2000). Sequence-specific 1H and 15N assignment and secondary structure of transforming growth factor beta3. *Journal of Biomolecular NMR*, 16(2), 179–180. <https://doi.org/10.1023/A:1008315600134>
- Bolognin, S., Fossépré, M., Qing, X., Jarazo, J., Ščančar, J., Moreno, E. L., Nickels, S. L., Wasner, K., Ouzren, N., Walter, J., Grünwald, A., Glaab, E., Salamanca, L., Fleming, R. M. T., Antony, P. M. A., & Schwamborn, J. C. (2019). 3D cultures of Parkinson's disease-specific dopaminergic neurons for high content Phenotyping and drug testing. *Advanced Science*, 6(1), 1–14. <https://doi.org/10.1002/ADVS.201800927>
- Bradburn, S., Murgatroyd, C., & Ray, N. (2019). Neuroinflammation in mild cognitive impairment and Alzheimer's disease: A meta-analysis. *Ageing Research Reviews*, 50, 1–8. <https://doi.org/10.1016/j.arr.2019.01.002>
- Carbonell, W. S., Murase, S. I., Horwitz, A. F., & Mandell, J. W. (2005). Migration of perilesional microglia after focal brain injury and modulation by CC chemokine receptor 5: An in situ time-lapse confocal imaging study. *Journal of Neuroscience*, 25(30), 7040–7047. <https://doi.org/10.1523/JNEUROSCI.5171-04.2005>
- Chan, A., Seguin, R., Magnus, T., Papadimitriou, C., Toyka, K. V., Antel, J. P., & Gold, R. (2003). Phagocytosis of apoptotic inflammatory cells by microglia and its therapeutic implications: Termination of CNS autoimmune inflammation and modulation by interferon-beta. *Glia*, 43(3), 231–242. <https://doi.org/10.1002/glia.10258>
- Chen, X., Zhang, K., Zhou, L., Gao, X., Wang, J., Yao, Y., He, F., Luo, Y., Yu, Y., Li, S., Cheng, L., & Sun, Y. E. (2016). Coupled electrophysiological recording and single cell transcriptome analyses revealed molecular mechanisms underlying neuronal maturation. *Protein & Cell*, 7(3), 175–186. <https://doi.org/10.1007/s13238-016-0247-8>
- Choi, S. H., Kim, Y. H., Hebisch, M., Sliwinski, C., Lee, S., D'Avanzo, C., Chen, H., Hooli, B., Asselin, C., Muffat, J., Klee, J. B., Zhang, C., Wainger, B. J., Peitz, M., Kovacs, D. M., Woolf, C. J., Wagner, S. L., Tanzi, R. E., & Kim, D. Y. (2014). A three-dimensional human neural cell culture model of Alzheimer's disease. *Nature*, 515(7526), 274–278. <https://doi.org/10.1038/nature13800>
- Choi, S. H., Veeraraghavalu, K., Lazarov, O., Marler, S., Ransohoff, R. M., Ramirez, J. M., & Sisodia, S. S. (2008). FAD-linked human Presenilin 1 variants impair environmental enrichment-induced hippocampal neural progenitor cell proliferation and differentiation in a non-cell-autonomous manner. *Neuron*, 59(4), 568. <https://doi.org/10.1016/J.NEURON.2008.07.033>
- Duffy, M. F., Collier, T. J., Patterson, J. R., Kemp, C. J., Luk, K. C., Tansey, M. G., Paumier, K. L., Kanaan, N. M., Fischer, D. L., Polinski, N. K., Barth, O. L., Howe, J. W., Vaikath, N. N., Majbour, N. K., el-Agnaf, O. M. A., & Sortwell, C. E. (2018). Lewy body-like alpha-synuclein inclusions trigger reactive microgliosis prior to nigral degeneration. *Journal of Neuroinflammation*, 15(1), 129. <https://doi.org/10.1186/s12974-018-1171-z>
- Galatro, T. F., Holtman, I. R., Lerario, A. M., Vainchtein, I. D., Brouwer, N., Sola, P. R., Veras, M. M., Pereira, T. F., Leite, R. E. P., Möller, T., Wes, P. D., Sogayar, M. C., Laman, J. D., den Dunnen, W., Pasqualucci, C. A., Oba-Shinjo, S. M., Boddeke, E. W. G. M., Marie, S. K. N., & Eggen, B. J. L. (2017). Transcriptomic analysis of purified human cortical microglia reveals age-associated changes. *Nature Neuroscience*, 20(8), 1162–1171. <https://doi.org/10.1038/nn.4597>
- Ginhoux, F., Greter, M., Leboeuf, M., Nandi, S., See, P., Gokhan, S., Mehler, M. F., Conway, S. J., Ng, L. G., Stanley, E. R., Samokhvalov, I. M., & Merad, M. (2010). Fate mapping analysis reveals that adult microglia derive from primitive macrophages. *Science*, 330(6005), 841–845. <https://doi.org/10.1126/science.1194637>
- Gomez-Giro, G., Arias-Fuenzalida, J., Jarazo, J., Zeuschner, D., Ali, M., Possemis, N., Bolognin, S., Halder, R., Jäger, C., Kuper, W. F. E., van Hasselt, P. M., Zaehres, H., del Sol, A., van der Putten, H., Schöler, H. R., & Schwamborn, J. C. (2019). Synapse alterations precede neuronal damage and storage pathology in a human cerebral organoid model of CLN3-juvenile neuronal ceroid lipofuscinosis. *Acta Neuropathologica Communications*, 7(1), 1–19. <https://doi.org/10.1186/s40478-019-0871-7>
- Grütter, C., Wilkinson, T., Turner, R., Podichetty, S., Finch, D., McCourt, M., Loning, S., Jermutus, L., & Grütter, M. G. (2008). A cytokine-neutralizing antibody as a structural mimetic of 2 receptor interactions. *Proceedings of the National Academy of Sciences of the United States of America*, 105(51), 20251–20256. <https://doi.org/10.1073/pnas.0807200106>
- Haenseler, W., Sanson, S. N., Buchrieser, J., Newey, S. E., Moore, C. S., Nicholls, F. J., Chintawar, S., Schnell, C., Antel, J. P., Allen, N. D., Cader, M. Z., Wade-Martins, R., James, W. S., & Cowley, S. A. (2017). A highly efficient human pluripotent stem cell microglia model displays a neuronal-co-culture-specific expression profile and inflammatory response. *Stem Cell Reports*, 8(6), 1727–1742. <https://doi.org/10.1016/j.stemcr.2017.05.017>
- Haenseler, W., Zambon, F., Lee, H., Vowles, J., Rinaldi, F., Duggal, G., Houlden, H., Gwinn, K., Wray, S., Luk, K. C., Wade-Martins, R., James, W. S., & Cowley, S. A. (2017). Excess  $\alpha$ -synuclein compromises phagocytosis in iPSC-derived macrophages. *Scientific Reports*, 7(1), 1, 9003–11. <https://doi.org/10.1038/s41598-017-09362-3>
- Hinck, A. P., Archer, S. J., Qian, S. W., Roberts, A. B., Sporn, M. B., Weatherbee, J. A., Tsang, M. L. S., Lucas, R., Zhang, B. L., Wenker, J., & Torchia, D. A. (1996). Transforming growth factor  $\beta$ 1: Three-dimensional structure in solution and comparison with the X-ray structure of transforming growth factor  $\beta$ 2. *Biochemistry*, 35(26), 8517–8534. <https://doi.org/10.1021/B19604946>
- Hu, S., Sheng, W. S., Peterson, P. K., & Chao, C. C. (1995). Cytokine modulation of murine microglial cell superoxide production. *Glia*, 13(1), 45–50. <https://doi.org/10.1002/GLIA.440130106>
- Jo, J., Xiao, Y., Sun, A. X., Cukuroglu, E., Tran, H.-D., Göke, J., Tan, Z. Y., Saw, T. Y., Tan, C. P., Lokman, H., Lee, Y., Kim, D., Ko, H. S., Kim, S. O., Park, J. H., Cho, N. J., Hyde, T. M., Kleinman, J. E., Shin, J. H., ... Ng, H. H. (2016). Midbrain-like organoids from human pluripotent stem cells contain functional dopaminergic and neuromelanin-producing neurons. *Cell Stem Cell*, 19(2), 248–257. <https://doi.org/10.1016/J.STEM.2016.07.005>

- Kim, H., Park, H. J., Choi, H., Chang, Y., Park, H., Shin, J., Kim, J., Lengner, C. J., Lee, Y. K., & Kim, J. (2019). Modeling G2019S-LRRK2 sporadic Parkinson's disease in 3D midbrain organoids. *Stem Cell Reports*, 12(3), 518–531. <https://doi.org/10.1016/j.stemcr.2019.01.020>
- Kim, W.-K., Hwang, S.-Y., Oh, E.-S., Piao, H. Z., Kim, K.-W., & Han, I.-O. (2004). TGF-beta1 represses activation and resultant death of microglia via inhibition of phosphatidylinositol 3-kinase activity. *Journal of Immunology*, 172(11), 7015–7023. <https://doi.org/10.4049/JIMMUNOL.172.11.7015>
- Klapal, L., Igelhorst, B. A., & Dietzel-Meyer, I. D. (2016). Changes in neuronal excitability by activated microglia: Differential Na<sup>+</sup> current upregulation in pyramid-shaped and bipolar neurons by TNF- $\alpha$  and IL-18. *Frontiers in Neurology*, 7(MAR), 1–13. <https://doi.org/10.3389/fneur.2016.00044>
- Kurbat, M. N., & Lelevich, V. V. (2009). Metabolism of amino acids in the brain. *Neurochemical Journal*, 3, 23–28. <https://doi.org/10.1134/S1819712409010036>
- la Manno, G., Gyllborg, D., Codeluppi, S., Nishimura, K., Salto, C., Zeisel, A., Borm, L. E., Stott, S. R. W., Toledo, E. M., Villaescusa, J. C., Lönnerberg, P., Ryge, J., Barker, R. A., Arenas, E., & Linnarsson, S. (2016). Molecular diversity of midbrain development in mouse, human, and stem cells. *Cell*, 167(2), 566–580.e19. <https://doi.org/10.1016/J.CELL.2016.09.027>
- Lake, B. B., Chen, S., Hoshi, M., Plongthongkum, N., Salamon, D., Knoten, A., Vijayan, A., Venkatesh, R., Kim, E. H., Gao, D., Gaut, J., Zhang, K., & Jain, S. (2019). A single-nucleus RNA-sequencing pipeline to decipher the molecular anatomy and pathophysiology of human kidneys. *Nature Communications*, 10(1), 1–15. <https://doi.org/10.1038/s41467-019-10861-2>
- Lancaster, M. A., Renner, M., Martin, C. A., Wenzel, D., Bicknell, L. S., Hurler, M. E., Homfray, T., Penninger, J. M., Jackson, A. P., & Knoblich, J. A. (2013). Cerebral organoids model human brain development and microcephaly. *Nature*, 501(7467), 373–379. <https://doi.org/10.1038/nature12517>
- Li, Q., & Barres, B. A. (2017). Microglia and macrophages in brain homeostasis and disease. *Nature Publishing Group*, 18(4), 225–242. <https://doi.org/10.1038/nri.2017.125>
- Lieb, K., Engels, S., & Fiebich, B. L. (2003). Inhibition of LPS-induced iNOS and NO synthesis in primary rat microglial cells. *Neurochemistry International*, 42(2), 131–137. [https://doi.org/10.1016/S0197-0186\(02\)00076-1](https://doi.org/10.1016/S0197-0186(02)00076-1)
- Lindborg, B. A., Brekke, J. H., Vegoe, A. L., Ulrich, C. B., Haider, K. T., Subramaniam, S., Venhuizen, S. L., Eide, C. R., Orchard, P. J., Chen, W., Wang, Q., Pelaez, F., Scott, C. M., Kokkoli, E., Keirstead, S. A., Dutton, J. R., Tolar, J., & O'Brien, T. D. (2016). Rapid induction of cerebral Organoids from human induced pluripotent stem cells using a chemically defined hydrogel and defined cell culture medium. *Stem Cells Translational Medicine*, 5(7), 970–979. <https://doi.org/10.5966/sctm.2015-0305>
- Mansour, A. A., Gonçalves, J. T., Bloyd, C. W., Li, H., Fernandes, S., Quang, D., Johnston, S., Parylak, S. L., Jin, X., & Gage, F. H. (2018). An in vivo model of functional and vascularized human brain organoids. *Nature Biotechnology*, 36(5), 432–441. <https://doi.org/10.1038/nbt.4127>
- Marton, R. M., & Paşca, S. P. (2020). Organoid and Assembloid Technologies for Investigating Cellular Crosstalk in human brain development and disease. *Trends in Cell Biology*, 30(2), 133–143. <https://doi.org/10.1016/j.tcb.2019.11.004>
- Mittelbronn, M., Dietz, K., Schluesener, H. J., & Meyermann, R. (2001). Local distribution of microglia in the normal adult human central nervous system differs by up to one order of magnitude. *Acta Neuropathologica*, 101(3), 249–255. <https://doi.org/10.1007/s004010000284>
- Modamio, J., Saraiva, C., Giro, G. G., Nickels, S. L., Jarazo, J., Antony, P., Peter Barbuti, Rashi Hadler, Christian Jäger, Rejko Krüger, Enrico Glaab, Schwamborn, J. C. (2021). Synaptic decline precedes dopaminergic neuronal loss in human midbrain organoids harboring a triplication of the SNCA gene. *BioRxiv*, 2021.07.15.452499. <https://doi.org/10.1101/2021.07.15.452499>
- Monzel, A. S., Smits, L. M., Hemmer, K., Hachi, S., Moreno, E. L., van Wuellen, T., Jarazo, J., Walter, J., Brüggemann, I., Boussaad, I., Berger, E., Fleming, R. M. T., Bolognin, S., & Schwamborn, J. C. (2017). Derivation of human midbrain-specific Organoids from Neuroepithelial stem cells. *Stem Cell Reports*, 8(5), 1144–1154. <https://doi.org/10.1016/J.STEMCR.2017.03.010>
- Muffat, J., Li, Y., Yuan, B., Mitalipova, M., Omer, A., Corcoran, S., Bakiasi, G., Tsai, L. H., Aubourg, P., Ransohoff, R. M., & Jaenisch, R. (2016). Efficient derivation of microglia-like cells from human pluripotent stem cells. *Nature Medicine*, 22(11), 1358–1367. <https://doi.org/10.1038/nm.4189>
- Muratsubaki, H., & Yamaki, A. (2011). Profile of plasma amino acid levels in rats exposed to acute hypoxic hypoxia. *Indian Journal of Clinical Biochemistry*, 26(4), 416–419. <https://doi.org/10.1007/s12291-011-0125-3>
- Nickels, S. L., Modamio, J., Mendes-Pinheiro, B., Monzel, A. S., Betsou, F., & Schwamborn, J. C. (2020). Reproducible generation of human midbrain organoids for in vitro modeling of Parkinson's disease. *Stem Cell Research*, 46, 1–13. <https://doi.org/10.1016/j.scr.2020.101870>
- Ormel, P. R., Vieira de Sá, R., van Bodegraven, E. J., Karst, H., Harschnitz, O., Sneebaer, M. A. M., Johansen, L. E., van Dijk, R. E., Scheefhals, N., Berdenis van Berlekom, A., Ribes Martínez, E., Kling, S., MacGillavry, H. D., van den Berg, L. H., Kahn, R. S., Hol, E. M., de Witte, L. D., & Pasterkamp, R. J. (2018). Microglia innately develop within cerebral organoids. *Nature Communications*, 9(1), 4167. <https://doi.org/10.1038/S41467-018-06684-2>
- Osorio, D., & Cai, J. J. (2021). Systematic determination of the mitochondrial proportion in human and mice tissues for single-cell RNA-sequencing data quality control. *Bioinformatics*, 37(7), 963–967. <https://doi.org/10.1093/BIOINFORMATICS/BTAA751>
- Paolicelli, R. C., Bolasco, G., Pagani, F., Maggi, L., Scianni, M., Panzanelli, P., Giustetto, M., Ferreira, T. A., Guiducci, E., Dumas, L., Ragozzino, D., & Gross, C. T. (2011). Synaptic pruning by microglia is necessary for normal brain development. *Science*, 333(6048), 1456–1458. <https://doi.org/10.1126/science.1202529>
- Pasca, S. P. (2019). Assembling human brain organoids. *Science*, 363(6423), 126–127. <https://doi.org/10.1126/science.aau5729>
- Qian, X., Nguyen, H. N., Song, M. M., Hadiono, C., Ogden, S. C., Hammack, C., Yao, B., Hamersky, G. R., Jacob, F., Zhong, C., Yoon, K. J., Jeang, W., Lin, L., Li, Y., Thakor, J., Berg, D. A., Zhang, C., Kang, E., Chickering, M., ... Ming, G. L. (2016). Brain-region-specific Organoids using mini-bioreactors for modeling ZIKV exposure. *Cell*, 165(5), 1238–1254. <https://doi.org/10.1016/j.cell.2016.04.032>
- Ramani, A., Müller, L., Ostermann, P. N., Gabriel, E., Abida-Islam, P., Müller-Schiffmann, A., Mariappan, A., Goureau, O., Gruell, H., Walker, A., Andrée, M., Hauka, S., Houwaart, T., Dilthey, A., Wohlgemuth, K., Omran, H., Klein, F., Wiczorek, D., Adams, O., ... Gopalakrishnan, J. (2020). SARS-CoV-2 targets neurons of 3D human brain organoids. *The EMBO Journal*, 39(20), e106230. <https://doi.org/10.15252/EMBJ.2020106230>
- Reinhardt, P., Glatza, M., Hemmer, K., Tsytsyura, Y., Thiel, C. S., Höing, S., Moritz, S., Parga, J. A., Wagner, L., Bruder, J. M., Wu, G., Schmid, B., Röpke, A., Klingauf, J., Schwamborn, J. C., Gasser, T., Schöler, H. R., & Sternecker, J. (2013). Correction: Derivation and expansion using only small molecules of human neural progenitors for neurodegenerative disease modeling. *PLoS One*, 8(11), 59252. <https://doi.org/10.1371/annotation/6a917a2e-df4a-4ad9-99bb-6aa7218b833e>
- Roussa, E., Wiehle, M., Dünker, N., Becker-Katins, S., Oehlke, O., & Kriegstein, K. (2006). Transforming growth factor  $\beta$  is required for differentiation of mouse Mesencephalic progenitors into dopaminergic neurons in vitro and in vivo: Ectopic induction in dorsal



- mesencephalon. *Stem Cells*, 24(9), 2120–2129. <https://doi.org/10.1634/STEMCELLS.2005-0514>
- Rymo, S. F., Gerhardt, H., Sand, F. W., Lang, R., Uv, A., & Betsholtz, C. (2011). A two-way communication between microglial cells and angiogenic sprouts regulates angiogenesis in aortic ring cultures. *PLoS One*, 6(1), e15846. <https://doi.org/10.1371/journal.pone.0015846>
- Schulz, C., Perdiguer, E. G., Chorro, L., Szabo-Rogers, H., Cagnard, N., Kierdorf, K., Prinz, M., Wu, B., Jacobsen, S. E. W., Pollard, J. W., Frampton, J., Liu, K. J., & Geissmann, F. (2012). A lineage of myeloid cells independent of Myb and hematopoietic stem cells. *Science (New York, N.Y.)*, 336(6077), 86–90. <https://doi.org/10.1126/science.1219179>
- Sellgren, C. M., Gracias, J., Watmuff, B., Biag, J. D., Thanos, J. M., Whittredge, P. B., Fu, T., Worringer, K., Brown, H. E., Wang, J., Kaykas, A., Karmacharya, R., Goold, C. P., Sheridan, S. D., & Perlis, R. H. (2019). Increased synapse elimination by microglia in schizophrenia patient-derived models of synaptic pruning. *Nature Neuroscience*, 22(3), 374–385. <https://doi.org/10.1038/s41593-018-0334-7>
- Shabab, T., Khanabdali, R., Moghadamtousi, S. Z., Kadir, H. A., & Mohan, G. (2017). Neuroinflammation pathways: A general review. *International Journal of Neuroscience*, 127(7), 624–633. <https://doi.org/10.1080/00207454.2016.1212854>
- Shi, Y., Kirwan, P., Smith, J., Robinson, H. P. C., & Livesey, F. J. (2012). Human cerebral cortex development from pluripotent stem cells to functional excitatory synapses. *Nature Neuroscience*, 15(3), 477–486. <https://doi.org/10.1038/nn.3041>
- Siddiqui, T. A., Lively, S., & Schlichter, L. C. (2016). Complex molecular and functional outcomes of single versus sequential cytokine stimulation of rat microglia. *Journal of Neuroinflammation*, 13(1), 66. <https://doi.org/10.1186/s12974-016-0531-9>
- Smits, L. M., Magni, S., Kinugawa, K., Grzyb, K., Luginbühl, J., Sabate-Soler, S., Bolognin, S., Shin, J. W., Mori, E., Skupin, A., & Schwamborn, J. C. (2020). Single-cell transcriptomics reveals multiple neuronal cell types in human midbrain-specific organoids. *Cell and Tissue Research*, 382(3), 463–476. <https://doi.org/10.1007/S00441-020-03249-Y>
- Smits, L. M., Reinhardt, L., Reinhardt, P., Glatza, M., Monzel, A. S., Stanslowsky, N., Rosato-Siri, M. D., Zanon, A., Antony, P. M., Bellmann, J., Nicklas, S. M., Hemmer, K., Qing, X., Berger, E., Kalmbach, N., Ehrlich, M., Bolognin, S., Hicks, A. A., Wegner, F., ... Schwamborn, J. C. (2019). Modeling Parkinson's disease in midbrain-like organoids. *Npj Parkinson's Disease*, 5(1), 5. <https://doi.org/10.1038/s41531-019-0078-4>
- Taylor, R. A., Chang, C. F., Goods, B. A., Hammond, M. D., Grory, B. M., Ai, Y., Steinschneider, A. F., Renfro, S. C., Askenase, M. H., McCullough, L. D., Kasner, S. E., Mullen, M. T., Hafler, D. A., Love, J. C., & Sansing, L. H. (2017). TGF- $\beta$ 1 modulates microglial phenotype and promotes recovery after intracerebral hemorrhage. *Journal of Clinical Investigation*, 127(1), 280–292. <https://doi.org/10.1172/JCI88647>
- Thion, M. S., Ginhoux, F., & Garel, S. (2018). Microglia and early brain development: An intimate journey. *Science*, 362(6411), 185–189. <https://doi.org/10.1126/science.aat0474>
- Tiwari, V., Ambadipudi, S., & Patel, A. B. (2013). Glutamatergic and GABAergic TCA cycle and neurotransmitter cycling fluxes in different regions of mouse brain. *Journal of Cerebral Blood Flow and Metabolism*, 33(10), 1523–1531. <https://doi.org/10.1038/jcbfm.2013.114>
- Tremblay, M. È., Stevens, B., Sierra, A., Wake, H., Bessis, A., & Nimmerjahn, A. (2011). The role of microglia in the healthy brain. *Journal of Neuroscience*, 31(45), 16064–16069. <https://doi.org/10.1523/JNEUROSCI.4158-11.2011>
- Tu, D., Gao, Y., Yang, R., Guan, T., Hong, J. S., & Gao, H. M. (2019). The pentose phosphate pathway regulates chronic neuroinflammation and dopaminergic neurodegeneration. *Journal of Neuroinflammation*, 16(1), 1–17. <https://doi.org/10.1186/s12974-019-1659-1>
- Ueno, M., Fujita, Y., Tanaka, T., Nakamura, Y., Kikuta, J., Ishii, M., & Yamashita, T. (2013). Layer v cortical neurons require microglial support for survival during postnatal development. *Nature Neuroscience*, 16(5), 543–551. <https://doi.org/10.1038/nn.3358>
- van Wilgenburg, B., Browne, C., Vowles, J., & Cowley, S. A. (2013). Efficient, long term production of monocyte-derived macrophages from human pluripotent stem cells under partly-defined and fully-defined conditions. *PLoS One*, 8(8), e71098. <https://doi.org/10.1371/journal.pone.0071098>
- Wake, H., Moorhouse, A. J., Jinno, S., Kohsaka, S., & Nabekura, J. (2009). Resting microglia directly monitor the functional state of synapses in vivo and determine the fate of ischemic terminals. *Journal of Neuroscience*, 29(13), 3974–3980. <https://doi.org/10.1523/JNEUROSCI.4363-08.2009>
- Weinberg, R. P., Koledova, V. V., Subramaniam, A., Schneider, K., Artamonova, A., Sambanthamurthi, R., Hayes, K. C., Sinskey, A. J., & Rha, C. K. (2019). Palm fruit bioactives augment expression of tyrosine hydroxylase in the Nile grass rat basal ganglia and alter the colonic microbiome. *Scientific Reports*, 9(1), 18625. <https://doi.org/10.1038/s41598-019-54461-y>
- Witting, A., Müller, P., Herrmann, A., Kettenmann, H., & Nolte, C. (2000). Phagocytic clearance of apoptotic neurons by microglia/brain macrophages in vitro: Involvement of lectin-, integrin-, and phosphatidylserine-mediated recognition. *Journal of Neurochemistry*, 75(3), 1060–1070. <https://doi.org/10.1046/j.1471-4159.2000.0751060.x>

## SUPPORTING INFORMATION

Additional supporting information may be found in the online version of the article at the publisher's website.

**How to cite this article:** Sabate-Soler, S., Nickels, S. L., Saraiva, C., Berger, E., Dubonyte, U., Barmppa, K., Lan, Y. J., Kouno, T., Jarazo, J., Robertson, G., Sharif, J., Koseki, H., Thome, C., Shin, J. W., Cowley, S. A., & Schwamborn, J. C. (2022). Microglia integration into human midbrain organoids leads to increased neuronal maturation and functionality. *Glia*, 70(7), 1267–1288. <https://doi.org/10.1002/glia.24167>

---

## Supporting information

### Supporting Figure Legends

**Figure S1. Microglia in assembloids show different morphologies and allow astrocyte differentiation** **A.** iPSCs from the line K7 (upper row), 163 (middle row) and EPI (bottom row) stained for the pluripotency markers TRA-1-60, Nanog (left), TRA-1-81, SOX2 (middle), SSEA-4 and Oct-4 (right). **B.** Zymosan and IBA1 staining on microglia from line K7 (top) and 163 (bottom) differentiated for 10 days. **C.** Immunostaining for IBA1, TH and TUJ1 of midbrain organoids and assembloids with microglia from line K7, 163 and EPI upon culture with midbrain organoid (MOm), microglia (MGLm) or co-culture (cc med) media). **D.** MAP2 positive (MAP2<sup>+</sup>) cells in midbrain organoids and assembloids (n (midbrain organoids) =5, 5 batches, n (assembloids) =15, 5 batches, 3 cell lines). For immunofluorescence images see Figure 2C and S1H. Data are represented as mean  $\pm$  SEM. Y axis is fold change compared to midbrain organoids. **E.** Immunostaining of neural precursor cells from line K7 for the pluripotency marker SOX2, the neural precursor marker Nestin and the forebrain and hindbrain marker PAX6, whose absence confirms the midbrain patterning of the cells. **F.** Bright field images of midbrain organoids (upper panels) and assembloids (bottom panels) at the co-culture day (0DOC, days of co-culture, left) and at 20DOC (right). **G.** Immunostaining of assembloids for IBA1 showing ramified (left), elongated (middle) and round (right) microglia. **H.** Immunostaining of an assembloid from the line 163 after 70 days of co-culture, for GFAP, IBA1 and MAP2. **I.** Immunofluorescence staining of midbrain organoids (left panels) and assembloids with microglia from line 163 (middle panels) and EPI (right panels) for IBA1, FOXA2 and MAP2 (upper panels), and for TH and TUJ1 (bottom panels). The images correspond to a maximum intensity projection from a z-stack of 70 $\mu$ m organoid sections.

**Figure S2. Cell type specific gene expression in assembloids.** Heatmap showing the cell type-specific gene expression throughout the different cell clusters in assembloids.

**Figure S3. Quality control of sn-RNAseq data using the Seurat R Package.** Quality controls of **A.** Midbrain organoids. **B.** Assembloids with microglia from line K7. **C.** Assembloids with microglia from line 163. i) Before quality controls; ii) After quality controls ( $100 < n_{\text{Feature\_RNA}} < 5000$  or  $\text{percent\_mt} < 25$ ); iii) Correlation between features and counts; iv) Correlation between microglial genes and counts. **D.** Volcano plot showing the most variable genes between midbrain organoids and assembloids. **E.** UMAP visualization of scRNA-seq data grouped by samples: Assembloids with microglia from 163 Assembloids\_163), Assembloids

---

with microglia from K7 (Assembloids\_K7) and midbrain organoids. **F.** Principle components analysis. 20 dimensions were chosen.

**Figure S4. Microglia in assembloids have a typical immune cell signature.** **A.** Heatmap showing the average expression of 100 most variable genes between midbrain organoids and assembloids. **B.** Expression of top 100 microglial marker genes across microglia cells in assembloids. **C.** Microglia core signature, expression of microglia marker genes as well as genes involved in adhesion, immune response, pathogen recognition and purinergic signaling. **D.** Gene expression levels of genes related to phagocytic activity. Violin plot shows average expression level. \* $p < 0.05$ , \*\* $p < 0.01$ , \*\*\* $p < 0.001$ , \*\*\*\* $p < 0.0001$  using a Wilcox one-sample tests, median in red, quantiles in black. Dots represent single cells.

**Figure S5. Microglia in assembloids lead to differential expression of multiple genes.** **A.** Heatmap of the average expression of 100 most significant differentially expressed genes across cell clusters in midbrain organoids and assembloids ( $p < 0.05$ ). **B.** Venn diagrams showing the number of DEG across cell types. Overlap within three neuronal clusters (left panel) and midNESC, PROG, RGL and NB (right panel). **C.** Complete enrichment analysis of cluster specific DEG between midbrain organoids and assembloids reveals significant network processes (FDR $< 0.05$ ).

**Figure S6. Microglia lead to a decrease in the inflammasome-related gene PPIA, and differences in synapse-related genes.** **A.** Expression of PPIA gene, involved in pyroptosis, across cell clusters in midbrain organoids and assembloids. **B.** Expression of *VMAT2* and *SNAP25*, involved in synaptic vesicle exocytosis, across cell clusters in midbrain organoids and assembloids. **C.** Expression levels of axonal guidance and growth-related genes: semaphorins (*SEMA3C*, *DPYSL2*), plexins, ephrins (*EPHA5*), neuropilins, neurofilaments and actin cytoskeleton (*NEFM*, *ACTB*) across cell clusters in midbrain organoids and assembloids. Data are represented as mean  $\pm$  SD. \*  $p < 0.05$  using a Wilcox test. Dots represent single cells. **D.** Boxplot from patch clamp data showing that neurons in midbrain organoids and assembloids show similar resting membrane potentials (left) and input resistances (middle), and fired repetitive action potentials in response to somatic current injections (right, n midbrain organoids = 14; n assembloids = 13 cells). **E.** Inward currents of an assembloid neuron triggered by voltage steps to different potentials starting from -70 mV in voltage-clamp mode. Voltage-gated currents appeared at -40mV and persisted until +30mV under whole-cell voltage-clamp conditions (left). Inward currents generated at -30 mV (red trace in left panel) between midbrain organoids and assembloids showed no significant difference between both groups (right). **F.** Heatmap showing extracellular metabolite levels in culture supernatants (n (midbrain

organoids) = 5, 5 batches, n (assembloids) = 15, 5 batches, 3 cell lines). Midbrain organoids cluster separately from assembloids from lines K7, 163 and EPI.

**Figure S7. Assembloids show a different extracellular metabolite profile compared to midbrain organoids.** **A.** Metabolite levels in the culture media from organoids and assembloids after 48h of culture. The levels of glucose and pyruvic acid were lower in media from assembloids compared to midbrain organoids. **B.** The levels of the amino acids phenylalanine, tyrosine, methionine, lysine, putrescine, threonine, leucine, isoleucine, valine, asparagine and serine in the media were lower in assembloids, whereas the glutamate levels were higher (n (midbrain organoids)= 3, 3 batches, n(assembloids)= 9, 3 batches, 3 cell lines). Each dot represents a replicate (medium 3 organoids or assembloids pooled). Data are represented as mean  $\pm$  SEM. \*p < 0.05, \*\*p<0.01, \*\*\*p<0.001, \*\*\*\*p<0.0001 using a Mann-Whitney or an unpaired t test.

### Supporting video legends

**Video S1.** Time-lapse of K7 microglia phagocytosing zymosan particles. 449.55 frames, 29.97 frames per second.

**Video S2.** Time-lapse of 163 microglia phagocytosing zymosan particles. 659.34 frames, 29.97 frames per second.

**Video S3.** Time-lapse of EPI microglia phagocytosing zymosan particles. 689.31, 29.97 frames per second.

**Video S4.** Z-stack images of microglia from lines K7, 163 and EPI showing internalized Zymosan particles. IBA1 shown in green, zymosan shown in red, nuclei shown in blue.

**Video S5.** 3D reconstruction from a microglia cell from line K7 showing internalized Zymosan particles. IBA1 shown in green, zymosan shown in red, nuclei shown in blue.

### Supporting Tables

Name	Simplified identifier	Identifier	Patient	Gender	Age of sampling	Source
K7	200	2.0.0.10.1.0	K7.1 WT/C4 WT	Female	81	Reinhardt et al., 2013
EPI	201	2.0.0.15.0.0	A13777	Female	Cord Blood	GIBCO/A13777
163	304	2.0.0.79.0.0	163	Male	66	SYSMED

**Table S1 related to experimental procedures.** iPS cell lines used in this study. Macrophage precursors were derived from iPSCs as described in the Experimental procedures section. Human neural precursors were derived from human iPSCs from the simplified identifier 200.

Human midbrain-specific organoids were generated with neural precursors as described in the Experimental procedures section.

Reagent name	Company	Catalog number	Concentration
<b>Advanced DMEM/F12</b>	Thermo Fisher	12634010	-
<b>N2</b>	Thermo Fisher	17502001	1x
<b>Pen/Strep</b>	Invitrogen	15140122	1x
<b>GlutaMax</b>	Thermo Fisher	35050061	1x
<b>2-mercaptoethanol</b>	Thermo Fisher	31350-010	50 $\mu$ M
<b>IL-34</b>	Peprtech	200-34	100 ng/mL
<b>GM-CSF</b>	Peprtech	300-03	10 ng/mL
<b>BDNF</b>	Peprtech	450-02	10 ng/mL
<b>GDNF</b>	Peprtech	450-10	10 ng/mL
<b>DAPT</b>	R&D Systems	2634/10	10 $\mu$ M
<b>Activin A</b>	Thermo Fisher	PHC9564	2.5 ng/mL

**Table S2 related to experimental procedures.** Co-culture medium composition.

Antibody	Host species	Source	Ref.-No.	Dilution
<b>IBA1</b>	Goat	Abcam	ab5076	1:250
<b>PU1</b>	Rabbit	Cell signalling	2258S	1:250
<b>CD45</b>	Mouse	Biologend	304002	1:1000
<b>TMEM119</b>	Rabbit	Sigma	HPA051870	1:250
<b>P2RY12</b>	Rabbit	Sigma	HPA014518	1:250
<b>FOXA2</b>	Mouse	Santa Cruz	sc-101060	1:250
<b>LMX1A</b>	Rabbit	Abcam	ab139726	1:100
<b>PAX6</b>	Rabbit	Biologend	901301	1:300
<b>SOX2</b>	Goat	R&D systems	AF2018	1:100
<b>SOX2</b>	Rabbit	Abcam	ab97959	1:100
<b>Nestin</b>	Mouse	Millipore	MAB5326	1:100
<b>TH</b>	Rabbit	Abcam	ab112	1:1000
<b>TUJ1</b>	Chicken	Millipore	AB9354	1:1000
<b>MAP2</b>	Chicken	Abcam	ab5392	1:1000
<b>MAP2</b>	Mouse	Millipore	MAB3418	1:200
<b>GFAP</b>	Chicken	Millipore	AB5541	1:1000
<b>SSEA-4</b>	Mouse	Millipore	MAB4304	1:50
<b>Oct-4</b>	Rabbit	Abcam	ab19857	1:400
<b>TRA-1-60</b>	Mouse	Millipore	MAB4360	1:50
<b>Nanog</b>	Rabbit	Millipore	AB5731	1:200
<b>TRA-1-81</b>	Mouse	Millipore	MAB4381	1:50
<b>VAMP2</b>	Rabbit	Abcam	ab215721	1:1000



<b>Actin-β</b>	Mouse	Cell signalling	3700	1:100000
<b>Alexa Fluor® 647 Anti-chicken</b>	Donkey	Jackson Immuno	703-605-155	1:1000
<b>Alexa Fluor® 488 anti-goat</b>	Donkey	Invitrogen	A-11055	1:1000
<b>Alexa Fluor® 568 anti-goat</b>	Donkey	Thermo Fisher	a11057	1:1000
<b>Alexa Fluor® 647 anti-goat</b>	Donkey	Invitrogen	a21447	1:1000
<b>Alexa Fluor® 488 anti-rabbit</b>	Donkey	Thermo Fisher	a21206	1:1000
<b>Alexa Fluor® 568 anti-rabbit</b>	Donkey	Invitrogen	a10042	1:1000
<b>Alexa Fluor® 647 anti-rabbit</b>	Donkey	Invitrogen	a31573	1:1000
<b>Alexa Fluor® 488 anti-mouse</b>	Donkey	Invitrogen	a21202	1:1000
<b>Alexa Fluor® 568 anti-mouse</b>	Donkey	Invitrogen	a10037	1:1000
<b>Hoechst 33342 Solution (20 mM)</b>	-	Invitrogen	62249	1:10000
<b>IgG H+L 800</b>	Rabbit	Cell signalling	5151	1:10000
<b>IgG H+L 680</b>	Mouse	Cell signalling	5470	1:10000

**Table S3 related to experimental procedures.** Antibodies used in this study.

Primer	Sequence (5' to 3')	Region (Purpose)
<b>h-RPL37A-F</b>	GTGGTTCCTGCATGAAGACAGTG	RT-PCR
<b>h-RPL37A-R</b>	TTCTGATGGCGGACTTTACCG	RT-PCR
<b>2241_AIF1_F</b>	AGACGTTCACTACCCTGACTT	RT-PCR
<b>2242_AIF1_R</b>	GGCCTGTTGGCTTTTCTTTTCTC	RT-PCR
<b>2243_CD68_F</b>	CTTCTCTCATTCCCCTATGGACA	RT-PCR
<b>2244_CD68_R</b>	GAAGGACACATTGTACTCCACC	RT-PCR
<b>2289_P2RY12 FW</b>	AAGAGCACTCAAGACTTTAC	RT-PCR
<b>2290_P2RY12 RV</b>	GGGTTTGAATGTATCCAGTAAG	RT-PCR
<b>2291_TMEM119 FW</b>	AGTCCTGTACGCCAAGGAAC	RT-PCR
<b>2292_TMEM119 RV</b>	GCAGCAACAGAAGGATGAGG	RT-PCR

**Table S4 related to experimental procedures.** Primers used in this study.

Stem cells	DA	VTA	Maturity	CN	GAN	GLN	SN
SOX2	NR4A2	ALDH1A	SPRYD7	CHAT	GAD1	SLC1A1	SLC6A4
PAX6	PBX1	1	TUBB2A	SLC18A	GAD2	SLC1A2	SLC18A2
HES5	GRIA3	TRHR	SKP1	3	GABARAP	SLC1A3	TPH1
ASCL1	TH	CD24	GNAI1	ACHE	GABARAP	SLC17A	TPH2
SOX1	EN1	SLC18A	MRAS		L1	6	FEV
PAX3	TMCC3	2	ATP1A3		GABARAP	SLC17A	HTR1D
	NTM	FGF1	MAGED1		L2	7	HTR1E

DACH 1 LMO3 NR2F1 PLAGL 1 LIX1 HOXA 2 FOXA2 SLC1A 3 MSI1 VIM NES SHH	DDC CAMK2 N1 ALDH1A 1 APP PDZRN4 PCDH10 ERBB4 SLC10A 4 BEX5 NPY1R GPC2 HTRA2 HTRA3 HTRA4 PTX3 OTX2 EN2 SOX6 FOXA2 LMX1A LMX1B KCNJ6 CALB1 SLC6A3 SHH NKX6-1	NRIP3 MPP6 NTS CCK SOX6 GRIN2C SNCG IGF1 ADCYA P1 GRP LPL CALB1 SLC32A 1 VIP TACR3 DCC OTX2 SATB1	ARL2 MCFD2 MORF4L 2 NRSN2 NAP1L3 NGRN OLFM1 DKK3 CCDC13 6 COX6C HSP90A B1 CALM2 ATP1B1 UQCRB COX4I1 PSMB5 FXYP7 RTN1 SEC62 COX7C CNTN1 FAIM2 SLC48A1 RAB3B NPTXR PDGFA NDUFC2 BEX2 UCHL1	ABAT	GLS GLS2 GRIN1 GRIN2A GRIN2B GRIN2 C GRIN2 D GRIN3A GRIN3B GRINA GRIA1 GRIA2 GRIA3 GRIA4 HTRA1	HTR1F HTR2A HTR2A-A S1 HTR2B HTR2C HTR3A HTR3B HTR3D HTR4 HTR5A HTR5A-A S1
-------------------------------------------------------------------------------------------------------------------	-------------------------------------------------------------------------------------------------------------------------------------------------------------------------------------------------------------------------------------------------	------------------------------------------------------------------------------------------------------------------------------------------------------------	---------------------------------------------------------------------------------------------------------------------------------------------------------------------------------------------------------------------------------------------------------------------------------------	------	------------------------------------------------------------------------------------------------------------------------------------------------	----------------------------------------------------------------------------------------------------------------

**Table S5 related to results.** Genes used for defining neuronal cell clusters and maturity. DA = Dopaminergic; VTA = ventral tegmental area; CN = Cholinergic; GAN = Gabaergic; GLN = Glutamatergic; SN = Serotonergic.

Name	Identifier
Cell 1	MgIk7_CATCAGAAGGCCATAG.1
Cell 2	MgIk7_AGGGATGGTGTCTCT.1
Cell 3	MgIk7_CTAAGACGTCTAGCGC.1
Cell 4	MgIk7_CCGTGGACATCCTTGC.1
Cell 5	MgIk7_AGTTGGTCAGCCTTTC.1
Cell 6	MgI163_ACGCCAGTCATTGCCC.1
Cell 7	MgI163_CATATTCTCCAATGGT.1
Cell 8	MgIk7_CGCTGGAGTCCAGTTA.1
Cell 9	MgIk7_AAGCCGCAGCTTCGCG.1
Cell 10	MgIk7_CTCCTAGTCCTGCTTG.1
Cell 11	MgIk7_CAAGGCCGTAGGCATG.1
Cell 12	MgIk7_ACAGCCGCAGCTGCAC.1

---

<b>Cell 13</b>	MgIK7_CAACCAACAGGAATGC.1
<b>Cell 14</b>	MgIK7_ACGGGCTGTACAAGTA.1
<b>Cell 15</b>	MgIK7_GTCTTCGCAATCCGAT.1
<b>Cell 16</b>	MgI163_GCACATACATCGGACC.1
<b>Cell 17</b>	MgI163_AGATCTGCAAACGTGG.1
<b>Cell 18</b>	MgI163_ACGTCAAAGTTTAGGA.1
<b>Cell 19</b>	MgIK7_GGATGTTGTCGCCATG.1
<b>Cell 20</b>	MgIK7_TGTTCCGCAAGAGGCT.1
<b>Cell 21</b>	MgIK7_GACTACAAGTAGGCCA.1
<b>Cell 22</b>	MgIK7_TTAGGACAGGTTACCT.1
<b>Cell 23</b>	MgIK7_GCTGGGTAGCGATATA.1
<b>Cell 24</b>	MgIK7_GCTTGAAAGATACACA.1
<b>Cell 25</b>	MgIK7_AAAGTAGGTGACTACT.1
<b>Cell 26</b>	MgIK7_TATCTCACAGGTTTCA.1

**Table S6 related to results.** Identifiers of the 26 microglia cells.

# Supporting Figures

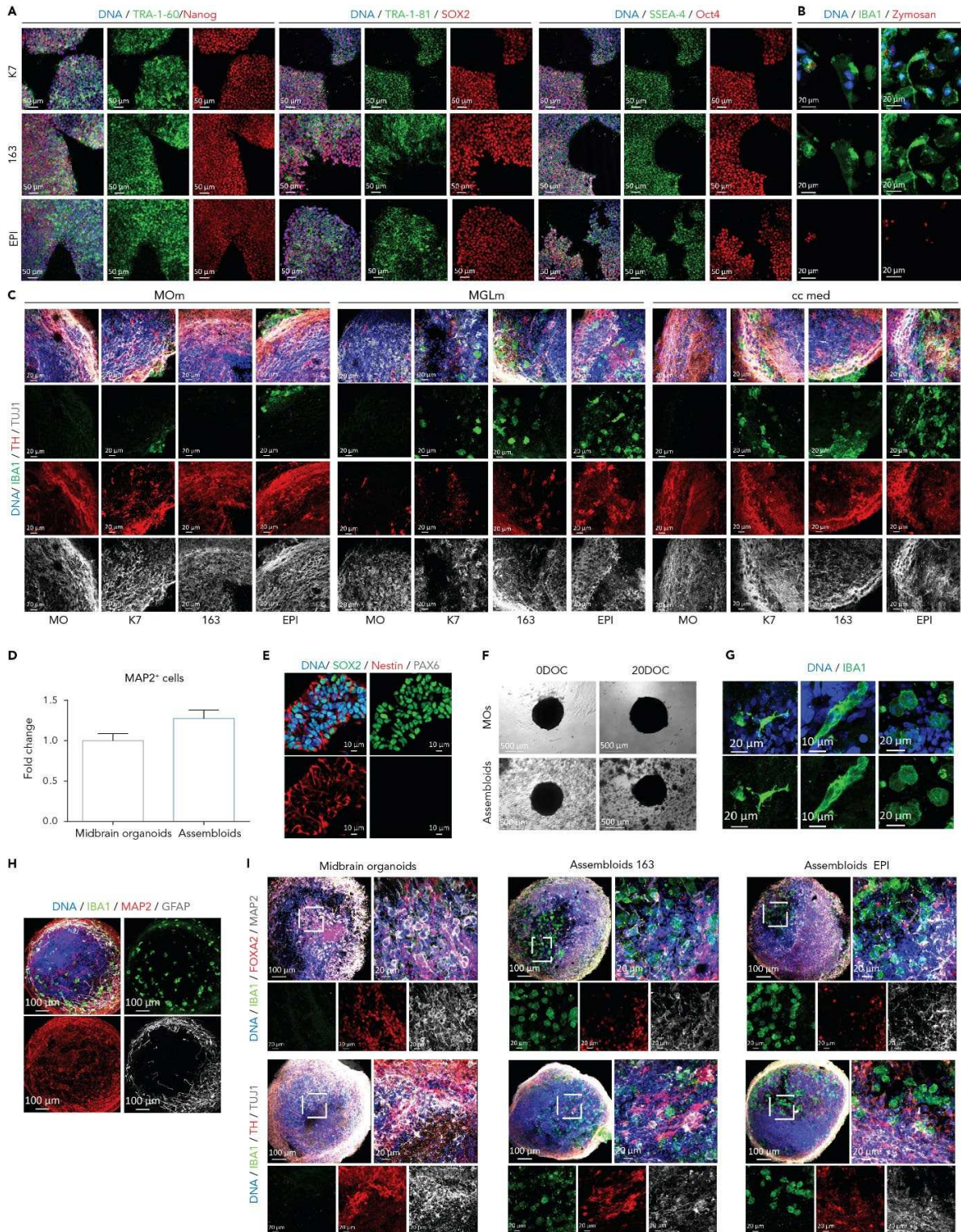
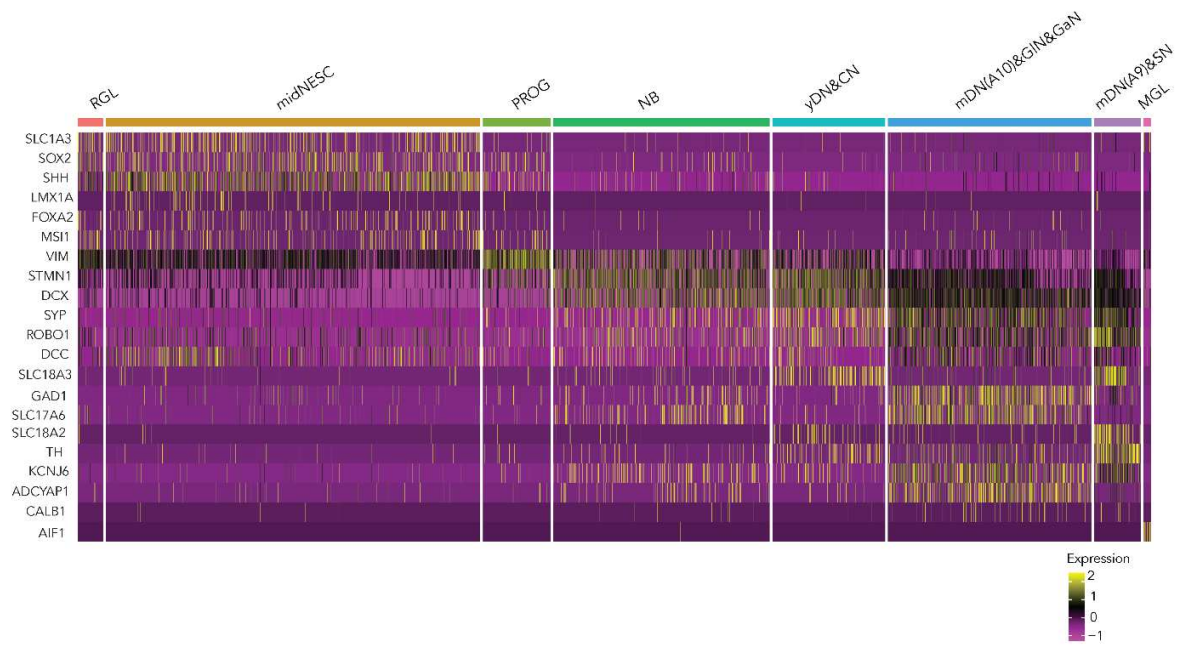
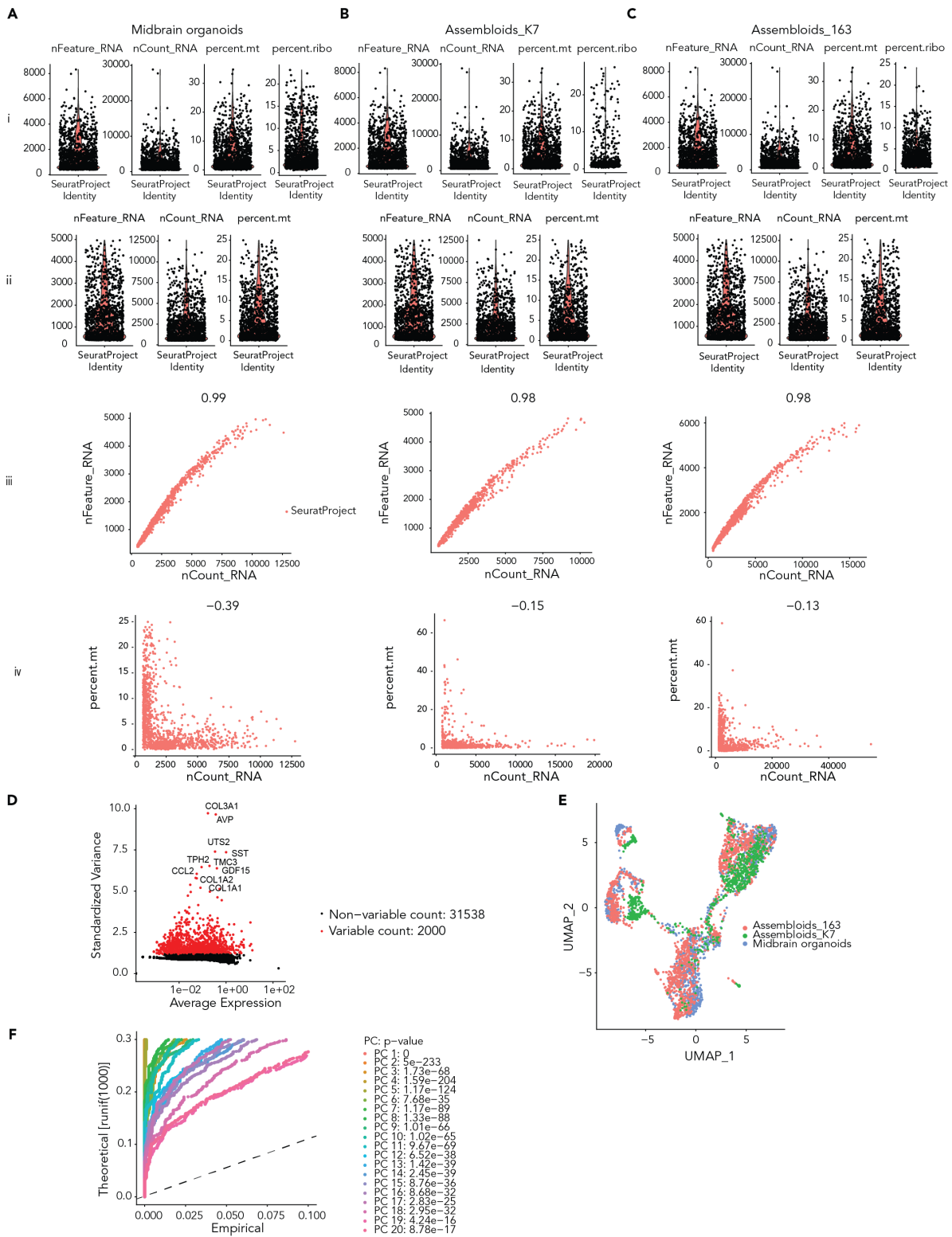


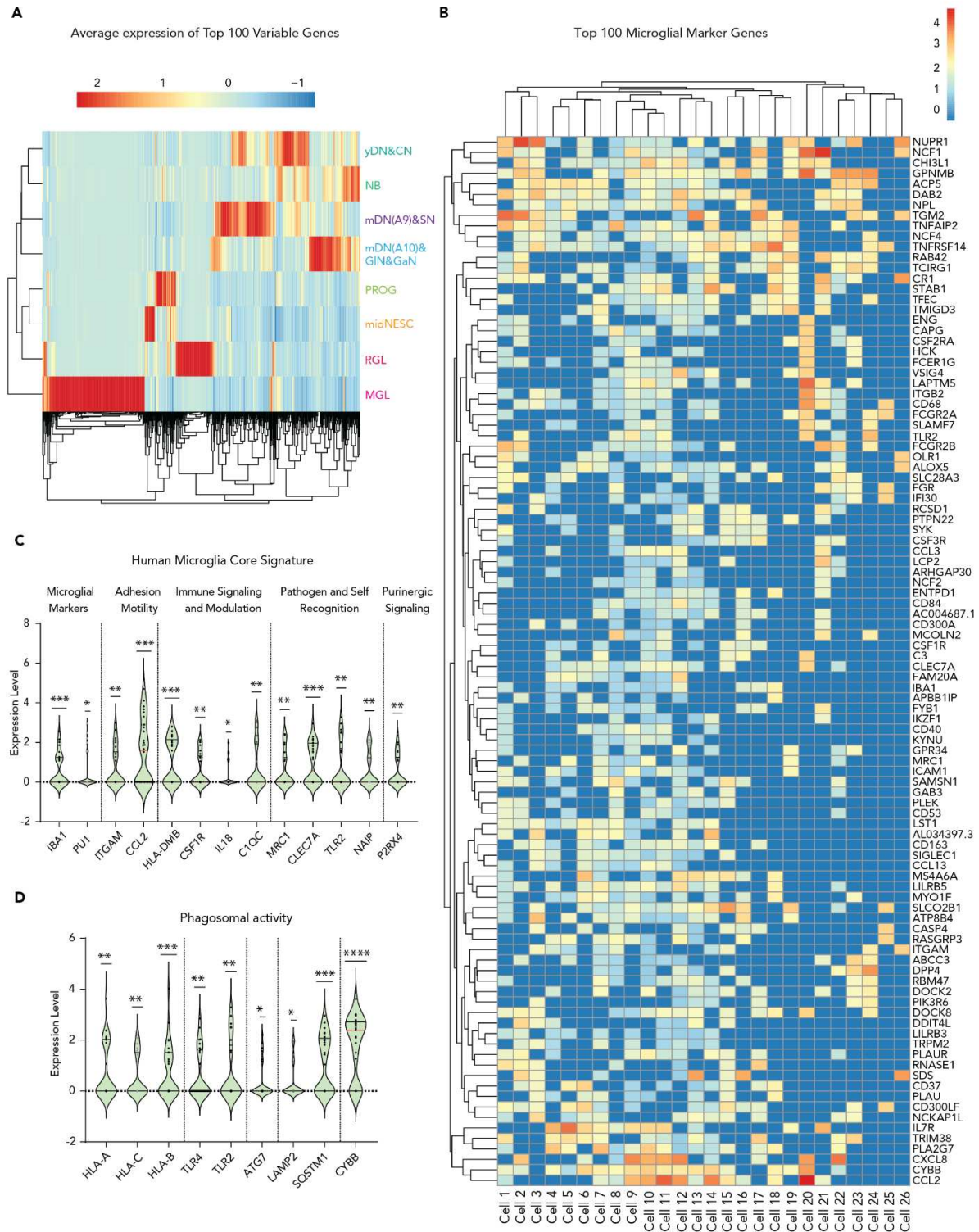
Figure S1.



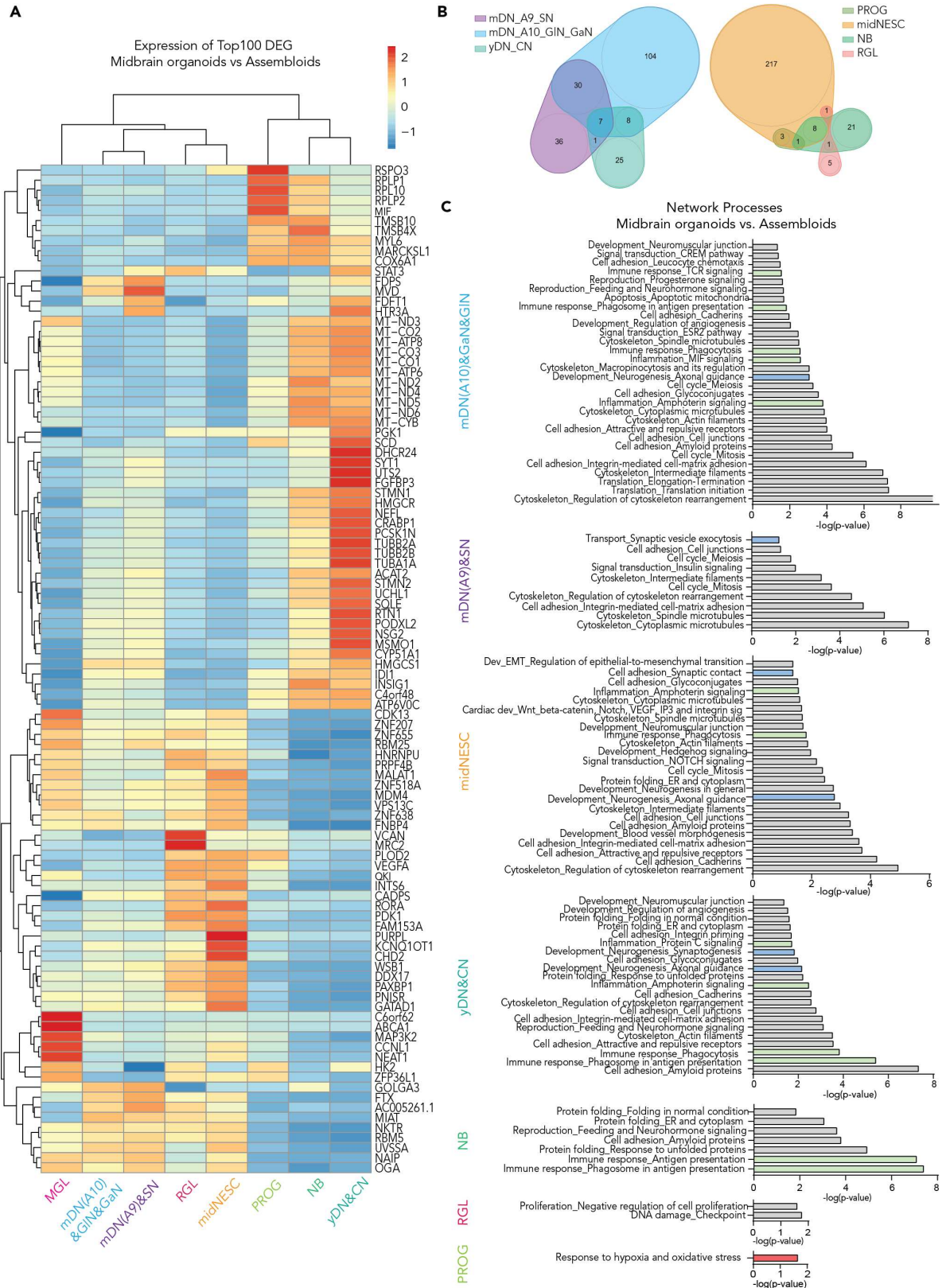
**Figure S2.**



**Figure S3.**



**Figure S4.**





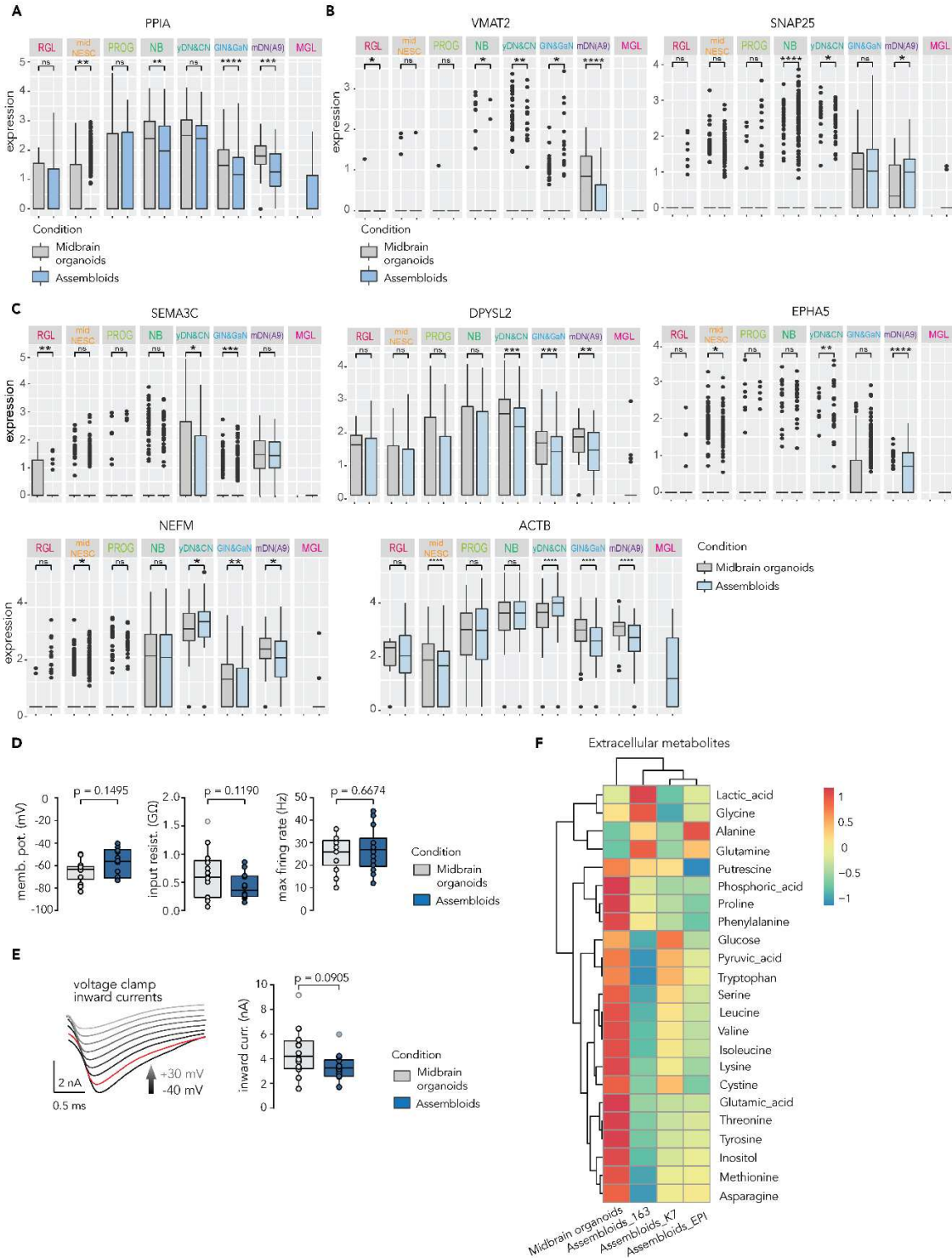
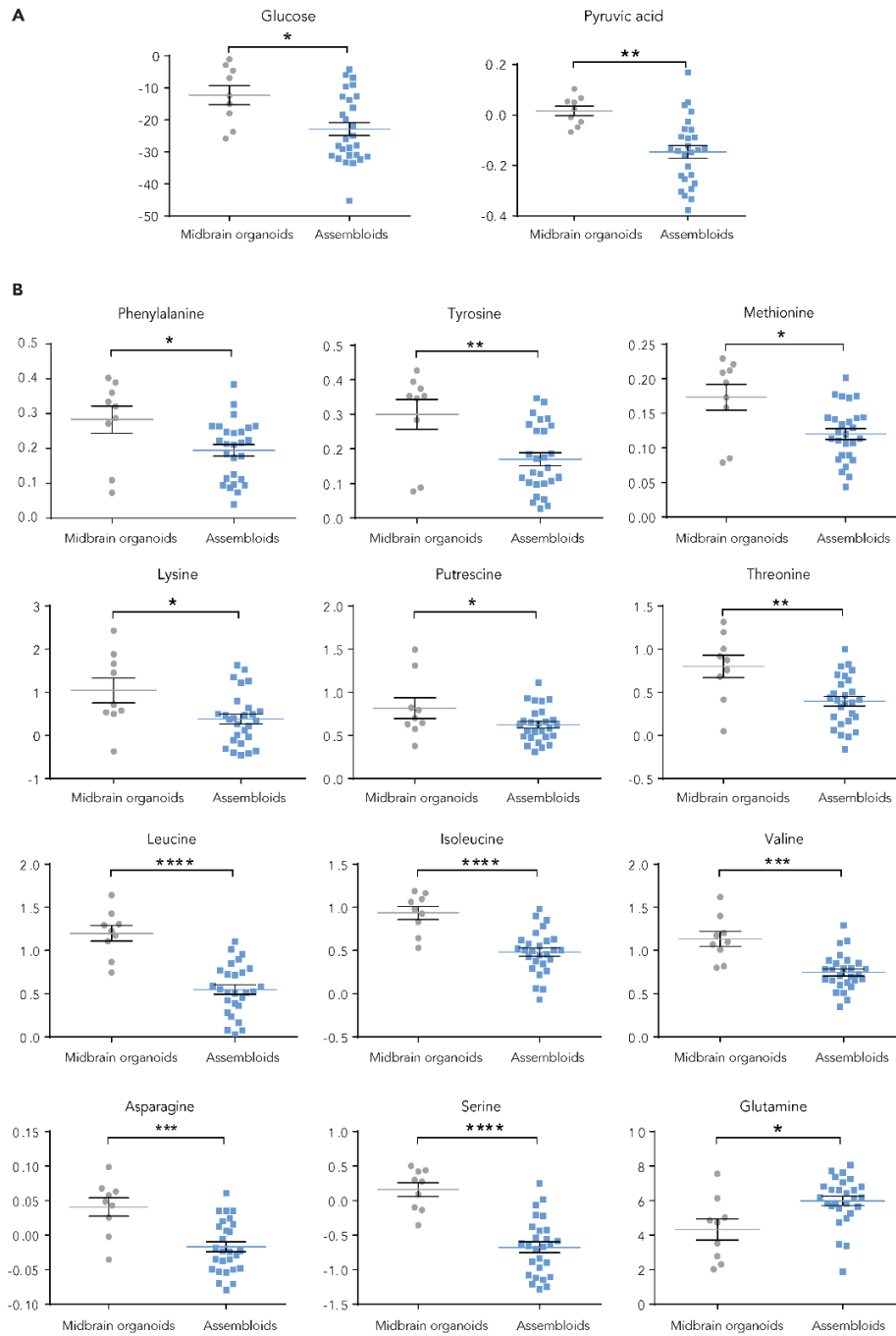


Figure S6.



**Figure S7.**

---

## **Manuscript III**

### **Age-induced midbrain-striatum assembloids model early phenotypes of Parkinson's disease**

**Kyriaki Barmpa**<sup>1</sup>, Claudia Saraiva<sup>1</sup>, Gemma Gomez-Giro<sup>1</sup>, Elisa Gabassi<sup>2</sup>, Sarah Spitz<sup>3</sup>, Konstanze Brandauer<sup>3</sup>, Juan E. Rodriguez Gatica<sup>4</sup>, Paul Antony<sup>1</sup>, Graham Robertson<sup>1</sup>, Florentia Papastefanaki<sup>5,6</sup>, Ulrich Kubitscheck<sup>4</sup>, Ahmad Salti<sup>2,7</sup>, Peter Ertl<sup>3</sup>, Rebecca Matsas<sup>5,6</sup>, Frank Edenhofer<sup>2</sup> and Jens C. Schwamborn<sup>1\*</sup>

<sup>1</sup>Developmental and Cellular Biology, Luxembourg Centre for Systems Biomedicine, University of Luxembourg, 7, Avenue des Hauts-Fourneaux, 4362 Esch-sur-Alzette, Luxembourg

<sup>2</sup>Laboratory of Genomics, Stem Cell Biology and Regenerative Medicine, Institute of Molecular Biology, University of Innsbruck, Technikerstr. 25, 6020 Innsbruck Austria

<sup>3</sup>Institute of Applied Synthetic Chemistry, Vienna University of Technology, Getreidemarkt 9, 1060 Vienna, Austria

<sup>4</sup>Clausius Institute of Physical and Theoretical Chemistry, University of Bonn, Wegeler Str. 12, 53115 Bonn, Germany

<sup>5</sup>Laboratory of Cellular and Molecular Neurobiology-Stem Cells, Hellenic Pasteur Institute, 127 Vassilissis Sofias Avenue, 11521 Athens, Greece

<sup>6</sup>Human Embryonic and Induced Pluripotent Stem Cell Unit, Hellenic Pasteur Institute, 127 Vassilissis Sofias Avenue, 11521 Athens, Greece

<sup>7</sup>Johannes Kepler University Linz, Kepler University Hospital, University Clinic for Ophthalmology and Optometry, Altenberger Strasse 69, 4040 Linz and Krankenhausstrasse 5, 4020 Linz, Austria

\*Corresponding author: Jens C. Schwamborn

The article is in bioRxiv. Submission to a peer reviewed journal is foreseen in the next weeks.

---

## **Preface**

The nigrostriatal pathway is formed by the dopaminergic neuronal projections from the SNpc to the dorsal striatum. In the case of PD, retrograde degeneration of the dopaminergic terminals in the striatum leads to DA depletion and dysregulation of the basal ganglia circuits that control behavior and movement. Research on PD has mainly focused on the dopaminergic neuronal loss, which is the ultimate state of the disease. More efforts are needed into elucidating the mechanisms of retrograde axonal degeneration of DANs, a phenotype that precedes the ultimate neuronal death in the SNpc (Tagliaferro and Burke 2016; L. H. Li et al. 2009; Heng et al. 2023).

Advanced 3D *in vitro* models such as midbrain organoids, are capable of recapitulating many aspects of PD making them a relevant model for studying the vulnerability of DANs in a microenvironment that resembles the adequate human midbrain composition better than the neuronal 2D models (Jarazo et al., 2021; H. Kim et al., 2019; Monzel et al., 2017; Smits et al., 2019). However, midbrain organoids cannot resemble the nigrostriatal connectivity which is crucially affected in PD. Here we present the generation of a midbrain striatum assembloid model. Characterisation of the model shows the identity specificity in the midbrain and striatum compartments in the assembloid, but also the ability of these two distinct organoids to communicate with the formation of active synapses. In parallel, we provide evidence of nigrostriatal pathway functionality in the model, with the release of catecholamines from the midbrain to striatum.

Another aspect that we take into consideration in this study, is the major risk factor of PD, which is aging. While *in vitro* iPSC-derived models are valuable for investigating neurodevelopmental defects that may contribute to the development of PD (Schwamborn, 2018), they cannot fully recapitulate aging dysregulated mechanisms (Simpson et al., 2021). To address this issue, we leveraged an iPSC line engineered to express a progerin transgene under the control of the Tet-On system. Overexpression of progerin with doxycycline supplementation induces aging characteristics in the assembloid model and leads to the development of early neurodegeneration phenotypes. The model described here represents the initial endeavour to induce aging in an iPSC-derived, brain-relevant 3D model, holding significant potential for its application in neurodegenerative research.

---

## **Contribution statement**

This article is the result of my main PhD project. I carried out the experimental planning, execution of most of the experiments and writing of the manuscript. The bulk RNA sequencing experiment and analysis was performed by the company Novogene, while I performed the analysis with the human post-mortem data comparison. Electrochemical measurements in tissue and analysis were performed by S. Spitz and K. Brandauer (Figure 3.B and Supplementary Figure 11.E, F). Analysis of the MEA data (Figure 1.G) was performed with the help of G. Robertson. P. Antony helped me with the troubleshooting of the image analysis MATLAB scripts. Single nuclei RNA sequencing experiment and data matrix generation was executed by the company Singleron, while I performed the downstream analysis. Whole mount imaging of assembloids (Figure 3.A and Supplementary Figure 11.B-C) was performed by J. E. Rodriguez-Gatica. The Rabies monosynaptic tracing experiment and analysis was executed by me, but previous optimisation of the method on assembloid models was done by G. Gomez-Giro. The viruses for this experiment were generated by F. Papastefanaki.

---

## Abstract

Parkinson's disease (PD), one of the most common aging-associated neurodegenerative disorders, is characterised by nigrostriatal pathway dysfunction, caused by the gradual loss of dopaminergic neurons in the substantia nigra pars compacta (SNpc) of the midbrain and the dopamine depletion in the striatum. State of the art, human *in vitro* models are enabling the study of the dopaminergic neurons' loss, but not the dysregulation of the dopaminergic network in the nigrostriatal pathway. Additionally, these models do not incorporate aging characteristics which potentially contribute to the development of PD. Therefore, it is conceivable that research conducted using these models overlooked numerous processes that contribute to disease's phenotypes. Here we present a nigrostriatal pathway model based on midbrain-striatum assembloids with inducible aging. We show that these assembloids are capable of developing characteristics of the nigrostriatal connectivity, with catecholamine release from the midbrain to striatum and synapse formation between midbrain and striatal neurons. Moreover, Progerin-overexpressing assembloids acquire aging traits that lead to early phenotypes of PD. This new model shall help to reveal the contribution of aging as well as nigrostriatal connectivity to the onset and progression of PD.

---

## Introduction

The nigrostriatal pathway connectivity is established through projections of the midbrain SNpc dopaminergic neurons to the dorsal striatum. Disruption of the nigrostriatal connectivity contributes to the development of PD symptoms, such as motor dysfunction, tremor, muscle stiffness, and bradykinesia (Caminiti et al., 2017; Ghosh et al., 2019). The gradual loss of dopaminergic neurons leads to dopamine depletion in the striatum, with consequences in the synaptic network organization and cellular complexity (Zhai et al., 2018). Before the onset of neuronal loss there is significant decrease of dopaminergic axons in the striatum. This reduction in dopaminergic axons is twice as pronounced in the striatum compared to the decrease in dopaminergic neuronal cells in the SNpc (Chung et al., 2020; Heng et al., 2023; L. H. Li et al., 2009; Tagliaferro & Burke, 2016). However, due to the research focus on the loss of neurons, which is the ultimate endpoint of the disease, the mechanisms of the retrograde dopaminergic axons' degeneration from the striatum are still not understood (Tagliaferro & Burke, 2016).

Animal models of PD have been used to elucidate cellular and molecular dysfunctions, but they cannot fully recapitulate the impairments that occur in the human nigrostriatal connectivity (Potashkin et al., 2011). More recently, human based cellular models such as induced pluripotent stem cells (iPSCs) derived 2D neuronal cell culture and the more advanced 3D midbrain organoids have been extensively used for PD modelling. Midbrain organoids have the advantage of better recapitulating the neuronal connectivity in a 3D environment with active neuronal electrophysiology and self-organization properties (J. Kim et al., 2020; Monzel et al., 2017). Midbrain organoids derived from PD patient cell lines exhibit phenotypes relevant to the disease and they present a great tool for further understanding the molecular and cellular mechanisms of neurodegeneration (Becerra-Calixto et al., 2023; Jarazo et al., 2019; Jo et al., 2021; H. Kim et al., 2019; S. W. Kim et al., 2021; Smits et al., 2019; Zagare et al., 2022). Although these models are useful for studying the dopaminergic neurons' vulnerability in PD, they do not recapitulate the nigrostriatal pathway connectivity dysfunction which is essential for unveiling the sources of PD onset and progression.

More advanced 3D models with the combination of two or more region specific brain organoids have started to pave the way towards cellular models with higher complexity that can effectively reflect the neuronal connectivity between different brain regions (Makrygianni & Chrousos, 2021; Panoutsopoulos, 2020; Paşca, 2018). For instance, recent studies have shown the

---

generation of pallium-subpallium, cortico-motor and cortico-striatal assembloids from human iPSCs (Andersen et al., 2020; Birey et al., 2017; Miura et al., 2020), and their capability to develop physiological functional networks that could provide essential insights in diseases' development and progression.

Here we present the development of a midbrain-striatum assembloid model that can recapitulate the nigrostriatal pathway connectivity, with catecholamines release from the midbrain to striatum and the formation of active synapses between the midbrain dopaminergic neurons and the striatal neurons. Although the midbrain-striatum assembloid model allows us to study aspects of the human nigrostriatal connectivity *in vitro*, it still lacks one major risk factor of PD, which is aging (Collier et al., 2017; Hindle, 2010; Lapasset et al., 2011). To address whether aging induction could lead to neurodegenerative phenotypes in assembloids, we used a genetically engineered iPSC line that carries a Progerin-GFP transgene under the control of the Tet-On system for the controllable overexpression of Progerin in the presence of doxycycline (Gabassi et al., *In Preparation*). Our results show that Progerin-overexpression can induce aging phenotypes in the midbrain-striatum assembloid model which subsequently leads to the development of PD-associated early neurodegeneration phenotypes.

## Methods

### iPSCs and NESCs

The induced pluripotent stem cells (iPSCs) that were used in this study are described in Supplementary Table 1. The iPSCs were cultured in 6-well plates (Thermo Fisher Scientific, 140675) coated with Geltrex (Life Technologies, A1413302). For the first 24 hours the cells were cultured in Essential 8 Basal medium (Thermo Fisher Scientific, A1517001) supplemented with 1% Penicillin/Streptomycin (Invitrogen, 15140122) and 10  $\mu$ M ROCK Inhibitor (Ri) (Y-27632, Millipore, SCM075). After the 24 hours, the cells were cultured in Essential 8 Basal Medium, with daily media changes. Confluent iPSCs (~70-90%) were splitted using UltraPure™ 0.5M EDTA, pH 8.0 (Thermo Fisher Scientific, 15575020). Immunofluorescence staining was performed to confirm the pluripotent identity of the iPSCs (Supplementary Figure



---

1.A-D). Neuroepithelial stem cells (NESCs) were generated from iPSCs using a previously described protocol (Reinhardt et al., 2013). Similar to the iPSCs, the NESCs were cultured in Geltrex-coated 6-well plates using supplemented N2B27 media, as described in (Monzel et al., 2017). The NESCs were passaged using Accutase (Sigma-Aldrich, A6964) and their neural stem cell identity was confirmed with immunofluorescence staining (Supplementary Figure 1.E-G).

### **Striatum Organoids**

Striatum organoids (StrOs) were generated using an adapted protocol (C4) from (Miura et al., 2020) (C3) after comparing it with two other conditions (RA and SR) in two time points of culture (day (D)35 and D50) (Supplementary Figure 2, Supplementary Figure 3). iPSCs at ~70% confluency were used for the StrOs generation. Before the procedure of spheroids formation, the cells were treated overnight with 1% DMSO (Sigma-Aldrich, D2650) in Essential 8 basal medium. For the spheroids formation (D -1), the iPSCs were first incubated into Accutase at 37 °C for 5 min. The accutase was stopped using 5x DMEM-F12 (Thermo Fisher Scientific, 21331-046). The cells were then resuspended in Essential 8 medium containing 20 µM Ri and counted using the Countless cell counting chambers slides (Invitrogen, C10313). For condition C4, 10000 cells were added per well in the BIOFLOAT™ 96-well plate U-bottom (faCellitate, F202003), centrifuged in 100g for 3 min and then incubated in the normal culture conditions of 37°C with 5% CO<sub>2</sub>. The spheroids were left intact for two days to form properly and at D1 the medium was exchanged with Essential 6 medium (Thermo Fisher Scientific, A1516401) supplemented with 10 µM Ri, 2.5 µM Dorsomorphin (Sigma-Aldrich, P5499) and 10 µM SB-431542 (Abcam, ab120163). The spheroids were cultured in the same medium until D5, with a reduction of the Ri concentration at 10 µM at D2, 5 µM at D3 until completely removed at D4. To start the differentiation process of the spheroids into StrOs, on D6 the medium was exchanged with a medium containing Neurobasal-A (Thermo Fisher Scientific, 10888022), 2% B-27 without vitamin A (Thermo Fisher Scientific, 12587010), 1% Penicillin/Streptomycin (Invitrogen, 15140122), 1% GlutaMAX (Thermo Fisher Scientific, 35050061) and supplemented with 2.5 µM IWP-2 (Selleckchem, S7085) and 50 ng/ml Activin A (Thermo Fisher Scientific, PHC9561). From D9 to 17, the media was additionally supplemented with 100 nM SR11237 (Tocris, 3411). Until D17 the medium was exchanged daily. From D17 to 35, the

---

media was changed to promote the neuronal differentiation and it was supplemented with 20 ng/ml BDNF (PeproTech, 450-02), 20 ng/ml NT-3 (Alomone labs, N-260), 200  $\mu$ M AA (Sigma-Aldrich, A4544) and 100  $\mu$ M cAMP (Biosynth, ND07996), with medium exchanges every 3 to 4 days. For condition C3, the same protocol as described in Miura and colleagues (Miura et al., 2020) was followed, without the addition of cis-4,7,10,13,16,19-docosahexaenoic acid (DHA) at D22 of differentiation.

For the generation of StrOs from the RA and SR conditions, iPSCs at ~70% confluency were collected using accutase as described above, and 9000 cells were plated in each well of the BIOFLOAT™ 96-well plate U-bottom (D -2). The media used for plating was containing 80% DMEM F12 (Thermo Fisher Scientific, 21331046), 20% KOSR (Thermo Fisher Scientific, 10828028), 3% FBS (Invitrogen, 16140071), 1% GlutaMAX, 1% NEAA (Thermo Fisher Scientific, 11140-050) and 0.7% 2-Mercaptoethanol 50 mM (Thermo Fisher Scientific, 31350-010). This media was supplemented with 10  $\mu$ M Ri and 40 ng/ml FGF-basic (PeproTech, 100-18B). After two days (D0 of culture) the media was exchanged with the Neural induction medium (NIM) containing 76.8% DMEM F12, 20% KOSR, 1% NEAA, 1% GlutaMAX, 1% Penicillin/Streptomycin and 0.2% 2-Mercaptoethanol 50 mM. From D0 to 2 the NIM was supplemented with 5  $\mu$ M DM, 10  $\mu$ M SB and 10  $\mu$ M Ri, while on D2 Ri was removed. From D2 to D16 the medium was exchanged daily. On D4 and 5 the medium was additionally supplemented with 5  $\mu$ M IWP-2. On D6, NIM was exchanged to the neural differentiation medium (NM) which contained 96% Neurobasal A medium, 2% B-27 without vitamin A, 1% GlutaMAX and 1% Penicillin/Streptomycin. From D6 to 8, NM was supplemented with 20 ng/ml FGF-basic, 20 ng/ml EGF (PeproTech, AF-100-15) and 5  $\mu$ M IWP-2. From D8 to 16, NM was supplemented with 20 ng/ml FGF-basic, 20 ng/ml EGF, 5  $\mu$ M IWP-2, 50 nM SAG (Merck Millipore, 566660), 50 ng/ml Activin A and 1 mM for condition RA or 100 nM SR11237 for condition SR. On D17 the media was exchanged with a non-supplemented NM. From D18 to D35 or D50, NM was supplemented with 20 ng/ml BDNF and 20 ng/ml NT3, with media changes every 3 to 4 days.

---

## Midbrain organoids

Midbrain organoids (MOs) were generated using NESCs as the starting population of cells. The protocol that was used is a slightly altered version of the one described in Monzel and colleagues (Monzel et al., 2017). At D0, 9000 NESCs were added per well in the BIOFLOAT™ 96-well plate U-bottom and cultured in maintenance medium for 2 days. At D3 the medium was exchanged with the differentiation medium containing 1  $\mu$ M purmorphamine and at D8 with the final differentiation medium without purmorphamine. The organoids were kept in static conditions and in the 96-well plates U-bottom, until used for the assembloids generation (described below).

## Assembloids

Assembloids of midbrain and striatum organoids were generated using midbrain organoids at D20 and striatum organoids at D35 of culture. Due to the different media composition of the organoids, an optimization of the co-culture medium was needed (Supplementary Figure 4, Supplementary Figure 5, Supplementary Figure 6). Four different media were tested. The Neural Medium (NM) was comprised of Neurobasal-A, 2% B-27 without vitamin A, 1% Penicillin/Streptomycin and 1% GlutaMAX, while the Neural Medium Plus (NMpl) was supplemented with B-27 plus (Thermo Fisher Scientific, A3582801) instead of the B-27 without Vitamin A. In the third condition, the Neural Medium++ (NM++) was tested, which was the NM medium supplemented with 20 ng/ml BDNF (PeproTech, 450-02), 10 ng/ml GDNF (PeproTech, 450-10), 20 ng/ml NT-3 (Alomone labs, N-260), 200  $\mu$ M AA (Sigma-Aldrich, A4544) and 100  $\mu$ M cAMP (Biosynth, ND07996). The optimal assembloid co-culture condition for the assembloid model was consisted of the N2B27 medium (described by Monzel and colleagues (Monzel et al., 2017)), which consists of DMEM F12 (Invitrogen)/Neurobasal (Invitrogen) 50:50 with 0.5% N2 supplement (Thermo Fisher Scientific, 17502001), 1% B-27 without Vitamin A, 1 % GlutaMAX and 1 % Penicillin/Streptomycin. The media was further supplemented with 20 ng/ml BDNF (PeproTech, 450-02), 10 ng/ml GDNF (PeproTech, 450-10), 20 ng/ml NT-3 (Alomone labs, N-260), 200  $\mu$ M AA (Sigma-Aldrich, A4544) and 100  $\mu$ M cAMP (Biosynth, ND07996). At D0 of the assembloids generation, each StrO was transferred in each well of the 96-well plate U-bottom that contained the MOs and the medium was

---

exchanged to the assembloid co-culture medium. After 4 days, the two organoids were merged into an assembloid, and they were transferred in 24 well ultra-low attachment plates (Celltreat, 229524). Some of the assembloids were embedded in 30  $\mu$ l Geltrex (Invitrogen, A1413302), as described before (Monzel et al., 2017). The assembloids were cultured in 37°C, 5% CO<sub>2</sub> under static conditions.

For the Progerin overexpression induction, assembloids that were generated from the Progerin-overexpressing cell line were treated with 4 ng/ $\mu$ l doxycycline (Sigma-Aldrich, D9891). Generation and validation of iPSC line expressing Progerin under control of the Tet-ON system is described elsewhere (Gabassi et al., *In Preparation*).

### **ATP and LDH assay**

Intracellular ATP in assembloids was measured using luminescence based CellTiter-Glo® 3D Cell Viability Assay (Promega, G9681). Three organoids per cell line and per condition were transferred each in one well of the imaging plate (PerkinElmer, 6055300). 50  $\mu$ l of CellTiter-Glo® reagent were added to each well and the plate was incubated for 30 min on a shaker at room temperature (RT). Luminescence was measured using Cytation5 M cell imaging reader (RRID:SCR\_019732). The experiment was repeated for three independent derivations (batches) at D30 assembloids. The mean signal of three assembloids of each cell line and condition was calculated and normalized to the mean size (area) of the assembloids. Brightfield images of random assembloids of the three batches taken with the ZEISS Axio Vert.A1+AxioCam ICM1 microscope and the area of each assembloid was calculated with the ZEN (blue edition) software (RRID:SCR\_013672). The mean area of all assembloids measured per line and conditions from each batch was used for the normalization.

For determining the cytotoxicity in the assembloids, the LDH-Glo™ Cytotoxicity Assay (Promega, J2381) was used. In the day of assembloids collections (D30 of culture) media from three assembloids per line and condition from three batches was collected and snap frozen in liquid nitrogen. For the LDH assay, the snap frozen media was thawed on ice. 50  $\mu$ l of media from each sample and 50  $\mu$ l of the enzyme and substrate mix was pipetted in a well of the imaging plate (PerkinElmer, 6055300). The plate was briefly mixed and incubated for 1 h at RT

---

avoiding exposure to light. Luminescence was measured using Cytation5 M cell imaging reader. Similar to the ATP assay, the mean signal of the assembloids was normalized to the mean of the assembloids' area.

### **Western Blotting – RIPA buffer**

For Western blotting, four non-embedded assembloids or six to eight organoids were lysed using RIPA buffer (Abcam, ab156034) supplemented with cOmplete™ Protease Inhibitor Cocktail (Roche, 11697498001) and Phosphatase Inhibitor Cocktail Set V (Merck Millipore, 524629). The samples were pipetted 10-20 times up and down until dissolved and were incubated on ice for 20 min. For DNA disruption, lysates were sonicated for 10 cycles (30 seconds on / 30 seconds off) using the Bioruptor Pico (Diagenode), followed by a centrifugation at 4°C for 20 min at 14000g. The protein concentration was measured using the Pierce™ BCA Protein Assay Kit (Thermo Fisher Scientific, 23225). Samples were adjusted to the same concentration by appropriate dilution with RIPA buffer and boiled at 95°C for 5 min in denaturing loading buffer. 2.5-10 µg of protein was loaded per sample for every Western blot. Protein separation was achieved using SDS polyacrylamide gel electrophoresis (Bolt™ 4-12% Bis-Tris Plus Gel, Thermo Fisher Scientific) and transferred onto a PVDF membrane using iBlot™ 2 Gel Transfer Device (Thermo Fisher Scientific). After transfer the membrane was dried for 10 min in 37°C and subsequently activated with 100% Methanol for 30 sec. The membranes were washed twice with PBS containing 0.02% Tween and they were blocked for 1 hour at RT in 5% skimmed milk powder dissolved in PBS. After blocking, the membranes were washed quickly with PBS containing 0.02% Tween and were incubated overnight at 4°C with the primary antibodies prepared in 5% BSA and 0.02% Tween in PBS (Supplementary Table 2). The next day, membranes were washed three times for 5 min with PBS containing 0.02% Tween and incubated with DyLight™ secondary antibodies at a dilution of 1:10000 (anti-rabbit IgG (H+L) 800, Cell Signaling, 5151P or anti-mouse IgG (H+L) 680, Cell Signaling, 5470P) for 1 hour. Membranes were revealed in the Odyssey® Fc 2800 Imaging System and exposure time was from 30 sec to 4 min, depending on the primary antibody used. Western blots were analyzed using ImageJ (RRID:SCR\_003070) software.

---

## Western Blotting – Nuclear and Cytoplasmic fractionation

The protocol described by Abcam (<https://www.abcam.com/protocols/nuclear-extraction-protocol-nuclear-fractionation-protocol>) was used for the nuclear-cytoplasmic fractionation. At the last step of the protocol both nuclear and cytoplasmic samples were sonicated for 10 cycles (30 seconds on / 30 seconds off) using the Bioruptor Pico (Diagenode). For the preparation of the nuclear extraction and fractionation buffer the reagents used were HEPES (Sigma-Aldrich, H3375), KCl (AppliChem, 8059), MgCl<sub>2</sub> (Sigma-Aldrich, M8266), EDTA (Sigma-Aldrich, E9884), EGTA (Sigma-Aldrich, E3889), DTT (Thermo Fisher Scientific, R0861), cOmplete™ Protease Inhibitor Cocktail and Phosphatase Inhibitor Cocktail Set V. The following Western blotting procedure is described in the previous section.

## Flow cytometry

Three embedded assembloids per condition were used for GFP<sup>+</sup>, live cells measurement in BD LSRFortessa flow cytometer (RRID:SCR\_019601). Geltrex embedded assembloids were first incubated at 37°C for 40-50 min on shaker in 500 µl of papain solution containing 20 ml DMEM-F12, 36 mg Papain (Sigma-Aldrich, P4762), 8 mg EDTA (Sigma-Aldrich, E6758) and 8 mg L-Cystein (Sigma-Aldrich, C6852). To start the dissociation process, papain solution was replaced with 500 µl accutase and the assembloids were pipetted with the 1000 pipette, followed by a 10 min incubation shaking. After that, pipetting with the 200 µl pipette and incubation cycles were continued until the complete dissociation of the assembloids. For the accutase and papain inhibition, 500 µl papain inhibitor solution containing 5 mg/ml BSA (Carl Roth, 8076.4) and 5 mg/ml Trypsin inhibitor (Sigma-Aldrich/Roche, 10109878001) in PBS was added. After transferring the total volume in 2 ml Eppendorf tube, the dissociated assembloids were centrifuged at 500xg for 5 min. Supernatant was discarded and the pellet was washed once with PBS. The pellet was resuspended in 300 µl DMEM (Thermo Fisher Scientific, A14430-01) containing 1:1000 concentration live-dead stain Zombie NIR (Biolegend, 423106), followed by incubation at 37°C for up to 30 min. Cells were then centrifuged at 500xg for 3 min and pellet was washed twice with PBS and centrifuged again with the same setting. After the final wash and centrifugation, the pellet was resuspended in DMEM and the samples were run in Becton Dickinson LSRFortessa, with 10000 events acquisition of GFP<sup>+</sup>, live-cells. Each sample was

---

run in two technical replicates. The data were analysed using the FlowJo software (v.10.7.2, RRID:SCR\_008520).

## **Rabies virus based retrograde monosynaptic tracing**

### Lentiviral vector and rabies virus vector productions

The construct pBOB-synP-HTB [gift from Edward Callaway & Liqun Luo (Addgene plasmid # 30195 ; <http://n2t.net/addgene:30195> ; RRID:Addgene\_30195)] (Miyamichi et al., 2011) was used for the production of the replication-deficient LV-GP-TVA-GFP lentiviral vector. High-titer preparations of lentiviral particles were produced, as previously described (Kutner et al., 2009). The titer of the preparation used was  $3 \times 10^8$  IU/mL.

For the production of RBV- $\Delta$ G-EnvA-RFP rabies viral particles, we followed stages III-VI of the previously established protocol for the amplification, pseudotyping, and concentration of the virus (Osakada & Callaway, 2013). Titer was  $4 \times 10^7$  IU/mL.

### Lentiviral vector and rabies virus vector transduction of assembloids

To assess the connectivity through active synapses between the midbrain and striatum neurons in the assembloid model, striatum organoids at D35 of culture were transduced by adding concentrated LV-GP-TVA-GFP viral particles at 1:500 dilution, in the culture medium. After 7 days the medium containing the lentiviral vector was discarded and the organoids were washed twice with fresh medium. The LV-transduced StrOs were then merged with MOs and the assembloids were infected by the addition of the concentrated RBV- $\Delta$ G-EnvA-RFP rabies viral particles at 1:500 dilution in the culture medium. Control experiments, with single infection of assembloids with only one of the vectors at a time, were performed to confirm the specificity of the signal. After 7 days the media was changed and the assembloids were cultured for up to D30. 70  $\mu$ m-thick sections were either imaged directly for the observation of the RFP and GFP signal from the viral infections or were immunostained using a tyrosine hydroxylase (TH) antibody (see **Immunofluorescence Staining** procedure and Supplementary Table 3 for the antibody) to assess the colocalization between TH and RFP.

---

## **β-galactosidase**

70 μm sections from assembloids were used in the β-galactosidase staining, using the Senescence Detection Kit (Abcam, ab65351). One section from two or three assembloids per condition from four batches were used. Images were taken using the colour camera setting with 4X objectives in the Olympus IX83 microscope (RRID:SCR\_020344). β-galactosidase positive areas were quantified using ImageJ. Positive areas in each section were summed and normalised to the total area of the section in the image. The normalised value was multiplied by 100 for calculating the % of positive β-galactosidase areas in the image.

## **Immunofluorescence Staining**

### **iPSCs and NESCs**

The procedure that was used for the immunofluorescence staining characterization of the iPSCs is detailed described by Gomez-Giro and colleagues (Gomez-Giro et al., 2019), a previous study from our lab.

For the NESCs' immunofluorescent staining characterization, NESCs were cultured on Geltrex-coated 96-well imaging plates (PerkinElmer, 6055300) until they reached approximately 70% confluency. Next, NESCs were fixed for 15 min at RT with 4% Paraformaldehyde (PFA), washed 3x for 5 min with PBS and permeabilized with 0.3% Triton X-100 in PBS for 15 min at RT. After permeabilization, NESCs were washed 3x for 5 min with PBS and then blocked with 10% fetal bovine serum (FBS) in PBS for 1 hour at RT. Primary antibodies (Supplementary Table 3) were diluted in 3% FBS in PBS and the cells were incubated overnight at 4°C. Then cells were washed 3x for 5 min with PBS and incubated for 1 hour at RT with secondary antibodies (Supplementary Table 3) and Hoechst 33342 (Invitrogen, 62249). After 3 washes for 5 min with PBS, cells were kept in 0.1% Sodium Azide (NaAz) in PBS until imaging with confocal microscopy.

### **Organoid and Assembloid Sections**

Assembloids and organoids were fixed with 4% PFA overnight at 4°C, and then washed with PBS three times for 15 min at RT. At least three organoids/assembloids per line and time point



---

were embedded in 3% low-melting point agarose (Biozym, 840100). 70  $\mu\text{m}$  sections were obtained using the vibratome (Leica VT1000s, RRID:SCR\_016495). The sections were permeabilized for 30 min in 0.5 % Triton X-100 and blocked for 2 h with blocking buffer containing 2.5% normal goat serum, 2.5 % BSA, 0.01% Triton X-100 and 0.1 % sodium azide in PBS at RT. Sections were incubated with the primary antibodies (Supplementary Table 3) diluted in blocking buffer for 48-72 hours at 4 °C. The sections were washed with 0.01% Triton X-100 for 5 min three times and then incubated with the secondary antibodies (Supplementary Table 3) and Hoechst at 1:1000 dilution for 2 hours at RT. The sections were then washed again with 0.01% Triton X-100 for 5 min three times at RT. After the last wash, the sections were kept in MilliQ water and mounted on slides as described by Nickels and colleagues (Nickels et al., 2020).

## **Microscopy**

For high-content image analysis, one 70  $\mu\text{m}$  section from three organoids/assembloids of each condition from at least three batches were acquired using the Yokogawa CV8000 high content screening microscope (RRID:SCR\_023270) with a 20X/0.75 numerical aperture (NA) objective.

For qualitative analysis, images were acquired using a confocal laser scanning microscope (Zeiss LSM 710, RRID:SCR\_018063) with the 20X/0.8 NA, 40X/1.3 NA or 63X/1.4 NA objective.

## **Light sheet fluorescence expansion microscopy**

### Sample preparation

The expansion microscopy protocol was adopted from Rodriguez-Gatica and colleagues (Rodriguez-Gatica et al., 2022) and used for whole assembloid preparation. Briefly, the labelled samples were incubated with 2 mM of methylacrylic acid-NHS linker for 24 hours on a shaker at RT, ensuring they were fully submerged in 1 ml of the solution. Following this, the samples were washed thrice, each time for 40 min in PBS. Subsequently, they were incubated in the

---

monomer solution (comprising 8.6% sodium acrylate, 2.5% acrylamide, 0.15% N,N'-methylenebisacrylamide, and 11.7% NaCl in 1× PBS) on a shaker at 4°C, using 0.9 ml of the solution to cover them.

The gelling solution was freshly prepared by adding 4-hydroxy-TEMPO (0.01%), TEMED (0.2%), and ammonium persulfate (0.2%) to new monomer solution. To prevent premature polymerization during the gelling process, the samples were placed in a 24-well plate on ice. After discarding the monomer and adding the gelling solution, the samples were shaken at 4°C for 5 min. They were then transferred to a gelling chamber that utilized 2 mm spacers to maintain the sample's integrity and prevent deformation. Post-transfer, the samples were left at 4°C overnight and subsequently incubated at 37°C for 2 hours. Upon gel formation, the samples were extracted from the gelling chamber and incubated at 37°C in the digestion buffer (containing 50 mM Tris, 1 mM EDTA, 0.5% Triton X-100, 0.8 M guanidine HCl, and 16 U/ml of proteinase K; pH 8.0). The digestion buffer was replaced every 24 hours, if required, until the samples became fully transparent. After digestion, the buffer was discarded, and the samples were washed three times with PBS. The samples were then stored in PBS, resulting in an expansion to approximately 1.5 times their original size.

The ability to preserve the fluorescence of autofluorescent proteins during the expansion procedure allowed for exclusive immunolabeling of the dopaminergic neurons. Owing to the enhanced retention capabilities of the protocol, nuclear staining was conducted post-digestion. To ensure complete penetration throughout the gel, samples were incubated with Hoechst 33342 (H3570, Invitrogen) in PBS for 24 hours at RT with a concentration of 2.5 µg/ml (1:4000).

#### Light sheet microscopy

Following the expansion protocol, whole-assembloids were imaged using light sheet microscopy to obtain information at both the mesoscale and microscopic scale. Specifically, we utilized the Blaze microscope LaVision-Miltenyi Biotec for whole-assembloid imaging and a custom-built setup for higher resolution imaging of selected regions of interest (ROIs).

#### Mesosopic Imaging

Mesosopic imaging and analysis provide insights into the topology of complete assembloids. This is particularly useful for analysing the distribution of dopaminergic neurons throughout the

---

entire sample. For imaging, the digested specimen was affixed to a coverslip using poly-L-lysine to prevent movement during measurement. This coverslip was then inserted into a custom sample holder and positioned within a large imaging chamber ( $183 \times 50 \times 64$  mm length–width–height) filled with PBS solution (1xPBS, 0.02% Sodium azide).

For mesoscopic imaging, the Blaze from LaVision-Miltenyi BioTec was employed. Fluorescence excitation was achieved using four fiber-coupled lasers emitting at 405, 488, 561, and 638 nm (from the LaVision laser beam combiner). Given the sample's transparency, a single illumination arm sufficed. The beam waist in the object plane was adjusted to a  $1/e^2$  diameter of  $6 \mu\text{m}$  for all laser lines. Fluorescence emission was detected by a 4X objective (LaVision-Miltenyi BioTec MI PLAN 4X/0.35 NA, working distance (WD) 15 mm with water dipping cap) and data was captured using a sCMOS camera (2048 x 2048 pixels, pixel size  $6.5 \mu\text{m}$ ) in global shutter mode, resulting in an effective field of view of  $(3328 \mu\text{m})^2$ . Due to the sample's extensive size, mosaic-style imaging was essential to capture the entire organoid.

### Microscopic Imaging

For microscopic scale imaging, assembloids were prepared as described above, producing a transparent specimen expanded by 1.5-fold. These were then examined using a high-resolution, long-distance objective with an NA of 1.1 (Nikon CFI75 25x/1.1 NA WD 2mm water immersion (WI)), achieving an optical resolution of approximately  $0.3 \mu\text{m}$  laterally and  $1.1 \mu\text{m}$  axially. Factoring in the sample expansion, this translated to an effective resolution of  $0.2$  and  $0.7 \mu\text{m}$ , respectively, enabling structural characterization at subcellular length scales. For samples where the projections were not clear with the 4X mesoscopic view, a 12X objective (LaVision-Miltenyi BioTec MI PLAN 4X/0.35 NA, WD 8.5 mm WI) was used as an intermediate imaging step with the Ultramicroscope.

Imaging of complete assembloids at this resolution is often not advisable due to the data generation (about 500 Gigabyte data per  $1 \text{mm}^3$  per channel). Instead, specific ROIs identified in the mesoscale data were chosen for subsequent microscopic scale analysis. To this end we employed a custom-built setup (Rodriguez-Gatica et al., 2022). Briefly, fluorescence excitation was achieved using four fiber-coupled lasers emitting at 405, 488, 561, and 638 nm (Hübner Photonics, Germany). A horizontally scanned light sheet was produced by a galvanometer system with silver-coated mirrors. Beam waist adjustment within the sample chamber was

---

facilitated by relay optics mounted on a precision linear stage. The beam waist in the object plane was set to specific  $1/e^2$  diameters for each laser line. For illumination, a Mitutoyo 10x NA 0.28 air objective was used.

Our custom sample chamber (165 × 60 × 40 mm length–width–height) featured an illumination window created by a standard 24x24 mm coverslip with a 0.17 mm thickness. Observation was from above using a Nikon 25X 1.1 NA WI objective with an additional 1.5x magnification (Nikon, Germany). The sample, mounted on a coverslip, was manoeuvrable in three spatial directions via motorized micro-translation stages. Data capture was facilitated by a sCMOS camera (3200 x 3200 pixels, pixel size 6.5  $\mu\text{m}$ , Kinetix, Teledyne Photometrics, USA), in global shutter mode, resulting in an effective field of view of (832  $\mu\text{m}$ )<sup>2</sup>. A custom-written LabView program managed all electronic components.

### Data processing

3D stacks of raw 16-bit images were processed using custom-written MATLAB scripts, facilitating parallel data processing. Selected image stacks were spatially deconvolved using Huygens (Professional version 22.04, Scientific Volume Imaging, The Netherlands). This deconvolution utilized theoretical point spread functions (PSFs) derived from the microscopy parameters. The classical maximum likelihood estimation algorithm was employed, with Acuity set to: -10 to 25. Signal-to-noise ratio (SNR) values ranged between 12 and 20, and the maximum number of iterations varied from 60 to 100.

Full 3D representations of the samples were achieved by stitching multiple 3D datasets together using FIJI (Schindelin et al., 2012) and the stitching plugin by Preibisch and colleagues (Preibisch et al., 2009). To optimize the stitching process, especially when datasets surpassed the available RAM of the workstation, a two-step approach was adopted. First, substacks of the 3D datasets were generated using a FIJI script, with each substack containing approximately 15% of the central data from the full stack. Subsequently, each substack was stitched to its adjacent counterpart, ensuring optimal overlap based on cross-correlation measures. Using the localization data from each substack post-stitching, the complete 3D stacks were then assembled.

---

The 3D data visualization was achieved using the Surpass view in Imaris (Version 10.0.1, Bitplane Inc., Zurich, Switzerland). All data processing tasks were executed on a HIVE workstation (ACQUIFER Imaging GmbH, Germany) equipped with dual Intel Xeon Gold 6252 CPUs (2.1 GHz, 24 cores), 1 TB of memory, and an Nvidia RTX A4000 GPU (16 GB GDDR6), operating on Windows Server 2019.

### **Image analysis**

Images obtained from the Yokogawa microscope were processed and analyzed in MATLAB (2021a, Mathworks, RRID:SCR\_001622) using a previously described image analysis pipeline (Bolognin et al., 2019; Monzel et al., 2020).

### **Electrochemical detection of catecholamines in neuronal tissues**

Commercially available Nafion-coated carbon fiber microelectrodes (World Precision Instruments, CF10-50) were employed to measure the presence of catecholaminergic neurotransmitters (e.g., dopamine) within the assembloids. Amperometric measurements were performed according to the manufacturer's instructions using a potentiostat (Bio-Logic, VMP3) equipped with a low current module (Bio-Logic) and a custom-made platform (Supplementary Figure 11.D). Electrodes were activated by applying a potential of 1.2V and simultaneous exposure to a 150 mM NaCl solution with a pH of 9.5. All measurements were conducted at a potential of 0.65V. Prior to the measurements, assembloids were washed three times using PBS. Assembloids were subsequently placed onto the custom-made platform, covered in 100 µl of PBS before electrodes were carefully inserted into the tissue using a laboratory jack. Measurements on StrOs alone and StrOs within D30 assembloids were conducted by introducing the electrode 1-2 times into the centre of the neuronal tissue. For the StrOs cultured in pre-used MOs media, the media was in contact with the MOs for 24 hours. Then it was transferred into the wells containing StrOs. StrOs were cultured in the pre-used MO media for 48 hours prior to the measurements. Due to the occasional occurrence of necrotic cores within assembloids electrochemical measurements on D60 assembloids were performed by introducing the electrodes at the border of the StrO. Measurements were conducted at five different locations

---

within the StrO of the assembloid. To exclude any cross-contaminations, electrodes were carefully washed, and background signals were recorded in between the measurement of each assembloid. Measurement results were averaged and unless stated otherwise data was background subtracted.

### **Quantitative PCR**

The RNeasy Mini Kit (Qiagen, 74106) was used for the total RNA extraction from striatum organoids. The RNA concentration was measured using the Nanodrop 2000c Spectrophotometer (Thermo Fisher Scientific, RRID:SCR\_020309). The High-Capacity RNA-to-cDNA™ Kit (Thermo Fisher Scientific, 4387406) was used for the cDNA synthesis. For the quantitative PCR reaction, the Maxima SYBR Green qPCR Master Mix (Thermo Fisher Scientific, K0221) was used with the primers listed in Supplementary Table 4. The Aria Mx Real-Time PCR system (Agilent) was used and the data were extracted from the AriaMx PC software.

### **RNA sequencing**

RNA was extracted from the assembloids using the RNeasy Mini Kit. Four assembloids were used per condition and from three batches. The RNA samples were shipped with dry ice to Novogene in UK for the RNA sequencing experiment and bioinformatic analysis. The following methodology was used:

#### Quality control of reads

In the process of obtaining clean reads, reads containing adapters, higher than 10% undetermined bases and low quality (Qscore of over 50% bases of the read is  $\leq 5$ ) were removed.

#### Library Construction, Quality Control and Sequencing

Poly-T oligo-attached magnetic beads were used to purify the messenger RNA from the total RNA. After fragmentation, the first strand cDNA was synthesized using random hexamer primers, followed by the second strand cDNA synthesis using dUTP for directional library. To quality control the library, Qubit and real time PCR were used for quantification, while for the size distribution detection bioanalyzer was used. The quantified libraries were combined and

---

sequenced on Illumina platforms, taking into consideration the optimal library concentration and desired data volume.

### Clustering and sequencing

The clustering of the index coded samples was performed according to the manufacturer's instructions. Following the generation of clusters, the library preparations underwent sequencing using an Illumina platform, resulting in the generation of paired-end reads.

## **RNA sequencing Data Analysis**

### Quality control

The initial processing of the raw data (raw reads) in fastq format involved utilizing the fastp software (RRID:SCR\_016962). This step involved removing reads that contained adapters, reads with poly-N sequences, and low-quality reads from the raw data, resulting in obtaining clean data (clean reads). Additionally, metrics such as Q20, Q30, and GC content were calculated for the clean data. All subsequent analyses were performed using the high-quality clean data.

### Reads mapping to the reference genome

The reference genome (hg38) and gene model annotation files were directly downloaded from the genome website. To enable alignment of the paired-end clean reads, an index of the reference genome was constructed using Hisat2 v2.0.5 (RRID:SCR\_015530). Subsequently, Hisat2 v2.0.5 was employed as the mapping tool of choice. We specifically chose Hisat2 due to its ability to generate a splice junction database utilizing the gene model annotation file, resulting in improved mapping accuracy compared to non-splice mapping tools.

### Quantification of gene expression level

To determine the number of reads mapped to each gene, featureCounts v1.5.0-p3 (RRID:SCR\_012919) was employed. Subsequently, the Fragments Per Kilobase of transcript sequence per Millions (FPKM) base pairs sequenced for each gene was calculated based on the gene's length and the count of reads mapped to it. FPKM is a widely utilized method for

---

estimating gene expression levels as it accounts for both the sequencing depth and gene length when considering the reads count. It provides a comprehensive measure of gene expression and is currently the most commonly used approach in this regard.

### Differential expression analysis

Differential expression analysis was conducted on two conditions/groups using the DESeq2 R package (version 1.20.0, RRID: SCR\_015687). DESeq2 utilizes a statistical model based on the negative binomial distribution to determine differential expression in digital gene expression data. The resulting P-values were adjusted using the Benjamini and Hochberg's method to control the false discovery rate. Genes with an adjusted P-value of less than or equal to 0.05, as determined by DESeq2, were identified as differentially expressed.

Before performing the differential gene expression analysis, the read counts for each sequenced library were adjusted using the edgeR package (version 3.22.5, RRID:SCR\_012802) by applying a scaling normalization factor. The differential expression analysis of the two conditions was carried out using the edgeR. The P-values were adjusted using the Benjamini and Hochberg's method. A corrected P-value threshold of 0.05 and an absolute fold change of 2 were set to determine significantly differential expression.

### Enrichment analysis of differentially expressed genes

The clusterProfiler (RRID:SCR\_016884) R package was used for Gene Ontology (GO) (RRID:SCR\_002811) enrichment analysis on the differentially expressed genes, with gene length bias being corrected. GO terms with a corrected P-value < 0.05 were deemed significantly enriched by the differentially expressed genes.

For the analysis of KEGG (RRID:SCR\_012773) pathways, which provide insights into the functions and utilities of biological systems, especially based on large-scale molecular datasets, the clusterProfiler R package was employed. The statistical enrichment of differentially expressed genes in KEGG pathways was assessed.



---

## Single nuclei RNA sequencing

### Samples processing

Samples were processed and sequenced by Singleron. 10 MOs, 10 StrOs and 4 assembloids per batch form 2 batches, generated from the same wild type (WT) line (201, Supplementary Table 1) were snap frozen in 1.5 ml Eppendorf tubes, and sent to Singleron in dry ice. The culture time point was D30 for assembloids, D50 for MOs and D65 for StrOs. As mentioned before, assembloids were generated by the merging of D20 MOs and D35 StrOs. MOs and StrOs that were cultured separately after D20 and D35, were cultured in the same media of the assembloid condition (optimized co-culture medium). Samples from the two batches were pulled together for nuclei extraction and sequencing by Singleron.

### Data analysis

Reads were mapped to Homo\_sapiens\_ensembl\_92 genome, and 10X matrices were generated for each sample. To perform the downstream analysis, we used R studio (23.06.1+504 version, RRID:SCR\_000432) and R 4.2.2 version (RRID:SCR\_001905). Using the Seurat package (version 4.3.0, RRID:SCR\_016341), Seurat objects were created for each sample and quality control filtering was performed. For all datasets, cells with >5% mitochondrial genes were filtered out. Additional filtering for cell debris and doublets was performed for each dataset. In MOs data cells with <100 and >1000 genes, in StrOs cells with <100 and >1800 genes and in assembloids cells with <100 and >4000 genes were filtered out. Similar to another study, after filtering, ribosomal and mitochondrial genes were removed from all datasets, as they are considered contamination in the single nuclei RNA sequencing experiments (Khan et al., 2021). After filtering, using the standard Seurat workflow, we analyzed each dataset separately, for identifying clusters specific to each model. LogNormalisation was performed in each dataset, followed by the identification of the 2000 most variable genes (FindVariableFeatures function). Next, data were scaled with the ScaleData function and linear dimensionality reduction was performed with the RunPCA function. 10 PCs were used for the MO dataset clustering and 15 PCs for the StrO and assembloid datasets. Clusters were identified using the FindNeighbors and FindClusters functions, at 0.5 resolution in all datasets. Determination of cell type identity in each cluster was performed with the evaluation of specific cellular markers expression using the DotPlot visualization method.

---

For identifying differentially expressed genes (DEGs) between assembloids and MOs or StrOs, integration analysis was performed (Butler et al., 2018). After integrating the data, DEG lists using the FindMarkers function were computed, defining the assembloid dataset as ident.1 and the MO or StrO dataset as ident.2. The DEG lists from both comparisons were imported in the Metacore (Clarivate, 2023) online software, where enrichment analysis with FDR threshold  $> 0.25$  and adjusted P.value  $< 0.05$  was performed. Enriched pathways from the “Process Networks” category were extracted. Genes related to the enrichment of the “Development\_Neurogenesis\_Axonal guidance” pathway were exported, and their expression pattern (up or down regulation) was evaluated. DEGs were also used to assess the expression pattern of genes related to neuronal maturity.

### **Multi-electrode Array**

Non-embedded assembloids were used for the electrophysiological analysis using the Axion Micro-electrode array (MEA) system. 48-well MEA plates (Axion, M768-tMEA-48B-5) were first coated with 0.1 mg/ml poly-D-lysine (Sigma-Aldrich, P7886) and incubated in 37°C, 5% CO<sub>2</sub> overnight, followed by an 1 hour incubation with 1 mg/ml laminin (Sigma-Aldrich, L2020). Laminin coating was removed, and the plates were washed twice with sterile PBS (Thermo Fisher Scientific, 14190250). Each assembloid was placed in the center of the well on the electrodes and after the media was carefully aspirated, it was left for 2-3 min to dry. Then, 15 µl of Geltrex was added on top of each assembloid and was left in the incubator for 5 min to polymerise. 500 µl of fresh culture medium was added in each well and the plate was kept in the incubator (37°C, 5% CO<sub>2</sub>) under static conditions. Electrophysiological data were acquired with the Axion Maestro Multiwell 768-channel MEA System (Axion Biosystems) and the Axis software (Axon Biosystems, RRID:SCR\_016308). For the analysis of the data the spike lists were exported from the Axis software and the data were processed with MATLAB (2021a, Mathworks, RRID:SCR\_001622). Plots of the MATLAB exported data were generated using R 4.2.2 version.

### **Data analysis and statistics**

---

Data were analysed using GraphPad Prism 9.0.0 or R studio (23.06.1+504 version) with R 4.2.2 version. Normality test was performed using the Shapiro test. If not stated otherwise, outlier removal was performed using the ROUT method Q 1% in GraphPad or the Inter-Quartile Range (IQR) proximity rule in R and data were batch normalized to the mean value of each batch. For normally distributed data, two-sided Wilcoxon test or Kruskal-Wallis with Dunn's multiple comparison test and Benjamini-Hochberg correction was implemented. For normally distributed data, Welch's t-test or one-way ANOVA with Tukey's multiple comparison test was performed. Significant P value is represented with asterisks in the order P<0.05 \*, P <0.01 \*\*, P <0.001 \*\*\*, P <0.0001 \*\*\*\*. Error bars represent mean  $\pm$  SD.

## Data availability

Raw and processed data that support the findings in this study, as well as scripts used for the analysis of the data are publicly available at this link: <https://doi.org/10.17881/4va5-e156>

Bulk RNA and single nuclei RNA sequencing data are available on Gene Expression Omnibus (GEO) under the accession codes GSE236458 and GSE241632 respectively.

## Results

### Development of the Midbrain-Striatum assembloid model

The nigrostriatal pathway is characterised by dopaminergic neuronal projections from the SNpc to the putamen and caudate of the dorsal striatum. To recapitulate this pathway *in vitro*, we generated a 3D *in vitro* model of midbrain and striatum organoids. MOs were generated based on our previously published protocols (Monzel et al., 2017; Nickels et al., 2020). For the generation of StrO different culture conditions were tested (RA, SR and C4) and compared to the recently published protocol (named C3) (Miura et al., 2020) with minor changes (Supplementary Figure 2). The purpose of this optimisation on the StrOs protocol generation was to reduce the lengthy culture time of 50-80 days to 35-50 days while preserving the mature population of medium spiny neurons (MSNs). For the conditions RA, SR and C4 organoids

---

were cultured for 35 and 50 days, while for the C3 organoids were cultured until D50 (the earliest time point described in (Miura et al., 2020)). In C4, the differentiation conditions are similar to C3 (Miura et al., 2020), but in the maturation phase (D17 to D35), DHA was excluded as it is susceptible to oxidation and to avoid the use of ethanol (the solvent for DHA) in the medium. The same medium was used until D50 without the addition of DAPT at D42 (Supplementary Figure 2.A). DHA was also excluded from the C3 (Supplementary Figure 2.B). For conditions RA and SR (Supplementary Figure 2.C, D) the previously published protocol which described the generation of ventral forebrain, subpallium-like organoids (Sloan et al., 2018), was adapted to shift the differentiation towards the LGE region and eventually to the dorsal striatum. In both conditions, SAG was added as it is neuroprotective and very important for neurodevelopment (Nguyen et al., 2021), while activin A has been shown to assist the differentiation of striatal projection neurons (Arber et al., 2015). As was demonstrated by Miura and colleagues (Miura et al., 2020), SR11237 was used to stimulate the RXRG receptor (SR condition), which has high expression in the development of the striatum as shown in the human brain transcriptome (HBT) database. Similarly, we also wanted to test the effects of RA supplementation (RA condition) as data in the HBT database show that RARB is also highly expressed in the first days of striatum development.

Gene expression analysis with qPCR for genes specific for the telencephalon and the LGE were used to confirm the differentiation of the organoids towards the dorsal striatum (Supplementary Figure 3.A). Although the forebrain marker Forkhead box protein G1 (*FOXP1*) was evenly expressed in all conditions, there were some differences in the expression of LGE progenitor genes. Achaete-Scute Family BHLH Transcription Factor 1 (*ASCL1*) showed a tendency of higher expression in the RA and SR conditions in both time points, indicating a slower differentiation of cells with higher number of progenitors at D50 of culture. In C4 at D35, *ASCL1* had similar expression with RA and SR conditions, but at D50 the expression was lower and similar to C3. Genetic-Screened Homeobox 2 (*GSX2*) is an essential transcription factor in LGE progenitors, that assists their differentiation towards neurons and glia cells in the dorsal striatum (Roychoudhury et al., 2020). In the here investigated conditions we show that *GSX2* is mainly expressed in the C4 and C3 at D50. The Forkhead Box P1 (*FOXP1*) and Forkhead Box P2 (*FOXP2*) genes are both transcription factors that are highly expressed in the striatum and are important for the development of MSNs (Fong et al., 2018). The expression of *FOXP1* was

---

similar in all conditions, but *FOXP2* had higher expression in C4 and C3 at D50, indicating a better differentiation of the neurons towards MSN fate. In addition COUP-TF-interacting protein 2 (*CTIP2*), another crucial transcription factor for the differentiation of MSNs (Arlotta et al., 2008), showed higher expression in the organoids of C4 and C3. Expression of *NKX2.1* and *OTX2* genes are important for the development of the medial ganglionic eminence (MGE) (Sandberg et al., 2018). The low expression of these genes in C3 and C4 further validates a LGE and dorsal striatum identity (Supplementary Figure 3.B). The presence of mature MSNs in the organoids was evaluated by the expression of the MSN specific marker Dopamine and cAMP-Regulated Neuronal Phosphoprotein 32 (*DARPP32*) and the dopaminergic receptors 1 and 2 (*DRD1* and *DRD2*). We observed that C4 had noticeable higher expression of *DARPP32*, while the expression of *DRD1* and *DRD2* was similar between C3 and C4 (Supplementary Figure 3.C). Similar patterns were observed in the protein levels, where *DARPP32* abundance was similar at D50 for conditions C3 and C4, *DRD1* was higher in C3 and C4 at D50 and there were no differences in the levels of *DRD2* between all conditions. Glutamic acid decarboxylase 65-kilodalton isoform (*GAD65*), important enzyme for the synthesis of GABA, was higher in C3. Overall, these results indicate that C4 and C3 have similar differentiation capacity towards dorsal striatum identity (Supplementary Figure 3.D-G). C4 seems to result in progenitor rich striatum organoids at D35 with differentiated characteristics at D50.

Since MOs and StrOs were differentiated independently for their identity specification, the generation of the assembloid model firstly required the optimisation of a suitable co-culture medium. Assembloids were generated between D20 of MOs derived from a GFP-expressing cell line and D35 or D50 of StrOs (Supplementary Figure 4.A), from the four StrO conditions described before (Supplementary Figure 2). Four different medium conditions were tested to ensure the optimal development and identity specificity of both organoids (Supplementary Figure 4.B). First, we evaluated the development of the dopaminergic neurons in GFP-expressing MOs cultured for up to 20 days by staining for TH and MAP2. MOs cultured in NM and NMpl media showed significant depletion of dopaminergic neurons, while the organoids in NM++ and N2B27++ medium did not show significant differences from the control condition (MOs standard media, see Midbrain organoids section in Methods) (Supplementary Figure 4.C). Then, the four different media were tested in assembloids cultured for 20 and 35 days to assess the impact on both dopaminergic neurons (TH staining) and MSNs (*DARPP32* staining).

---

Similar to the observations in MOs, assembloids cultured with NM<sup>++</sup> and N2B27<sup>++</sup> media, showed high levels of TH neurons in both time points of assembloid culture, specifically in C4 and C3 (Supplementary Figure 5). Since these two conditions were more suitable for the development of TH-positive neurons and the N2B27<sup>++</sup> was slightly more favourable for the DARPP32 positive neurons in C4 (Supplementary Figure 6), we used N2B27<sup>++</sup> as the optimal co-culture medium for the assembloids (Figure 1.A). Overall, based on these data, in order to reduce the time of cultures and achieve the desired differentiation capacity in assembloids, StrOs generated with the strategy C4 at D35 of differentiation were used for the generation of assembloids in the subsequent experiments.

### **Midbrain and striatum specific identity in the assembloid model**

Characterisation was performed on assembloids cultured for 30 days. Microscopy assessment with immunofluorescence staining showed that the midbrain and the striatum organoids retain their identity in the assembloid model (Figure 1.B-F). Midbrain progenitors positive for FOXA2 and CORIN were identified only in the midbrain side of the assembloid, while striatal progenitors positive for ASCL1 and CTIP2 appear only in the striatum side (Figure 1.B, C, D). Additionally, mature neurons of midbrain and striatal identity were observed with the positive immunofluorescence staining of TH and DARPP32, respectively (Figure 1.E, F). To validate that the assembloid model exhibits neuronal activity, electrophysiological measurement with MEA were performed on assembloids generated from two independent WT cell lines. Analysis of the MEA recordings showed that assembloids from both lines display similar electrophysiological activity with no differences in the number of spikes, the interspike interval and the burst frequency (Figure 1.G).

To confirm the qualitative observations, we performed single nuclei RNA sequencing on pooled assembloids from two batches, generated from the WT 1 cell line (see Supplementary Table 1) and cultured for 30 days. From the same batches, we also sequenced MOs and StrOs that after D20 and D35 respectively (time points used for assembloid generation) were cultured independently for 30 more days in the same assembloid co-culture medium. Datasets from the three models were analysed separately following the standard Seurat workflow. For the assembloid model, eight different clusters were identified and visualised with UMAP (Figure 2.A). The identity of each cluster was defined based on the expression of cellular specific

---

markers from gene lists identified by literature (Bhaduri et al., 2020; Kamath et al., 2022; La Manno et al., 2016) and the PanglaoDB database (Supplementary Figure 7). Calculation of the percentage of each cellular identity in the assembloid model revealed the presence of 5% A10 dopaminergic neurons (DANs(A10)), 6% of GABAergic neurons, 7% progenitors of the LGE (LGE Prog), 14% of radial glia cells (RGCs), 15% of medium spiny GABAergic neurons (MSNs), 16% of non-defined progenitors (Progenitors), 17% of A9 dopaminergic neurons (DANs(A9)) and 21% young neurons (yNeurons) (Figure 2.B). Hierarchical clustering of the cellular populations based on their top 500 variable genes, demonstrated the similar transcriptomic identity of the dopaminergic neuronal clusters, followed by the other mature neuronal populations of MSNs and GABAergic neurons, while young neurons and progenitor cells cluster together (Figure 2.C). The identity similarity between clusters is further demonstrated by the Spearman's correlation matrix (Figure 2.D). This illustrates the close correlation of the progenitor clusters (LGE Prog, RGCs and Progenitors) that weakly correlate with the more mature populations. Additionally, there is a weak correlation between the A9 and A10 DANs, indicating their distinct genetic signature. Although A10 DANs exhibit low correlation with all the clusters, their slightly better correlation with the RGCs and Progenitors clusters, suggests a more immature identity. On the other hand, A9 DANs correlate with the more mature clusters (GABAergic Neur and MSNs), while showing a weak correlation with the progenitor clusters. Finally, yNeuron cluster exhibits an unidentified young neuronal identity, correlating with Progenitors, DANs(A9) and GABAergic neurons, but with highest correlation to the MSN cluster.

The same analysis was performed for the MO and StrO datasets, with the presence of cell clusters more specific to the midbrain and striatum identity respectively. MOs are comprised of dopaminergic neuronal clusters (DANs and DANs2, 28% and 3% respectively) but also GABAergic neurons (33%), general neurons with no specific identity (Neurons, 14%), radial glia cells (RGCs, 20%) and a small proportion of oligodendrocyte precursor cells (OPCs, 1%) (Supplementary Figure 8.A, B). Heatmap of the 500 most variable genes, shows the clustering of RGCs in the middle, giving rise to the DANs, GABAergic neurons and Neurons clusters, while DANs2 and OPCs cluster separately, showing a more specified identity (Supplementary Figure 8.C). In Spearman's correlation, DANs2 cluster shows a more mature identity with a very weak correlation to the progenitor RGCs cluster and a stronger correlation with the

---

GABAergic Neur and Neurons clusters. On the other hand, DANs cluster shows a less mature identity (Supplementary Figure 8.D). The clustering was confirmed by the expression of different cellular markers (Supplementary Figure 8.E-J).

StrOs show a striatum specific cellular composition with 42% MSNs, 39% GABAergic interneurons, 10% LGE progenitors, 8% Neural progenitors and 1% of more general Telencephalic progenitors (Supplementary Figure 9.A-B). Similarly here, hierarchical clustering of the 500 most variable genes shows the close association of the progenitor clusters, followed but the more mature populations of MSNs and GABAergic interneurons (Supplementary Figure 9.C). The maturity of the MSNs is further confirmed by the Spearman's correlation matrix, with their weak correlation to LGE and Telencephalic progenitors, and their strong correlation to the GABAergic interneurons (Supplementary Figure 9.D). The identity of each cellular cluster was also here validated by the expression of cellular specific markers (Supplementary Figure 9.E-K).

To be able to compare the three datasets and evaluate the genes that are differentially expressed between assembloids and the individual organoids, we performed integration analysis using the Seurat workflow (Butler et al., 2018). A clear shift of cellular populations from the MOs and StrOs into the assembloid model is visible in the UMAP plot of the integrated object based on the clusters identified separately in each model (Supplementary Figure 10.A). The progenitor clusters in all models appear in the upper part of the UMAP. DANs(A10) population clusters closer to the RGCs, illustrating once more their immature identity. Between the progenitor and mature clusters appears an intermediate more general cluster of progenitors in the assembloids model (Progenitors). This progenitor cluster seems to evolve into neuronal identity cells, given its close association with the yNeurons cluster. DANs cluster, that has a more immature identity in MOs, was not present in the assembloid model, while the general neuronal cluster in MOs, seems to have been shifted towards the DANs(A9) identity in assembloids. The MSNs cluster from StrOs, was preserved in assembloids. The strong correlation between GABAergic interneurons and MSNs is likely the reason why this cluster is not observable in the assembloid model (Supplementary Figure 10.B). Additionally, a small number of OPCs is only present in MOs. Given their correlation with neuronal cluster, this cluster probably consists of cells with mixed identity (Supplementary Figure 10.B).



---

Enrichment analysis using the DEGs of assembloids-MOs and assembloids-StrOs, revealed the enrichment of several processes related to synaptic contact, cell adhesion but also neurogenesis and axonal guidance (Figure 2.E). Concerning the developmental neurogenesis and axonal guidance pathway, which was the second most enriched pathway in both comparisons, we observed that the majority of responsible genes for enriching this pathway are upregulated in the assembloid model compared to the MO and StrO models (Figure 2.F). Additionally, we evaluated the expression of genes related to neuronal maturity and identified six genes, all showing upregulation in the assembloid model (Figure 2.G). Finally, genes related to cellular and oxidative stress were found downregulated in assembloids compared to MOs and StrOs (Supplementary Figure 10.C, Supplementary Table 5).

### **Midbrain-striatum assembloid model resembles the nigrostriatal pathway connectivity**

For validating the existence of nigrostriatal pathway connectivity, we examined the presence of dopaminergic projections from the midbrain into the striatum in the assembloid model. First, to confirm that TH<sup>+</sup> signal in the striatum of the assembloids originates from the MOs TH<sup>+</sup> neurons innervation, we examined the presence of TH<sup>+</sup> neurons in GFP-expressing MOs and StrOs cultured separately in the assembloid co-culture media for the same culture period as the assembloids (D30 assembloids, D50 MOs and D65 StrOs). We observed that MOs develop a high number of TH<sup>+</sup> neurons, while the StrOs have almost no TH<sup>+</sup> signal (Supplementary Figure 11.A). Next, for visualising the TH<sup>+</sup> neurite projections from the midbrain to the striatum in the assembloid model, we performed whole mount imaging of D30 assembloids containing GFP-expressing MOs. We were able to identify neurons that have TH<sup>+</sup>/GFP<sup>+</sup> soma, indicating their midbrain identity, with TH<sup>+</sup> axons projecting towards the striatum side of the assembloid (Figure 3.A, Supplementary Figure 11.B, C).

Nigrostriatal pathway connectivity and functionality in the assembloid model were further investigated. Catecholamine levels were assessed by inserting a Nafion-coated carbon electrode into the neuronal tissues (Supplementary Figure 11.D). We have previously shown that electrochemical monitoring of catecholamine levels in the supernatant of MOs can provide valuable insights into the presence of dopamine (DA), due to neglectable levels of the interfering cationic catecholamines norepinephrine and epinephrine within the system (Zanetti et al., 2021). As expected, we observed higher levels of catecholamines in the MO side of the assembloid

---

compared to the StrO side (Supplementary Figure 11.E). No differences in StrO and StrO cultured in MO-conditioned media were detected, indicating no significant catecholamine or DA uptake from the medium (Supplementary Figure 11.F). Finally, we measured catecholamine levels in StrOs alone and StrOs in the assembloid model. The results showed that the StrOs in the assembloid model displayed higher signals compared to StrOs cultured alone (Figure 3.B), suggesting the active secretion of the catecholamine DA from midbrain dopaminergic neurons that are projecting to the striatum in the assembloid model.

To further determine whether neurons of MO and StrO are connected through active synapses in the assembloid model, we established a rabies virus-based retrograde monosynaptic tracing system. This system allows tracing of monosynaptic connections between neurons, using a lentiviral vector (Miyamichi et al., 2011) that expresses histone 2B-tagged green fluorescent protein (GFP), the avian tumor virus A (TVA) receptor (for selective infection by EnvA-pseudotyped rabies virus), and rabies virus envelope spike glycoprotein (GP) (to allow for rabies virus transsynaptic spreading) (LV-GP-TVA-GFP), in combination with a recombinant G-deleted ( $\Delta$ G) rabies viral vector, pseudotyped with EnvA envelope protein (selectively binding to TVA), and red fluorescent protein (RFP)-tagged (RBV- $\Delta$ G-EnvA-RFP). LV-GP-TVA-GFP-transduced neurons (starter neurons) are identified by nuclear GFP expression. Following infection with the RBV- $\Delta$ G-EnvA-RFP, the double-transduced starter neurons are traced by co-expression of nuclear GFP and RFP, and because of GP expression, allow  $\Delta$ G-rabies virus to form infectious particles in their cytoplasm. Neurons laying presynaptic inputs on the targeted starter neurons, are rendered RFP<sup>+</sup> due to the selective retrograde transmission of rabies virus across active synapses (target neurons) (Ugolini, 1995). Therefore, target neurons are RFP<sup>+</sup>/GFP<sup>-</sup> whereas starter neurons are RFP<sup>+</sup>/GFP<sup>+</sup>. Only first-order synapses are traced because GP expression is confined to the starter neurons, not allowing for further propagation of  $\Delta$ G-rabies virus (Etessami et al., 2011; Grealish et al., 2015; Osakada & Callaway, 2013).

StrOs at D35 of culture were transduced with LV-GP-TVA-GFP expressing the H2B-GFP fusion protein under the human Synapsin promoter. One week later, transduced StrOs were merged with MOs expressing GFP to generate assembloids, and together they were infected with RBV- $\Delta$ G-EnvA-RFP. The targeted starter neurons in the StrO were RFP<sup>+</sup>/GFP<sup>+</sup>. One week later, the media was changed and the assembloids were further cultured for up to 30 days (Figure 3.C). Sections from fixed assembloids were analysed with confocal microscopy for RFP

---

and GFP expression (Figure 3.D). Starter neurons (RFP+/GFP+, arrowheads in Figure 3.D StrO side) as well as target neurons (RFP+/GFP-, arrowheads in Figure 3.D MO side) were detected in the striatum side of the assembloid, demonstrating high connectivity of the nearby neurons with the starter neurons in the striatum organoid. Notably, RFP+ (arrowheads in Figure 3.D MO side) target neurons were additionally present more distantly in the MO compartment, indicating active synaptic connectivity between the two organoids on the assembloid level. TH-immunostaining revealed TH+/RFP+ target neurons in the MO side of the assembloid, suggesting the presence of synapse connectivity between dopaminergic neurons in the MO and starter neurons in the StrO (Figure 3.E). Target neurons (RFP+/GFP-) presence was also confirmed in assembloids where MOs were derived from iPSCs that initially did not express GFP (Supplementary Figure 11.G).

### **Doxycycline inducible Progerin overexpression in the assembloid system**

For the induction of aging phenotypes in the assembloid model we used an iPSC line that was genetically engineered with a transgene containing the modified *LMNA* gene for the transcription of Progerin, under the control of the Tet-On system, where doxycycline supplementation is needed for the induction of the transgene expression (Gabassi et al., *In Preparation*). For better identification of the Progerin+ cells, Progerin is co-expressed with the GFP fluorescent protein. This line was used to generate assembloids (Figure 4.A), and optimal concentration of doxycycline supplementation was determined by testing three different concentrations (1, 2 and 4 ng/μl). Assembloids were treated with doxycycline from D4 to D30 of culture. At D30, three assembloids per condition and from three batches were used in flow cytometry to measure the amount of GFP positive cells. Approximately 50% of cells were GFP-positive in assembloids treated with the highest concentration of doxycycline (4 ng/μl), which was significantly higher than in the other conditions (Figure 4.B). Similar to what was observed for the GFP levels, Progerin levels, validated by Western blot using the LMNA antibody (see Supplementary Table 2), were significantly higher in the 4 ng/μl doxycycline concentration (Figure 4.C). To evaluate the viability of assembloids treated with doxycycline we performed ATP and LDH assays (Supplementary Figure 12). Here, we also used assembloids generated from the isogenic line (without the Progerin transgene, referred to as WT assembloids) as a control. In the LDH assay, we show significant higher levels of LDH in the 4 ng/μl doxycycline

---

treatment (WT\_4\_Dox) which indicates that doxycycline could cause some cytotoxicity in the model. However, we noticed a different pattern of LDH levels in the assembloids with the Progerin transgene (Progerin assembloids), with no significant differences between the untreated (Progerin\_0\_Dox) and the 4 ng/μl doxycycline treated assembloids (Progerin\_4\_Dox) (Supplementary Figure 12.A). In the ATP assay, we detected no differences between the conditions, indicating no changes in the viability and metabolic activity of the model when treated with doxycycline (Supplementary Figure 12.B). These findings suggest that 4 ng/μl doxycycline concentration is acceptable for generating a mosaic Progerin-overexpressing assembloid model.

### **Progerin-overexpressing assembloids show aging characteristics**

To determine whether neurons that express Progerin in the assembloids acquire aging characteristics, we stained assembloid sections from D30 and D60 assembloids treated with 4 ng/μl doxycycline for aging-associated markers (Figure 5). Colocalization of H2AX and 53BP1 positive foci is a marker of DNA double-strand breaks. We were able to see that D60 assembloids had significantly higher levels of H2AX/53BP1 positive foci in the Progerin-expressing cells (marked as GFP+) compared to the non-Progerin-expressing cells (Figure 5.A). Similarly, aging-associated markers such as p21, p16 and p53 were all significantly elevated not only in the Progerin-expressing cells, but more specifically in Progerin-expressing neurons (MAP2/GFP-double positive) in D60 assembloids (Figure 5.B, C, D).

Next, we explored the impact of the Progerin-expressing cells on the whole assembloid model. For that, we performed transcriptomic analysis with bulk RNA sequencing on assembloids generated from the Progerin-expressing cell line and its respective isogenic control. In both cases, we used the doxycycline treated (WT\_DOX, PROG\_DOX) and the untreated conditions (WT\_UNTR, PROG\_UNTR). Principle component analysis (PCA) plot shows the clustering of the samples based on their transcriptomic similarity. In this case, all the Progerin-expressing (PROG\_DOX) samples were clustered completely separately from the rest of the samples (Figure 6.A). Similarly, a heatmap of the DEGs shows that the Progerin-expressing samples have a distinct expression pattern (Supplementary Figure 13.A). Additionally, the number of DEGs of assembloids with Progerin overexpression (PROG\_DOX group) versus the control groups (PROG\_UNTR, WT\_UNTR, WT\_DOX) was 2 or 3-fold higher (Supplementary Figure

---

13.B). These data demonstrated that assembloids with Progerin overexpression acquire a distinct transcriptomic profile. To explore possible aging-related transcriptomic changes, relevant to the human brain in the Progerin-overexpressing assembloids, we pooled the DEG lists from the comparisons between the Progerin-overexpressing assembloids with the controls (PROG\_DOXvsPROG\_UNTR, PROG\_DOXvsWT\_UNTR and PROG\_DOXvsWT\_DOX) and we compared them to the differentially expressed genes of aged human post-mortem brain transcriptomic data from two studies (Berchtold et al., 2008; González-Velasco et al., 2020). For these comparison, we extracted the significant DEGs (adj. pvalue < 0.05) that are commonly up or downregulated in the post-mortem and assembloid datasets (Extended data 1-4). From these genes we focused on the ones with a log2FoldChange higher than 2. Additionally, we included the expression of *PNOG* (foldchange = -1.34) and *GMPR* (foldchange = 1.72) genes. The expression pattern of these two genes is best associated with aging, according to González-Velasco and colleagues (González-Velasco et al., 2020) (Figure 6.B). The aging associate genes *VIP*, *SST*, *NRGN*, *NETO1*, *KCNAB1*, *GRM4*, *GABRA4*, *DRD2*, *DRD1*, *DLX6*, *CRH*, *COBL*, *CHCHD2*, *IER3*, *GMPR*, *COL21A1* and *CHI3L1* were all significantly differentially expressed. Confirming the transcriptomic changes, we were also able to observe significant reduction of the LAMINB1 protein levels, another aging-related phenotype, in the Progerin-overexpressing assembloids (Figure 6.C). Finally, the  $\beta$ -galactosidase staining on assembloid sections, revealed significant higher levels of senescent cells in the Progerin-overexpressing assembloids (Figure 6.D). Overall, we consider that these results reveal a successful induction of aging in the assembloid model with the inducible expression of Progerin.

### **Neurodegeneration phenotypes in the Progerin-inducible aged assembloids**

Next, we investigated whether the Progerin-overexpressing aged assembloids, at D60 of culture, lead to PD relevant neurodegeneration phenotypes. First, we measured the catecholamine levels in the StrO tissue in assembloids from the control (WT\_Untreated, WT\_DOX and Progerin\_Untreated) and aged conditions (Progerin\_DOX) (Figure 7.A). Catecholamine levels were significantly lower in the striatum of the aged assembloid model. These data along with the RNA sequencing analysis, showing the clustering of all the control samples (Figure 6.A), demonstrates a similar phenotype between the 3 control conditions. Therefore, in the following experiments we only compared assembloids generated from the Progerin line without

---

doxycycline treatment (Progerin\_Untreated) with assembloids from the same line with doxycycline supplementation for inducing the Progerin overexpression (Progerin\_DOX). KEGG and GO enrichment analysis from the bulk RNA sequencing transcriptomic data revealed significant dysregulation of synaptic and DA transmission related pathways (Figure 7.B), with the majority of the responsible genes to be downregulated in the Progerin-overexpressing assembloids (Supplementary Figure 14.A-E). To confirm these results at the protein level, we performed Western blotting for the postsynaptic protein Gephyrin and the presynaptic proteins VAMP2 and Synaptotagmin1 (SYN). Importantly, the three of them were significantly downregulated in Progerin-overexpressing assembloids (Figure 7.C-E).

Loss of TH positive dopaminergic neurons which leads to striatal DA depletion is the key characteristic of PD (Chung et al., 2020). The lower catecholamine levels detected in the striatal compartment of aged assembloids, is a first indication that this pathology hallmark is recapitulated in the aging model. To further substantiate this finding, we assessed the levels of TH protein in the Progerin-overexpressing assembloids via Western blotting. Consistent with the electrochemical measurements, also the TH protein levels are reduced upon induced aging (Figure 7.F). Finally, we investigated the integrity of the dopaminergic neuronal population within the assembloid model. Strikingly, this revealed an increase in the fragmentation of neurites from TH positive dopaminergic neurons, which is an early sign of degeneration (Figure 7.G-H). The TH fragmentation was calculated using our automated image analysis method (Bolognin et al., 2019). Altogether, these data suggest that there is indeed an early loss of dopaminergic neurons' function in induced aged assembloids that mimics early stages of PD pathology. Accordingly, this new model could be very valuable to investigate early alterations during the onset and progression of PD.

## **Discussion**

In this study, we developed a midbrain-striatum assembloid model that resembles the physiological nigrostriatal pathway connectivity. This model represents a relevant tool for the investigation of PD. To date, most studies on PD research with advanced cellular 3D models are based on the use of midbrain organoids (Becerra-Calixto et al., 2023; H. Kim et al., 2019; Monzel et al., 2017; Smits et al., 2019). Although these organoids have proven to be an excellent

---

tool for studying the dopaminergic neurons' vulnerability in different PD-related conditions, they are not able to recapitulate the dysregulated connectivity in the nigrostriatal pathway, which is crucially affected in PD (Fuxe et al., 2006; Singh et al., 2015). For the reconstruction of the nigrostriatal pathway connectivity, here we show the generation of a midbrain-striatum assembloid model that retains the identity of the two regions with the expression of midbrain and striatum specific markers respectively.

Single nuclei RNA sequencing analysis further revealed the identity specificity of MOs and StrOs, while the assembloid model demonstrated the preservation of cellular populations from both organoids, with additionally the identification of A9 and A10 dopaminergic neuronal clusters that are not clearly detected in our MOs dataset. A9 dopaminergic neurons were revealed by the high expression of *KCNJ6* that encodes GIRK2 protein (H. Li et al., 2022), while expression of *OTX2* was found only in the A10 cluster. *OTX2* encodes a transcription factor that is crucial for the specification of the A10 dopaminergic neurons (Grealish et al., 2014). In parallel, the MSN population in the assembloid model is specified by the co-expression of *ARPP21* and *PPP1R1B*, a strong indication of an MSN identity (Ivkovic & Ehrlich, 1999; Straccia et al., 2015), which is not evident in the StrOs dataset where only *ARPP21* expression was found. This illustrates that the assembloid model, probably through a functional communication between both regions, favours the further specification of the midbrain dopaminergic neurons as well as the MSNs of the striatum.

Enrichment analysis of the DEGs between assembloids and MOs, and assembloids and StrOs, revealed the upregulation of genes related to developmental neurogenesis, axonal guidance, and neuronal maturity. In line with the importance of brain's interregional communication in neuronal maturity and functionality (Qin et al., 2015; Voytek & Knight, 2015), it is possible that neurogenesis and neuronal maturity are promoted by the interactions formed between midbrain and striatal neurons in the assembloid model. These observations align with another study in cortico-thalamic assembloids, where neuronal maturity was observed in the assembloid level compared to individual organoids (Xiang et al., 2019). Moreover, this assumption is further supported by the reduced expression of cellular and oxidative stress related genes in midbrain-striatum assembloids, as elevated stress levels in cerebral organoids have been linked with impaired cellular maturity (Bhaduri et al., 2020).

---

Nigrostriatal pathway connectivity and functionality are also confirmed in assembloids, with the formation of active synapses between midbrain and striatal neurons and the release of catecholamines from the midbrain to striatum. This is specifically important, as the catecholamine DA release in the dorsal striatum from the SNpc dopaminergic neuronal axons is the major functionality of the nigrostriatal pathway and it is crucial for behaviour and movement control (Aarts et al., 2011; Sulzer et al., 2016).

A limitation of iPSC-derived organoid models in the research of age-related neurodegenerative diseases is that their developmental nature lacks the aging-specific phenotypes (Simpson et al., 2021). Since aging is the major risk factor in PD, we aimed to model this aspect in midbrain-striatum assembloids. To achieve this, we leveraged the overexpression of Progerin for introducing aging characteristics to our model. Similar approach has been previously described, where transient Progerin overexpression in iPSC derived dopaminergic neurons resulted in aging and neurodegeneration phenotypes (Miller et al., 2013). In our approach for Progerin overexpression, we used iPSCs carrying a Progerin transgene under the control of the Tet-On system (Gabassi et al., *In Preparation*), where doxycycline supplementation is essential for the inducible expression. Our optimised concentration of doxycycline for Progerin overexpression can be safely used in our system, as it does not affect the viability and metabolic activity in assembloids, and it does not introduce major changes in their transcriptome profile. Progerin overexpression was achieved in approximately half of the cells in doxycycline treated assembloids carrying the Progerin transgene, creating a mosaic Progerin-overexpressing model. In this mosaic model, we found that Progerin-overexpressing cells acquire aging characteristics compared to the non-Progerin-expressing cells. Some of these characteristics are the increased levels of DNA double strand breaks marked with the double positive H2AX-53BP1 nucleus foci (Shibata & Jeggo, 2020). Moreover, Progerin-overexpressing cells and neurons had significantly higher levels of p21<sup>CIP1</sup>, p53 and p16<sup>INK4A</sup>. The upregulation of these three proteins has been shown to be associated with cellular senescence and aging (Kumari & Jat, 2021; Wagner & Wagner, 2022).

To assess how Progerin-overexpressing cells affect the whole assembloid model we performed transcriptomic analysis with bulk RNA sequencing. Clustering of the data based on their transcriptomic similarity and the differential gene expression revealed a distinct transcriptomic profile for assembloids with Progerin overexpression. To investigate whether there are aging-



---

related transcriptomic differences we performed a benchmarking analysis with the use of human brain post-mortem transcriptomic data from aged individuals (Berchtold et al., 2008; González-Velasco et al., 2020). An aging-related transcriptomic profile was observed in Progerin-overexpressing assembloids, with the identification of aging-related genes with a common expression pattern between assembloids and human brain post-mortem data. Noteworthy, Progerin assembloids DEG showed *PNOC* downregulation and *GMPR* upregulation, that were found to correlate best with the biological age of the human brain post-mortem data (Velasco et al., 2020). Significantly upregulated genes found in Progerin assembloids have also been associated with aging and neurodegeneration. Specifically, higher expression of *CHI3L1* has been linked to aging and neurodegeneration (Moreno-Rodriguez et al., 2020; Sanfilippo et al., 2019), *COL21A1* upregulation has been correlated with Alzheimer's disease (AD) (Kong et al., 2009) and *IER3* gene has been implicated in cellular stress response and it is upregulated in inflammatory conditions (Arlt & Schäfer, 2011). From the significant downregulated genes, *PNOC* and *VIP* are associated with inhibitory neurotransmission in GABAergic neurons and are both significantly downregulated in human aged brains (Loerch et al., 2008). *SST* and *CRH* downregulation has been found in aging brain but also in AD genetic signature (Berchtold et al., 2013; Loerch et al., 2008; Peng et al., 2021). Similarly, downregulation of *NRGN* expression correlates with higher density of amyloid plaques in post mortem brains of AD patients (Sun et al., 2021). *GRM4* which encodes for the Glutamate Metabotropic Receptor 4 has also been found to be reduced in the prefrontal of aged rats (Hernandez et al., 2018). *KCNAB1* and *GABRA4* have a positive co-expression with *BDNF* which shows gradual downregulation in aging human prefrontal cortex (Oh et al., 2016). Additionally, *DRD1* and *DRD2* DA receptors' downregulation correlates with brain aging (Lubec et al., 2021). Both receptors are crucial for DA signalling in the striatum, and their reduced expression can be linked to motor and cognitive abnormalities (Hemby et al., 2003). *DLX6* encodes an important transcription factor for the regulation of GABAergic neurons (Lombares et al., 2019) and therefore its downregulation could be associated with aging. *NETO1* is essential for the regulation of the connectivity of glutamatergic neurons (Orav et al., 2017; Straub et al., 2011) and its downregulation could cause dysfunction in synaptic circuits. Reduction of *COBL* has been linked with reduced dendrite arborisation (Ahuja et al., 2007). Lastly, downregulation of *CHCHD2* could be associated with the aging brain and development of PD, as studies have shown that mutations in this gene are

---

tied to dysfunctional mitochondria (Kee et al., 2021; Meng et al., 2017), while at the same time reduction of *CHCHD2* mRNA levels has been found in erythrocytes of PD patients (Liu et al., 2021). The aging phenotype observed in the transcriptomic profile of the Progerin-overexpressing assembloids was further validated by the significant reduction of the LAMINB1 protein levels and the significant increase in senescence-activated  $\beta$ -galactosidase positive areas. Both these phenotypes have been considered hallmarks of aging and senescence (Dodig et al., 2019; Matias et al., 2022; Miller et al., 2013).

Many of the genes mentioned previously are not only related to aging but also to neurodegenerative diseases such as AD and PD, highlighting the interconnected relationship between aging and neurodegeneration. Synaptic dysfunction in the aging brain is one of the major promoters of neurodegeneration (Azam et al., 2021; Buss et al., 2021; Talyansky & Brinkman, 2021). Dysregulation of synaptic and DA neurotransmission pathways revealed in the transcriptomic data of Progerin-overexpressing assembloids, was further validated by the downregulation of the post-synaptic protein Gephyrin, an important scaffolding protein that regulates the organisation of post-synapses in striatal GABAergic neurons (Choi & Ko, 2015), and the pre-synaptic proteins VAMP2 and Synaptotagmin1. VAMP2 regulates the fusion of synaptic vesicles and neurotransmitter release through the SNARE complex (Yan et al., 2022) and Synaptotagmin1 is an essential  $\text{Ca}^{2+}$  sensor for the fast release of DA (Banerjee et al., 2020, 2022). In parallel, catecholamine measurements showed significantly lower catecholamine levels in the striatum of the Progerin-overexpressing assembloids, indicating dysregulation of DA release in the aged-induced model, a PD-relevant phenotype (Jiang et al., 2019). These results reveal a defective synaptic and DA release system in Progerin-overexpressing assembloids.

Moreover, low TH protein levels in Progerin-overexpressing assembloids could be linked to dysregulated DA synthesis system and the presence of vulnerable dopaminergic neurons. TH is the key enzyme of DA synthesis (Daubner et al., 2011). Lower TH protein levels have been previously observed in surviving dopaminergic neurons of PD patients, indicating their vulnerability to the disease (Kastner et al., 1993). Moreover, loss of TH activity followed by TH protein decline has been linked to DA deficiency in PD (Tabrez et al., 2012). Additionally, quantification of the fragmentation index of the TH<sup>+</sup> neurites revealed that dopaminergic neurons in the age-induced assembloids are more fragmented, demonstrating a degeneration

---

phenotype prior to their neuronal death (Lin et al., 2016). The axonal fragmented phenotype has been previously described in iPSC-derived PD neuronal models (Kouroupi et al., 2017). These results support that our age-induced assembloids display an early PD-relevant neurodegeneration phenotype, with dysregulation in the DA synthesis and release systems indicative of axonal degeneration preceding the eventual loss of dopaminergic neurons' soma, in retrograde fashion as typically observed in PD (Cheng et al., 2011; Chu et al., 2012; L. H. Li et al., 2009; Miwa et al., 2005).

The here presented age-induced midbrain-striatum assembloid model offers new possibilities for PD research. Given the crucial role of aging in PD development, it is imperative to diligently consider its influence when studying the disease's phenotypes through *in vitro* models. By incorporating aging characteristics in cellular models derived from PD patient cell lines, we can more accurately recapitulate the disease state of patients and unveil cellular dysfunctions that remain unnoticed in the current developmental models. Studies with cell lines sourced from PD patients in the future will provide further insights into the model's robustness and its potential applications in personalised medicine.

## **Authors Contribution**

K.B. designed and executed experiments, analysed and interpreted data, prepared figures, and wrote the original draft. C.S. designed and executed experiments for the striatum organoids optimisation, reviewed and edited the manuscript. G.G.G. contributed on the optimisation of the Rabies monosynaptic tracing experiment in assembloids. E.G. contributed to the generation and quality control of the Progerin iPSCs. S.S. and K.B. performed the electrochemical measurements in organoids and assembloids. J.E.R.G. performed the whole mount imaging of assembloids and analysis. P.A. supervised the high-content imaging workflow. G.R. contributed to the analysis of microelectrode array data. F.P. generated the RBV and LV viruses for the Rabies monosynaptic tracing experiment. U.K., P.E. and R.M. reviewed and edited the manuscript. A.S. and F.E. provided scientific feedback in regular project meetings, reviewed, and edited the manuscript. J.C.S. conceived and supervised the project and edited the manuscript.

---

## **Acknowledgements**

This study was supported by the Luxembourg National Fund FNR-Inter and the Austrian Science Fund FWF (FWF-INTER – INTER/FWF/19/14117540/PDage; FWF-SFB F78/P1040-016-015). Special thanks to Prof. Alexander Skupin for his scientific input on single nuclei RNA sequencing analysis data and Dr. Henry Kurniawan for his feedback on the flow cytometry experiment.

Rights retention statement: This research was funded in whole by the FNR-Luxembourg. For the purpose of Open Access, the author has applied a CC BY public copyright license to any Author Accepted Manuscript (AAM) version arising from this submission.

## **Competing interest statement**

JCS is a co-inventor on a patent covering the generation of the here-described midbrain organoids (WO2017060884A1). Furthermore, JCS is a co-founder and shareholder of the company OrganoTherapeutics which makes use of midbrain organoid technology. The other authors declare no competing interests.

## **Ethical approval**

Ethics Review Panel (ERP) of the University of Luxembourg and the national Luxembourgish research ethics committee (CNER, Comité National d'Ethique de Recherche) have approved the work with induced pluripotent stem cells (iPSCs). CNER No. 201901/01; ivPD

---

## References

- Aarts, E., van Holstein, M., & Cools, R. (2011). Striatal dopamine and the interface between motivation and cognition. *Frontiers in Psychology*, 2(JUL), 1–11. <https://doi.org/10.3389/fpsyg.2011.00163>
- Ahuja, R., Pinyol, R., Reichenbach, N., Custer, L., Klingensmith, J., Kessels, M. M., & Qualmann, B. (2007). Cordon-Bleu Is an Actin Nucleation Factor and Controls Neuronal Morphology. *Cell*, 131(2), 337–350. <https://doi.org/10.1016/j.cell.2007.08.030>
- Andersen, J., Revah, O., Miura, Y., Thom, N., Amin, N. D., Kelley, K. W., Singh, M., Chen, X., Thete, M. V., Walczak, E. M., Vogel, H., Fan, H. C., & Paşca, S. P. (2020). Generation of Functional Human 3D Cortico-Motor Assembloids. *Cell*, 183(7), 1913–1929.e26. <https://doi.org/10.1016/j.cell.2020.11.017>
- Arber, C., Precious, S. V., Cambray, S., Risner-Janiczek, J. R., Kelly, C., Noakes, Z., Fjodorova, M., Heuer, A., Ungless, M. A., Rodríguez, T. A., Rosser, A. E., Dunnett, S. B., & Li, M. (2015). Activin a directs striatal projection neuron differentiation of human pluripotent stem cells. *Development (Cambridge)*, 142(7), 1375–1386. <https://doi.org/10.1242/dev.117093>
- Arlotta, P., Molyneaux, B. J., Jabaudon, D., Yoshida, Y., & Macklis, J. D. (2008). *Ctip2 Controls the Differentiation of Medium Spiny Neurons and the Establishment of the Cellular Architecture of the Striatum*. <https://doi.org/10.1523/JNEUROSCI.2986-07.2008>
- Arlt, A., & Schäfer, H. (2011). Role of the immediate early response 3 (IER3) gene in cellular stress response, inflammation and tumorigenesis. *European Journal of Cell Biology*, 90(6–7), 545–552. <https://doi.org/10.1016/j.ejcb.2010.10.002>
- Azam, S., Haque, M. E., Balakrishnan, R., Kim, I. S., & Choi, D. K. (2021). The Ageing Brain: Molecular and Cellular Basis of Neurodegeneration. In *Frontiers in Cell and Developmental Biology* (Vol. 9). <https://doi.org/10.3389/fcell.2021.683459>
- Banerjee, A., Imig, C., Balakrishnan, K., Kershberg, L., Lipstein, N., Uronen, R. L., Wang, J., Cai, X., Benseler, F., Rhee, J. S., Cooper, B. H., Liu, C., Wojcik, S. M., Brose, N., & Kaeser, P. S. (2022). Molecular and functional architecture of striatal dopamine release sites. *Neuron*, 110(2), 248–265.e9. <https://doi.org/10.1016/j.neuron.2021.10.028>
- Banerjee, A., Lee, J., Nemcova, P., Liu, C., & Kaeser, P. S. (2020). Synaptotagmin-1 is the Ca<sup>2+</sup> sensor for fast striatal dopamine release. *ELife*, 9, 1–16.

---

<https://doi.org/10.7554/eLife.58359>

- Becerra-Calixto, A., Mukherjee, A., Ramirez, S., Sepulveda, S., Sinha, T., Al-Lahham, R., De Gregorio, N., Gherardelli, C., & Soto, C. (2023). Lewy Body-like Pathology and Loss of Dopaminergic Neurons in Midbrain Organoids Derived from Familial Parkinson's Disease Patient. *Cells*, *12*(4). <https://doi.org/10.3390/cells12040625>
- Berchtold, N. C., Coleman, P. D., Cribbs, D. H., Rogers, J., Gillen, D. L., & Cotman, C. W. (2013). Synaptic genes are extensively downregulated across multiple brain regions in normal human aging and Alzheimer's disease. *Neurobiology of Aging*, *34*(6), 1653–1661. <https://doi.org/10.1016/j.neurobiolaging.2012.11.024>
- Berchtold, N. C., Cribbs, D. H., Coleman, P. D., Rogers, J., Head, E., Kim, R., Beach, T., Miller, C., Troncoso, J., Trojanowski, J. Q., Ronald Zielke, H., & Cotman, C. W. (2008). *Gene expression changes in the course of normal brain aging are sexually dimorphic*. [www.pnas.org/cgi/content/full/](http://www.pnas.org/cgi/content/full/)
- Bhaduri, A., Andrews, M. G., Mancina Leon, W., Jung, D., Shin, D., Allen, D., Jung, D., Schmunk, G., Haeussler, M., Salma, J., Pollen, A. A., Nowakowski, T. J., & Kriegstein, A. R. (2020). Cell stress in cortical organoids impairs molecular subtype specification. *Nature*, *578*(7793), 142–148. <https://doi.org/10.1038/s41586-020-1962-0>
- Birey, F., Andersen, J., Makinson, C. D., Islam, S., Wei, W., Huber, N., Fan, H. C., Metzler, K. R. C., Panagiotakos, G., Thom, N., O'Rourke, N. A., Steinmetz, L. M., Bernstein, J. A., Hallmayer, J., Huguenard, J. R., & Pasca, S. P. (2017). Assembly of functionally integrated human forebrain spheroids. *Nature*, *545*(7652), 54–59. <https://doi.org/10.1038/nature22330>
- Bolognin, S., Fossépré, M., Qing, X., Jarazo, J., Ščančar, J., Moreno, E. L., Nickels, S. L., Wasner, K., Ouzren, N., Walter, J., Grünewald, A., Glaab, E., Salamanca, L., Fleming, R. M. T., Antony, P. M. A., & Schwamborn, J. C. (2019). 3D Cultures of Parkinson's Disease-Specific Dopaminergic Neurons for High Content Phenotyping and Drug Testing. *Advanced Science*, *6*(1), 1–14. <https://doi.org/10.1002/advs.201800927>
- Buss, E. W., Corbett, N. J., Roberts, J. G., Ybarra, N., Musial, T. F., Simkin, D., Molina-Campos, E., Oh, K. J., Nielsen, L. L., Ayala, G. D., Mullen, S. A., Farooqi, A. K., D'Souza, G. X., Hill, C. L., Bean, L. A., Rogalsky, A. E., Russo, M. L., Curlik, D. M., Antion, M. D., ... Nicholson, D. A. (2021). Cognitive aging is associated with redistribution of

- 
- synaptic weights in the hippocampus. *Proceedings of the National Academy of Sciences of the United States of America*, 118(8), 1–10. <https://doi.org/10.1073/pnas.1921481118>
- Butler, A., Hoffman, P., Smibert, P., Papalexi, E., & Satija, R. (2018). Integrating single-cell transcriptomic data across different conditions, technologies, and species. *Nature Biotechnology*, 36(5), 411–420. <https://doi.org/10.1038/nbt.4096>
- Caminiti, S. P., Presotto, L., Baroncini, D., Garibotto, V., Moresco, R. M., Gianolli, L., Volonté, M. A., Antonini, A., & Perani, D. (2017). Axonal damage and loss of connectivity in nigrostriatal and mesolimbic dopamine pathways in early Parkinson's disease. *NeuroImage: Clinical*, 14(March), 734–740. <https://doi.org/10.1016/j.nicl.2017.03.011>
- Cheng, H. C., Kim, S. R., Oo, T. F., Kareva, T., Yarygina, O., Rzhetskaya, M., Wang, C., Doring, M., Talloczy, Z., Tanaka, K., Komatsu, M., Kobayashi, K., Okano, H., Kholodilov, N., & Burke, R. E. (2011). Akt suppresses retrograde degeneration of dopaminergic axons by inhibition of macroautophagy. *Journal of Neuroscience*, 31(6), 2125–2135. <https://doi.org/10.1523/JNEUROSCI.5519-10.2011>
- Choi, G., & Ko, J. (2015). Gephyrin: a central GABAergic synapse organizer. *Experimental & Molecular Medicine*, 47. <https://doi.org/10.1038/emm.2015.5>
- Chu, Y., Morfini, G. A., Langhamer, L. B., He, Y., Brady, S. T., & Kordower, J. H. (2012). Alterations in axonal transport motor proteins in sporadic and experimental Parkinson's disease. *Brain*, 135(7), 2058–2073. <https://doi.org/10.1093/brain/aws133>
- Chung, S. J., Lee, H. S., Yoo, H. S., Lee, Y. H., Lee, P. H., & Sohn, Y. H. (2020). Patterns of striatal dopamine depletion in early Parkinson disease: Prognostic relevance. *Neurology*, 95(3), E280–E290. <https://doi.org/10.1212/WNL.00000000000009878>
- Collier, T. J., Kanaan, N. M., & Kordower, J. H. (2017). Aging and Parkinson's disease: Different sides of the same coin? *Movement Disorders*, 32(7), 983–990. <https://doi.org/10.1002/mds.27037>
- Daubner, S. C., Le, T., & Wang, S. (2011). Tyrosine hydroxylase and regulation of dopamine synthesis. *Archives of Biochemistry and Biophysics*, 508(1), 1–12. <https://doi.org/10.1016/j.abb.2010.12.017>
- Dodig, S., Čepelak, I., & Pavić, I. (2019). Hallmarks of senescence and aging. *Biochimica Medica*, 29(3), 1–15. <https://doi.org/10.11613/BM.2019.030501>
- Etessami, R., Conzelmann, K., Fadai-ghotbi, B., Natelson, B., Tsiang, H., & Ceccaldi, P. (2011).

- 
- Spread and pathogenic characteristics of a G-deficient rabies virus recombinant- an in vitro and in vivo study. *Journal of General Virology*, 81(9), 2147–2153. [papers2://publication/uuid/BDB7C790-A842-498C-AC14-A623401118A4](https://doi.org/10.1099/jgv.2000.8109-2147)
- Fong, W. L., Kuo, H. Y., Wu, H. L., Chen, S. Y., & Liu, F. C. (2018). Differential and Overlapping Pattern of Foxp1 and Foxp2 Expression in the Striatum of Adult Mouse Brain. In *Neuroscience* (Vol. 388). IBRO. <https://doi.org/10.1016/j.neuroscience.2018.07.017>
- Fuxe, K., Manger, P., Genedani, S., & Agnati, L. (2006). The nigrostriatal DA pathway and Parkinson's disease. *Journal of Neural Transmission, Supplement*, 70, 71–83. [https://doi.org/10.1007/978-3-211-45295-0\\_13](https://doi.org/10.1007/978-3-211-45295-0_13)
- Ghosh, B., Zhang, C., Ziemba, K. S., Fletcher, A. M., Yurek, D. M., & Smith, G. M. (2019). Partial Reconstruction of the Nigrostriatal Circuit along a Preformed Molecular Guidance Pathway. *Molecular Therapy - Methods and Clinical Development*, 14(September), 217–227. <https://doi.org/10.1016/j.omtm.2019.06.008>
- Gomez-Giro, G., Arias-Fuenzalida, J., Jarazo, J., Zeuschner, D., Ali, M., Possemis, N., Bolognin, S., Halder, R., Jäger, C., Kuper, W. F. E., Van Hasselt, P. M., Zaehres, H., Del Sol, A., Van Der Putten, H., Schöler, H. R., & Schwamborn, J. C. (2019). Synapse alterations precede neuronal damage and storage pathology in a human cerebral organoid model of CLN3-juvenile neuronal ceroid lipofuscinosis. *Acta Neuropathologica Communications*, 7(1), 1–19. <https://doi.org/10.1186/s40478-019-0871-7>
- González-Velasco, O., Papy-García, D., Le Douaron, G., Sánchez-Santos, J. M., & De Las Rivas, J. (2020). Transcriptomic landscape, gene signatures and regulatory profile of aging in the human brain. *Biochimica et Biophysica Acta - Gene Regulatory Mechanisms*, 1863(6), 194491. <https://doi.org/10.1016/j.bbagr.2020.194491>
- Grealish, S., Diguët, E., Kirkeby, A., Mattsson, B., Heuer, A., Bramouille, Y., Van Camp, N., Perrier, A. L., Hantraye, P., Björklund, A., & Parmar, M. (2014). Human ESC-derived dopamine neurons show similar preclinical efficacy and potency to fetal neurons when grafted in a rat model of Parkinson's disease. *Cell Stem Cell*, 15(5), 653–665. <https://doi.org/10.1016/j.stem.2014.09.017>
- Grealish, S., Heuer, A., Cardoso, T., Kirkeby, A., Jönsson, M., Johansson, J., Björklund, A., Jakobsson, J., & Parmar, M. (2015). Monosynaptic Tracing using Modified Rabies Virus Reveals Early and Extensive Circuit Integration of Human Embryonic Stem Cell-Derived



- 
- Neurons. *Stem Cell Reports*, 4(6), 975–983. <https://doi.org/10.1016/j.stemcr.2015.04.011>
- Hemby, S. E., Trojanowski, J. Q., & Ginsberg, S. D. (2003). Neuron-specific age-related decreases in dopamine receptor subtype mRNAs. *Journal of Comparative Neurology*, 456(2), 176–183. <https://doi.org/10.1002/cne.10525>
- Heng, N., Malek, N., Lawton, M. A., Nodehi, A., Pitz, V., Grosset, K. A., Ben-Shlomo, Y., & Grosset, D. G. (2023). Striatal Dopamine Loss in Early Parkinson’s Disease: Systematic Review and Novel Analysis of Dopamine Transporter Imaging. In *Movement Disorders Clinical Practice* (Vol. 10, Issue 4, pp. 539–546). <https://doi.org/10.1002/mdc3.13687>
- Hernandez, C. M., Mcquail, J. A., Schwabe, M. R., Bizon, J. L., Burke, S. N., & Setlow, B. (2018). *Age-Related Declines in Prefrontal Cortical Expression of Metabotropic Glutamate Receptors that Support Working Memory*. 5(June).
- Hindle, J. V. (2010). Ageing, neurodegeneration and Parkinson’s disease. *Age and Ageing*, 39(2), 156–161. <https://doi.org/10.1093/ageing/afp223>
- Ivkovic, S., & Ehrlich, M. E. (1999). *Expression of the Striatal DARPP-32/ARPP-21 Phenotype in GABAergic Neurons Requires Neurotrophins In Vivo and In Vitro*.
- Jarazo, J., Barmppa, K., Rosety, I., Smits, L. M., Arias-Fuenzalida, J., Walter, J., Gomez-Giro, G., Monzel, A. S., Qing, X., Cruciani, G., Boussaad, I., Jäger, C., Rakovic, A., Berger, E., Bolognin, S., Antony, P. M. A., Klein, C., Krüger, R., Seibler, P., & Schwamborn, J. C. (2019). Parkinson’s disease phenotypes in patient specific brain organoids are improved by HP- $\beta$ -CD treatment. *BioRxiv*, 813089. <https://doi.org/10.1101/813089>
- Jiang, P., Scarpa, J. R., Gao, V. D., Vitaterna, M. H., Kasarskis, A., & Turek, F. W. (2019). Parkinson’s Disease is Associated with Dysregulations of a Dopamine-Modulated Gene Network Relevant to Sleep and Affective Neurobehaviors in the Striatum. *Scientific Reports*, 9(1), 1–14. <https://doi.org/10.1038/s41598-019-41248-4>
- Jo, J., Yang, L., Tran, H.-D., Yu, W., Xuyang Sun, A., Yin Chang, Y., Chul Jung, B., Lee, S.-J., Yih Saw, T., Xiao, B., Tze Ting Khoo, A., Yaw, L.-P., Jiabin Xie, J., Lokman, H., Ong, W.-Y., Gui Yin Lim, G., Lim, K.-L., Tan, E.-K., Ng, H.-H., & Shawn Je, H. (2021). *Lewy Body-like Inclusions in Human Midbrain Organoids Carrying Glucocerebrosidase and  $\alpha$ -Synuclein Mutations*. <https://doi.org/10.1002/ana.26166>
- Kamath, T., Abdulraouf, A., Burris, S. J., Langlieb, J., Gazestani, V., Nadaf, N. M., Balderrama, K., Vanderburg, C., & Macosko, E. Z. (2022). Single-cell genomic profiling of human

- 
- dopamine neurons identifies a population that selectively degenerates in Parkinson's disease. *Nature Neuroscience*, 25(5), 588–595. <https://doi.org/10.1038/s41593-022-01061-1>
- Kastner, A., Hirsch, E. C., Agid, Y., & Javoy-Agid, F. (1993). Tyrosine hydroxylase protein and messenger RNA in the dopaminergic nigral neurons of patients with Parkinson's disease. *Brain Research*, 606(2), 341–345. [https://doi.org/10.1016/0006-8993\(93\)91005-D](https://doi.org/10.1016/0006-8993(93)91005-D)
- Kee, T. R., Gonzalez, P. E., Wehinger, J. L., Bukhari, M. Z., Ermekbaeva, A., Sista, A., & Kotsiviras, P. (2021). *Mitochondrial CHCHD2: Disease-Associated Mutations, Physiological Functions, and Current Animal Models*. 13(April), 1–15. <https://doi.org/10.3389/fnagi.2021.660843>
- Khan, T., Seetharam, A. S., Zhou, J., Bivens, N. J., Schust, D. J., Ezashi, T., Tuteja, G., & Roberts, R. M. (2021). Single Nucleus RNA Sequence (snRNAseq) Analysis of the Spectrum of Trophoblast Lineages Generated From Human Pluripotent Stem Cells in vitro. *Frontiers in Cell and Developmental Biology*, 9(July). <https://doi.org/10.3389/fcell.2021.695248>
- Kim, H., Park, H. J., Choi, H., Chang, Y., Park, H., Shin, J., Kim, J., Lengner, C. J., Lee, Y. K., & Kim, J. (2019). Modeling G2019S-LRRK2 Sporadic Parkinson's Disease in 3D Midbrain Organoids. *Stem Cell Reports*, 12(3), 518–531. <https://doi.org/10.1016/j.stemcr.2019.01.020>
- Kim, J., Koo, B. K., & Knoblich, J. A. (2020). Human organoids: model systems for human biology and medicine. In *Nature Reviews Molecular Cell Biology* (Vol. 21, Issue 10, pp. 571–584). <https://doi.org/10.1038/s41580-020-0259-3>
- Kim, S. W., Woo, H. J., Kim, E. H., Kim, H. S., Suh, H. N., Kim, S. hyun, Song, J. J., Wulansari, N., Kang, M., Choi, S. Y., Choi, S. J., Jang, W. H., Lee, J., Kim, K. H., Lee, W., Kim, S. H., Yang, J., Kyung, J., Lee, H. S., ... Lee, S. H. (2021). Neural stem cells derived from human midbrain organoids as a stable source for treating Parkinson's disease: Midbrain organoid-NSCs (Og-NSC) as a stable source for PD treatment. *Progress in Neurobiology*, 204(May), 102086. <https://doi.org/10.1016/j.pneurobio.2021.102086>
- Kong, W., Mou, X., Liu, Q., Chen, Z., Vanderburg, C. R., Rogers, J. T., & Huang, X. (2009). *Molecular Neurodegeneration Independent component analysis of Alzheimer's DNA*

---

*microarray gene expression data.* <https://doi.org/10.1186/1750-1326-4-5>

- Kouroupi, G., Taoufik, E., Vlachos, I. S., Tsioras, K., Antoniou, N., Papastefanaki, F., Chroni-Tzartou, D., Wrasidlo, W., Bohl, D., Stellas, D., Politis, P. K., Vekrellis, K., Papadimitriou, D., Stefanis, L., Bregestovski, P., Hatzigeorgiou, A. G., Masliah, E., & Matsas, R. (2017). Defective synaptic connectivity and axonal neuropathology in a human iPSC-based model of familial Parkinson's disease. *Proceedings of the National Academy of Sciences of the United States of America*, *114*(18), E3679–E3688. <https://doi.org/10.1073/pnas.1617259114>
- Kumari, R., & Jat, P. (2021). Mechanisms of Cellular Senescence: Cell Cycle Arrest and Senescence Associated Secretory Phenotype. *Frontiers in Cell and Developmental Biology*, *9*(March), 1–24. <https://doi.org/10.3389/fcell.2021.645593>
- Kutner, R. H., Zhang, X. Y., & Reiser, J. (2009). Production, concentration and titration of pseudotyped HIV-1-based lentiviral vectors. *Nature Protocols*, *4*(4), 495–505. <https://doi.org/10.1038/nprot.2009.22>
- La Manno, G., Gyllborg, D., Codeluppi, S., Nishimura, K., Salto, C., Zeisel, A., Borm, L. E., Stott, S. R. W., Toledo, E. M., Villaescusa, J. C., Lönnerberg, P., Ryge, J., Barker, R. A., Arenas, E., & Linnarsson, S. (2016). Molecular Diversity of Midbrain Development in Mouse, Human, and Stem Cells. *Cell*, *167*(2), 566–580.e19. <https://doi.org/10.1016/j.cell.2016.09.027>
- Lapasset, L., Milhavet, O., Prieur, A., Besnard, E., Babled, A., Ät-Hamou, N., Leschik, J., Pellestor, F., Ramirez, J. M., De Vos, J., Lehmann, S., & Lemaitre, J. M. (2011). Rejuvenating senescent and centenarian human cells by reprogramming through the pluripotent state. *Genes and Development*, *25*(21), 2248–2253. <https://doi.org/10.1101/gad.173922.111>
- Li, H., Jiang, H., Li, H., Li, L., Yan, Z., & Feng, J. (2022). Generation of human A9 dopaminergic pacemakers from induced pluripotent stem cells. *Molecular Psychiatry*, *27*(11), 4407–4418. <https://doi.org/10.1038/s41380-022-01628-1>
- Li, L. H., Qin, H. Z., Wang, J. L., Wang, J., Wang, X. L., & Gao, G. D. (2009). Axonal degeneration of nigra-striatum dopaminergic neurons induced by 1-methyl-4-phenyl-1,2,3,6-tetrahydropyridine in mice. *Journal of International Medical Research*, *37*(2), 455–463. <https://doi.org/10.1177/147323000903700221>

- 
- Lin, L., Göke, J., Cukuroglu, E., Dranias, M. R., VanDongen, A. M. J., & Stanton, L. W. (2016). Molecular Features Underlying Neurodegeneration Identified through In Vitro Modeling of Genetically Diverse Parkinson's Disease Patients. *Cell Reports*, *15*(11), 2411–2426. <https://doi.org/10.1016/j.celrep.2016.05.022>
- Liu, X., Wang, Q., Yang, Y., Stewart, T., Shi, M., Soltys, D., Liu, G., Thorland, E., Cilento, E. M., Hou, Y., Liu, Z., Feng, T., & Zhang, J. (2021). Reduced erythrocytic CHCHD2 mRNA is associated with brain pathology of Parkinson's disease. *Acta Neuropathologica Communications*, 1–16. <https://doi.org/10.1186/s40478-021-01133-6>
- Loerch, P. M., Lu, T., Dakin, K. A., Vann, J. M., Isaacs, A., Geula, C., Wang, J., Pan, Y., Gabuzda, D. H., Li, C., Prolla, T. A., & Yankner, B. A. (2008). Evolution of the aging brain transcriptome and synaptic regulation. *PLoS ONE*, *3*(10). <https://doi.org/10.1371/journal.pone.0003329>
- Lombares, C. De, Heude, E., Alfama, G., Fontaine, A., Hassouna, R., Vernochet, C., Chaumont, F. De, Olivo-marin, C., Ey, E., Tronche, F., Bourgeron, T., Luquet, S., & Levi, G. (2019). *Dlx5 and Dlx6 expression in GABAergic neurons controls behavior, metabolism, healthy aging and lifespan*. *11*(17), 6638–6656.
- Lubec, J., Kalaba, P., Hussein, A. M., Feyissa, D. D., Kotob, M. H., Mahmmoud, R. R., Wieder, O., Garon, A., Sagheddu, C., Ilic, M., Dragačević, V., Cybulska-Klosowicz, A., Zehl, M., Wackerlig, J., Sartori, S. B., Ebner, K., Kouhnavardi, S., Roller, A., Gajic, N., ... Lubec, G. (2021). Reinstatement of synaptic plasticity in the aging brain through specific dopamine transporter inhibition. *Molecular Psychiatry*, *26*(12), 7076–7090. <https://doi.org/10.1038/s41380-021-01214-x>
- Makrygianni, E. A., & Chrousos, G. P. (2021). From Brain Organoids to Networking Assembloids: Implications for Neuroendocrinology and Stress Medicine. *Frontiers in Physiology*, *12*(June). <https://doi.org/10.3389/fphys.2021.621970>
- Matias, I., Pereira, L., Isabella, D., Damico, V., Paula, A., Araujo, B., Neves, S., Vargas, G., Leite, R. E. P., Suemoto, C. K., Jacob, R. N. W., Grinberg, L. T., Hol, E. M., Middeldorp, J., Carvalho, F., & Gomes, A. (2022). *Loss of lamin-B1 and defective nuclear morphology are hallmarks of astrocyte senescence in vitro and in the aging human hippocampus*. *February 2021*, 1–18. <https://doi.org/10.1111/accel.13521>
- Meng, H., Yamashita, C., Shiba-fukushima, K., Inoshita, T., Funayama, M., Sato, S., Hatta, T.,

- 
- Natsume, T., Umitsu, M., Takagi, J., & Imai, Y. (2017). Loss of Parkinson's disease-associated protein CHCHD2 affects mitochondrial crista structure and destabilizes cytochrome c. *Nature Communications*, 8, 1–18. <https://doi.org/10.1038/ncomms15500>
- Miller, J. D., Ganat, Y. M., Kishinevsky, S., Bowman, R. L., Liu, B., Tu, E. Y., Mandal, P. K., Vera, E., Shim, J. W., Kriks, S., Taldone, T., Fusaki, N., Tomishima, M. J., Krainc, D., Milner, T. A., Rossi, D. J., & Studer, L. (2013). Human iPSC-based modeling of late-onset disease via progerin-induced aging. *Cell Stem Cell*, 13(6), 691–705. <https://doi.org/10.1016/j.stem.2013.11.006>
- Miura, Y., Li, M. Y., Birey, F., Ikeda, K., Revah, O., Thete, M. V., Park, J. Y., Puno, A., Lee, S. H., Porteus, M. H., & Pasca, S. P. (2020). Generation of human striatal organoids and cortico-striatal assembloids from human pluripotent stem cells. *Nature Biotechnology*, 38(12), 1421–1430. <https://doi.org/10.1038/s41587-020-00763-w>
- Miwa, H., Kubo, T., Suzuki, A., Nishi, K., & Kondo, T. (2005). Retrograde dopaminergic neuron degeneration following intrastriatal proteasome inhibition. *Neuroscience Letters*, 380(1–2), 93–98. <https://doi.org/10.1016/j.neulet.2005.01.024>
- Miyamichi, K., Amat, F., Moussavi, F., Wang, C., Wickersham, I., Wall, N. R., Taniguchi, H., Tasic, B., Huang, Z. J., He, Z., Callaway, E. M., Horowitz, M. A., & Luo, L. (2011). Cortical representations of olfactory input by trans-synaptic tracing. *Nature*. <https://doi.org/10.1038/nature09714>
- Monzel, A. S., Hemmer, K., Kaoma, T., Smits, L. M., Bolognin, S., Lucarelli, P., Rosety, I., Zagare, A., Antony, P., Nickels, S. L., Krueger, R., Azuaje, F., & Schwamborn, J. C. (2020). Machine learning-assisted neurotoxicity prediction in human midbrain organoids. *Parkinsonism and Related Disorders*, 75(May), 105–109. <https://doi.org/10.1016/j.parkreldis.2020.05.011>
- Monzel, A. S., Smits, L. M., Hemmer, K., Hachi, S., Moreno, E. L., van Wuellen, T., Jarazo, J., Walter, J., Brüggemann, I., Boussaad, I., Berger, E., Fleming, R. M. T., Bolognin, S., & Schwamborn, J. C. (2017). Derivation of Human Midbrain-Specific Organoids from Neuroepithelial Stem Cells. *Stem Cell Reports*, 8(5), 1144–1154. <https://doi.org/10.1016/j.stemcr.2017.03.010>
- Moreno-Rodriguez, M., Perez, S. E., Nadeem, M., Malek-Ahmadi, M., & Mufson, E. J. (2020). Frontal cortex chitinase and pentraxin neuroinflammatory alterations during the

- 
- progression of Alzheimer's disease. *Journal of Neuroinflammation*, 17(1), 1–15. <https://doi.org/10.1186/s12974-020-1723-x>
- Nguyen, V., Chavali, M., Larphaveesarp, A., Kodali, S., Gonzalez, G., Franklin, R. J. M., Rowitch, D. H., & Gonzalez, F. (2021). Neuroprotective effects of Sonic hedgehog agonist SAG in a rat model of neonatal stroke. *Pediatric Research*, 90(6), 1161–1170. <https://doi.org/10.1038/s41390-021-01408-7>
- Nickels, S. L., Modamio, J., Mendes-Pinheiro, B., Monzel, A. S., Betsou, F., & Schwamborn, J. C. (2020). Reproducible generation of human midbrain organoids for in vitro modeling of Parkinson's disease. *Stem Cell Research*, 46(June), 101870. <https://doi.org/10.1016/j.scr.2020.101870>
- Oh, H., Lewis, D. A., & Sibille, E. (2016). *The Role of BDNF in Age-Dependent Changes of Excitatory and Inhibitory Synaptic Markers in the Human Prefrontal Cortex*. 2, 3080–3091. <https://doi.org/10.1038/npp.2016.126>
- Orav, E., Atanasova, T., Shintyapina, A., Kesaf, S., Kokko, M., Partanen, J., Taira, T., & Lauri, S. E. (2017). NETO1 guides development of glutamatergic connectivity in the hippocampus by regulating axonal kainate receptors. *ENeuro*, 4(3). <https://doi.org/10.1523/ENEURO.0048-17.2017>
- Osakada, F., & Callaway, E. M. (2013). Design and generation of recombinant rabies virus vectors. *Nature Protocols*, 8(8), 1583–1601. <https://doi.org/10.1038/nprot.2013.094>
- Panoutsopoulos, A. A. (2020). Organoids, Assembloids, and Novel Biotechnology: Steps Forward in Developmental and Disease-Related Neuroscience. *Neuroscientist*. <https://doi.org/10.1177/1073858420960112>
- Paşca, S. P. (2018). The rise of three-dimensional human brain cultures. *Nature*, 553(7689), 437–445. <https://doi.org/10.1038/nature25032>
- Peng, S., Zeng, L., Haure-Mirande, J. V., Wang, M., Huffman, D. M., Haroutunian, V., Ehrlich, M. E., Zhang, B., & Tu, Z. (2021). Transcriptomic Changes Highly Similar to Alzheimer's Disease Are Observed in a Subpopulation of Individuals During Normal Brain Aging. *Frontiers in Aging Neuroscience*, 13(December), 1–16. <https://doi.org/10.3389/fnagi.2021.711524>
- Potashkin, J. A., Blume, S. R., & Runkle, N. K. (2011). Limitations of animal models of Parkinson's disease. In *Parkinson's Disease* (Vol. 658083).

---

<https://doi.org/10.4061/2011/658083>

- Preibisch, S., Saalfeld, S., & Tomancak, P. (2009). Globally optimal stitching of tiled 3D microscopic image acquisitions. *Bioinformatics*, 25(11), 1463–1465. <https://doi.org/10.1093/bioinformatics/btp184>
- Qin, J., Chen, S. G., Hu, D., Zeng, L. L., Fan, Y. M., Chen, X. P., & Shen, H. (2015). Predicting individual brain maturity using dynamic functional connectivity. *Frontiers in Human Neuroscience*, 9(JULY). <https://doi.org/10.3389/fnhum.2015.00418>
- Reinhardt, P., Glatza, M., Hemmer, K., Tsytsyura, Y., Thiel, C. S., Höing, S., Moritz, S., Parga, J. A., Wagner, L., Bruder, J. M., Wu, G., Schmid, B., Röpke, A., Klingauf, J., Schwamborn, J. C., Gasser, T., Schöler, H. R., & Sternecker, J. (2013). Derivation and Expansion Using Only Small Molecules of Human Neural Progenitors for Neurodegenerative Disease Modeling. *PLoS ONE*, 8(3). <https://doi.org/10.1371/journal.pone.0059252>
- Rodriguez-Gatica, J. E., Iefremova, V., Sokhranyaeva, L., Yeung, S. W. C. A., Breitkreuz, Y., Brüstle, O., Schwarz, M. K., & Kubitscheck, U. (2022). Imaging three-dimensional brain organoid architecture from meso- to nanoscale across development. *Development*, 149(20). <https://doi.org/10.1242/dev.200439>
- Roychoudhury, K., Salomone, J., Qin, S., Cain, B., Adam, M., Steven Potter, S., Nakafuku, M., Gebelein, B., & Campbell, K. (2020). Physical interactions between Gsx2 and Ascl1 balance progenitor expansion versus neurogenesis in the mouse lateral ganglionic eminence. *Development (Cambridge)*, 147(7). <https://doi.org/10.1242/dev.185348>
- Sandberg, M., Taher, L., Hu, J., Black, B. L., Nord, A. S., & Rubenstein, J. L. R. (2018). Genomic analysis of transcriptional networks directing progression of cell states during MGE development 06 Biological Sciences 0604 Genetics. *Neural Development*, 13(1), 1–12. <https://doi.org/10.1186/s13064-018-0119-4>
- Sanfilippo, C., Castrogiovanni, P., Imbesi, R., Kazakowa, M., Musumeci, G., Blennow, K., Zetterberg, H., & Di Rosa, M. (2019). Sex difference in CHI3L1 expression levels in human brain aging and in Alzheimer’s disease. *Brain Research*, 1720(June), 146305. <https://doi.org/10.1016/j.brainres.2019.146305>
- Schindelin, J., Arganda-Carreras, I., Frise, E., Kaynig, V., Longair, M., Pietzsch, T., Preibisch, S., Rueden, C., Saalfeld, S., Schmid, B., Tinevez, J. Y., White, D. J., Hartenstein, V., Eliceiri, K., Tomancak, P., & Cardona, A. (2012). Fiji: An open-source platform for

- 
- biological-image analysis. *Nature Methods*, 9(7), 676–682.  
<https://doi.org/10.1038/nmeth.2019>
- Shibata, A., & Jeggo, P. A. (2020). Roles for 53BP1 in the repair of radiation-induced DNA double strand breaks. *DNA Repair*, 93, 102915.  
<https://doi.org/10.1016/j.dnarep.2020.102915>
- Simpson, D. J., Olova, N. N., & Chandra, T. (2021). Cellular reprogramming and epigenetic rejuvenation. *Clinical Epigenetics*, 13(1), 1–10. <https://doi.org/10.1186/s13148-021-01158-7>
- Singh, A., Liang, L., Kaneoke, Y., Cao, X., & Papa, S. M. (2015). Dopamine regulates distinctively the activity patterns of striatal output neurons in advanced parkinsonian primates. *Journal of Neurophysiology*, 113(5), 1533–1544.  
<https://doi.org/10.1152/jn.00910.2014>
- Sloan, S. A., Andersen, J., Paşca, A. M., Birey, F., & Paşca, S. P. (2018). Generation and assembly of human brain region-specific three-dimensional cultures. *Nature Protocols*, 13(9), 2062–2085. <https://doi.org/10.1038/s41596-018-0032-7>
- Smits, L. M., Reinhardt, L., Reinhardt, P., Glatza, M., Monzel, A. S., Stanslowsky, N., Rosato-Siri, M. D., Zanon, A., Antony, P. M., Bellmann, J., Nicklas, S. M., Hemmer, K., Qing, X., Berger, E., Kalmbach, N., Ehrlich, M., Bolognin, S., Hicks, A. A., Wegner, F., ... Schwamborn, J. C. (2019). Modeling Parkinson's disease in midbrain-like organoids. *Npj Parkinson's Disease*, 5(1). <https://doi.org/10.1038/s41531-019-0078-4>
- Straccia, M., Barriga, G. G. D., Sanders, P., Bombau, G., Carrere, J., Mairal, P. B., Vinh, N. N., Yung, S., Kelly, C. M., Svendsen, C. N., Kemp, P. J., Arjomand, J., Schoenfeld, R. C., Alberch, J., Allen, N. D., Rosser, A. E., & Canals, J. M. (2015). Quantitative high-throughput gene expression profiling of human striatal development to screen stem cell-derived medium spiny neurons. *Molecular Therapy - Methods and Clinical Development*, 2(July), 15030. <https://doi.org/10.1038/mtm.2015.30>
- Straub, C., Hunt, D. L., Yamasaki, M., Kim, K. S., Watanabe, M., Castillo, P. E., & Tomita, S. (2011). Distinct functions of kainate receptors in the brain are determined by the auxiliary subunit Neto1. *Nature Neuroscience*, 14(7), 866–873. <https://doi.org/10.1038/nn.2837>
- Sulzer, D., Cragg, S. J., & Rice, M. E. (2016). Striatal dopamine neurotransmission: Regulation of release and uptake. *Basal Ganglia*, 6(3), 123–148.



---

<https://doi.org/10.1016/j.baga.2016.02.001>

- Sun, X., Zhang, B., Wang, Q., Blennow, K., Zetterberg, H., Yue, Z., Mccarthy, M., Loewenstein, D. A., & Vontell, R. (2021). *Association of neurogranin gene expression with Alzheimer ' s disease pathology in the perirhinal cortex*. *January*, 1–9. <https://doi.org/10.1002/trc2.12162>
- Tabrez, S., R. Jabir, N., Shakil, S., H. Greig, N., Alam, Q., M. Abuzenadah, A., A. Damanhour, G., & A. Kamal, M. (2012). A Synopsis on the Role of Tyrosine Hydroxylase in Parkinson's Disease. *CNS & Neurological Disorders - Drug Targets*, *11*(4), 395–409. <https://doi.org/10.2174/187152712800792785>
- Tagliaferro, P., & Burke, R. E. (2016). Retrograde Axonal Degeneration in Parkinson Disease. *Journal of Parkinson ' s Disease*, *6*(1), 1–15. <https://doi.org/10.3233/JPD-150769>
- Talyansky, S., & Brinkman, B. A. W. (2021). Dysregulation of excitatory neural firing replicates physiological and functional changes in aging visual cortex. *PLoS Computational Biology*, *17*(1), 1–29. <https://doi.org/10.1371/JOURNAL.PCBI.1008620>
- Ugolini, G. (1995). Specificity of rabies virus as a transneuronal tracer of motor networks: Transfer from hypoglossal motoneurons to connected second-order and higher order central nervous system cell groups. *Journal of Comparative Neurology*, *356*(3), 457–480. <https://doi.org/10.1002/cne.903560312>
- Voytek, B., & Knight, R. T. (2015). Dynamic network communication as a unifying neural basis for cognition, development, aging, and disease. *Biological Psychiatry*, *77*(12), 1089–1097. <https://doi.org/10.1016/j.biopsych.2015.04.016>
- Wagner, K. D., & Wagner, N. (2022). The Senescence Markers p16INK4A, p14ARF/p19ARF, and p21 in Organ Development and Homeostasis. *Cells*, *11*(12). <https://doi.org/10.3390/cells11121966>
- Xiang, Y., Tanaka, Y., Cakir, B., Patterson, B., Kim, K. Y., Sun, P., Kang, Y. J., Zhong, M., Liu, X., Patra, P., Lee, S. H., Weissman, S. M., & Park, I. H. (2019). hESC-Derived Thalamic Organoids Form Reciprocal Projections When Fused with Cortical Organoids. *Cell Stem Cell*, *24*(3), 487–497.e7. <https://doi.org/10.1016/j.stem.2018.12.015>
- Yan, C., Jiang, J., Yang, Y., Geng, X., & Dong, W. (2022). The function of VAMP2 in mediating membrane fusion: An overview. *Frontiers in Molecular Neuroscience*, *15*(December), 1–15. <https://doi.org/10.3389/fnmol.2022.948160>

- 
- Zagare, A., Barmpha, K., Smajic, S., Smits, L. M., Grzyb, K., Grünewald, A., Skupin, A., Nickels, S. L., & Schwamborn, J. C. (2022). Midbrain organoids mimic early embryonic neurodevelopment and recapitulate LRRK2-p.Gly2019Ser-associated gene expression. *American Journal of Human Genetics*, *109*(2), 311–327. <https://doi.org/10.1016/j.ajhg.2021.12.009>
- Zanetti, C., Spitz, S., Berger, E., Bolognin, S., Smits, L. M., Crepaz, P., Rothbauer, M., Rosser, J. M., Marchetti-Deschmann, M., Schwamborn, J. C., & Ertl, P. (2021). Monitoring the neurotransmitter release of human midbrain organoids using a redox cycling microsensor as a novel tool for personalized Parkinson's disease modelling and drug screening †. *Cite This: Analyst*, *146*, 2358. <https://doi.org/10.1039/d0an02206c>
- Zhai, S., Tanimura, A., Graves, S. M., Shen, W., & Surmeier, D. J. (2018). Striatal synapses, circuits, and Parkinson's disease. *Current Opinion in Neurobiology*, *48*, 9–16. <https://doi.org/10.1016/j.conb.2017.08.004>

---

## Figure Legends

### **Figure 1: Generation of midbrain-striatum assembloid model with identity specificity.**

**A.** Schematic representation of the assembloid model generation. **B.** Representative confocal image of a 70  $\mu\text{m}$  assembloid section immunostained with Hoechst, FOXA2 visible in the MO side and CTIP2 visible in the StrO side of the assembloid. GFP fluorescence is intrinsic in the midbrain part of the assembloids. **C.** Representative confocal image of a 70  $\mu\text{m}$  assembloid section immunostained with Hoechst and ASCL1 visible in the StrO side of the assembloid. GFP fluorescence is intrinsic in the MO part of the assembloids. **D.** Representative confocal image of a 70  $\mu\text{m}$  assembloid section immunostained with Hoechst and CORIN visible in the MO side of the assembloid. GFP fluorescence is intrinsic in the midbrain part of the assembloids. **E.** Representative confocal image of a 70  $\mu\text{m}$  assembloid section immunostained with Hoechst and TH visible in the MO side of the assembloid. GFP fluorescence is intrinsic in the midbrain part of the assembloids. **F.** Representative confocal image of a 70  $\mu\text{m}$  assembloid section immunostained with Hoechst and DARPP32 visible in the StrO side of the assembloid. GFP fluorescence is intrinsic in the midbrain part of the assembloids. **G.** Representative brightfield image of an assembloid in a well of the 48-well MEA plate. Plots showing the quantification of the Number of Spikes, Inter-spike Interval in seconds and the Burst Frequency in Hz between assembloids generated from two independent human WT cell lines. The data in the plots represent recordings of individual assembloids for the culture periods D32 to D43, from 3-4 batches. Batch correction was applied by normalising each value to the mean of the values for each batch. Outliers were calculated in GraphPad Prism using the ROUT method Q 1%. Two-sided Wilcoxon test was performed in R 4.2.2.

### **Figure 2: Single nuclei RNA sequencing analysis in the assembloid model.**

**A.** UMAP embedding of the different cellular clusters in assembloids. **B.** Percentage of the cellular composition in the assembloid model. **C.** Unsupervised hierarchical clustering of cell clusters, using the average expression with Z-score normalisation of the top 500 most variable genes. **D.** Spearman's correlation between the different cell types in assembloids. **E.** Enriched pathways identified by Metacore using the DEGs between assembloid and MO, and between assembloid and StrO, after integration of the three datasets with the Seurat workflow. **F.** Plot showing the number of genes that were identified in the enrichment of the "Developmental Neurogenesis

---

and Axonal guidance” pathway in both comparisons Assembloid vs MO and Assembloid vs StrO. **G.** Barplot showing the upregulation of neuronal maturity related genes in both DEG lists, of Assembloid vs MO and Assembloid vs StrO.

**Figure 3: Midbrain-Striatum assembloids develop nigrostriatal pathway connectivity. A.** Representative microscopic images of a whole assembloid (4X objective) and of ROI, observed with fluorescence microscopy (25X objective). The assembloid was immunostained with Hoechst and TH. The ROI (right panel) shows the GFP+/TH+ neuron’s soma in the MO-GFP side of the assembloid with TH+ projection towards the striatum side in the different planes along the Z stack (Z.190-280). White arrowheads show the progression of the TH+ projection in images from the different planes. 3D reconstruction of the neuron across the planes shows the complete TH+ neuronal projection. **B.** Bar pot showing the electrochemical measurements in tissue in StrOs and in the StrO side of the assembloid model at D30. Welch’s t-test was performed, StOs n=8, StrOs in assembloid n=9, where n is the average measurements in one organoid or assembloid, for three batches, generated from the same line (390, see Supplementary Table 1). Error bars represent mean  $\pm$  SD. Data were plotted in GraphPad Prism 9.0.0. \*p<0.05, \*\*p<0.01, \*\*\*p<0.001. **C.** Schematic representation of the Rabies monosynaptic tracing experiments in midbrain-striatum assembloids. **D.** Representative confocal image of 70  $\mu$ m assembloid section showing the GFP and RFP positive cells from the LV-GP-TVA-GFP and RBV- $\Delta$ G-EnvA-RFP infections respectively. The GFP signal in the StrO side of the assembloid is coming from the LV-GP-TVA-GFP infection, while GFP fluorescence in the MO side of the assembloid is cell intrinsic. White arrowheads indicate the RFP positive signal in the MO side, and the RFP/GFP positive signal in the StrO side of the assembloid. **E.** Representative confocal images of 70  $\mu$ m assembloids sections showing the MO sides of the assembloids with GFP and RFP positive cells from the cell intrinsic GFP expression and RBV- $\Delta$ G-EnvA-RFP infections respectively and immunostained with Hoechst and TH. Zoomed in regions (indicated by the white squares) show the TH+/RFP+ colocalization in the midbrain side of the assembloids.

**Figure 4: Optimisation of the Progerin-overexpression in the assembloid model. A.** Schematic representation of the assembloid model generation using the Progerin cell line for the

---

inducible overexpression of Progerin after doxycycline supplementation. **B.** FACs data showing the % of the GFP positive signal measured in live cells of dissociated assembloids, treated with different doxycycline concentrations (Progerin\_0\_Dox = Untreated, Progerin\_1\_Dox = 1 ng/ $\mu$ l, Progerin\_2\_Dox = 2 ng/ $\mu$ l, Progerin\_4\_Dox = 4 ng/ $\mu$ l). One-way ANOVA, with Tukey's multiple comparison test was performed in R 4.2.2. For all conditions n = 3 with each point representing the average of two technical replicates per batch for 3 batches. \*p<0.05, \*\*p<0.01, \*\*\*p<0.001. **C.** Western blot for Progerin protein levels in assembloids treated with the different doxycycline concentrations. One-way ANOVA, with Tukey's multiple comparison test was performed in R 4.2.2. Error bars represent mean  $\pm$  SD. For all conditions n =3 with each point representing 3-4 polled assembloids per batch, for 4 batches. \*p<0.05, \*\*p<0.01, \*\*\*p<0.001. Batch correction was applied by normalising each value to the mean of the values for each batch. Outliers were calculated in GraphPad Prism using the ROUT method Q 1%.

**Figure 5: Progerin-overexpressing cells with aging characteristics in the assembloid model.** **A.** Immunofluorescence staining quantification of the H2AX and 53BP1 positive nuclear foci voxels normalised to the total nucleus voxels in 70  $\mu$ m Progerin-overexpressing assembloid sections from D30 and D60 cultures. For D30 data, Welch's t-test was performed with n = 9 for both conditions where each point represents one section per assembloid per batch for 3 batches. For D60 data two-sided Wilcoxon test was performed with n = 12 for both conditions where each point represents one section per assembloid per batch for 4 batches. \*p<0.05, \*\*p<0.01, \*\*\*p<0.001. **B.** Immunofluorescence staining quantification of the P16 voxels normalised to the total nucleus voxels, and P16 and MAP2 double positive voxels normalised to the total MAP2 voxels in 70  $\mu$ m Progerin-overexpressing assembloid sections from D60 cultures. Two-sided Wilcoxon test for both plots was performed, with n = 11 where each point represents one section per assembloid per batch for 4 batches. \*p<0.05, \*\*p<0.01, \*\*\*p<0.001. **C.** Immunofluorescence staining quantification of the P21 voxels normalised to the total nucleus voxels, and P21 and MAP2 double positive voxels normalised to the total MAP2 voxels in 70  $\mu$ m Progerin-overexpressing assembloid sections from D60 cultures. Welch's t-test and two-sided Wilcoxon test was performed respectively, with n = 12 for both conditions where each point represents one section per assembloid per batch for 4 batches. \*p<0.05, \*\*p<0.01, \*\*\*p<0.001. **D.** Immunofluorescence staining quantification of the P53

---

voxels normalised to the total nucleus voxels, and P53 and MAP2 double positive voxels normalised to the total MAP2 voxels in 70  $\mu\text{m}$  Progerin-overexpressing assembloid sections from D60 cultures. Welch's t-test and two-sided Wilcoxon test was performed respectively, with  $n = 12$  for both conditions where each point represents one section per assembloid per batch for 4 batches. \* $p < 0.05$ , \*\* $p < 0.01$ , \*\*\* $p < 0.001$ . In all plots batch correction was applied by normalising each value to the mean of the values for each batch. Outlier removal was performed based on the Inter-Quartile Range (IQR) proximity rule. Data were plotted in R 4.2.2.

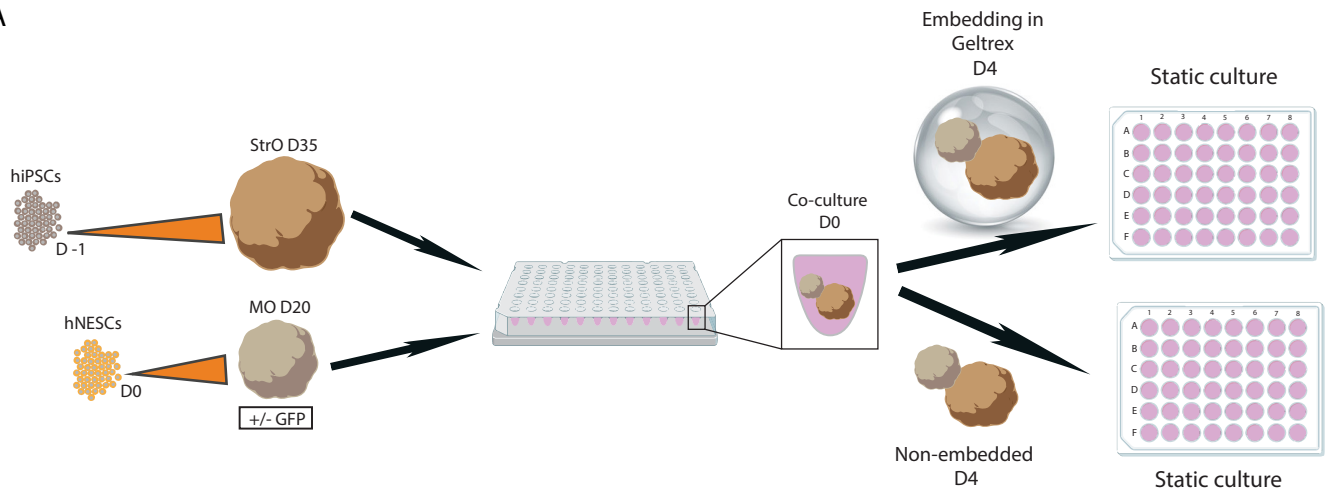
**Figure 6: Evident aging phenotype in the Progerin-overexpressing assembloid model. A.** PCA plot of the two first principal components on the gene expression value (FPKM) of all samples. Each sample represents data from 4 pooled assembloids from one batch. **B.** Plot showing the log<sub>2</sub> fold change of significant differentially expressed genes between Progerin-overexpressing assembloids (PROG\_DOX) and control (WT\_UNTR, WT\_DOX, PROG\_UNTR) samples. This list of genes was extracted after the comparison of the assembloid data with post mortem human brain data (Berchtold et al., 2008; González-Velasco et al., 2020). **C.** Western blot showing the protein levels of LAMINB1 normalised to H3 housekeeping protein and batch corrected by normalising to the mean of the values for each batch. Outliers were calculated in GraphPad Prism using the ROUT method Q 1%. One-way ANOVA, with Tukey's multiple comparison test was performed. For all conditions  $n = 4$  with each point representing 3-4 pooled assembloids per batch, for 4 batches. Error bars represent mean  $\pm$  SD. Data were plotted in GraphPad Prism 9.0.0. \* $p < 0.05$ , \*\* $p < 0.01$ , \*\*\* $p < 0.001$ . **D.**  $\beta$ -galactosidase staining for all the different assembloid conditions. Positive  $\beta$ -galactosidase areas were measured with ImageJ and normalised to the area of the section in each image and batch corrected by normalising to the mean of the values for each batch. Kruskal-Wallis test with Benjamini-Hochberg correction and Dunn's multiple comparison test was performed. For all conditions  $n = 6$  with each point representing one section per assembloid, per batch, for 3 batches. \* $p < 0.05$ , \*\* $p < 0.01$ , \*\*\* $p < 0.001$ . Batch correction was applied by normalising each value to the mean of the values for each batch. Outlier removal was performed based on the Inter-Quartile Range (IQR) proximity rule. Data were plotted in R 4.2.2.

---

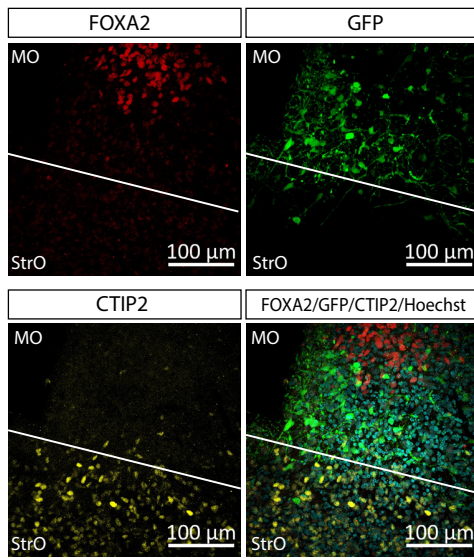
**Figure 7: Early neurodegeneration phenotypes in Progerin-overexpressing assembloids.**

**A.** Bar blot showing the electrochemical measurements in the StrO side of assembloids from the different conditions at D60. One-way ANOVA with Tukey's multiple comparison test was performed. For all conditions  $n =$  the mean of measurements from 5 different positions in 3-4 assembloids per batch for 3 batches (WT\_Untreated  $n = 11$ , WT\_DOX  $n = 10$ , Progerin\_Untreated  $n = 11$ , Progerin\_DOX  $n = 9$ ). Error bars represent mean  $\pm$  SD. **B.** KEGG and GO pathway enrichment analysis of the DEGs between PROG-DOX and PROG\_UNTR samples. **C.** Western blot for the protein levels of VAMP2 normalised to  $\beta$ -Actin. **D.** Western blot for the protein levels of Synaptotagmin1 (SYN) normalised to  $\beta$ -Actin. **E.** Western blot for the protein levels of Gephyrin normalised to  $\beta$ -Actin. **F.** Western blot for the protein levels of TH normalised to  $\beta$ -Actin. **G.** Representative confocal image of the MO side of a 70  $\mu$ m Progerin-overexpressing assembloid section with TH and Hoechst immunostaining. The white square indicates the zoomed in region showing a representative image of a fragmented TH+ neurite. **H.** Plot showing the TH fragmentation index as quantified by our neuronal skeleton quantification approach with MATLAB (Bolognin et al., 2019). Welch's t-test was performed with  $n = 8$  for each condition, where each point represents the average of 3-5 sections per assembloid per batch, for 4 batches. In all plots batch correction was applied by normalising each value to the mean of the values for each batch. \* $p < 0.05$ , \*\* $p < 0.01$ , \*\*\* $p < 0.001$ . For C-F plots, Welch's t-test was performed in each plot with  $n = 7$  for each condition, where each point represents 3-4 pooled assembloid per batch, for 7 batches. Outliers were calculated in GraphPad Prism 9.0.0 using the ROUT method Q 1%. Error bars represent mean  $\pm$  SD. For plot H, data were plotted in R 4.2.2 and outlier removal was performed based on the Inter-Quartile Range (IQR) proximity rule.

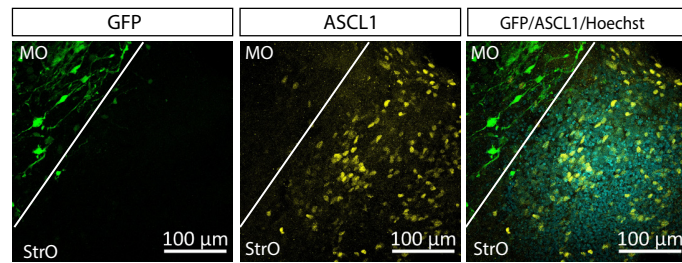
A



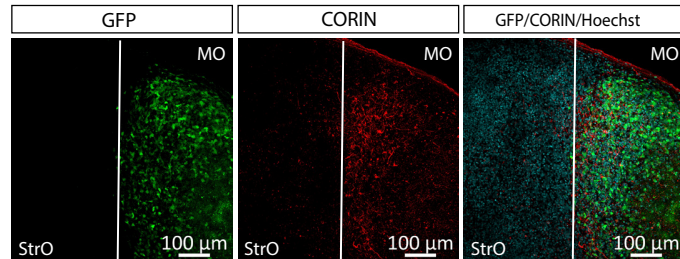
B



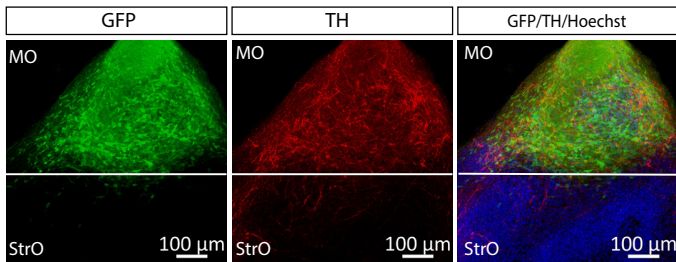
C



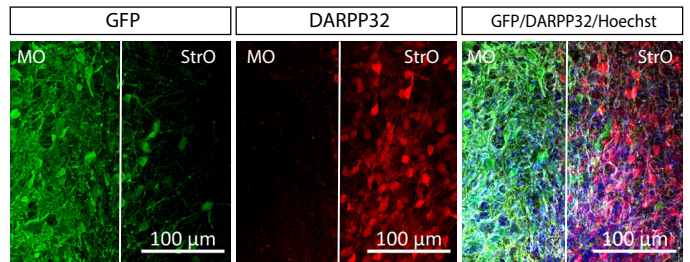
D



E



F



G

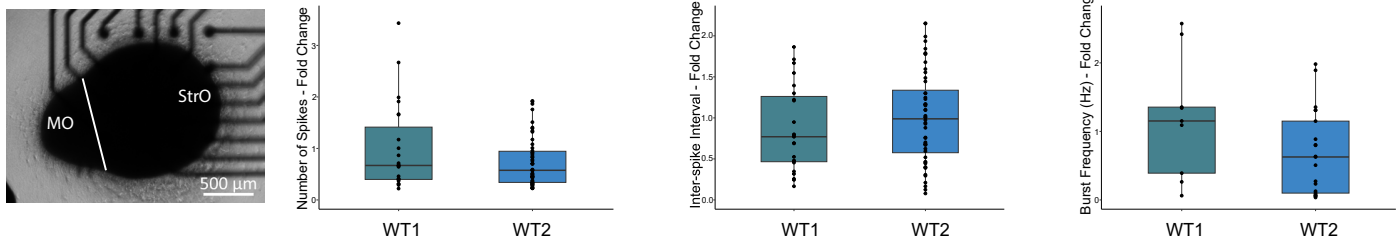


Figure 1



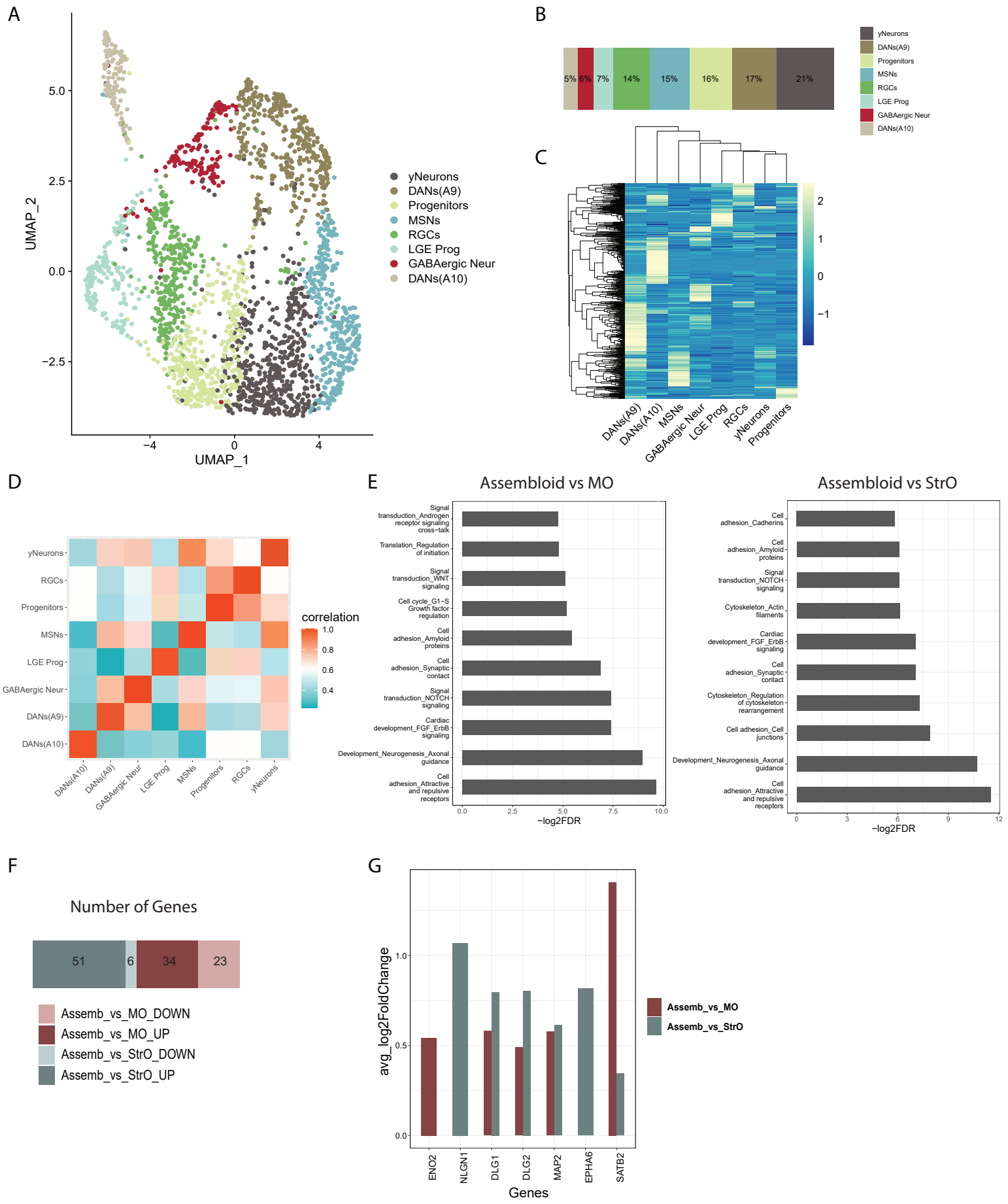


Figure 2

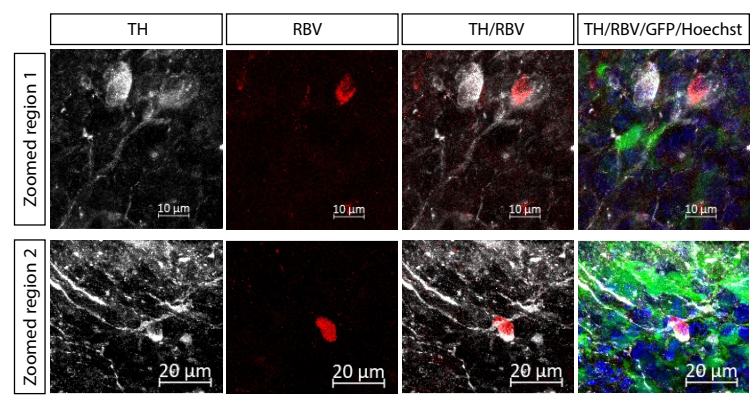
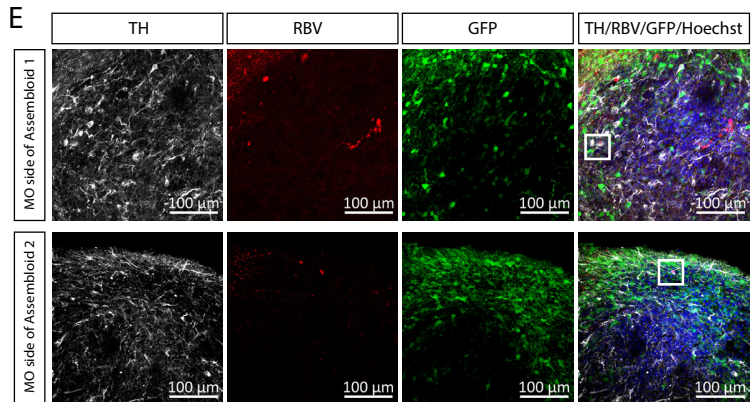
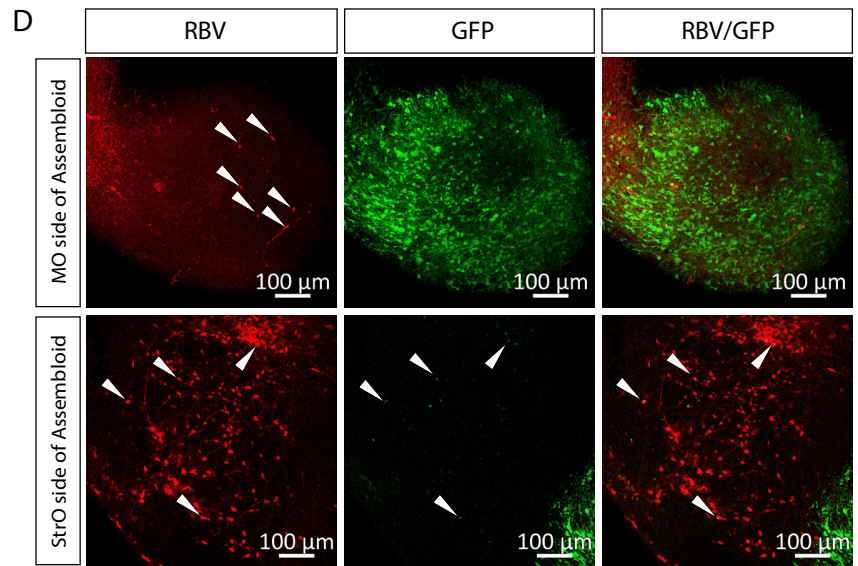
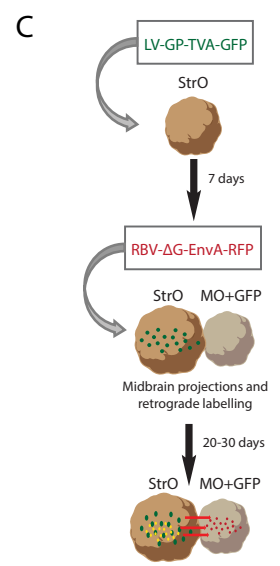
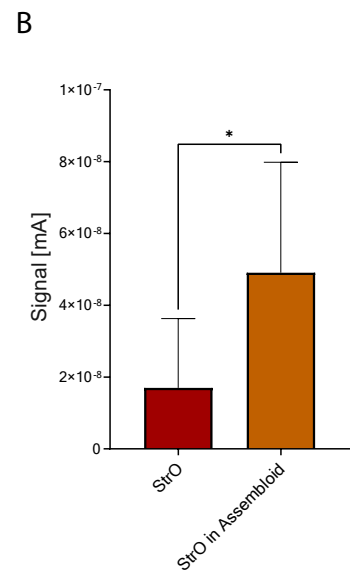
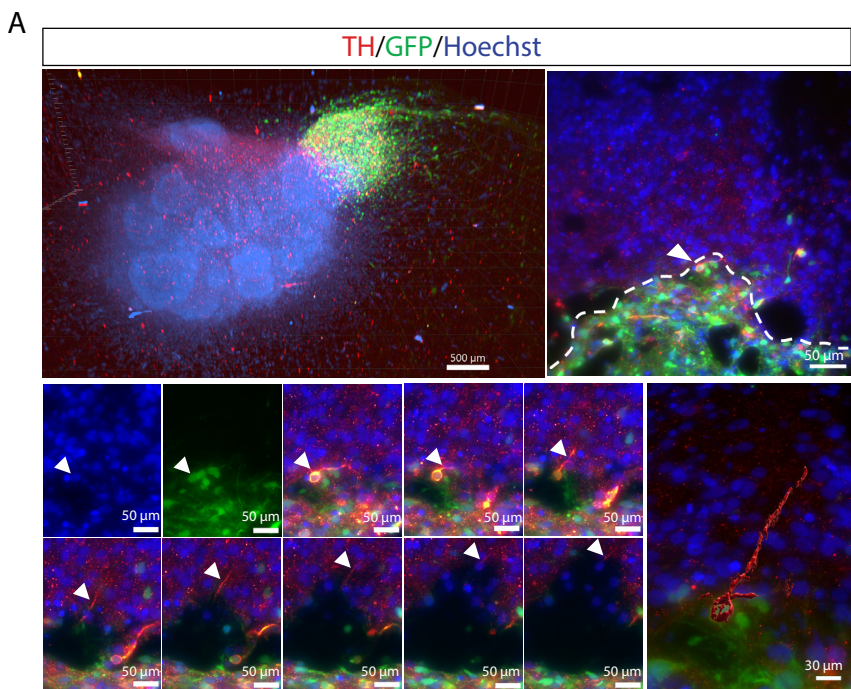
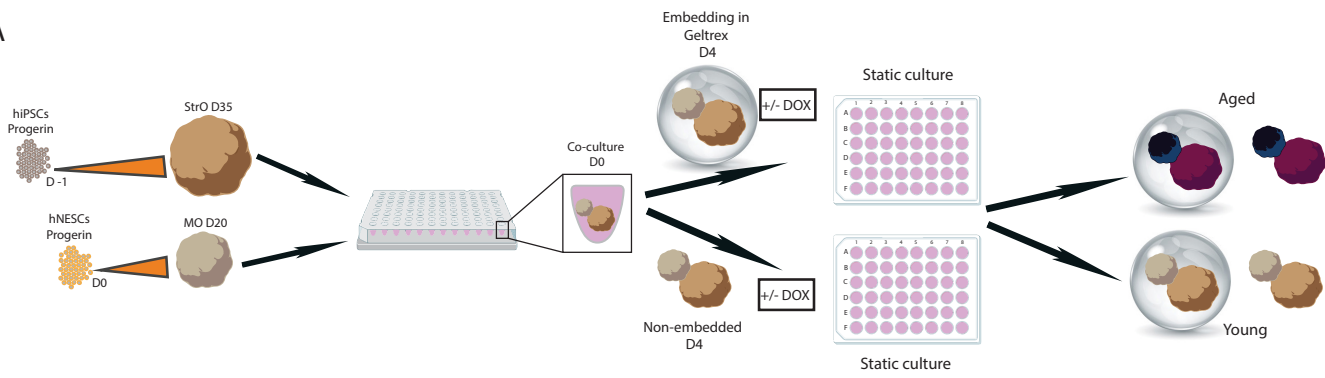
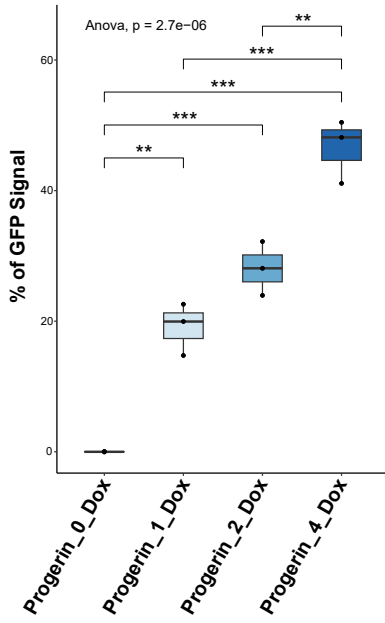


Figure 3

A



B



C

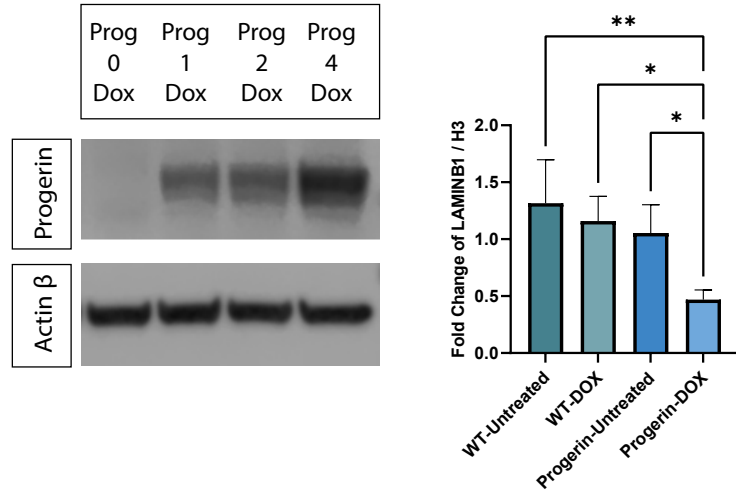


Figure 4

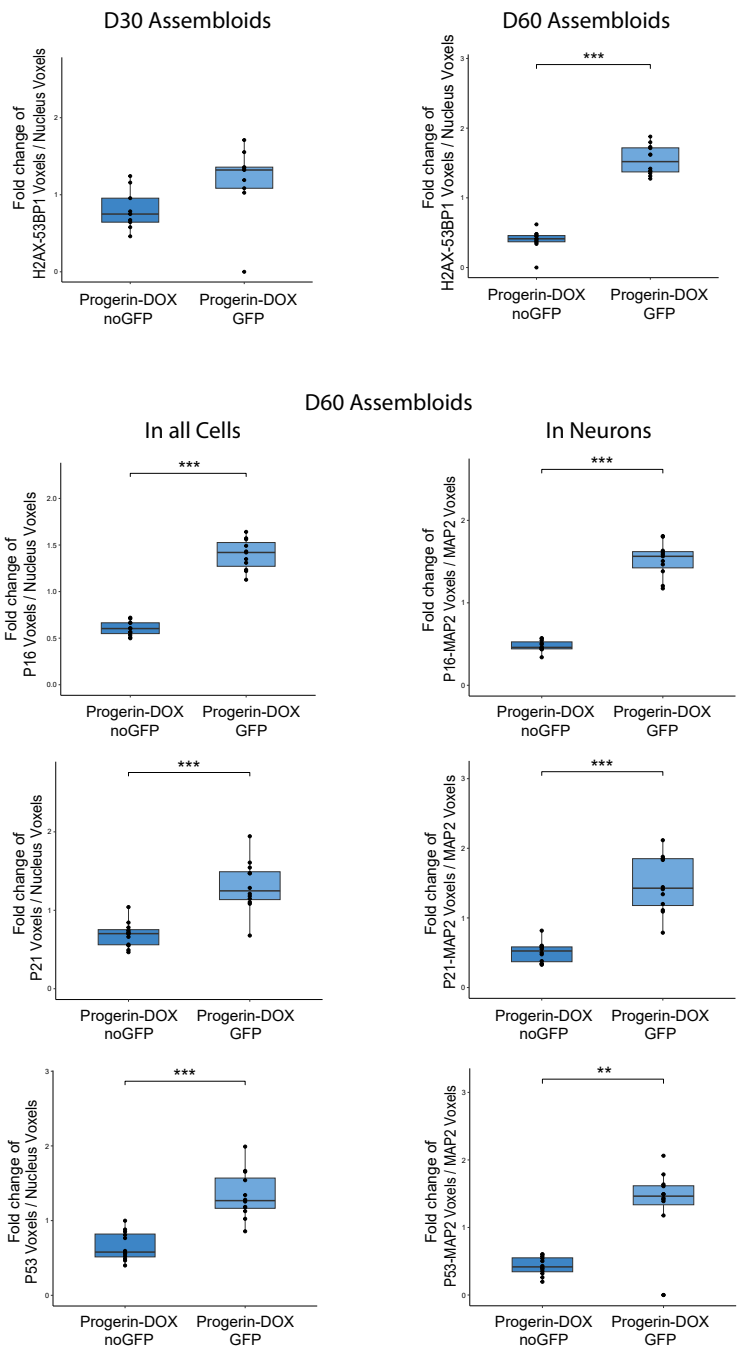
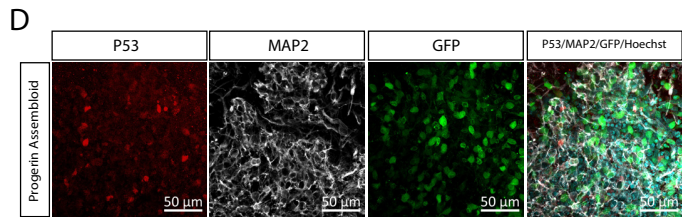
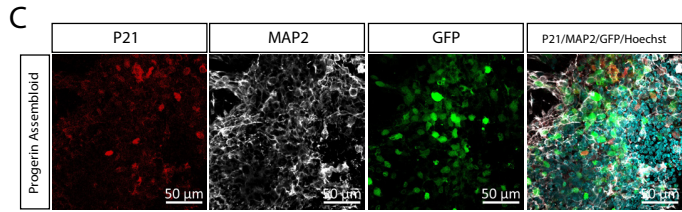
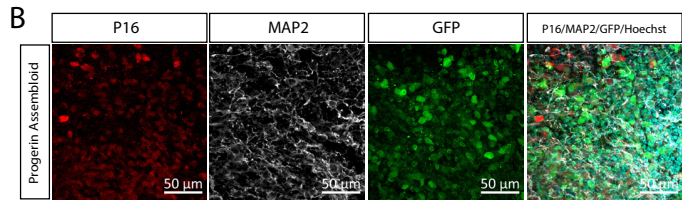
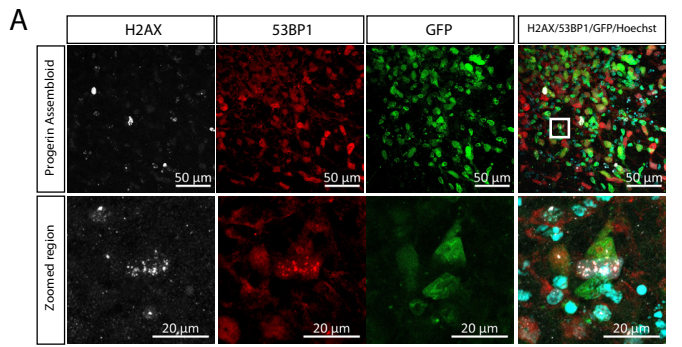


Figure 5

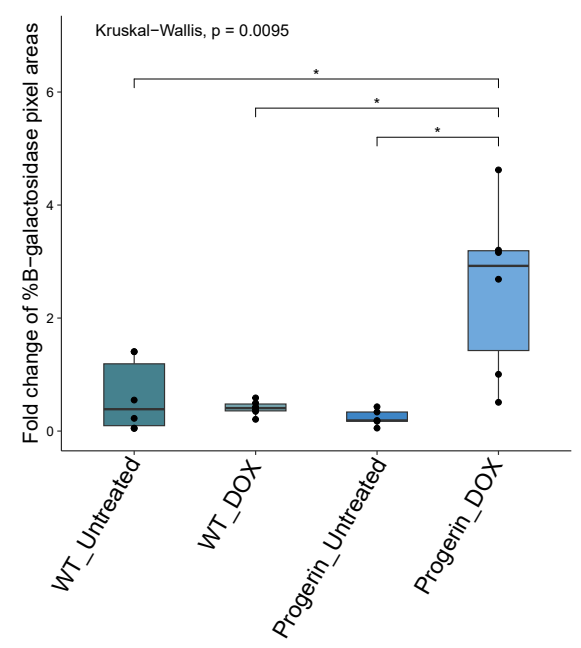
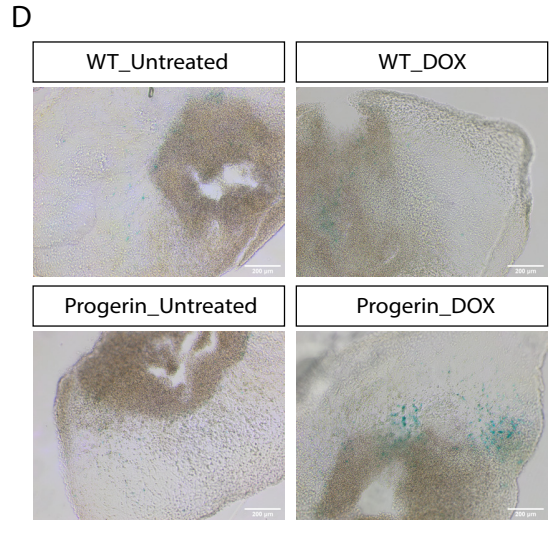
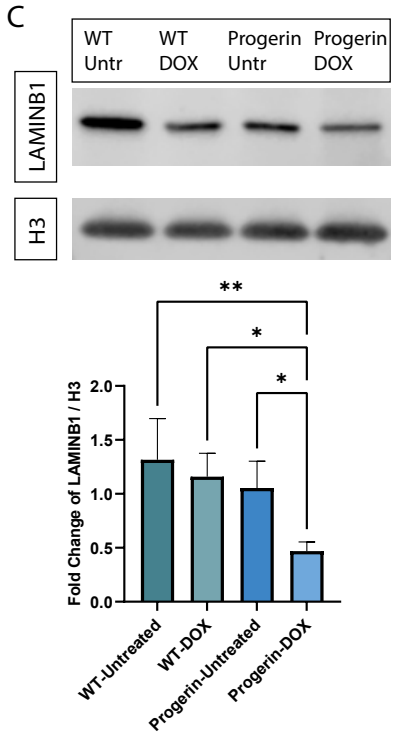
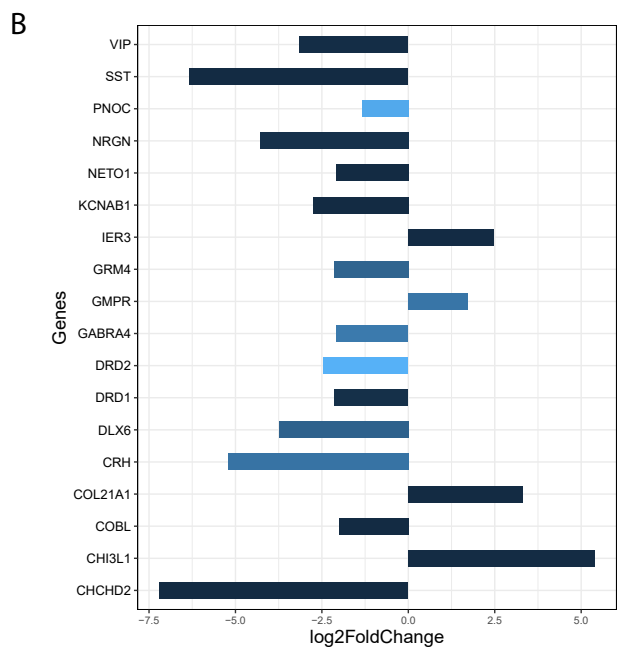
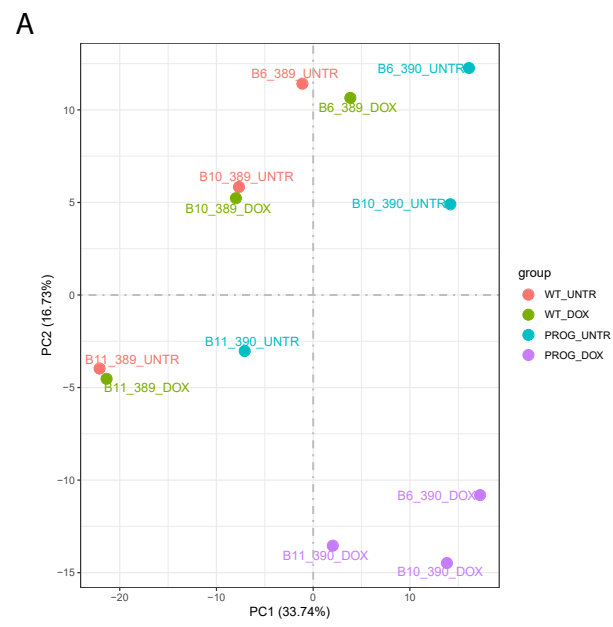


Figure 6

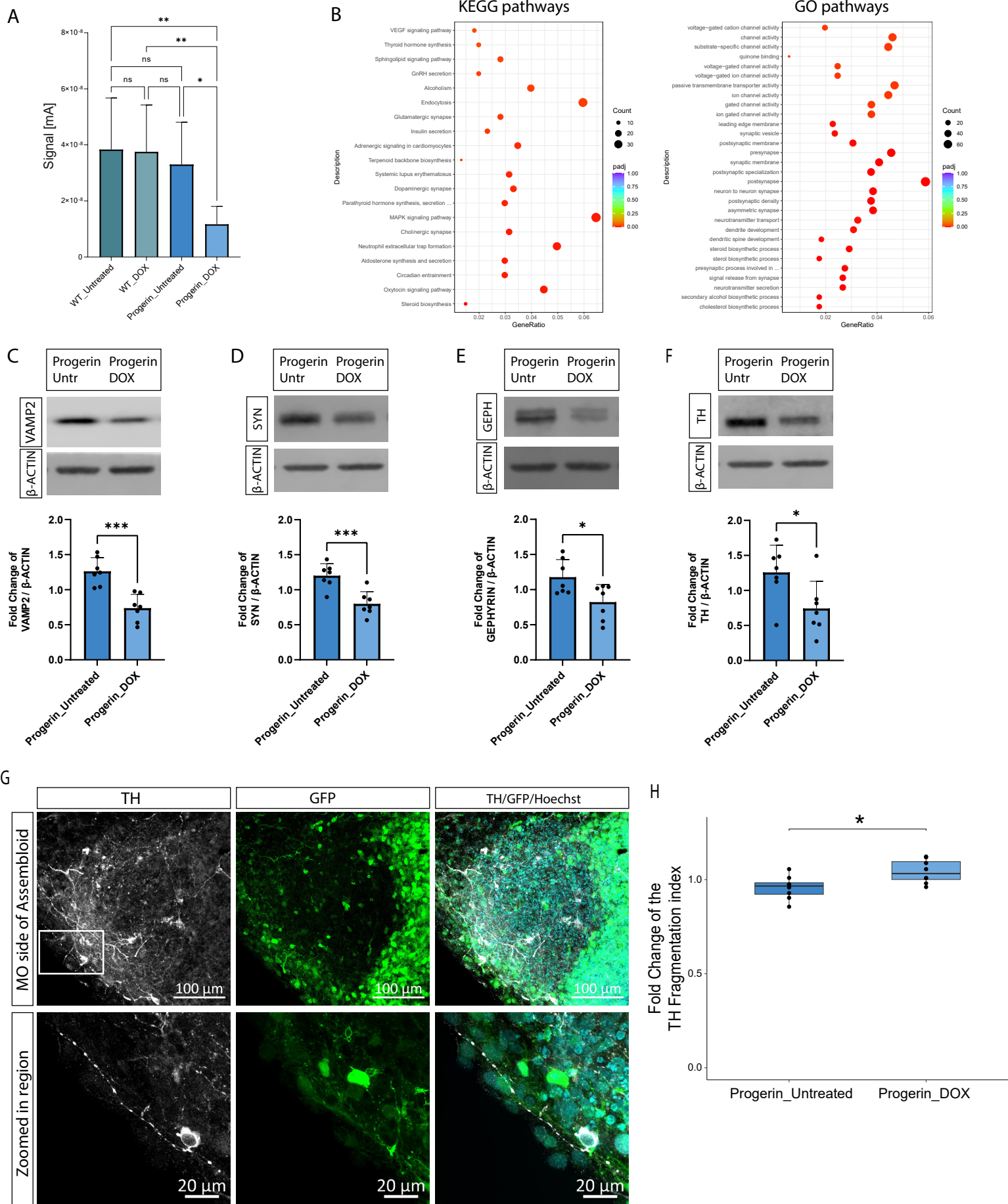


Figure 7

---

## Supplementary Figure Legends

**Supplementary Figure 1: Characterisation of iPSC and NESC lines with immunofluorescence staining.** iPSCs and NESCs were immunostained for the detection of pluripotent and neuroepithelial stem cell markers respectively. **A.** iPSCs of the 200 cell line were immunostained for SSEA-4, NANOG, OCT4 and Hoechst. **B.** iPSCs of the 201 cell line were immunostained for SSEA-4, OCT4, NANOG, TRA1-60 and Hoechst. **C.** iPSCs of the 389 and 390 cell lines were immunostained for SSEA-4, OCT4 and Hoechst. **D.** iPSCs of the 389 and 390 cell lines were immunostained for NANOG, TRA1-60 and Hoechst. **E.** NESCs of the 201 and 200 cell lines were immunostained for PAX6, NESTIN and Hoechst. These lines were previously genetically engineered for the intrinsic expression of GFP. **F.** NESCs of the 201 and 200 cell lines were immunostained for SOX1, SOX2 and Hoechst. These lines were previously genetically engineered for the intrinsic expression of GFP. **G.** NESCs of the 389 and 390 cell lines were immunostained for PAX6, SOX2, NESTIN and Hoechst.

**Supplementary Figure 2: Different conditions used for the generation of striatum organoids. A-D.** Schematic representation of the different steps in the differentiation process of StrOs generation in the condition C4 (A), in the condition C3 (B), in the condition RA (C) and in the condition SR (D).

**Supplementary Figure 3: Striatum organoids characterisation. A.** qPCR plots showing the relative expression of progenitor markers specific to the LGE and striatum brain regions. For *FOXG1*, *ASCL1*, *GSX2* and *CTIP2*, Kruskal-Wallis test with Benjamini-Hochberg correction and Dunn's multiple comparison test was performed. For *FOXP1* and *FOXP2*, one-way ANOVA, with Tukey's multiple comparison test was performed. **B.** qPCR plots showing the relative expression of progenitor markers specific to the MGE region of the brain. For *NKX2.1*, Kruskal-Wallis test with Benjamini-Hochberg correction and Dunn's multiple comparison test was performed. For *OTX2*, one-way ANOVA, with Tukey's multiple comparison test was performed. **C.** qPCR plots showing the relative expression of striatum specific markers. For *DARPP32*, one-way ANOVA, with Tukey's multiple comparison test was performed. For *DRD1* and *DRD2*, Kruskal-Wallis test with Benjamini-Hochberg correction and Dunn's multiple comparison test was performed. **D.** Western blot showing the protein levels of

---

DARPP32 in the different conditions of StrOs. One-way ANOVA, with Tukey's multiple comparison test was performed. **E.** Western blot showing the protein levels of DRD1 in the different conditions of StrOs. One-way ANOVA, with Tukey's multiple comparison test was performed. **F.** Western blot showing the protein levels of DRD2 in the different conditions of StrOs. One-way ANOVA, with Tukey's multiple comparison test was performed. **G.** Western blot showing the protein levels of GAD65 in the different conditions of StrOs. One-way ANOVA, with Tukey's multiple comparison test was performed. For all plots,  $n = 3-5$ , where each point is one sample of pooled 6-8 pooled organoids, from 3-5 batches.  $*p < 0.05$ ,  $**p < 0.01$ ,  $***p < 0.001$ . qPCR data were normalised to ACTINB expression and fold change to the C4\_D35 condition was calculated. For the western blots, data were normalised to  $\beta$ -Actin levels and batch correction was applied by normalising each value to the mean of the values for each batch. Error bars represent mean  $\pm$  SD. In all plots, outliers were calculated in GraphPad Prism using the ROUT method Q 1%. Data were plotted in GraphPad Prism 9.0.0.

**Supplementary Figure 4: Co-culture media optimisation for the assembloid model.** **A.** Schematic representation of the protocol used for the generation of assembloids. **B.** Table showing the different media that were tested for the optimisation of the co-culture condition. **C.** Immunostaining of MO 70  $\mu$ m sections for the expression of TH, cultured for 20 days in the different co-culture conditions. Images were acquired with the Yokogawa high content imaging microscope. Kruskal-Wallis test with Benjamini-Hochberg correction and Dunn's multiple comparison test was performed.  $N = 6$ , where each point represents the average of 2 sections per organoids per batch, for 3 batches. Batch correction was applied by normalising each value to the mean of the values for each batch.  $*p < 0.05$ ,  $**p < 0.01$ ,  $***p < 0.001$ ,  $****p < 0.001$ . Outlier removal was performed based on the Inter-Quartile Range (IQR) proximity rule. Data were plotted in R 4.2.2.

**Supplementary Figure 5: Immunostaining for TH in assembloids cultured in the different co-culture conditions.** 70  $\mu$ m assembloid sections cultured for 20 and 35 days in the different co-culture and StrO conditions, were immunostained with TH and Hoechst for the quantification of the TH positive cells. Images were acquired with the Yokogawa high content imaging microscope. Kruskal-Wallis test with Benjamini-Hochberg correction and Dunn's multiple



---

comparison test was performed.  $N = 6-9$ , where each point represents one section, per assembloid, per batch, for 3 batches. In all plots batch correction was applied by normalising each value to the mean of the values for each batch.  $*p < 0.05$ ,  $**p < 0.01$ ,  $***p < 0.001$ . Outlier removal was performed based on the Inter-Quartile Range (IQR) proximity rule. Data were plotted in R 4.2.2.

**Supplementary Figure 6: Immunostaining for DARPP32 in assembloids cultured in the different co-culture conditions.** 70  $\mu\text{m}$  assembloid sections cultured for 20 and 35 days in the different co-culture and StrO conditions, were immunostained with DARPP32 and Hoechst for the quantification of the DARPP32 positive cells. Images were acquired with the Yokogawa high content imaging microscope. Kruskal-Wallis test with Benjamini-Hochberg correction and Dunn's multiple comparison test was performed.  $N = 6-9$ , where each point represents one section, per assembloid, per batch, for 3 batches. In all plots batch correction was applied by normalising each value to the mean of the values for each batch.  $*p < 0.05$ ,  $**p < 0.01$ ,  $***p < 0.001$ . Outlier removal was performed based on the Inter-Quartile Range (IQR) proximity rule. Data were plotted in R 4.2.2.

**Supplementary Figure 7: Markers expression in the different clusters of assembloids, identified by single nuclei RNA sequencing analysis. A-I.** Dot plots showing the expression of markers specific to dopaminergic neurons (DANs) (A-B), mature neurons (C), GABAergic neurons (D), medium spiny neurons (MSNs) (E-F), LGE progenitors (G), radial glia cells (RGCs) (H) and glia progenitors (I).

**Supplementary Figure 8: Single nuclei RNA sequencing analysis of midbrain organoids.** **A.** UMAP embedding of the different cellular clusters in MOs. **B.** Percentage of the cellular composition in MOs. **C.** Unsupervised hierarchical clustering of cell clusters, using the average expression with Z-score normalisation of the top 500 most variable genes. **D.** Spearman's correlation between the different cell types in MOs. **E-J.** Dot plots showing the expression of markers specific to dopaminergic neurons (E-F), GABAergic neurons (G), mature neurons (H), oligodendrocyte precursor cells (OPCs) (I) and radial glia cells (RGCs) (J).

---

**Supplementary Figure 9: Single nuclei RNA sequencing analysis of striatum organoids.** **A.** UMAP embedding of the different cellular clusters in StrOs. **B.** Percentage of the cellular composition in StrOs. **C.** Unsupervised hierarchical clustering of cell clusters, using the average expression with Z-score normalisation of the top 500 most variable genes. **D.** Spearman's correlation between the different cell types in StrOs. **E-K.** Dot plots showing the expression of markers specific to mature neurons (E), Telencephalic progenitors (F), MSNs progenitors (G), dopaminergic neurons (H), GABAergic neurons and MSNs (I-J) and GABAergic interneurons (K).

**Supplementary Figure 10: Single nuclei RNA sequencing integration analysis.** **A.** UMAP embedding of the integrated object, showing the predefined cellular identities in each model. **B.** Spearman's correlation between the different cell types. **C.** Expression of genes related to cellular and oxidative stress response in assembloids compared to MOs and StrOs. Dots represent single cells. Two-sided Wilcoxon test was performed between assembloids-MOs and assembloids-StrOs. \* $p < 0.05$ , \*\* $p < 0.01$ , \*\*\* $p < 0.001$ , \*\*\*\* $p < 0.0001$ . Data were plotted in R 4.2.2.

**Supplementary Figure 11: Nigrostriatal connectivity in the assembloid model.** **A.** Representative confocal images of MO and StrO 70  $\mu\text{m}$  sections immunostained for TH, MAP2 and Hoechst. **B.** Representative light sheet microscopic image (12X objective) of a whole assembloid and a ROI. The assembloid was immunostained with Hoechst and TH. The ROI shows the GFP+/TH+ neuron's soma in the MO-GFP side of the assembloid with TH+ projections towards the striatum side in the different planes (Z.236-280) along the Z stack. White arrowheads show the progression of the TH+ projection in images from the different planes. **C.** Representative light sheet microscopic image of a whole assembloid (4X objective) and the ROI (25X objective), in light sheet fluorescence microscopy. The assembloid was immunostained with Hoechst and TH. The ROI shows the GFP+/TH+ neuron's soma in the MO-GFP side of the assembloid with TH+ projections towards the striatum side in the different planes along the Z stack (Z.660-755). White arrowheads show the progression of the TH+ projection in images from the different planes. 3D reconstruction of the neuron across the planes shows the complete TH+ neuronal projection. **D.** Schematic representation of the electrochemical measurement set

---

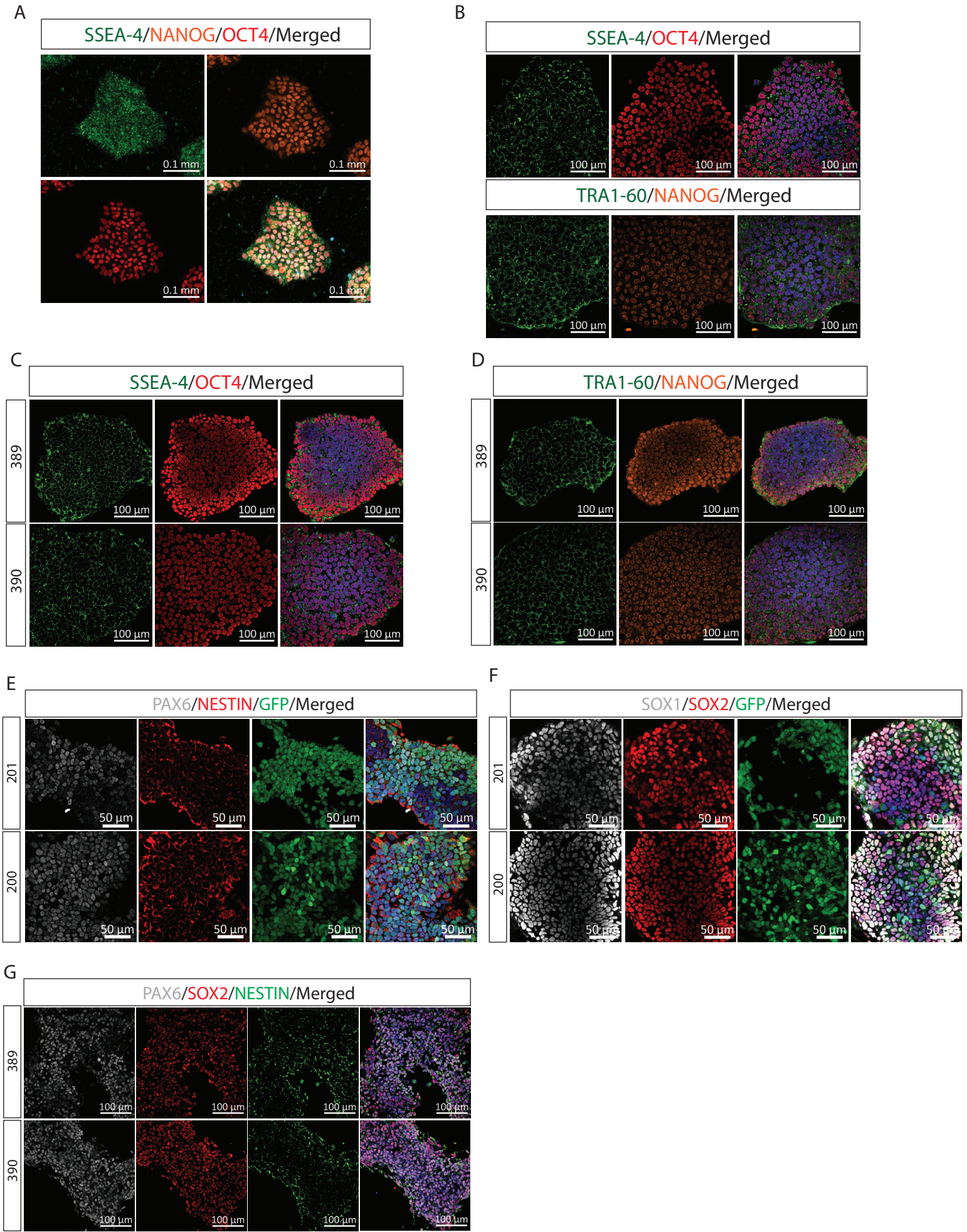
up in assembloids. **E.** Barplot showing the electrochemical measurements of catecholamines in tissue approximate to the MO and StrO sides of the assembloid model. Welch's t-test was performed. N = 8, where each point represents the average of the 3 technical electrochemical measurements in the MO and StrO side respectively, in each assembloid, for 2 batches. Background measurement was not subtracted in these measurements. Data were plotted in GraphPad Prism 9.0.0. \*p<0.05, \*\*p<0.01, \*\*\*p<0.001. Error bars represent mean ± SD. **F.** Bar plot showing the electrochemical measurements of catecholamines in StrOs cultured in their normal conditions and StrOs cultured in pre-used media in MOs culture. Welch's t-test was performed. N = 3-8, where each point represents the average measurement value with the background subtracted (PBS measurements) of each organoid per batch, for 3 batches. Data were plotted in GraphPad Prism 9.0.0. \*p<0.05, \*\*p<0.01, \*\*\*p<0.001. Error bars represent mean ± SD. **G.** Representative confocal images of a 70 µm assembloid section showing the GFP and RFP positive cells from the LV-GP-TVA-GFP and RBV-ΔG-EnvA-RFP infections respectively and immunostained with Hoechst and TH. Close up images indicated by the white square, show the colocalization of Rabies and TH signal in the MO side of the assembloid.

**Supplementary Figure 12: Toxicity assessment of doxycycline.** **A.** Boxplot showing the quantification of the LDH luminescence signal normalised to the average area of assembloids. One-way ANOVA, with Tukey's multiple comparison test was performed. N = 3, where each point represents the average of 3 technical replicates per batch, for 3 batches. Statistics show the pairwise comparisons of interest between the treatments in the same condition (Progerin or WT) and between the conditions with the same treatment. **B.** Boxplot showing the quantification of the ATP luminescence signal normalised to the average area of assembloids. One-way ANOVA, with Tukey's multiple comparison test was performed. N = 3, where each point represents the average of two technical replicates per batch, for 3 batches. \*p<0.05, \*\*p<0.01, \*\*\*p<0.001. Data were plotted in R 4.2.2.

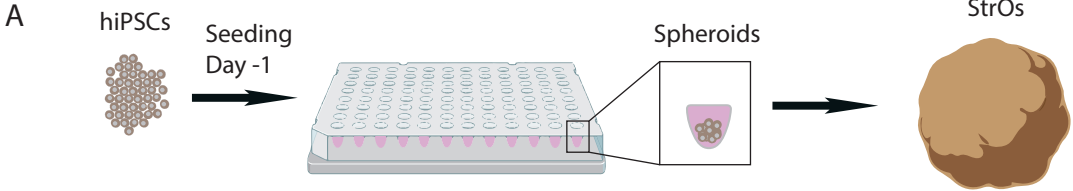
**Supplementary Figure 13: Differential expression gene profile in aged and young assembloids.** **A.** Heatmap showing the hierarchical clustering of samples with similar expression patterns, after Z-score homogenisation of the expression data. **B.** Histogram showing the number of differential genes (up-regulated and down-regulated) for each comparison.

---

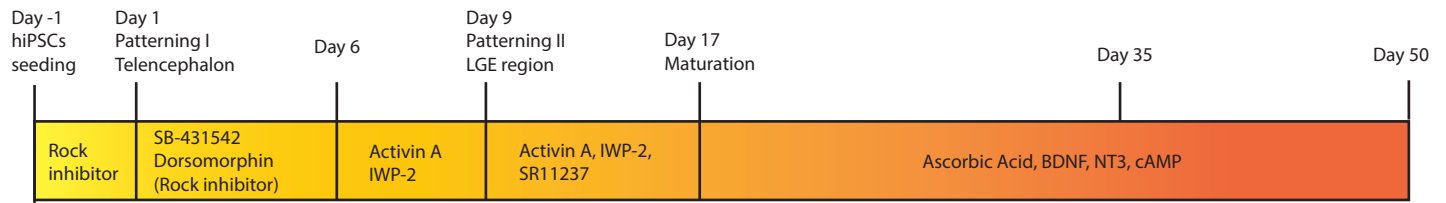
**Supplementary Figure 14: Expression of genes relevant to the synaptic pathways in GO and KEGG enrichment analysis.** Fold change expression of genes in Progerin-overexpressing assembloids (PROG\_DOX) versus non-Progerin-expressing assembloids (PROG\_UNTR), responsible for the enrichment of Dopaminergic Synapse KEGG pathway (A), Neuron to neuron synapses GO pathway (B), Neurotransmitter secretion GO pathway (C), Postsynapses GO pathway (D) and Presynapses GO pathway (E).



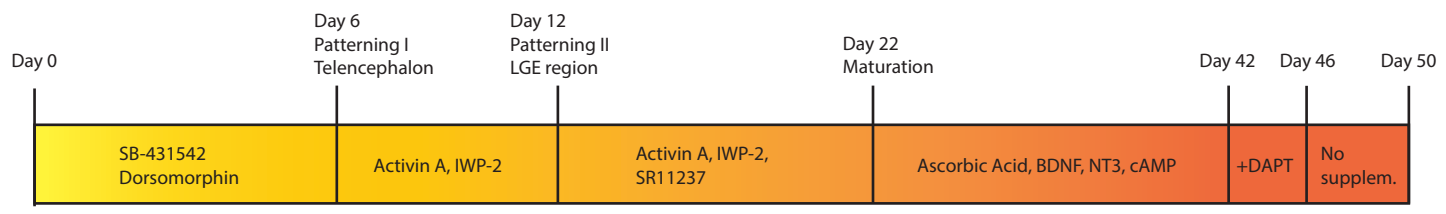
Supplementary Figure 1



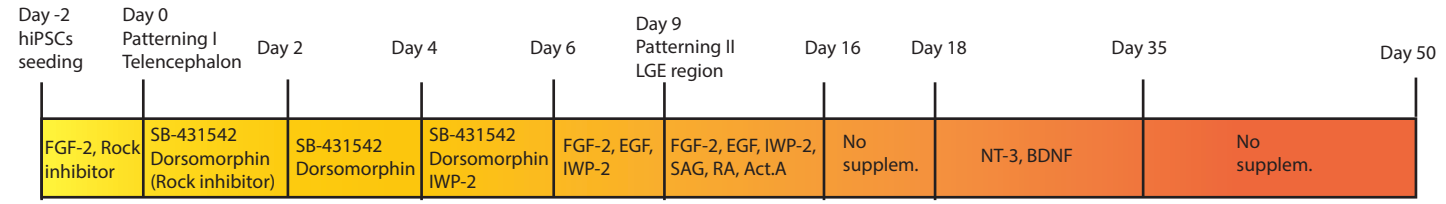
**Condition C4**



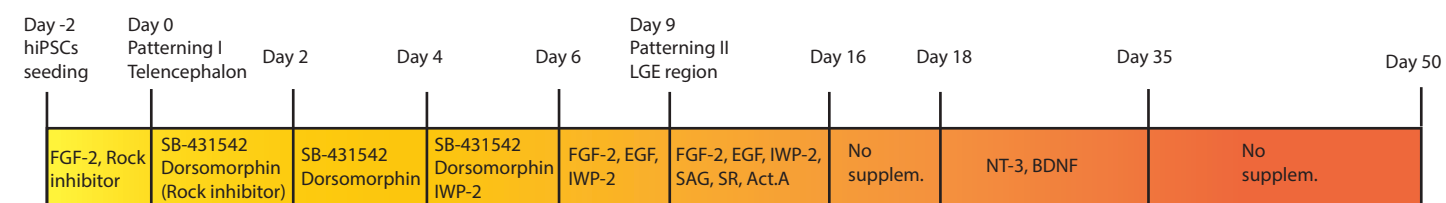
**Condition C3**



**Condition RA**

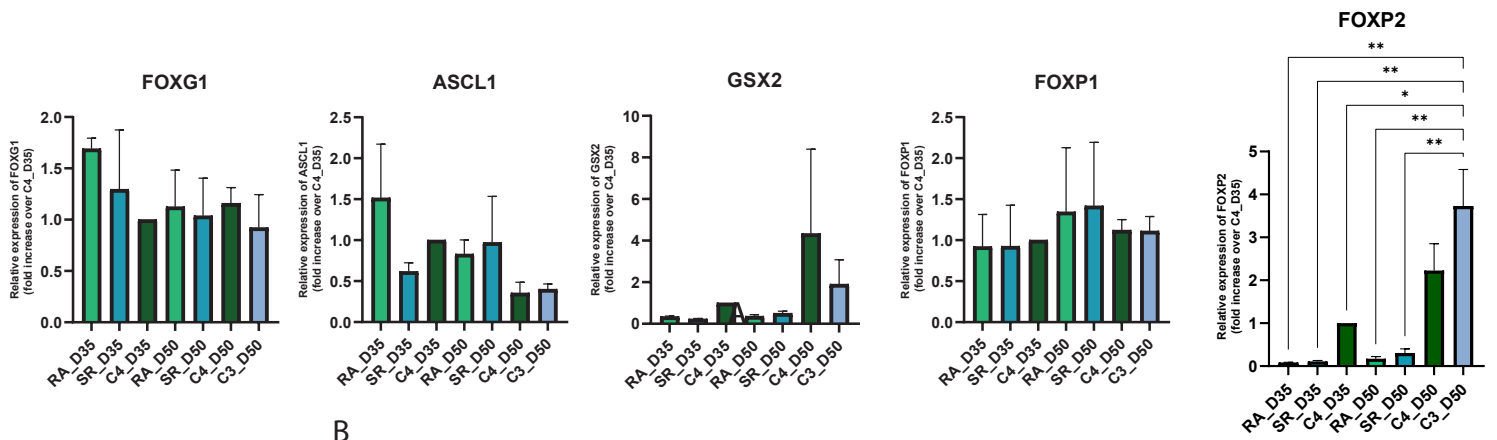


**Condition SR**

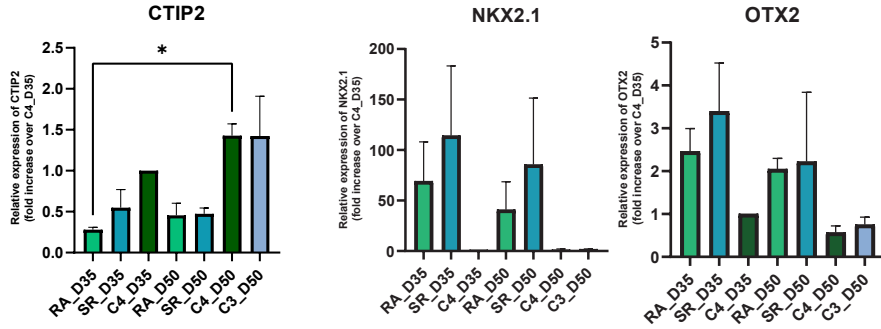


Supplementary Figure 2

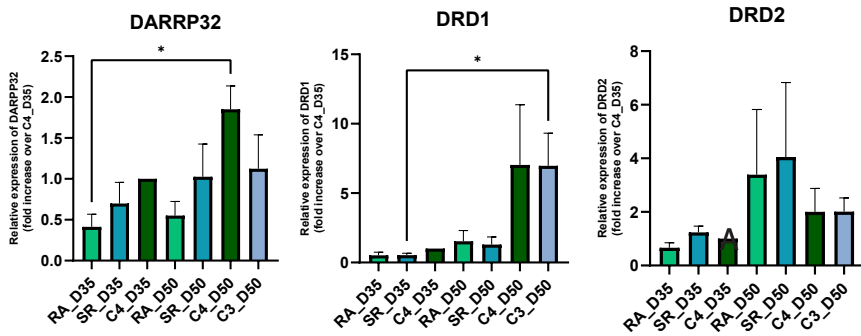
A



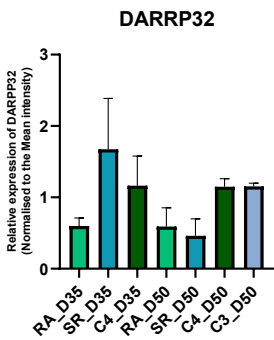
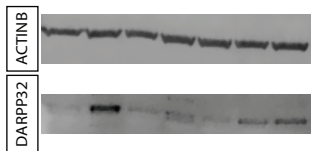
B



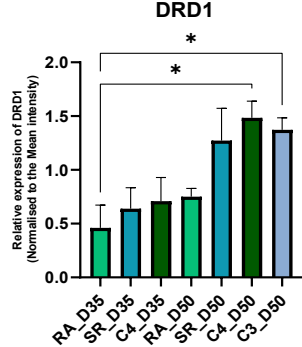
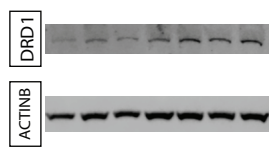
C



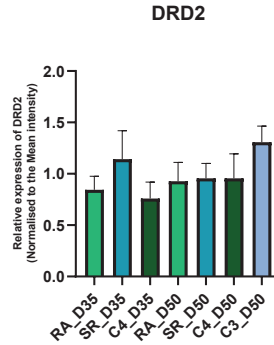
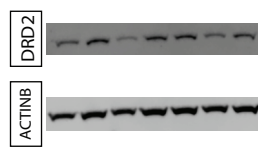
D



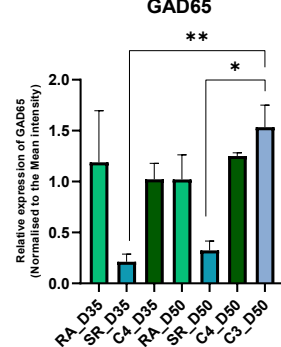
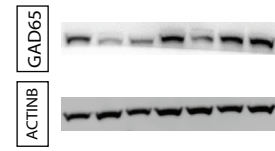
E



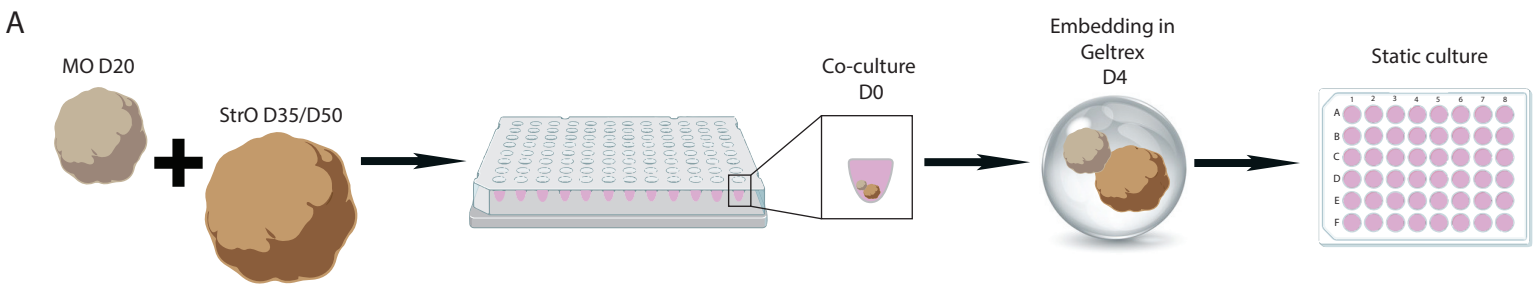
F



G

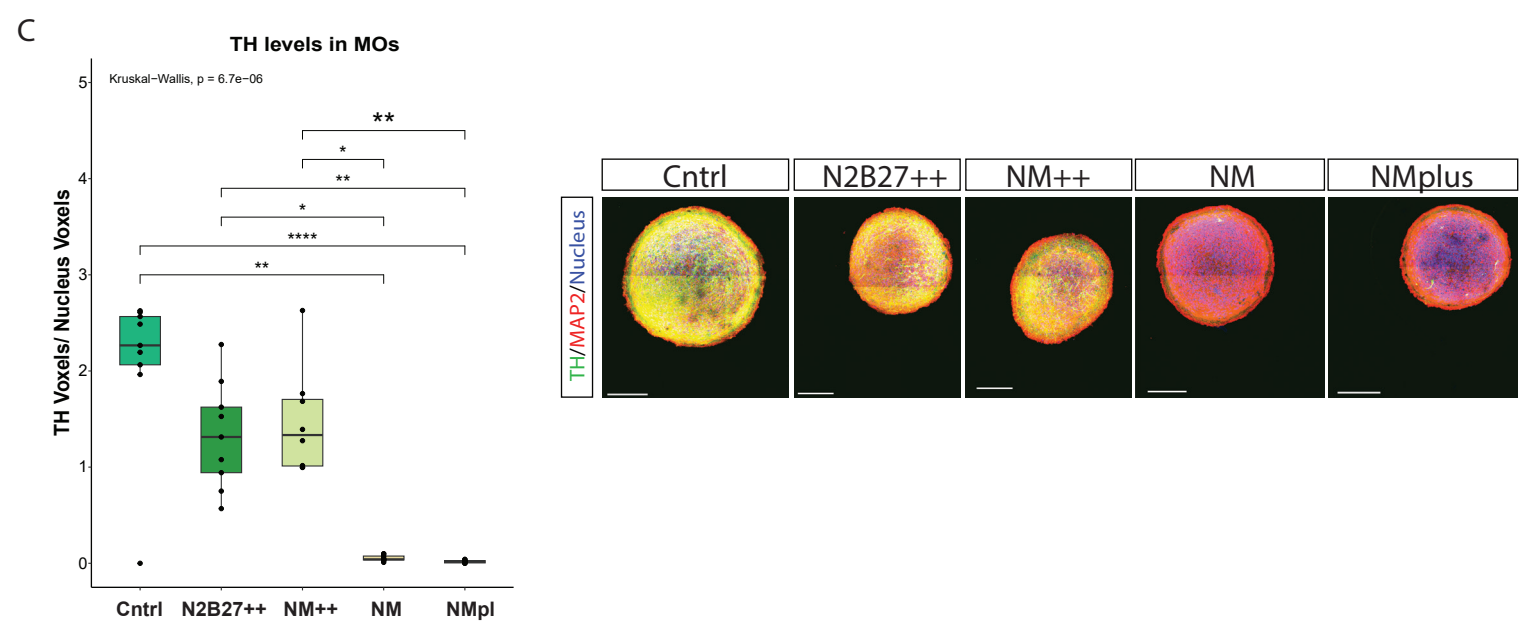


Supplementary Figure 3



**B**

	Media Composition	Small Molecules
Neural Medium	Neurobasal A, B27, Glutamax, P/S	-
Neural Medium Plus	Neurobasal A, <b>B27 plus</b> , Glutamax, P/S	-
Neural Medium ++	Neurobasal A, B27, Glutamax, P/S	AA, db cAMP, BDNF, GDNF, NT3
N2B27 ++	Neurobasal, DMEM/F12, B27, N2, Glutamax, P/S	AA, db cAMP, BDNF, GDNF, NT3



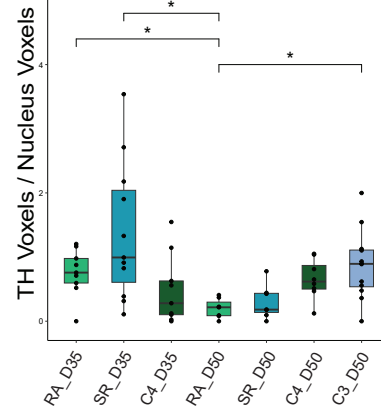
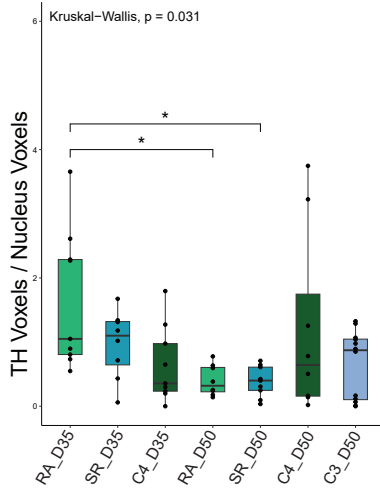
Supplementary Figure 4



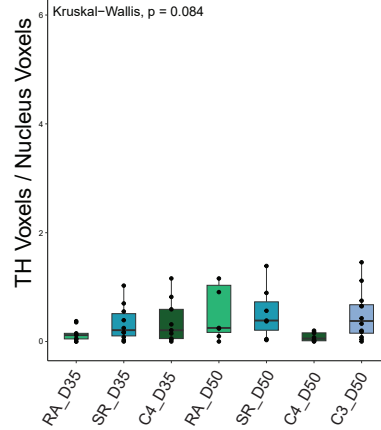
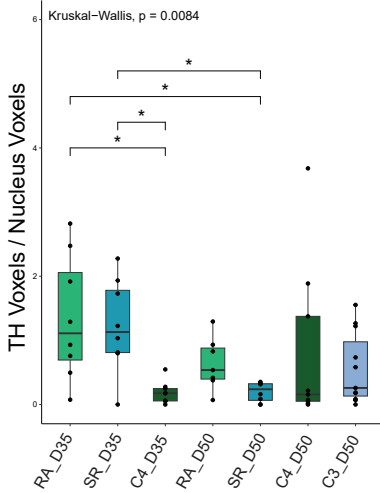
## Assembloids D20

## Assembloids D35

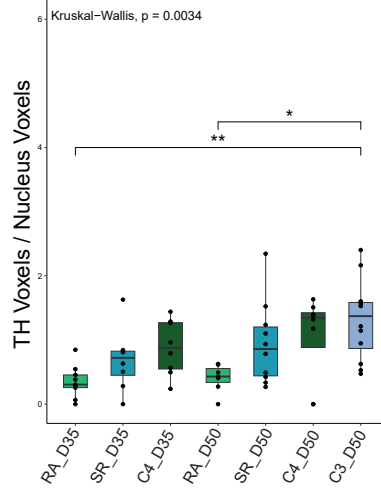
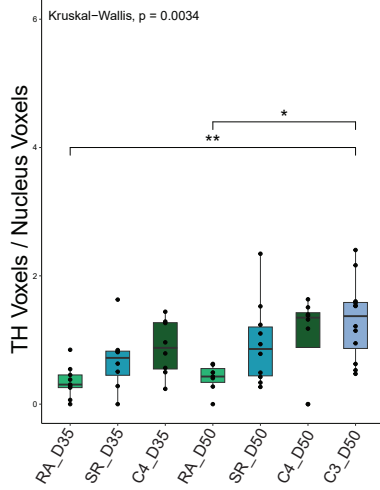
**TH total  
NM Media**



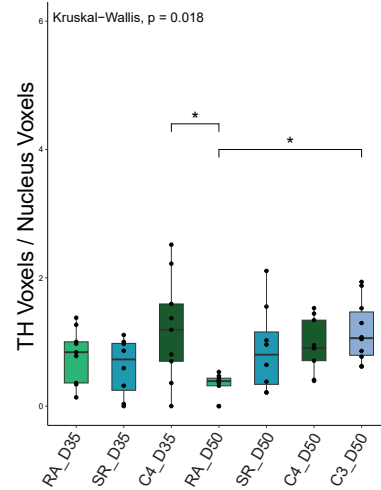
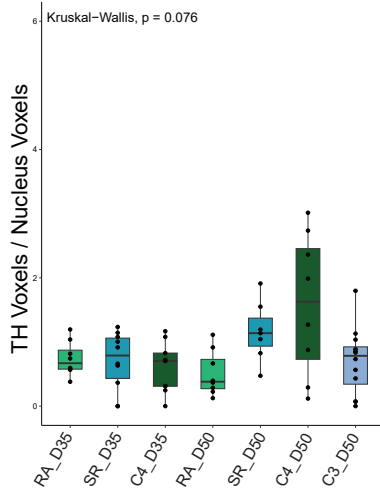
**TH total  
NM plus Media**



**TH total  
NM++ Media**

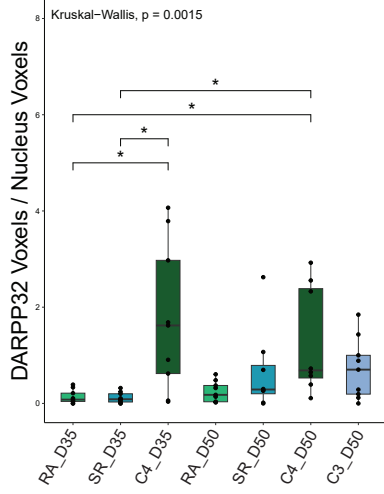


**TH total  
N2B27++ Media**

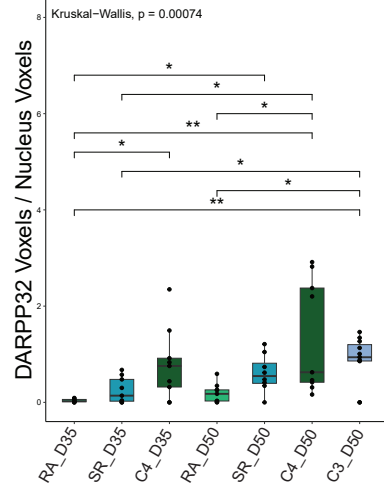


## Assembloids D20

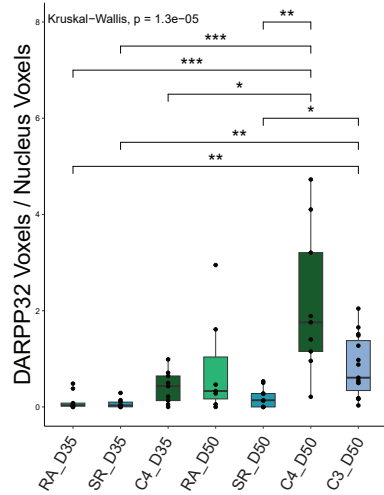
DARPP32 total  
NM Media



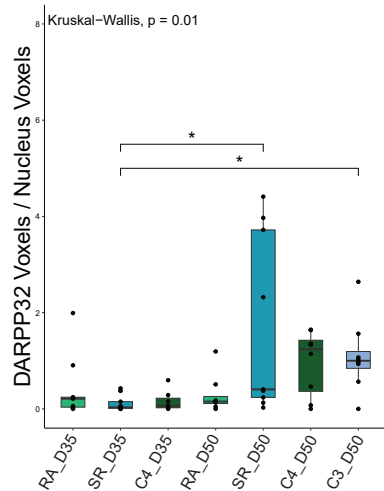
DARPP32 total  
NM plus Media



DARPP32 total  
NM++ Media

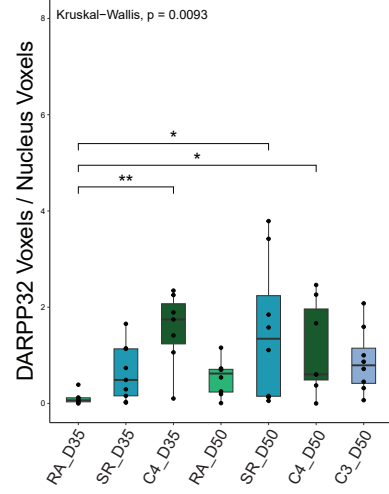


DARPP32 total  
N2B27++ Media

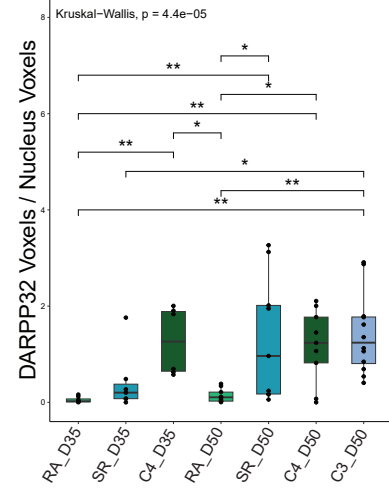


## Assembloids D35

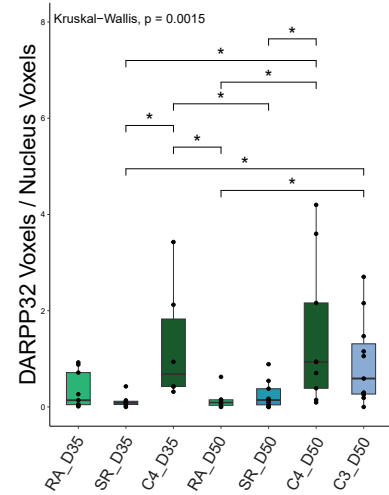
DARPP32 total  
NM Media



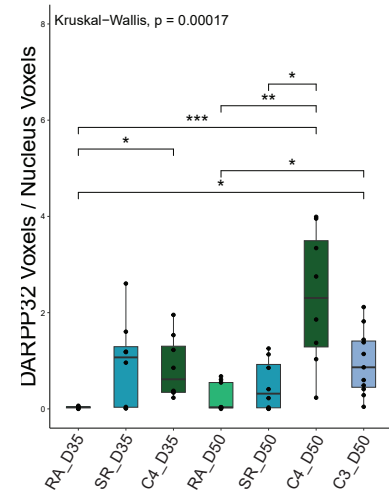
DARPP32 total  
NM plus Media

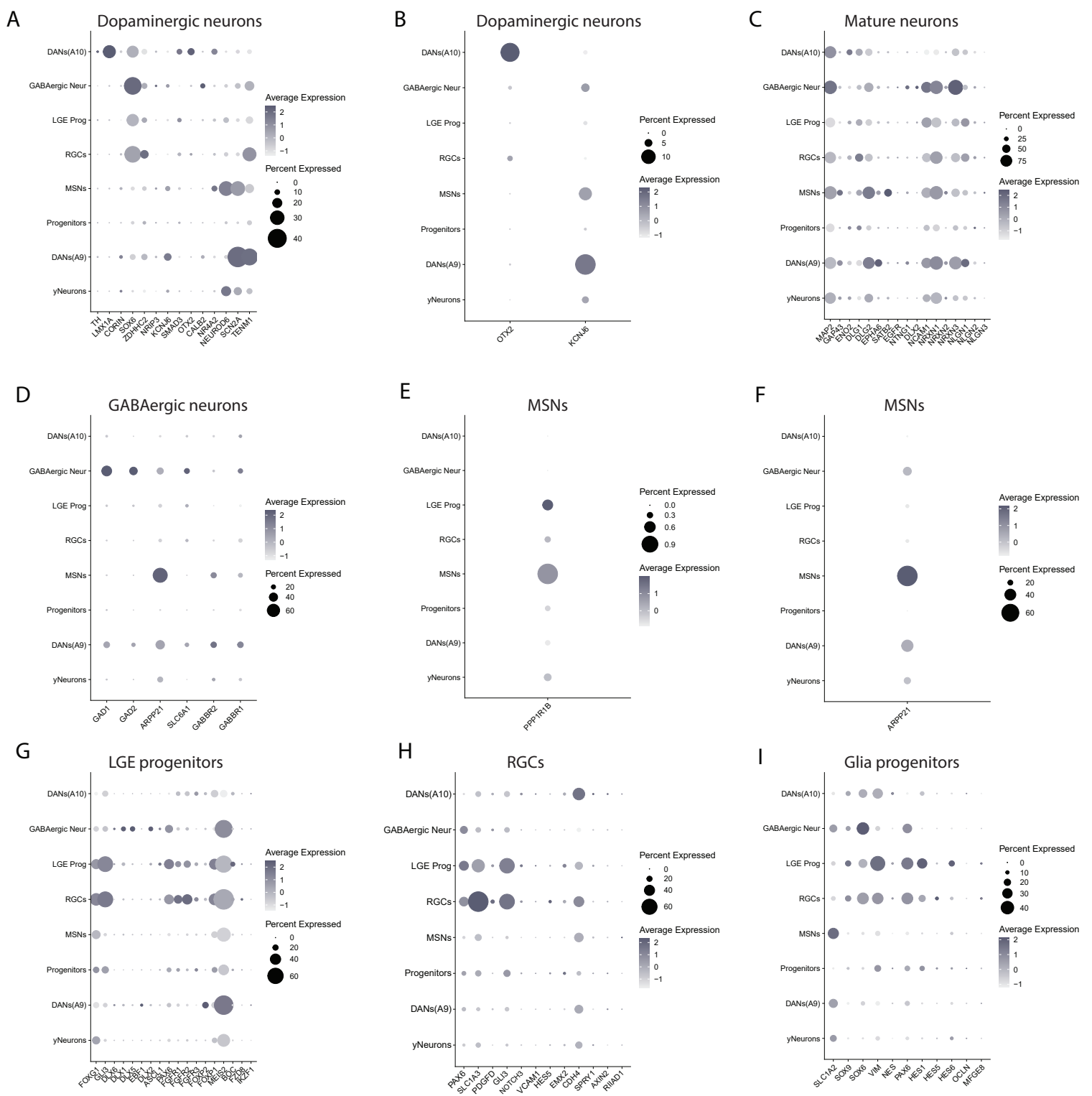


DARPP32 total  
NM++ Media

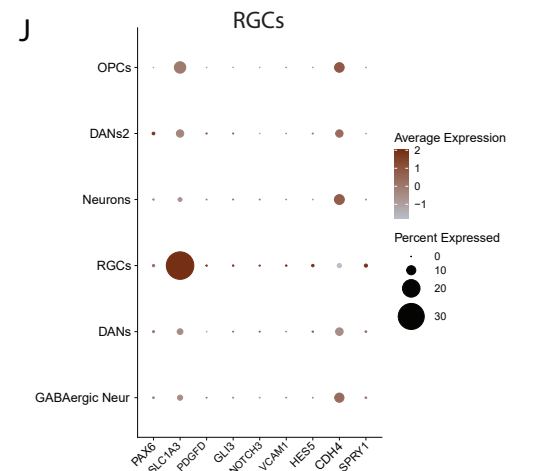
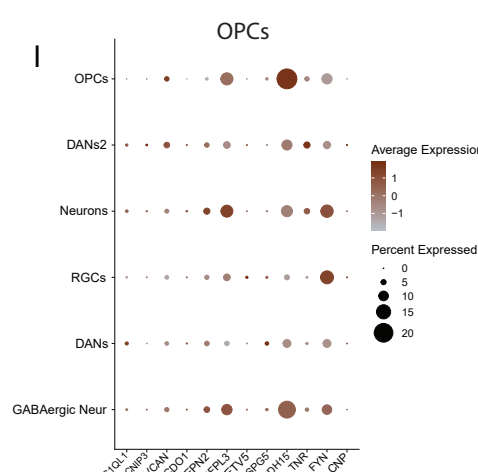
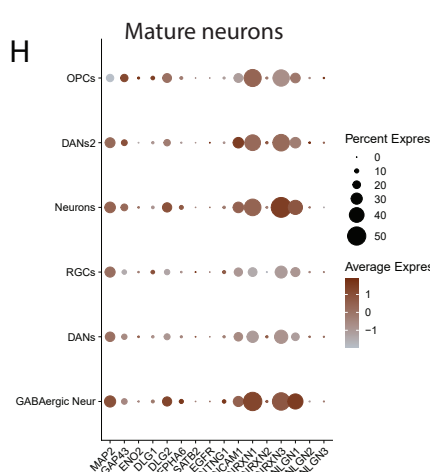
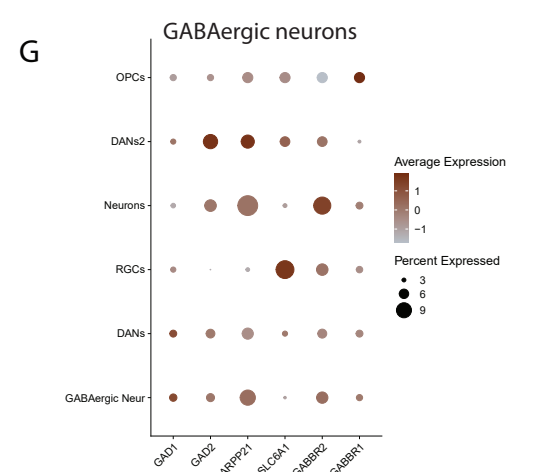
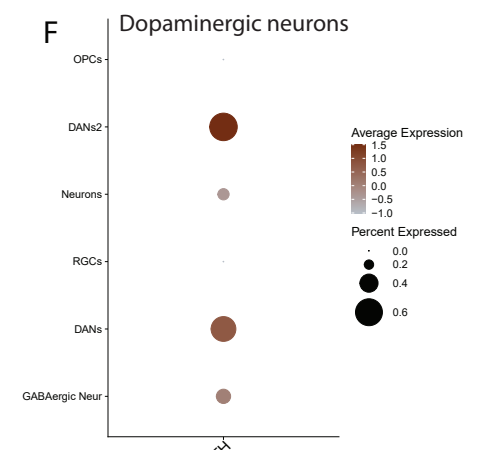
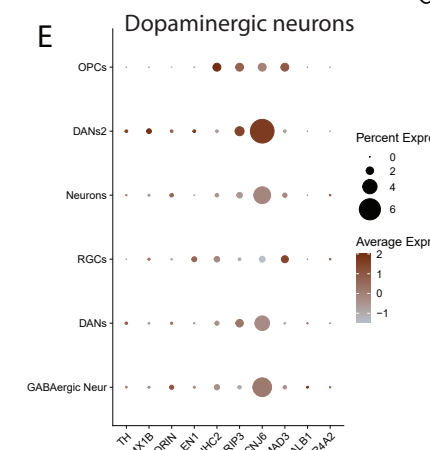
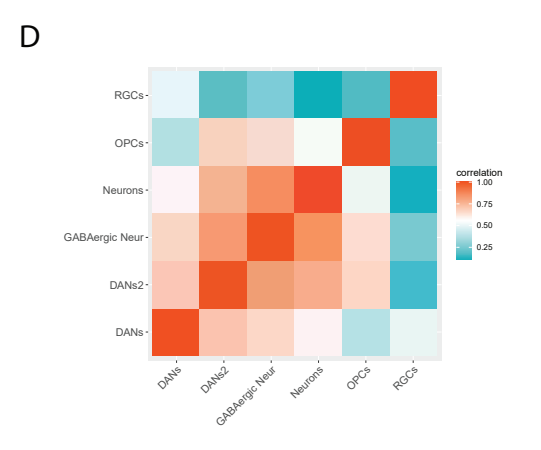
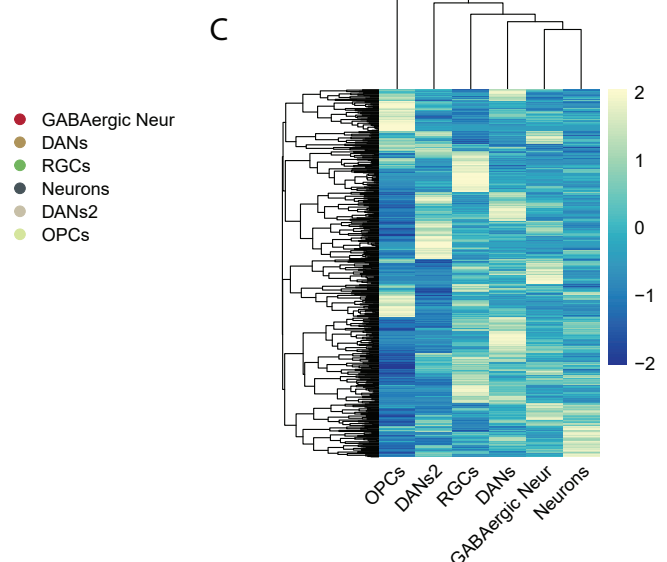
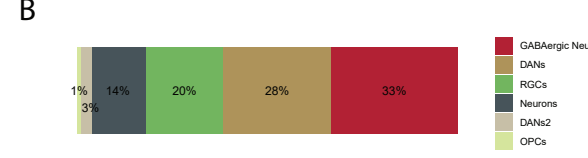
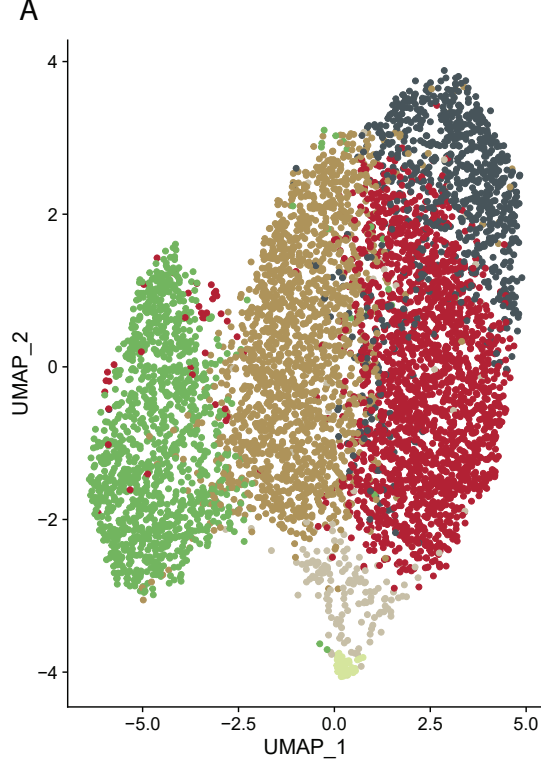


DARPP32 total  
N2B27++ Media

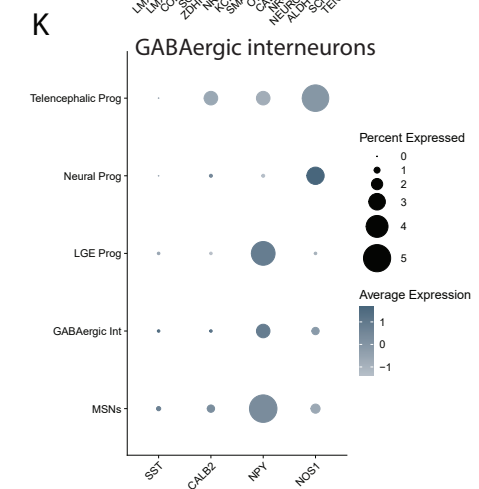
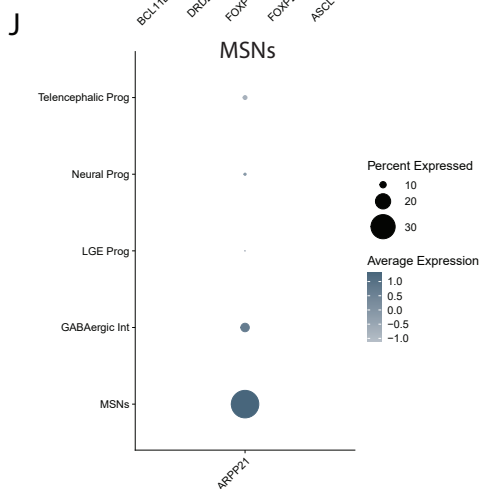
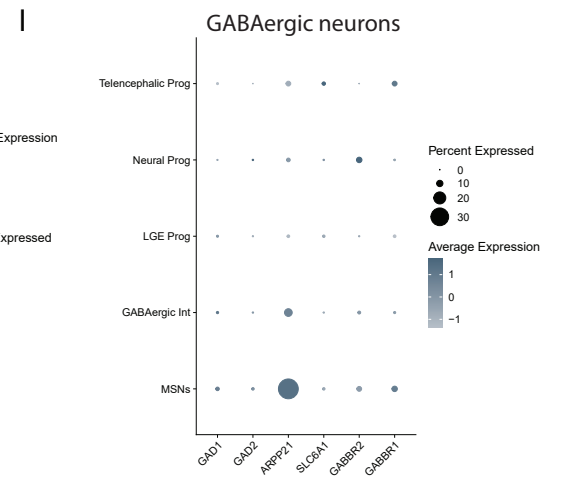
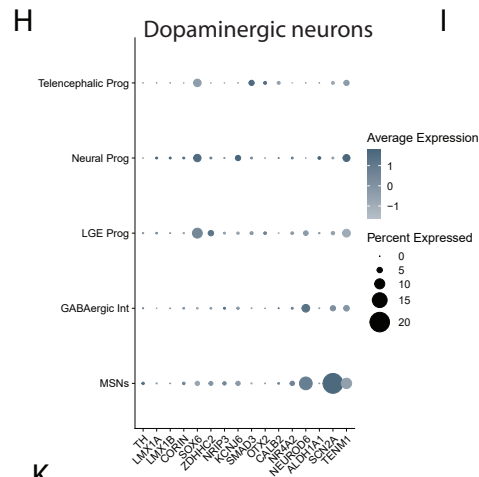
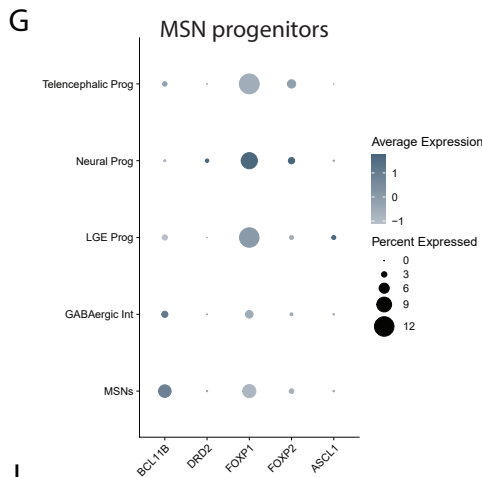
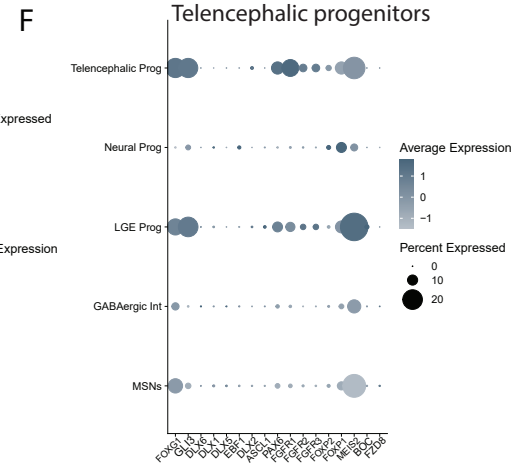
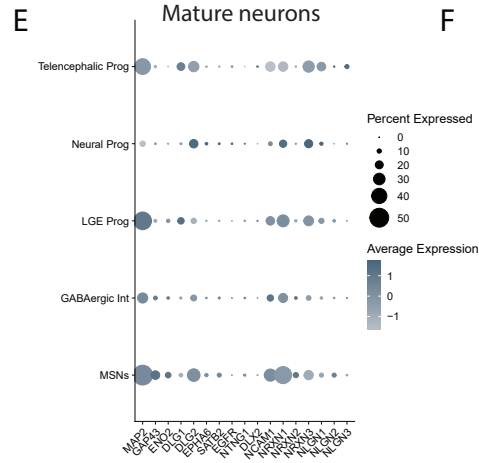
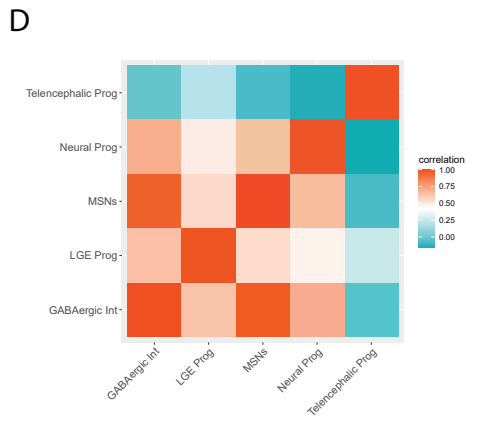
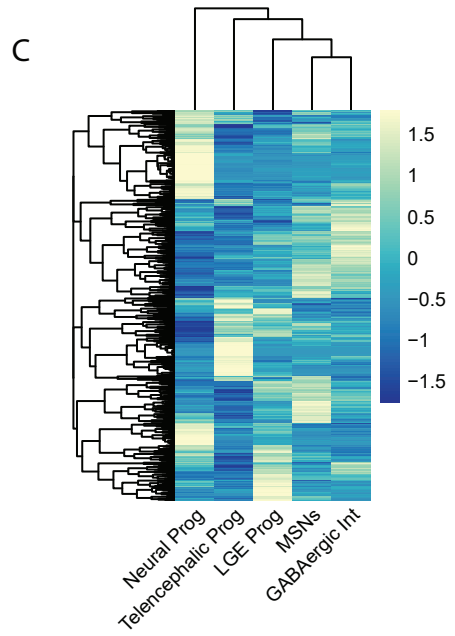
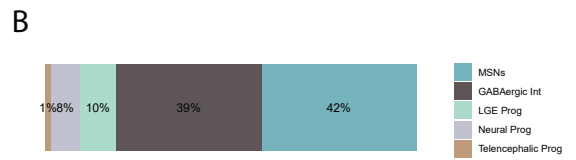
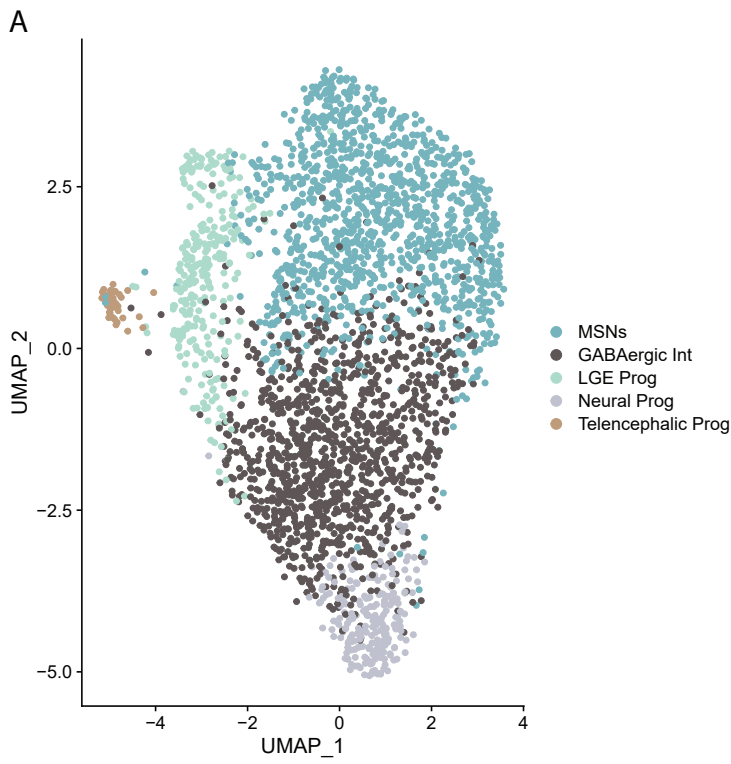


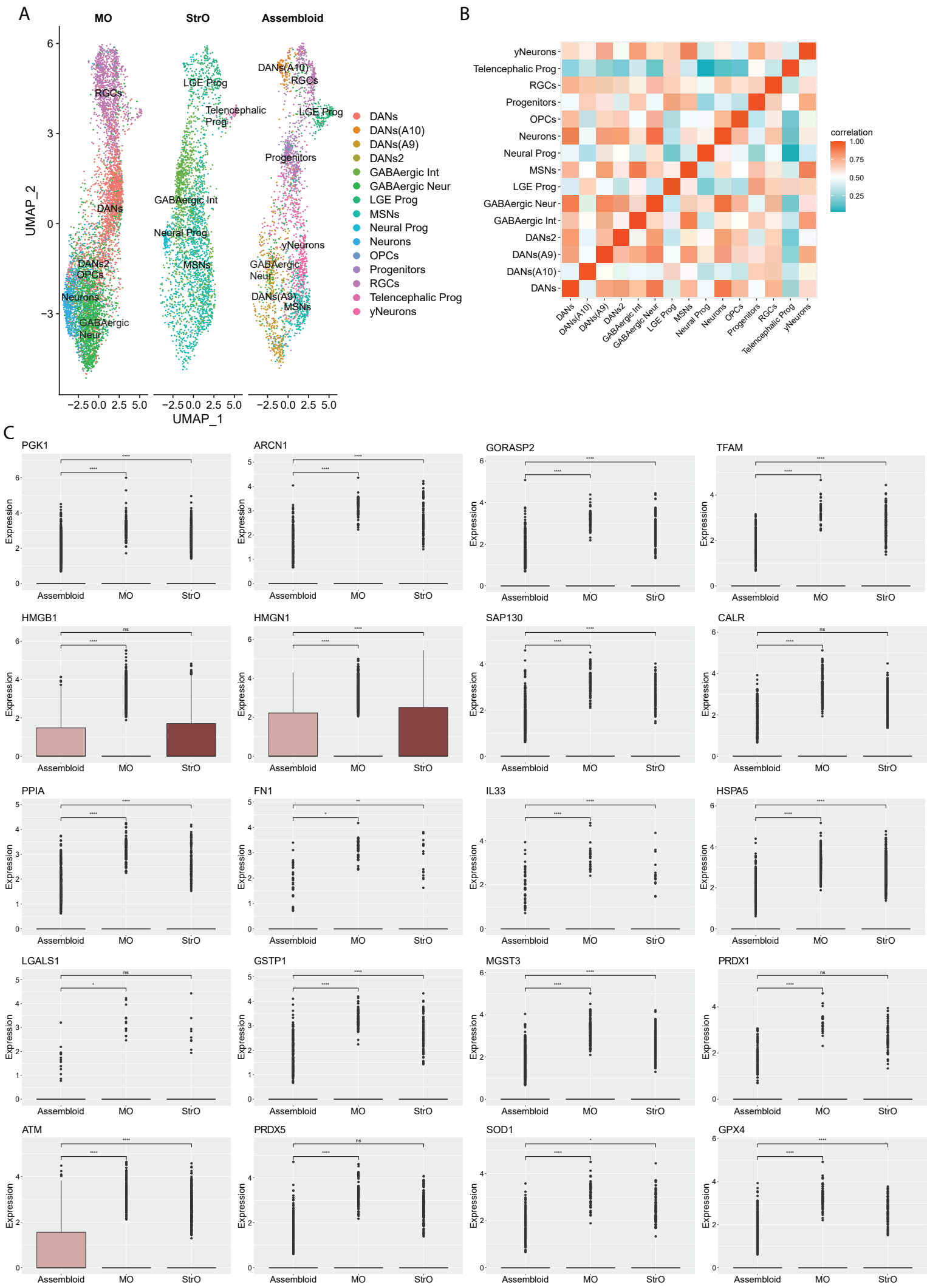


Supplementary Figure 7

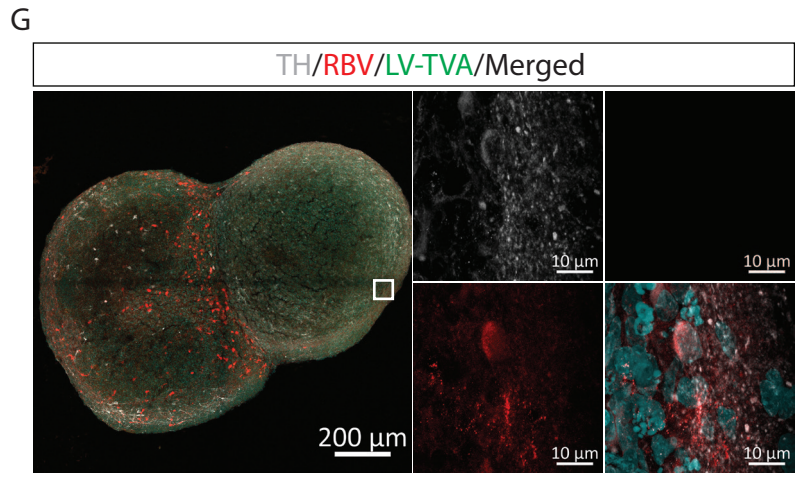
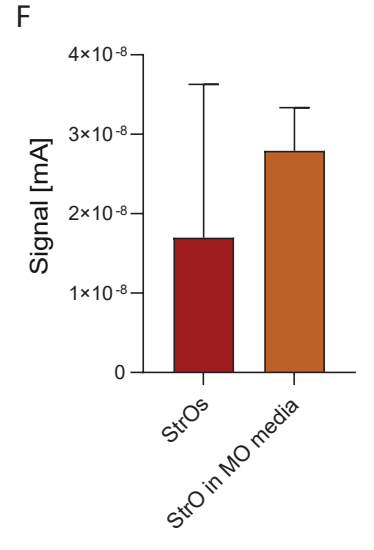
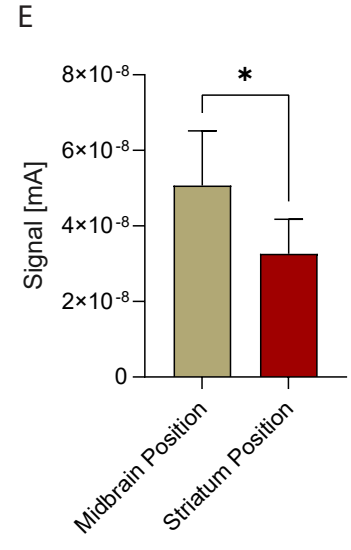
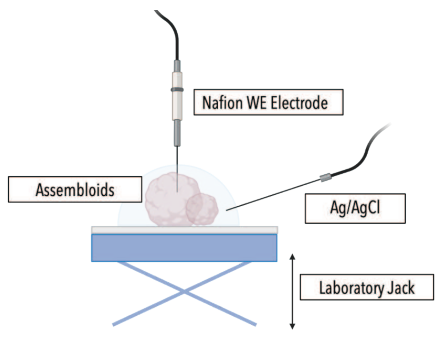
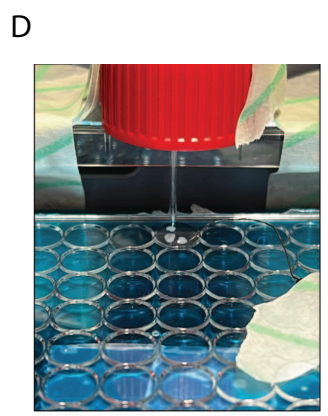
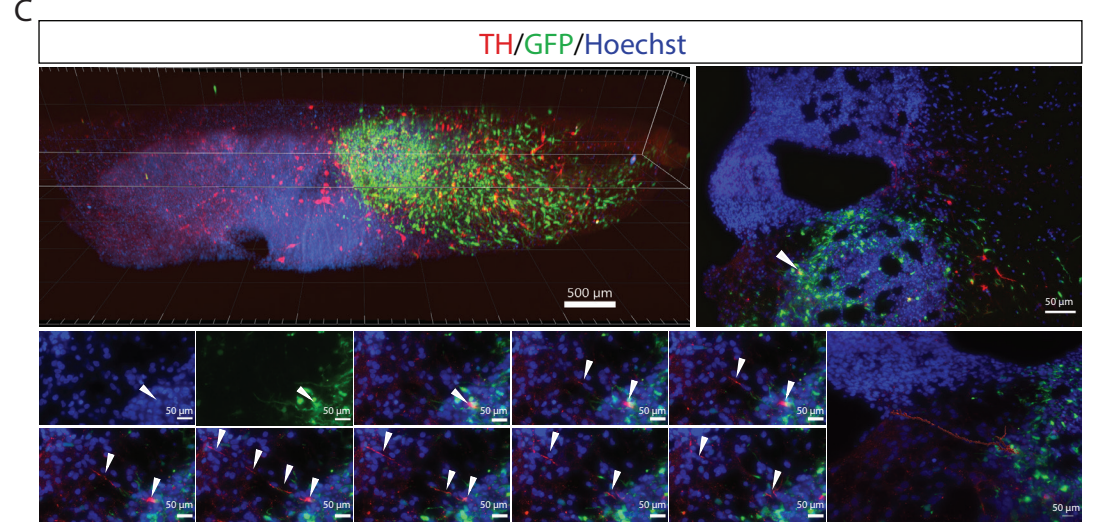
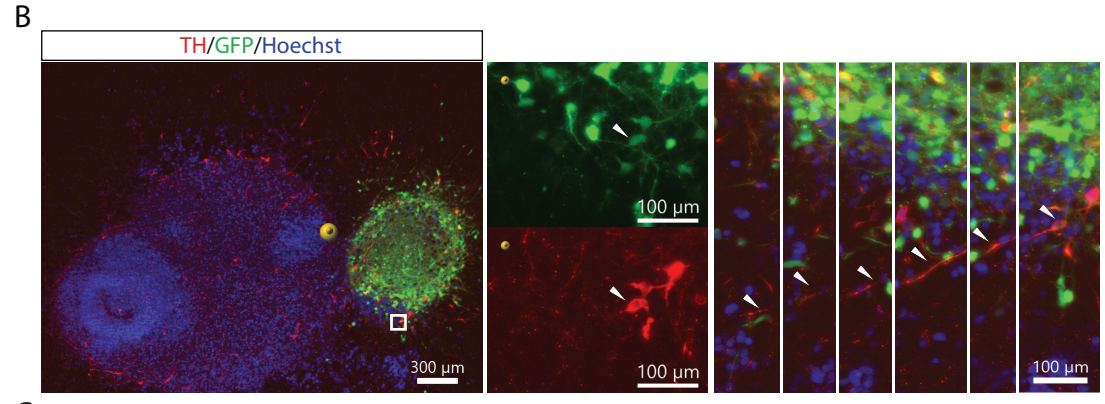
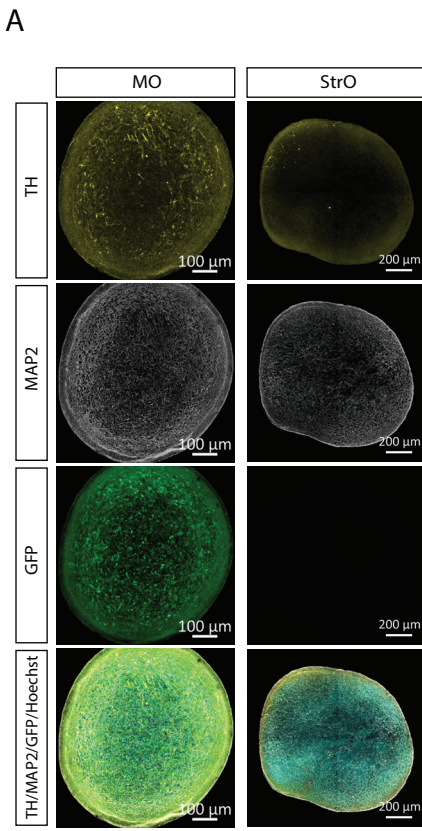


Supplementary Figure 8



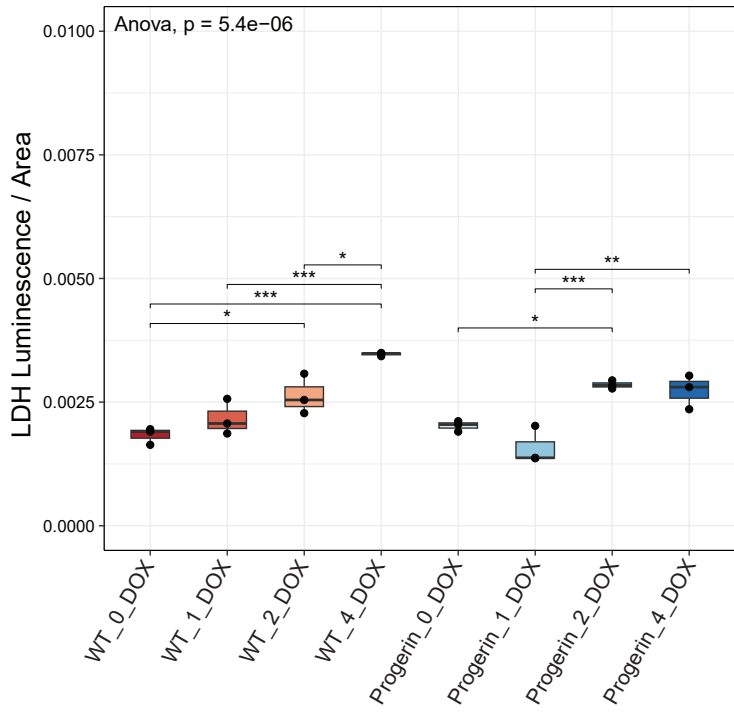


Supplementary Figure 10

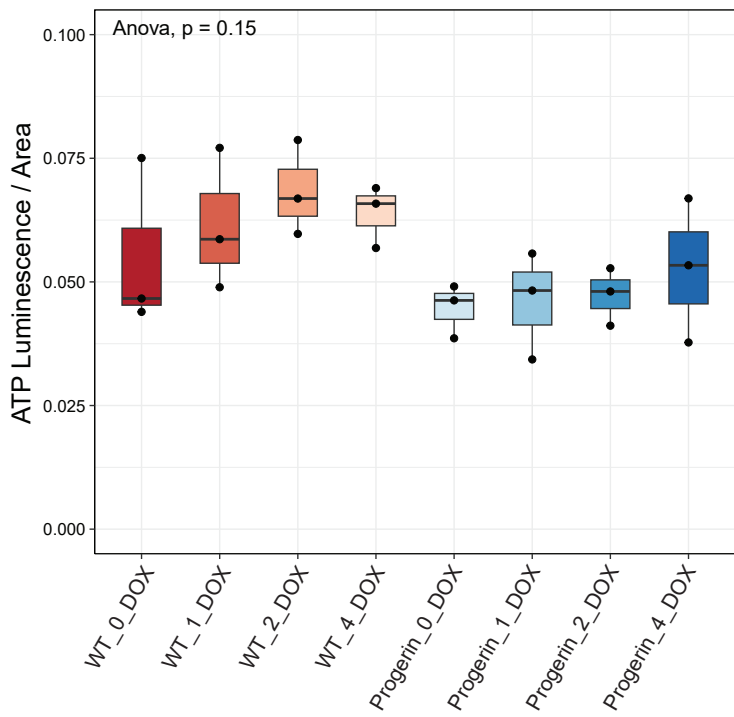


Supplementary Figure 11

A



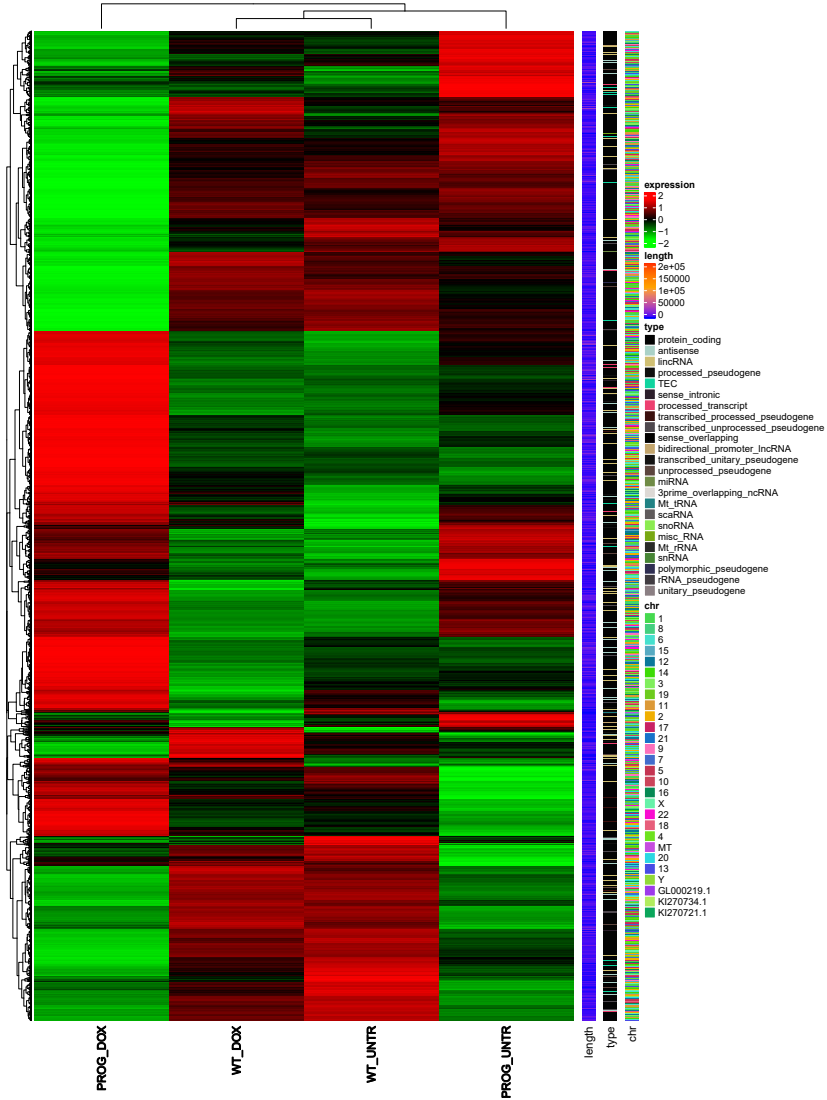
B



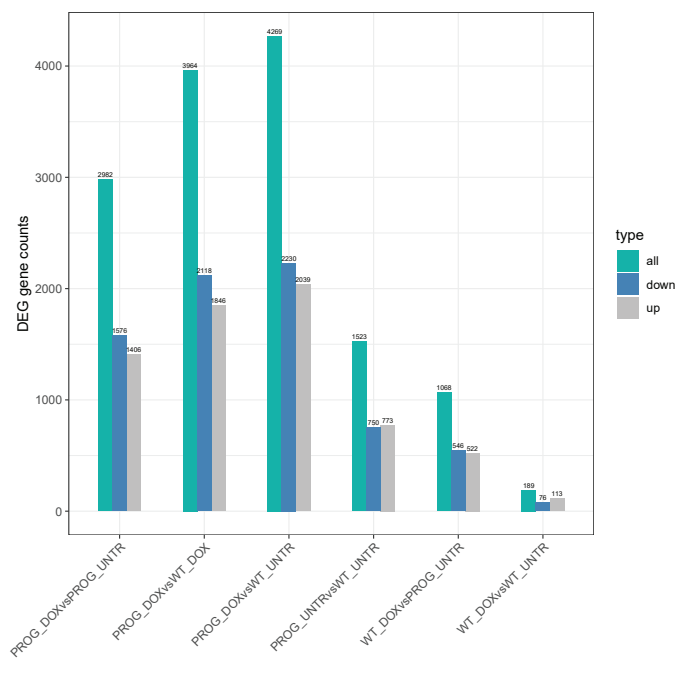
Supplementary Figure 12



A



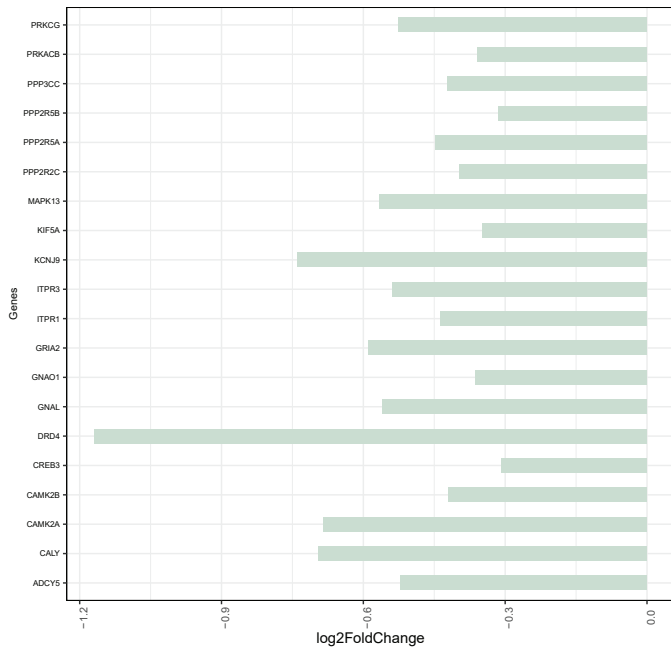
B



Supplementary Figure 13

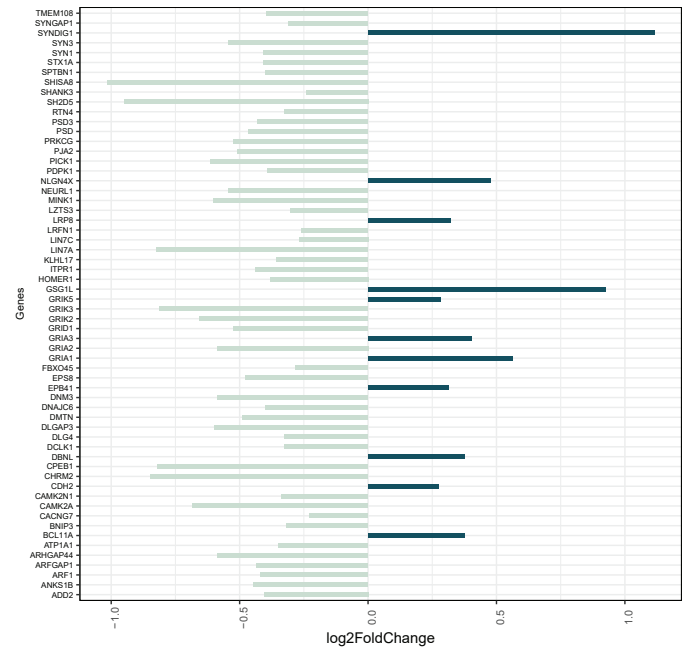
A

## Dopaminergic Synapse (KEGG)



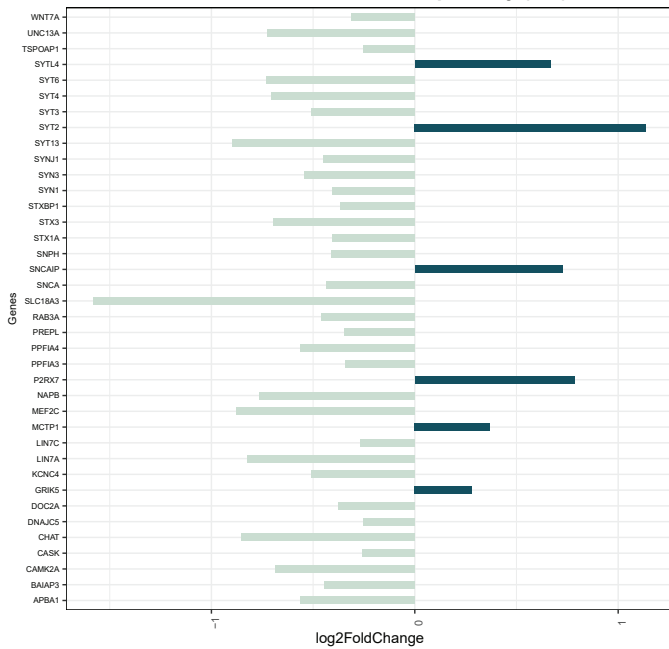
B

## Neuron to Neuron synapses (GO)



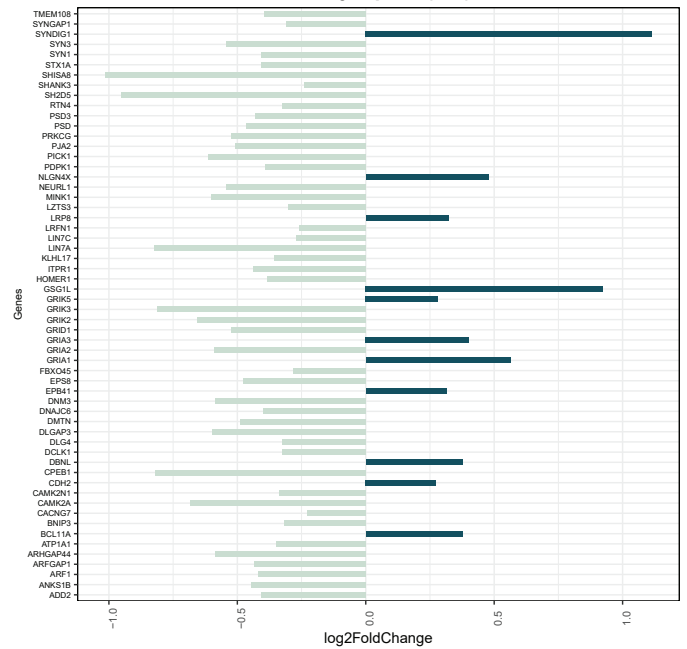
C

## Neurotransmitter secretion pathway (GO)



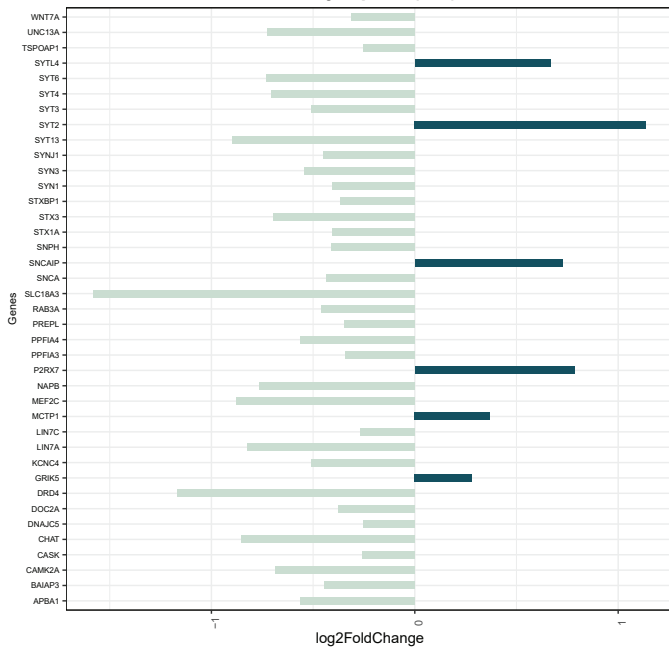
D

## Postsynapses (GO)



E

## Presynapses (GO)



**Supplementary Table 1: Cell lines used in the study.**

<b>Lab identifier</b>	<b>Name</b>	<b>Sex</b>	<b>Age of sampling</b>	<b>Source</b>	<b>Reference Name</b>	<b>Karyotype</b>
201	WT 1	F	-	GIBCO	A13777	Normal
200	WT 2	F	83	Reinhardt <i>et al.</i> , 2013	K7.1	Chr1-mosaic gain q21.2 Chr1- gain q25.3
389	WT	M	6	Promocell	NHDF	Chr20q - gain
390	Progerin	M	6	Innsbruck, Prof. Frank Edenhover	NHDF progerin	Chr20q - gain

**Supplementary Table 2: Primary and secondary antibodies used in Western blots.**

<b>Antibody</b>	<b>Source</b>	<b>Ref.no.</b>	<b>RRID</b>	<b>Species</b>	<b>Dilution</b>
$\beta$ -Actin	Cell Signaling	3700S	<i>AB_2242334</i>	Mouse	1:20000
LAMINB1	Abcam	ab16048	<i>AB_443298</i>	Rabbit	1:500
LMNA	Sigma	L1293	<i>AB_532254</i>	Rabbit	1:500
DRD1	Abcam	ab216644	<i>AB_2941932</i>	Rabbit	1:300
DRD2	Abcam	ab85367	<i>AB_10674739</i>	Rabbit	1:300
Histone H3	Millipore	05-1341	<i>AB_1977240</i>	Mouse	1:20000
TUJ1	BioLegend	801201	<i>AB_2313773</i>	Mouse	1:20000
TAU	Abcam	ab80579	<i>AB_1603723</i>	Mouse	1:1000
Synaptotagmin1	Synaptic Systems	105011	<i>AB_2619761</i>	Mouse	1:200
VAMP2	Abcam	ab215721	<i>AB_2923382</i>	Rabbit	1:1000
TH	Abcam	ab112	<i>AB_297840</i>	Rabbit	1:600
DARPP32	Abcam	ab40801	<i>AB_731843</i>	Rabbit	1:400
GAD65	R&D systems	AF2247	<i>AB_2108039</i>	Goat	1:1000
ECL anti-goat	Santa Cruz	sc-2020	<i>AB_631728</i>	Donkey	1:1000
Anti-rabbit H+L 800	Cell Signaling	5151	<i>AB_10697505</i>	Goat	1:10000
Anti-mouse H+L 680	Cell Signaling	5470	<i>AB_10696895</i>	Goat	1:10000

**Supplementary Table 3: Primary and secondary antibodies used in immunofluorescence stainings.**

<b>Antibody</b>	<b>Source</b>	<b>Cat.no.</b>	<b>RRID</b>	<b>Species</b>	<b>Dilution</b>
NESTIN	BD Bioscience	611659	<i>AB_399177</i>	Mouse	1:600
PAX6	Biolegend	901302	<i>AB_2749901</i>	Rabbit	1:300
FOXA2	Santa Cruz	sc-101060	<i>AB_1124660</i>	Mouse	1:100
MASH1/ASCL1	BD Bioscience	556604	<i>AB_396479</i>	Mouse	1:200
CORIN	R&D systems	MAB2209	<i>AB_2082224</i>	Rat	1:200
TRA-1-60	Millipore	MAB4360	<i>AB_2119183</i>	Mouse	1:50
SSEA-4	Millipore	MAB4304	<i>AB_177629</i>	Mouse	1:50
NANOG	Millipore	AB5731	<i>AB_2267042</i>	Rabbit	1:200
OCT4	Abcam	ab19857	<i>AB_445175</i>	Rabbit	1:400
CTIP2	Abcam	ab18465	<i>AB_2064130</i>	Rat	1:300
TH	Abcam	ab112	<i>AB_297840</i>	Rabbit	1:600
MAP2	Abcam	ab92434	<i>AB_2138147</i>	Chicken	1:1000
SOX1	R&D systems	AF3369	<i>AB_2239879</i>	Goat	1:100
SOX2	Abcam	ab97959	<i>AB_2341193</i>	Rabbit	1:200
SOX2	R&D Systems	AF2018	<i>AB_355110</i>	Goat	1:200
DARPP32	Abcam	ab40801	<i>AB_731843</i>	Rabbit	1:400
P21 Waf1/Cip1	Cell Signaling	2946	<i>AB_2260325</i>	Mouse	1:200
P16INK4a	Abcam	ab108349	<i>AB_10858268</i>	Rabbit	1:200
P53	Thermo Fisher Scientific	MA5-12557	<i>AB_10989883</i>	Mouse	1:200

H2AX	Millipore	05-636-I	<i>AB_2755003</i>	Mouse	1:200
53BP1	Novus	NB100-304	<i>AB_10003037</i>	Rabbit	1:200
Anti-mouse 488	Invitrogen	A21202	<i>AB_141607</i>	Donkey	1:1000
Anti-mouse 568	Invitrogen	A10037	<i>AB_2534013</i>	Donkey	1:1000
Anti-goat 657	Invitrogen	A21447	<i>AB_2535864</i>	Donkey	1:1000
Anti-rabbit 647	Invitrogen	A31573	<i>AB_2536183</i>	Donkey	1:1000
Anti-chicken 568	Invitrogen	A11041	<i>AB_2534098</i>	Goat	1:1000
Anti-chicken 647	Invitrogen	A21449	<i>AB_2535866</i>	Goat	1:1000
Anti-mouse 488	Invitrogen	A11029	<i>AB_2534088</i>	Goat	1:1000
Anti-mouse 568	Invitrogen	A11031	<i>AB_144696</i>	Goat	1:1000
Anti-mouse 647	Invitrogen	A21236	<i>AB_2535805</i>	Goat	1:1000
Anti-rabbit 568	Invitrogen	A11036	<i>AB_10563566</i>	Goat	1:1000
Anti-rabbit 647	Invitrogen	A21244	<i>AB_2535812</i>	Goat	1:1000

**Supplementary Table 4: Primers used in qPCRs for the striatum organoids characterization.**

<b>Gene</b>	<b>Forward Primer</b>	<b>Reverse Primer</b>
DARPP32	CCTGAAGGTCATCAGGCAGT	GGTCTTCCACTTGGTCCTCA
DRD1	AGGGACATGTCTTTGGCTTCAG	GGAACAGTGTTAGCACCTGTT
DRD2	CTGAGGGCTCCACTAAAGGAG	CATTCTTCTCTGGTTTGGCG
CTIP2	ATCCTCAGCCCCTTTTGTTT	GCCGTTGTTCTGAATTGTT
ASCL1	GTCCTGTGCGCCACCATCTC	CCCTCCCAACGCCACTGAC
FOXP1	TGTTGACTCAGAACTCGCTGG	CTGCTCTGCGAAGTCATTGAC
FOXP2	GCAGTTACAGCAGCAGCACCTCC	CAGCCTGGCCACTTGCATACACC
FOXP2	AATGTGGGAGCCATACGAAG	GCCTGCCTTATGAGAGTTGC
OTX2	TCAACTTGCCCGAGTCGAGG	CAATGGTCGGGACTGAGGTG
NKX1.2	CGCATCCAATCTCAAGGAAT	TGTGCCCAGAGTGAAGTTTG
GSX2	ATGTCGCGCTCCTTCTATGTC	ATGCCAAGCGGGATGAAGAAA
ACTINB	TCAAGATCATTGCTCCTCCTGAG	ACATCTGCTGGAAGGTGGACA

**Supplementary Table 5:** Genes related to cellular and oxidative stress.

<b>Genes</b>	<b>Role in Cellular/Oxidative stress</b>	<b>References</b>
PGK1 (Phosphoglycerate Kinase 1)	A protein kinase responsible for governing mitochondrial activity and cell stress-triggered autophagy. Downregulation has been linked to oxidative stress inhibition.	(Bhaduri et al., 2020; Xu et al., 2022)
ARCN1 (Archain 1)	Involvement in ER stress response.	(Bhaduri et al., 2020; Izumi et al., 2016)
GORASP2 (Golgi Reassembly Stacking Protein 2)	Involvement in ER stress response.	(Bhaduri et al., 2020; Zhang & Wang, 2018)
TFAM (Transcription Factor A, Mitochondrial)	Stress response induced by mitochondria dysfunction.	(Hunt et al., 2019)
HMGB1 (High Mobility Group Box 1)	Cytokine with a role in initiating neuroinflammation.	(Paudel et al., 2020)
HMGN1 (High Mobility Group Nucleosome Binding Domain 1)	Chromatin architectural protein. Can contribute to neuroinflammation.	(Farley et al., 2022; Furusawa & Cherukuri, 2010)
SAP130 (Sin3A Associated Protein 130)	It is increased in neuroinflammation.	(Y. Wang et al., 2019)
CALR (Calreticulin)	ER Ca <sup>2+</sup> binding protein. Is activated by environmental stress.	(Chen et al., 2023; Michalak, 2023)
PPIA (Peptidylprolyl Isomerase A)	It has a role as molecular chaperone. Increased levels in ALS.	(Lauranzano et al., 2015)
FN1 (Fibronectin 1)	Extracellular matrix glycoprotein. Increased expression in cellular stress response.	(Dhanani et al., 2017)
IL33 (Interleukin 33)	Cytokine with a role in neuroinflammation.	(Sun et al., 2021; Zharichenko & Njoku, 2020)
HSPA5 (Heat Shock Protein Family A (Hsp70) Member 5)	Upregulated under ER stress for the clearing of misfolded proteins.	(Nowakowska et al., 2020)
LGALS1 (Galectin 1)	Highly expressed during neuroinflammation.	(Aalinkeel & Mahajan, 2016; J. Wang et al., 2015)
GSTP1 (Glutathione S-Transferase)	Increased levels have been associated with cancer and neurodegenerative diseases.	(Allocati et al., 2018)
MGST3 (microsomal Glutathione S-Transferase)	Possible role in neuroinflammation, with the production of LCT4 for the biosynthesis of proinflammatory LTs.	(Fetissov et al., 2002)
PRDX1 (Peroxiredoxin 1)	An antioxidant enzyme that protects the brain against oxidative stress. Increased levels have been found in AD patients.	(Kim et al., 2022; Szeliga, 2020)
ATM (ATM Serine/Threonine Kinase)	It is activated by oxidative stress and is important for the repair of DNA damage.	(Berger et al., 2017; Kozlov et al., 2016)
PRDX5 (Peroxiredoxin 5)	Antioxidant enzyme, protecting cells against oxidative stress (similar to PRDX1).	(Tavleeva et al., 2022; Yuan et al., 2004)
SOD1 (Superoxide Dismutase 1)	It is oxidative stress dependent and is upregulated during brain inflammation.	(Dell'Orco et al., 2021; Dimayuga et al., 2007)
GPX4 (Glutathione Peroxidase 4)	It is overexpressed during ferroptosis and neuroinflammation.	(Fang et al., 2023)



## Supplementary References

- Aalinkeel, R., & Mahajan, S. D. (2016). Neuroprotective role of galectin-1 in central nervous system pathophysiology. *Neural Regeneration Research*, *11*(6), 896–897.  
<https://doi.org/10.4103/1673-5374.184455>
- Allocati, N., Masulli, M., Di Ilio, C., & Federici, L. (2018). Glutathione transferases: Substrates, inhibitors and pro-drugs in cancer and neurodegenerative diseases. *Oncogenesis*, *7*(1).  
<https://doi.org/10.1038/s41389-017-0025-3>
- Berger, N. D., Stanley, F. K. T., Moore, S., & Goodarzi, A. A. (2017). ATM-dependent pathways of chromatin remodelling and oxidative DNA damage responses. *Philosophical Transactions of the Royal Society B: Biological Sciences*, *372*(1731).  
<https://doi.org/10.1098/rstb.2016.0283>
- Bhaduri, A., Andrews, M. G., Mancina Leon, W., Jung, D., Shin, D., Allen, D., Jung, D., Schmunk, G., Haeussler, M., Salma, J., Pollen, A. A., Nowakowski, T. J., & Kriegstein, A. R. (2020). Cell stress in cortical organoids impairs molecular subtype specification. *Nature*, *578*(7793), 142–148. <https://doi.org/10.1038/s41586-020-1962-0>
- Chen, C. J., Hu, Y. C., Chien, Y., Huang, W. C., Wu, C. S., Tsai, C. Y., Lin, Y. H., Lee, M. S., Chien, C. S., Yang, Y. P., Lee, M. C., Tseng, C. C., & Chi, H. C. (2023). Calreticulin Expression Controls Cellular Redox, Stemness, and Radiosensitivity to Function as a Novel Adjuvant for Radiotherapy in Neuroblastoma. *Oxidative Medicine and Cellular Longevity*, *2023*. <https://doi.org/10.1155/2023/8753309>
- Dell'Orco, M., Sardone, V., Gardiner, A. S., Pansarasa, O., Bordoni, M., Perrone-Bizzozero, N. I., & Cereda, C. (2021). HuD regulates SOD1 expression during oxidative stress in differentiated neuroblastoma cells and sporadic ALS motor cortex. *Neurobiology of Disease*, *148*(June 2018), 105211. <https://doi.org/10.1016/j.nbd.2020.105211>
- Dhanani, K. C. H., Samson, W. J., & Edkins, A. L. (2017). Fibronectin is a stress responsive gene regulated by HSF1 in response to geldanamycin. *Scientific Reports*, *7*(1).  
<https://doi.org/10.1038/s41598-017-18061-y>
- Dimayuga, F. O., Wang, C., Clark, J. M., Dimayuga, E. R., Dimayuga, V. M., & Bruce-Keller,

- A. J. (2007). SOD1 overexpression alters ROS production and reduces neurotoxic inflammatory signaling in microglial cells. *Journal of Neuroimmunology*, *182*(1–2), 89–99. <https://doi.org/10.1016/j.jneuroim.2006.10.003>
- Fang, J., Yuan, Q., Du, Z., Zhang, Q., Yang, L., Wang, M., Yang, W., Yuan, C., Yu, J., Wu, G., & Hu, J. (2023). Overexpression of GPX4 attenuates cognitive dysfunction through inhibiting hippocampus ferroptosis and neuroinflammation after traumatic brain injury. *Free Radical Biology and Medicine*, *204*(April), 68–81. <https://doi.org/10.1016/j.freeradbiomed.2023.04.014>
- Farley, S. J., Grishok, A., & Zeldich, E. (2022). Shaking up the silence: consequences of HMGN1 antagonizing PRC2 in the Down syndrome brain. *Epigenetics and Chromatin*, *15*(1), 1–27. <https://doi.org/10.1186/s13072-022-00471-6>
- Fetissov, S. O., Schröder, O., Jakobsson, P. J., Samuelsson, B., Haeggström, J. Z., & Hökfelt, T. (2002). Expression of microsomal glutathione S-transferase type 3 mRNA in the rat nervous system. *Neuroscience*, *115*(3), 891–897. [https://doi.org/10.1016/S0306-4522\(02\)00411-6](https://doi.org/10.1016/S0306-4522(02)00411-6)
- Furusawa, T., & Cherukuri, S. (2010). Developmental function of HMGN proteins. *Biochimica et Biophysica Acta - Gene Regulatory Mechanisms*, *1799*(1–2), 69–73. <https://doi.org/10.1016/j.bbagr.2009.11.011>
- Hunt, R. J., Granat, L., McElroy, G. S., Ranganathan, R., Chandel, N. S., & Bateman, J. M. (2019). Mitochondrial stress causes neuronal dysfunction via an ATF4-dependent increase in L-2-hydroxyglutarate. *Journal of Cell Biology*, *218*(12), 4007–4016. <https://doi.org/10.1083/jcb.201904148>
- Izumi, K., Brett, M., Nishi, E., Drunat, S., Tan, E. S., Fujiki, K., Lebon, S., Cham, B., Masuda, K., Arakawa, M., Jacquinet, A., Yamazumi, Y., Chen, S. T., Verloes, A., Okada, Y., Katou, Y., Nakamura, T., Akiyama, T., Gressens, P., ... Shirahige, K. (2016). ARCN1 Mutations Cause a Recognizable Craniofacial Syndrome Due to COPI-Mediated Transport Defects. *American Journal of Human Genetics*, *99*(2), 451–459. <https://doi.org/10.1016/j.ajhg.2016.06.011>
- Kim, S., Lee, W., Jo, H., Sonn, S. K., Jeong, S. J., Seo, S., Suh, J., Jin, J., Kweon, H. Y., Kim, T.

- K., Moon, S. H., Jeon, S., Kim, J. W., Kim, Y. R., Lee, E. W., Shin, H. K., Park, S. H., & Oh, G. T. (2022). The antioxidant enzyme Peroxiredoxin-1 controls stroke-associated microglia against acute ischemic stroke. *Redox Biology*, *54*(May), 102347. <https://doi.org/10.1016/j.redox.2022.102347>
- Kozlov, S. V., Waardenberg, A. J., Engholm-Keller, K., Arthur, J. W., Graham, M. E., & Lavin, M. (2016). Reactive oxygen species (ROS)-activated ATM-dependent phosphorylation of cytoplasmic substrates identified by large-scale phosphoproteomics screen. *Molecular and Cellular Proteomics*, *15*(3), 1032–1047. <https://doi.org/10.1074/mcp.M115.055723>
- Lauranzano, E., Pozzi, S., Pasetto, L., Stucchi, R., Massignan, T., Paoletta, K., Mombrini, M., Nardo, G., Lunetta, C., Corbo, M., Mora, G., Bendotti, C., & Bonetto, V. (2015). Peptidylprolyl isomerase A governs TARDBP function and assembly in heterogeneous nuclear ribonucleoprotein complexes. *Brain*, *138*(4), 974–991. <https://doi.org/10.1093/brain/awv005>
- Michalak, M. (2023). Calreticulin: Endoplasmic reticulum Ca<sup>2+</sup> gatekeeper. *Journal of Cellular and Molecular Medicine*, *June*, 1–19. <https://doi.org/10.1111/jcmm.17839>
- Nowakowska, M., Gualtieri, F., von Rüden, E. L., Hansmann, F., Baumgärtner, W., Tipold, A., & Potschka, H. (2020). Profiling the Expression of Endoplasmic Reticulum Stress Associated Heat Shock Proteins in Animal Epilepsy Models. *Neuroscience*, *429*, 156–172. <https://doi.org/10.1016/j.neuroscience.2019.12.015>
- Paudel, Y. N., Angelopoulou, E., Piperi, C., Othman, I., & Shaikh, M. F. (2020). Hmgb1-mediated neuroinflammatory responses in brain injuries: Potential mechanisms and therapeutic opportunities. *International Journal of Molecular Sciences*, *21*(13), 1–29. <https://doi.org/10.3390/ijms21134609>
- Sun, Y., Wen, Y., Wang, L., Wen, L., You, W., Wei, S., Mao, L., Wang, H., Chen, Z., & Yang, X. (2021). Therapeutic Opportunities of Interleukin-33 in the Central Nervous System. *Frontiers in Immunology*, *12*(May), 1–10. <https://doi.org/10.3389/fimmu.2021.654626>
- Szeliga, M. (2020). Peroxiredoxins in neurodegenerative diseases. *Antioxidants*, *9*(12), 1–19. <https://doi.org/10.3390/antiox9121203>

- Tavleeva, M. M., Belykh, E. S., Rybak, A. V., Rasova, E. E., Chernykh, A. A., Ismailov, Z. B., & Velegzhaninov, I. O. (2022). Effects of Antioxidant Gene Overexpression on Stress Resistance and Malignization In Vitro and In Vivo: A Review. *Antioxidants*, *11*(12), 1–25. <https://doi.org/10.3390/antiox11122316>
- Wang, J., Xia, J., Zhang, F., Shi, Y., Wu, Y., Pu, H., Liou, A. K. F., Leak, R. K., Yu, X., Chen, L., & Chen, J. (2015). Galectin-1-secreting neural stem cells elicit long-term neuroprotection against ischemic brain injury. *Scientific Reports*, *5*. <https://doi.org/10.1038/srep09621>
- Wang, Y., Yin, J., Wang, C., Hu, H., Li, X., Xue, M., Liu, J., Cheng, W., Wang, Y., Li, Y., Shi, Y., Tan, J., Li, X., Liu, F., Liu, Q., & Yan, S. (2019). Microglial Mincle receptor in the PVN contributes to sympathetic hyperactivity in acute myocardial infarction rat. *Journal of Cellular and Molecular Medicine*, *23*(1), 112–125. <https://doi.org/10.1111/jcmm.13890>
- Xu, M., Wang, W., Lu, W., Ling, X., Rui, Q., & Ni, H. (2022). Evodiamine prevents traumatic brain injury through inhibiting oxidative stress via PGK1/NRF2 pathway. *Biomedicine and Pharmacotherapy*, *153*(May), 113435. <https://doi.org/10.1016/j.biopha.2022.113435>
- Yuan, J., Murrell, G. A. C., Trickett, A., Landtmeters, M., Knoop, B., & Wang, M. X. (2004). Overexpression of antioxidant enzyme peroxiredoxin 5 protects human tendon cells against apoptosis and loss of cellular function during oxidative stress. *Biochimica et Biophysica Acta - Molecular Cell Research*, *1693*(1), 37–45. <https://doi.org/10.1016/j.bbamcr.2004.04.006>
- Zhang, X., & Wang, Y. (2018). The Golgi stacking protein GORASP2/GRASP55 serves as an energy sensor to promote autophagosome maturation under glucose starvation. *Autophagy*, *14*(9), 1649–1651. <https://doi.org/10.1080/15548627.2018.1491214>
- Zharichenko, N., & Njoku, D. B. (2020). The role of pro-inflammatory and regulatory signaling by il-33 in the brain and liver: A focused systematic review of mouse and human data and risk of bias assessment of the literature. *International Journal of Molecular Sciences*, *21*(11). <https://doi.org/10.3390/ijms21113933>

---

## Conclusions and Perspectives

The research presented in this Thesis is focused on the development and use of advanced 3D brain organoid and assembloid models for PD research. In contrast to the classical 2D cultures, DANs in MOs interact with other neurons and glia cells, creating a microenvironment that is physiologically relevant. The physiological resemblance of MOs with the human embryonic midbrain is supported by the results of Manuscript I, with the identification of shared cellular composition and the high correlation of their mutual genetic expression signature. Additionally, we illustrated the potential of MOs in PD modelling. The genetic signature of MOs derived from a cell line carrying the PD-relevant mutation LRRK2 p.Gly2019Ser illustrates dysregulated pathways known to be affected in PD. In parallel, our analysis validates the developmental defect of MUT MOs, that was also previously described in PD models carrying the LRRK2 p.Gly2019Ser mutation (Smits et al., 2019; Walter et al., 2021). This study also highlights that the integration of the LRRK2 p.Gly2019Ser mutation into the healthy genetic background of the donor line can induce significant alterations in the MO's genetic expression profile, relevant to PD pathophysiology even from an early developmental stage, underlying the impact of a single mutation in the development of the pathology.

Regardless of the thorough quality control of our samples and data during the scRNAseq experiment and analysis, the use of only one pair of mutant and control lines in our study, renders it potentially susceptible to certain technical constraints. In scRNAseq experiments, the procedure followed to obtain a pure population of single cells can lead to significant loss of sample and induce a stress-related transcriptomic profile in the purified cells. Additionally, the transcripts obtained from each cell are significantly less than the whole transcriptome, limiting the accurate representation of the biological processes and possible dysregulations (X. Li & Wang, 2021). Similar studies involving MOs generated from a larger cohort of patient and CRISPR/Cas9-engineered cell lines would be necessary to further validate our findings. Additionally, since LRRK2 p.Gly2019Ser mutation is considered one of the most penetrant mutations in PD, it would be interesting to incorporate cell lines that carry similar (such as GBA-N370S) or different levels of penetrance (Tran et al., 2020) and evaluate the common and distinct transcriptomic changes in each case. These studies could help identify more specific dysregulated processes that might currently be masked due to technical limitations and shed light on general, mutation-independent transcriptomic changes that are causative of PD.

---

Despite the great potential of MOs in PD research, there are still some aspects of the disease that cannot be addressed. In the case of PD, neuroinflammation caused by the chronic activation of microglia is detrimental for the survival of neurons and contributes to accelerated neurodegeneration phenotypes. Due to the neuroectodermal origin of MOs, microglia cells that are derived from the mesoderm cannot be developed innately in the model. In Manuscript II, we show the successful integration of microglia into MOs and their contribution to MOs' homeostasis, with the removal of dead cells and remodelling of the synaptic network. Although healthy microglia in MOs have an amoeboid morphology, indicative of reactivity (Torres-Platas et al., 2014), our analysis showed no significant signs of microgliosis driven neuronal damage in our model. In this case, microglia activation is likely a result of the high number of dead cells in the centre of the organoid, where nutrients and oxygen are scarce. In this regard, more efforts are needed to reduce the stress levels in 3D *in vitro* models. Better perfusion of oxygen and nutrients in the centre of organoids is a necessary step towards the optimisation of the model, for achieving microglia physiological morphology closer to the healthy CNS environment. This optimisation is essential for the utility of MO-MGL model in PD-relevant neuroinflammation studies, as the microglia morphological differences between healthy and neurodegenerative states is a crucial phenotype for assessing neuroinflammation. Some ways to achieve this optimisation are either with the use of a microfluidic system, where organoids are cultured in chips with the controlled perfusion of fresh media and oxygen (Saorin et al., 2023), or with the vascularization of organoids (Rademakers et al., 2019), an important physiological system that is not present in the current brain organoid models.

Depending on the research question, we should use the adequate model that holds the necessary physiological characteristics and complexity needed to address the hypothesis. In Manuscript III, we present the generation of a midbrain-striatum assembloid model, that can recapitulate the nigrostriatal pathway connectivity. This manuscript is a first attempt to generate an *in vitro* human iPSC-derived 3D model of the nigrostriatal pathway, particularly important in PD research, as the reasons that drive the degeneration of dopaminergic terminals in the striatum are understudied. Nigrostriatal pathway connectivity is demonstrated in our assembloid model by the release of catecholamines from the midbrain into the striatum and the formation of active synapses between the midbrain and striatum compartments. However, future studies could yield valuable insights into enhancing our understanding of the model's synaptic organization. Specifically, a deeper characterization could be achieved by exploring the visual colocalization of pre and postsynaptic markers between dopaminergic and striatal neurons, using fluorescent and electron microscopy. Additionally, connectivity could be further

---

addressed with electrophysiological approaches such as MEA and patch clamp. In our lab, we have been working on a patch clamp approach where we can stimulate one side of the assembloid (e.g. in the midbrain organoid) and record the activity on the other side (e.g. in the striatum organoid). Moreover, using MEA and micro-devices, we can place the midbrain and striatum organoids in specific positions and record the electrophysiological activity occurring between the two organoids. With these experiments we could further assess the effect of the interregional connectivity in the neuronal firing capacity. Finally, optogenetics coupled with calcium imaging is another approach that could be used to evaluate the formation of active neuronal circuits between the two organoids in the assembloid model. This method has been successfully used by Miura and colleagues, in the cortico-striatal assembloid model (Miura et al., 2020).

Another important characteristic of the assembloid model that hasn't been addressed, is the directionality of the neuronal projections. While with simple immunofluorescence staining we were able to identify the formation of dopaminergic projections from the MO (TH-positive axons) towards the StrO in the assembloid, the possible formation of striatal medium spiny neuronal projections towards the MOs has not been examined. The main marker (DARPP32) used to identify the MSNs population in StrOs, could not be used to visualise their axons, as it is mainly visible in the soma and dendrites of these neurons. More elaborate methods, such as viral labelling of MSNs and DANs in the assembloid, would be a targeted approach to visually inspect the developing neuronal projections. Similar approach was followed by Miura and colleagues (Miura et al., 2020), where they used viral labelling to investigate the neuronal projections between striatum and cortical organoids in their cortico-striatum assembloid model. However, this method does also come with limitations, as the generation of a viral vector containing gene expression elements, such as reporters and enhancers, for its targeted expression in specific cell types can be laborious and with low selective expression efficiency. In line with the further model optimisation, one limitation that needs to be considered is the random cellular migration between the region-specific organoids in the assembloid model. Although in our assembloid model the two organoids retain in a high extend their identity and regional specificity and integrity, we could notice some migration of GFP-positive midbrain cells into the striatum and specifically around the surface of the organoid. This was mostly visible when assembloids were embedded into geltrex, as cells tend to migrate from the organoid core part towards the empty space covered by geltrex. Geltrex is similar to Matrigel, they are both derived from the secretions of Engelbreth-Holm-Swarm mouse sarcoma cells and they are enriched with extracellular matrix proteins (Gargotti et al., 2018). Although geltrex can provide

---

the organoid culture with chemical cues important for cellular differentiation, adhesion, and spatial organisation, it is still not clear how geltrex or matrigel affects the development of organoids (Raz et al., 2005). Therefore, it is possible that geltrex contributes to the random migration observed in our model. Alternatives of geltrex, such as synthetic hydrogels could be specifically engineered to provide chemical cues needed for the arrangement of organoids towards the target tissue (S. Kim et al., 2022; Z. Li et al., 2022). In our case, using a synthetic hydrogel that will provide the mechanical properties and extracellular matrix elements needed for the organisation of the cells towards the nigrostriatal pathway arrangement, could assist the physiological organisation in our assembloid model. However, the generation of such hydrogels require exact knowledge of the extracellular matrix features and signalling pathways, necessary for the development and regional organisation of the cells involved in the nigrostriatal pathway connectivity.

Aging is the major risk factor for developing PD and our *in vitro* models cannot fully recapitulate the dysregulated processes that occur during aging. Here, the induction of aged characteristics in our midbrain-striatum assembloid model with the overexpression of progerin, reveals synaptic dysregulation and early neurodegeneration phenotypes, relevant to PD. This is a very important step into the generation of iPSC-derived brain 3D models with aged characteristics. However, these results should be taken with caution and more studies are needed to evaluate the relevance with the normal human brain aging. In our study we performed a benchmarking analysis comparing human brain post-mortem RNA sequencing data with data from the aged assembloids. Although we were able to observe a common aged-relevant expression profile, this comparison cannot recapitulate accurately the aged profile in our model, as the post-mortem tissue was not specific to striatum and midbrain brain regions. Studies have shown that aging can affect differently each brain region (Berchtold et al., 2008; González-Velasco et al., 2020; Raz et al., 2005). Therefore, direct comparison of midbrain-striatum human post-mortem tissue with the progerin-overexpressing aged midbrain-striatum assembloids would be instrumental in examining the degree of physiological aging in our region-specific *in vitro* model. In our study we also show that p21<sup>CIP1</sup>, p53 and p16<sup>INK4A</sup> are increased in neurons that overexpress progerin. As discussed in 1.2 section, neuronal senescence has been shown by several studies in *in vitro* neuronal cultures and animal models. It is possible that increased DNA damage, an aging-related stress stimuli, can lead to senescent-like phenotypes in neurons (Jurk et al., 2012). However, the exact mechanism by which p21<sup>CIP1</sup>, p53 and p16<sup>INK4A</sup> are involved in neuronal senescence still needs to be explored. Progerin-overexpressing assembloids could contribute to studies on cellular and neuronal senescence. Although here



---

we show the presence of some key aging-senescent associated markers, further investigation on the presence of aging hallmarks such as mitochondrial and lysosomal dysfunction, and inflammation, would be beneficial for the further characterisation of aging and senescence in the model. Additionally, the use of this model to investigate aging and senescence not only on neurons but also on astrocytes and stem cells, would be essential to understand whether specific cell types are more vulnerable to aging stimuli in the brain and how this affects their neighbouring cells. It is also important to point out that due to the unavailability of more progerin cell lines, our results are based on one cell line. Subsequent investigations with the use of more progerin engineered lines would be advantageous to further validate the consistency of the aged phenotypes in our model.

Finally, for further enhancing the complexity and physiological relevance of our model, microglia integration in midbrain-striatum assembloids has already been achieved in our lab (data not shown here). More specifically, we have optimized the co-culture conditions of assembloids with macrophage precursors, and similar with the MO-MGL model, we have achieved the successful differentiation of microglia in the assembloid model. Future studies using this model will enable deciphering the role of neuroinflammation on the nigrostriatal pathway dopaminergic axons degeneration.

Without disregarding the limitations and needs for further improvement, *in vitro* models carry considerable prospects in advancing the development of novel therapeutic strategies aimed at addressing both the early and late stages of neurodegeneration. Here we show how brain organoid and assembloid models can evolve from the standard region-specific organoids to even more complex and physiological relevant structures, with better identity specificity of cellular populations and phenotypes of neuronal maturation. Following the assembloid generation strategies we can efficiently combine not only different organoids of neuroectodermal origin but also cell types originated from different germ layers, such as microglia. We show that the presence of microglia in MOs creates a more homeostatic environment with increased neuronal excitation and reduced expression of stress-related genes. On the same line, midbrain-striatum assembloids seem to also promote neuronal maturity with the increased expression of relevant genes. In parallel, midbrain-striatum assembloids can recreate neuronal circuits of the nigrostriatal pathway, rendering them an invaluable tool in PD studies where nigrostriatal connectivity is crucially affected. Finally, the ability to induce aging characteristics in these models paves the way towards studies that can assess the evolvement of observed developmental defects into an aged microenvironment,

---

allowing the observation of biological alterations that might contribute to onset and progression of PD.

Overall, enhancing the complexity of *in vitro* brain models improves their physiological relevance to the human brain conditions. This is particularly important as it is not only necessary for considering all the different factors contributing to PD development but also for their efficacy in advancing drug discoveries and therapeutic strategies for PD.

---

## References

- Aarts, E., van Holstein, M., & Cools, R. (2011). Striatal dopamine and the interface between motivation and cognition. *Frontiers in Psychology, 2*(JUL), 1–11. <https://doi.org/10.3389/fpsyg.2011.00163>
- Abud, E. M., Ramirez, R. N., Martinez, E. S., Healy, L. M., Nguyen, C. H. H., Newman, S. A., Yeromin, A. V., Scarfone, V. M., Marsh, S. E., Fimbres, C., Caraway, C. A., Fote, G. M., Madany, A. M., Agrawal, A., Kayed, R., Gylys, K. H., Cahalan, M. D., Cummings, B. J., Antel, J. P., ... Blurton-Jones, M. (2017). iPSC-Derived Human Microglia-like Cells to Study Neurological Diseases. *Neuron, 94*(2), 278–293.e9. <https://doi.org/10.1016/j.neuron.2017.03.042>
- Ahuja, R., Pinyol, R., Reichenbach, N., Custer, L., Klingensmith, J., Kessels, M. M., & Qualmann, B. (2007). Cordon-Bleu Is an Actin Nucleation Factor and Controls Neuronal Morphology. *Cell, 131*(2), 337–350. <https://doi.org/10.1016/j.cell.2007.08.030>
- Alejandra Morato Torres, C., Wassouf, Z., Zafar, F., Sastre, D., Outeiro, T. F., & Schüle, B. (2020). The role of alpha-synuclein and other parkinson's genes in neurodevelopmental and neurodegenerative disorders. In *International Journal of Molecular Sciences* (Vol. 21, Issue 16, pp. 1–32). <https://doi.org/10.3390/ijms21165724>
- Anderegg, A., Poulin, J. F., & Awatramani, R. (2015). Molecular heterogeneity of midbrain dopaminergic neurons - Moving toward single cell resolution. *FEBS Letters, 589*(24), 3714–3726. <https://doi.org/10.1016/j.febslet.2015.10.022>
- Andersen, J., Revah, O., Miura, Y., Thom, N., Amin, N. D., Kelley, K. W., Singh, M., Chen, X., Thete, M. V., Walczak, E. M., Vogel, H., Fan, H. C., & Paşca, S. P. (2020). Generation of Functional Human 3D Cortico-Motor Assembloids. *Cell, 183*(7), 1913–1929.e26. <https://doi.org/10.1016/j.cell.2020.11.017>
- Anichtchik, O., Diekmann, H., Fleming, A., Roach, A., Goldsmith, P., & Rubinsztein, D. C. (2008). Loss of PINK1 function affects development and results in neurodegeneration in zebrafish. *Journal of Neuroscience, 28*(33), 8199–8207. <https://doi.org/10.1523/JNEUROSCI.0979-08.2008>
- Arber, C., Precious, S. V., Cambrey, S., Risner-Janiczek, J. R., Kelly, C., Noakes, Z., Fjodorova, M., Heuer, A., Ungless, M. A., Rodríguez, T. A., Rosser, A. E., Dunnett, S. B., & Li, M. (2015). Activin a directs striatal projection neuron differentiation of human pluripotent stem cells. *Development (Cambridge), 142*(7), 1375–1386. <https://doi.org/10.1242/dev.117093>
- Arias-Fuenzalida, J., Jarazo, J., Qing, X., Walter, J., Gomez-Giro, G., Nickels, S. L., Zaehres, H., Schöler, H. R., & Schwamborn, J. C. (2017). FACS-Assisted CRISPR-Cas9 Genome Editing Facilitates Parkinson's

- 
- Disease Modeling. *Stem Cell Reports*, 9(5), 1423–1431.  
<https://doi.org/10.1016/j.stemcr.2017.08.026>
- Arlotta, P., Molyneaux, B. J., Jabaudon, D., Yoshida, Y., & Macklis, J. D. (2008). *Ctip2 Controls the Differentiation of Medium Spiny Neurons and the Establishment of the Cellular Architecture of the Striatum*. <https://doi.org/10.1523/JNEUROSCI.2986-07.2008>
- Arlt, A., & Schäfer, H. (2011). Role of the immediate early response 3 (IER3) gene in cellular stress response, inflammation and tumorigenesis. *European Journal of Cell Biology*, 90(6–7), 545–552.  
<https://doi.org/10.1016/j.ejcb.2010.10.002>
- Arnaud, K., Moreira, V. O., Vincent, J., Dallerac, G., Dubreuil, C., Dupont, E., Richter, M., Müller, U. C., Rondi-Reig, L., Prochiantz, A., & Di Nardo, A. A. (2021). Choroid plexus APP regulates adult brain proliferation and animal behavior. *Life Science Alliance*, 4(11), 1–11.  
<https://doi.org/10.26508/lsa.202000703>
- Arranz, A. M., Delbroek, L., van Kolen, K., Guimarães, M. R., Mandemakers, W., Daneels, G., Matta, S., Calafate, S., Shaban, H., Baatsen, P., de Bock, P. J., Gevaert, K., Berghe, P. Vanden, Verstreken, P., de Strooper, B., & Moechars, D. (2015). LRRK2 functions in synaptic vesicle endocytosis through a kinasedependent mechanism. *Journal of Cell Science*, 128(3), 541–552.  
<https://doi.org/10.1242/jcs.158196>
- Asai, H., Morita, S., & Miyata, S. (2011). Effect of pleiotrophin on glutamate-induced neurotoxicity in cultured hippocampal neurons. *Cell Biochemistry and Function*, 29(8), 660–665.  
<https://doi.org/10.1002/cbf.1802>
- Aveleira, C. A., Ferreira-Marques, M., Cortes, L., Valero, J., Pereira, D., Pereira de Almeida, L., & Cavadas, C. (2020). Neuropeptide Y Enhances Progerin Clearance and Ameliorates the Senescent Phenotype of Human Hutchinson-Gilford Progeria Syndrome Cells. *The Journals of Gerontology. Series A, Biological Sciences and Medical Sciences*, 75(6), 1073–1078.  
<https://doi.org/10.1093/gerona/glz280>
- Azam, S., Haque, M. E., Balakrishnan, R., Kim, I. S., & Choi, D. K. (2021). The Ageing Brain: Molecular and Cellular Basis of Neurodegeneration. In *Frontiers in Cell and Developmental Biology* (Vol. 9).  
<https://doi.org/10.3389/fcell.2021.683459>
- Baek, J. H., Schmidt, E., Viceconte, N., Strandgren, C., Pernold, K., Richard, T. J. C., Van Leeuwen, F. W., Dantuma, N. P., Damberg, P., Hultenby, K., Ulfhake, B., Mugnaini, E., Rozell, B., & Eriksson, M. (2015). Expression of progerin in aging mouse brains reveals structural nuclear abnormalities without detectable significant alterations in gene expression, hippocampal stem cells or behavior.

- 
- Human Molecular Genetics*, 24(5), 1305–1321. <https://doi.org/10.1093/hmg/ddu541>
- Bagley, J. A., Reumann, D., Bian, S., Lévi-Strauss, J., & Knoblich, J. A. (2017). Fused cerebral organoids model interactions between brain regions. *Nature Methods*, 14(7), 743–751. <https://doi.org/10.1038/nmeth.4304>
- Banerjee, A., Imig, C., Balakrishnan, K., Kershberg, L., Lipstein, N., Uronen, R. L., Wang, J., Cai, X., Benseler, F., Rhee, J. S., Cooper, B. H., Liu, C., Wojcik, S. M., Brose, N., & Kaeser, P. S. (2022). Molecular and functional architecture of striatal dopamine release sites. *Neuron*, 110(2), 248–265.e9. <https://doi.org/10.1016/j.neuron.2021.10.028>
- Banerjee, A., Lee, J., Nemcova, P., Liu, C., & Kaeser, P. S. (2020). Synaptotagmin-1 is the Ca<sup>2+</sup> sensor for fast striatal dopamine release. *ELife*, 9, 1–16. <https://doi.org/10.7554/eLife.58359>
- Becerra-Calixto, A., Mukherjee, A., Ramirez, S., Sepulveda, S., Sinha, T., Al-Lahham, R., De Gregorio, N., Gherardelli, C., & Soto, C. (2023). Lewy Body-like Pathology and Loss of Dopaminergic Neurons in Midbrain Organoids Derived from Familial Parkinson's Disease Patient. *Cells*, 12(4). <https://doi.org/10.3390/cells12040625>
- Bedrosian, T. A., Houtman, J., Eguiguren, J. S., Ghassemzadeh, S., Rund, N., Novaresi, N. M., Hu, L., Parylak, S. L., Denli, A. M., Randolph-Moore, L., Namba, T., Gage, F. H., & Toda, T. (2021). Lamin B1 decline underlies age-related loss of adult hippocampal neurogenesis. *The EMBO Journal*, 40(3), 1–21. <https://doi.org/10.15252/embj.2020105819>
- Behl, T., Kaur, G., Fratila, O., Buhas, C., Judea-Pusta, C. T., Negrut, N., Bustea, C., & Bungau, S. (2021). Cross-talks among GBA mutations, glucocerebrosidase, and  $\alpha$ -synuclein in GBA-associated Parkinson's disease and their targeted therapeutic approaches: a comprehensive review. *Translational Neurodegeneration*, 10(1), 1–13. <https://doi.org/10.1186/s40035-020-00226-x>
- Berchtold, N. C., Coleman, P. D., Cribbs, D. H., Rogers, J., Gillen, D. L., & Cotman, C. W. (2013). Synaptic genes are extensively downregulated across multiple brain regions in normal human aging and Alzheimer's disease. *Neurobiology of Aging*, 34(6), 1653–1661. <https://doi.org/10.1016/j.neurobiolaging.2012.11.024>
- Berchtold, N. C., Cribbs, D. H., Coleman, P. D., Rogers, J., Head, E., Kim, R., Beach, T., Miller, C., Troncoso, J., Trojanowski, J. Q., Ronald Zielke, H., & Cotman, C. W. (2008). *Gene expression changes in the course of normal brain aging are sexually dimorphic*. [www.pnas.org/cgi/content/full/](http://www.pnas.org/cgi/content/full/)
- Berwick, D. C., & Harvey, K. (2012). LRRK2 functions as a wnt signaling scaffold, bridging cytosolic proteins and membrane-localized LRP6. *Human Molecular Genetics*, 21(22), 4966–4979. <https://doi.org/10.1093/hmg/dd342>

- 
- Berwick, D. C., Harvey, K., Blandini, F., & Mondino, C. (2013). *LRRK2: an éminence grise of Wnt-mediated neurogenesis?* <https://doi.org/10.3389/fncel.2013.00082>
- Bhaduri, A., Andrews, M. G., Mancia Leon, W., Jung, D., Shin, D., Allen, D., Jung, D., Schmunk, G., Haeussler, M., Salma, J., Pollen, A. A., Nowakowski, T. J., & Kriegstein, A. R. (2020). Cell stress in cortical organoids impairs molecular subtype specification. *Nature*, *578*(7793), 142–148. <https://doi.org/10.1038/s41586-020-1962-0>
- Bidault, G., Garcia, M., Capeau, J., Morichon, R., Vigouroux, C., & Béréziat, V. (2020). Progerin Expression Induces Inflammation, Oxidative Stress and Senescence in Human Coronary Endothelial Cells. *Cells*, *9*(5). <https://doi.org/10.3390/cells9051201>
- bin Imtiaz, M. K., Jaeger, B. N., Bottes, S., Machado, R. A. C., Vidmar, M., Moore, D. L., & Jessberger, S. (2021). Declining lamin B1 expression mediates age-dependent decreases of hippocampal stem cell activity. *Cell Stem Cell*, *28*(5), 967–977.e8. <https://doi.org/10.1016/j.stem.2021.01.015>
- Birey, F., Andersen, J., Makinson, C. D., Islam, S., Wei, W., Huber, N., Fan, H. C., Metzler, K. R. C., Panagiotakos, G., Thom, N., O'Rourke, N. A., Steinmetz, L. M., Bernstein, J. A., Hallmayer, J., Huguenard, J. R., & Pasca, S. P. (2017). Assembly of functionally integrated human forebrain spheroids. *Nature*, *545*(7652), 54–59. <https://doi.org/10.1038/nature22330>
- Birtele, M., Storm, P., Sharma, Y., Kajtez, J., Wahlestedt, J. N., Sozzi, E., Nilsson, F., Stott, S., He, X. L., Mattsson, B., Ottosson, D. R., Barker, R. A., Fiorenzano, A., & Parmar, M. (2022). *Single-cell transcriptional and functional analysis of dopaminergic neurons in organoid-like cultures derived from human fetal midbrain*. <https://doi.org/10.1242/dev.200504>
- Bitar, M., & Barry, G. (2020). Building a Human Brain for Research. *Frontiers in Molecular Neuroscience*, *13*, 22. <https://doi.org/10.3389/fnmol.2020.00022>
- Blesa, J., & Przedborski, S. (2014). Parkinson's disease: Animal models and dopaminergic cell vulnerability. *Frontiers in Neuroanatomy*, *8*(DEC), 1–12. <https://doi.org/10.3389/fnana.2014.00155>
- Bohnen, N. I. (2020). Vulnerabilities of aging and biological effects of physical activity provide new clues for interventions in Parkinson's disease. *Journals of Gerontology - Series A Biological Sciences and Medical Sciences*, *75*(4), 687–689. <https://doi.org/10.1093/gerona/glaa026>
- Bolognin, S., Fossépré, M., Qing, X., Jarazo, J., Ščančar, J., Moreno, E. L., Nickels, S. L., Wasner, K., Ouzren, N., Walter, J., Grünewald, A., Glaab, E., Salamanca, L., Fleming, R. M. T., Antony, P. M. A., & Schwamborn, J. C. (2019). 3D Cultures of Parkinson's Disease-Specific Dopaminergic Neurons for High Content Phenotyping and Drug Testing. *Advanced Science*, *6*(1), 1–14.

- 
- <https://doi.org/10.1002/adv.201800927>
- Book, A., Guella, I., Candido, T., Brice, A., Hattori, N., Jeon, B., & Farrer, M. J. (2018). A meta-analysis of  $\alpha$ -synuclein multiplication in familial parkinsonism. *Frontiers in Neurology*, *9*, 1021. <https://doi.org/10.3389/fneur.2018.01021>
- Braak, H., Del Tredici, K., Rüb, U., De Vos, R. A. I., Jansen Steur, E. N. H., & Braak, E. (2003). Staging of brain pathology related to sporadic Parkinson's disease. *Neurobiology of Aging*, *24*(2), 197–211. [https://doi.org/10.1016/S0197-4580\(02\)00065-9](https://doi.org/10.1016/S0197-4580(02)00065-9)
- Brennand, K. J. (2013). Inducing cellular aging: Enabling neurodegeneration-in-a-dish. *Cell Stem Cell*, *13*(6), 635–636. <https://doi.org/10.1016/j.stem.2013.11.017>
- Buss, E. W., Corbett, N. J., Roberts, J. G., Ybarra, N., Musial, T. F., Simkin, D., Molina-Campos, E., Oh, K. J., Nielsen, L. L., Ayala, G. D., Mullen, S. A., Farooqi, A. K., D'Souza, G. X., Hill, C. L., Bean, L. A., Rogalsky, A. E., Russo, M. L., Curlik, D. M., Antion, M. D., ... Nicholson, D. A. (2021). Cognitive aging is associated with redistribution of synaptic weights in the hippocampus. *Proceedings of the National Academy of Sciences of the United States of America*, *118*(8), 1–10. <https://doi.org/10.1073/pnas.1921481118>
- Butler, A., Hoffman, P., Smibert, P., Papalexi, E., & Satija, R. (2018). Integrating single-cell transcriptomic data across different conditions, technologies, and species. *Nature Biotechnology*, *36*(5), 411–420. <https://doi.org/10.1038/nbt.4096>
- Cabin, D. E., Gispert-Sanchez, S., Murphy, D., Auburger, G., Myers, R. R., & Nussbaum, R. L. (2005). Exacerbated synucleinopathy in mice expressing A53T SNCA on a Snca null background. *Neurobiology of Aging*, *26*(1), 25–35. <https://doi.org/10.1016/j.neurobiolaging.2004.02.026>
- Caminiti, S. P., Presotto, L., Baroncini, D., Garibotto, V., Moresco, R. M., Gianolli, L., Volonté, M. A., Antonini, A., & Perani, D. (2017). Axonal damage and loss of connectivity in nigrostriatal and mesolimbic dopamine pathways in early Parkinson's disease. *NeuroImage: Clinical*, *14*(March), 734–740. <https://doi.org/10.1016/j.nicl.2017.03.011>
- Camp, J. G., Badsha, F., Florio, M., Kanton, S., Gerber, T., Wilsch-Bräuninger, M., Lewitus, E., Sykes, A., Hevers, W., Lancaster, M., Knoblich, J. A., Lachmann, R., Pääbo, S., Huttner, W. B., & Treutlein, B. (2015). Human cerebral organoids recapitulate gene expression programs of fetal neocortex development. *Proceedings of the National Academy of Sciences of the United States of America*, *112*(51), 15672–15677. <https://doi.org/10.1073/pnas.1520760112>
- Centeno, E. G. Z., Cimarosti, H., & Bithell, A. (2018). 2D versus 3D human induced pluripotent stem cell-derived cultures for neurodegenerative disease modelling. In *Molecular Neurodegeneration* (Vol.

---

13, Issue 1). <https://doi.org/10.1186/s13024-018-0258-4>

- Cetin, S., Knez, D., Gobec, S., Kos, J., & Pišlar, A. (2022). Cell models for Alzheimer's and Parkinson's disease: At the interface of biology and drug discovery. *Biomedicine and Pharmacotherapy*, *149*(February). <https://doi.org/10.1016/j.biopha.2022.112924>
- Chanoumidou, K., Mozafari, S., Baron-Van Evercooren, A., & Kuhlmann, T. (2020). Stem cell derived oligodendrocytes to study myelin diseases. *GLIA*, *68*(4), 705–720. <https://doi.org/10.1002/glia.23733>
- Cheng, H. C., Kim, S. R., Oo, T. F., Kareva, T., Yarygina, O., Rzhetskaya, M., Wang, C., During, M., Talloczy, Z., Tanaka, K., Komatsu, M., Kobayashi, K., Okano, H., Kholodilov, N., & Burke, R. E. (2011). Akt suppresses retrograde degeneration of dopaminergic axons by inhibition of macroautophagy. *Journal of Neuroscience*, *31*(6), 2125–2135. <https://doi.org/10.1523/JNEUROSCI.5519-10.2011>
- Chiu, C. C., Weng, Y. H., Huang, Y. Z., Chen, R. S., Liu, Y. C., Yeh, T. H., Lu, C. S., Lin, Y. W., Chen, Y. J., Hsu, C. C., Chiu, C. H., Wang, Y. T., Chen, W. S., Liu, S. Y., & Wang, H. L. (2020). (D620N) VPS35 causes the impairment of Wnt/ $\beta$ -catenin signaling cascade and mitochondrial dysfunction in a PARK17 knockin mouse model. *Cell Death and Disease*, *11*(11). <https://doi.org/10.1038/s41419-020-03228-9>
- Choi, I., Kim, B., Byun, J. W., Baik, S. H., Huh, Y. H., Kim, J. H., Mook-Jung, I., Song, W. K., Shin, J. H., Seo, H., Suh, Y. H., Jou, I., Park, S. M., Kang, H. C., & Joe, E. H. (2015). LRRK2 G2019S mutation attenuates microglial motility by inhibiting focal adhesion kinase. *Nature Communications*, *6*. <https://doi.org/10.1038/ncomms9255>
- Choi, G., & Ko, J. (2015). Gephyrin: a central GABAergic synapse organizer. *Experimental & Molecular Medicine*, *47*. <https://doi.org/10.1038/emm.2015.5>
- Chu, Y., Morfini, G. A., Langhamer, L. B., He, Y., Brady, S. T., & Kordower, J. H. (2012). Alterations in axonal transport motor proteins in sporadic and experimental Parkinson's disease. *Brain*, *135*(7), 2058–2073. <https://doi.org/10.1093/brain/aws133>
- Chung, C. Y., Licznerski, P., Alavian, K. N., Simeone, A., Lin, Z., Martin, E., Vance, J., & Isacson, O. (2010). The transcription factor orthodenticle homeobox 2 influences axonal projections and vulnerability of midbrain dopaminergic neurons. *Brain*, *133*(7), 2022–2031. <https://doi.org/10.1093/brain/awq142>
- Chung, S. J., Lee, H. S., Yoo, H. S., Lee, Y. H., Lee, P. H., & Sohn, Y. H. (2020). Patterns of striatal dopamine depletion in early Parkinson disease: Prognostic relevance. *Neurology*, *95*(3), E280–E290. <https://doi.org/10.1212/WNL.0000000000009878>



- 
- Collier, T. J., Kanaan, N. M., & Kordower, J. H. (2017). Aging and Parkinson's disease: Different sides of the same coin? *Movement Disorders*, *32*(7), 983–990. <https://doi.org/10.1002/mds.27037>
- Colonna, M., & Butovsky, O. (2017). Microglia function in the central nervous system during health and neurodegeneration. *Annual Review of Immunology*, *35*, 441–468. <https://doi.org/10.1146/annurev-immunol-051116-052358>
- Cooper, O., Hargus, G., Deleidi, M., Blak, A., Osborn, T., Marlow, E., Lee, K., Levy, A., Perez-Torres, E., Yow, A., & Isacson, O. (2010). Differentiation of human ES and Parkinson's disease iPS cells into ventral midbrain dopaminergic neurons requires a high activity form of SHH, FGF8a and specific regionalization by retinoic acid. *Molecular and Cellular Neuroscience*, *45*(3), 258–266. <https://doi.org/10.1016/j.mcn.2010.06.017>
- Coronel, R., Bernabeu-Zornoza, A., Palmer, C., Muñiz-Moreno, M., Zambrano, A., Cano, E., & Liste, I. (2018). Role of Amyloid Precursor Protein (APP) and Its Derivatives in the Biology and Cell Fate Specification of Neural Stem Cells. In *Molecular Neurobiology* (Vol. 55, Issue 9, pp. 7107–7117). <https://doi.org/10.1007/s12035-018-0914-2>
- Correia Guedes, L., Mestre, T., Outeiro, T. F., & Ferreira, J. J. (2020). Are genetic and idiopathic forms of Parkinson's disease the same disease? In *Journal of Neurochemistry* (Vol. 152, Issue 5, pp. 515–522). <https://doi.org/10.1111/jnc.14902>
- Das, A. T., Zhou, X., Metz, S. W., Vink, M. A., & Berkhout, B. (2016). Selecting the optimal Tet-On system for doxycycline-inducible gene expression in transiently transfected and stably transduced mammalian cells. *Biotechnology Journal*, *11*(1), 71–79. <https://doi.org/10.1002/biot.201500236>
- Daubner, S. C., Le, T., & Wang, S. (2011). Tyrosine hydroxylase and regulation of dopamine synthesis. *Archives of Biochemistry and Biophysics*, *508*(1), 1–12. <https://doi.org/10.1016/j.abb.2010.12.017>
- De Gregorio, R., Pulcrano, S., De Sanctis, C., Volpicelli, F., Guatteo, E., von Oerthel, L., Latagliata, E. C., Esposito, R., Piscitelli, R. M., Perrone-Capano, C., Costa, V., Greco, D., Puglisi-Allegra, S., Smidt, M. P., di Porzio, U., Caiazzo, M., Mercuri, N. B., Li, M., & Bellenchi, G. C. (2018). miR-34b/c Regulates Wnt1 and Enhances Mesencephalic Dopaminergic Neuron Differentiation. *Stem Cell Reports*, *10*(4), 1237–1250. <https://doi.org/10.1016/j.stemcr.2018.02.006>
- De Haas, A. H., Van Weering, H. R. J., De Jong, E. K., Boddeke, H. W. G. M., & Biber, K. P. H. (2007). Neuronal chemokines: Versatile messengers in central nervous system cell interaction. *Molecular Neurobiology*, *36*(2), 137–151. <https://doi.org/10.1007/s12035-007-0036-8>
- De Masi, C., Spitalieri, P., Murdocca, M., Novelli, G., & Sangiuolo, F. (2020). Application of CRISPR/Cas9 to human-induced pluripotent stem cells: From gene editing to drug discovery. *Human Genomics*,

- 
- 14(1), 1–12. <https://doi.org/10.1186/s40246-020-00276-2>
- Deng, H., & Yuan, L. (2014). Genetic variants and animal models in SNCA and Parkinson disease. *Ageing Research Reviews*, 15(1), 161–176. <https://doi.org/10.1016/j.arr.2014.04.002>
- di Domenico, A., Carola, G., Calatayud, C., Pons-Espinal, M., Muñoz, J. P., Richaud-Patin, Y., Fernandez-Carasa, I., Gut, M., Faella, A., Parameswaran, J., Soriano, J., Ferrer, I., Tolosa, E., Zorzano, A., Cuervo, A. M., Raya, A., & Consiglio, A. (2019). Patient-Specific iPSC-Derived Astrocytes Contribute to Non-Cell-Autonomous Neurodegeneration in Parkinson’s Disease. *Stem Cell Reports*, 12(2), 213–229. <https://doi.org/10.1016/j.stemcr.2018.12.011>
- Di Salvio, M., Di Giovannantonio, L. G., Omodei, D., Acampora, D., & Simeone, A. (2010). Otx2 expression is restricted to dopaminergic neurons of the ventral tegmental area in the adult brain. *International Journal of Developmental Biology*, 54(5), 939–945. <https://doi.org/10.1387/ijdb.092974ms>
- Dodig, S., Čepelak, I., & Pavić, I. (2019). Hallmarks of senescence and aging. *Biochemia Medica*, 29(3), 1–15. <https://doi.org/10.11613/BM.2019.030501>
- Dommershuijsen, L. J., Boon, A. J. W., & Ikram, M. K. (2021). Probing the Pre-diagnostic Phase of Parkinson’s Disease in Population-Based Studies. *Frontiers in Neurology*, 12, 702502. <https://doi.org/10.3389/fneur.2021.702502>
- Dovonou, A., Bolduc, C., Soto Linan, V., Gora, C., Peralta, M. R., & Lévesque, M. (2023). Animal models of Parkinson’s disease: bridging the gap between disease hallmarks and research questions. *Translational Neurodegeneration*, 12(1), 1–25. <https://doi.org/10.1186/s40035-023-00368-8>
- Ehrlich, M., Mozafari, S., Glatza, M., Starost, L., Velychko, S., Hallmann, A. L., Cui, Q. L., Schambach, A., Kim, K. P., Bachelin, C., Marteyn, A., Hargus, G., Johnson, R. M., Antel, J., Sternecker, J., Zaehres, H., Schöler, H. R., Baron-Van Evercooren, A., & Kuhlmann, T. (2017). Rapid and efficient generation of oligodendrocytes from human induced pluripotent stem cells using transcription factors. *Proceedings of the National Academy of Sciences of the United States of America*, 114(11), E2243–E2252. <https://doi.org/10.1073/pnas.1614412114>
- Eigenhuis, K. N., Somsen, H. B., van der Kroeg, M., Smeenk, H., Korporaal, A. L., Kushner, S. A., de Vrij, F. M. S., & van den Berg, D. L. C. (2023). A simplified protocol for the generation of cortical brain organoids. *Frontiers in Cellular Neuroscience*, 17. <https://doi.org/10.3389/fncel.2023.1114420>
- Etessami, R., Conzelmann, K., Fadai-ghotbi, B., Natelson, B., Tsiang, H., & Ceccaldi, P. (2011). Spread and pathogenic characteristics of a G-deficient rabies virus recombinant- an in vitro and in vivo study. *Journal of General Virology*, 81(9), 2147–2153. [papers2://publication/uuid/BDB7C790-](https://doi.org/10.1099/jgv.0.019000-0)

---

A842-498C-AC14-A623401118A4

- Fathi, A., Mathivanan, S., Kong, L., Petersen, A. J., Harder, C. R. K., Block, J., Miller, J. M., Bhattacharyya, A., Wang, D., & Zhang, S. C. (2022). Chemically induced senescence in human stem cell-derived neurons promotes phenotypic presentation of neurodegeneration. *Aging Cell*, *21*(1), 1–21. <https://doi.org/10.1111/accel.13541>
- Ferrer, I., Martinez, A., Boluda, S., Parchi, P., & Barrachina, M. (2008). Brain banks: Benefits, limitations and cautions concerning the use of post-mortem brain tissue for molecular studies. *Cell and Tissue Banking*, *9*(3), 181–194. <https://doi.org/10.1007/s10561-008-9077-0>
- Fiorenzano, A., Sozzi, E., Birtele, M., Kajtez, J., Giacomoni, J., Nilsson, F., Bruzelius, A., Sharma, Y., Zhang, Y., Mattsson, B., Emnéus, J., Ottosson, D. R., Storm, P., & Parmar, M. (2021a). Single-cell transcriptomics captures features of human midbrain development and dopamine neuron diversity in brain organoids. *Nature Communications*, *12*(1), 1–19. <https://doi.org/10.1038/s41467-021-27464-5>
- Fiorenzano, A., Sozzi, E., Birtele, M., Kajtez, J., Giacomoni, J., Nilsson, F., Bruzelius, A., Sharma, Y., Zhang, Y., Mattsson, B., Emnéus, J., Ottosson, D. R., Storm, P., & Parmar, M. (2021b). Single-cell transcriptomics captures features of human midbrain development and dopamine neuron diversity in brain organoids. *Nature Communications*, *12*(1). <https://doi.org/10.1038/s41467-021-27464-5>
- Fong, W. L., Kuo, H. Y., Wu, H. L., Chen, S. Y., & Liu, F. C. (2018). Differential and Overlapping Pattern of Foxp1 and Foxp2 Expression in the Striatum of Adult Mouse Brain. In *Neuroscience* (Vol. 388). IBRO. <https://doi.org/10.1016/j.neuroscience.2018.07.017>
- Fu, R., Shen, Q., Xu, P., Luo, J. J., & Tang, Y. (2014). Phagocytosis of microglia in the central nervous system diseases. *Molecular Neurobiology*, *49*(3), 1422–1434. <https://doi.org/10.1007/s12035-013-8620-6>
- Fujii, M., & Sato, T. (2021). Somatic cell-derived organoids as prototypes of human epithelial tissues and diseases. In *Nature Materials* (Vol. 20, Issue 2, pp. 156–169). <https://doi.org/10.1038/s41563-020-0754-0>
- Fujita, Y., & Yamashita, T. (2021). Neuroprotective function of microglia in the developing brain. *Neuronal Signaling*, *5*(1), 1–10. <https://doi.org/10.1042/NS20200024>
- Fuxe, K., Manger, P., Genedani, S., & Agnati, L. (2006). The nigrostriatal DA pathway and Parkinson's disease. *Journal of Neural Transmission, Supplement*, *70*, 71–83. [https://doi.org/10.1007/978-3-211-45295-0\\_13](https://doi.org/10.1007/978-3-211-45295-0_13)

- 
- Garcia-Reitboeck, P., Anichtchik, O., Dalley, J. W., Ninkina, N., Tofaris, G. K., Buchman, V. L., & Spillantini, M. G. (2013). Endogenous alpha-synuclein influences the number of dopaminergic neurons in mouse substantia nigra. *Experimental Neurology*, *248*, 541–545. <https://doi.org/10.1016/j.expneurol.2013.07.015>
- Gargotti, M., Lopez-Gonzalez, U., Byrne, H. J., & Casey, A. (2018). Comparative studies of cellular viability levels on 2D and 3D in vitro culture matrices. *Cytotechnology*, *70*(1), 261–273. <https://doi.org/10.1007/s10616-017-0139-7>
- Geng, Y. Q., Guan, J. T., Xu, X. H., & Fu, Y. C. (2010). Senescence-associated beta-galactosidase activity expression in aging hippocampal neurons. *Biochemical and Biophysical Research Communications*, *396*(4), 866–869. <https://doi.org/10.1016/j.bbrc.2010.05.011>
- George, S., Rey, N. L., Reichenbach, N., Steiner, J. A., & Brundin, P. (2013).  $\alpha$ -Synuclein: The long distance runner. *Brain Pathology*, *23*(3), 350–357. <https://doi.org/10.1111/bpa.12046>
- Ghosh, B., Zhang, C., Ziemba, K. S., Fletcher, A. M., Yurek, D. M., & Smith, G. M. (2019). Partial Reconstruction of the Nigrostriatal Circuit along a Preformed Molecular Guidance Pathway. *Molecular Therapy - Methods and Clinical Development*, *14*(September), 217–227. <https://doi.org/10.1016/j.omtm.2019.06.008>
- Ginhoux, F., Lim, S., Hoeffel, G., Low, D., & Huber, T. (2013). Origin and differentiation of microglia. In *Frontiers in Cellular Neuroscience* (Issue MAR). <https://doi.org/10.3389/fncel.2013.00045>
- Gómez-Benito, M., Granado, N., García-Sanz, P., Michel, A., Dumoulin, M., & Moratalla, R. (2020). Modeling Parkinson's Disease With the Alpha-Synuclein Protein. In *Frontiers in Pharmacology* (Vol. 11, p. 1). <https://doi.org/10.3389/fphar.2020.00356>
- Gomez-Giro, G., Arias-Fuenzalida, J., Jarazo, J., Zeuschner, D., Ali, M., Possemis, N., Bolognin, S., Halder, R., Jäger, C., Kuper, W. F. E., Van Hasselt, P. M., Zaehres, H., Del Sol, A., Van Der Putten, H., Schöler, H. R., & Schwamborn, J. C. (2019). Synapse alterations precede neuronal damage and storage pathology in a human cerebral organoid model of CLN3-juvenile neuronal ceroid lipofuscinosis. *Acta Neuropathologica Communications*, *7*(1), 1–19. <https://doi.org/10.1186/s40478-019-0871-7>
- González-Castillo, C., Ortuño-Sahagún, D., Guzmán-Brambila, C., Pallàs, M., & Rojas-Mayorquín, A. E. (2015). Pleiotrophin as a central nervous system neuromodulator, evidences from the hippocampus. *Frontiers in Cellular Neuroscience*, *8*(JAN), 1–7. <https://doi.org/10.3389/fncel.2014.00443>
- González-Velasco, O., Papy-García, D., Le Douaron, G., Sánchez-Santos, J. M., & De Las Rivas, J. (2020).

- 
- Transcriptomic landscape, gene signatures and regulatory profile of aging in the human brain. *Biochimica et Biophysica Acta - Gene Regulatory Mechanisms*, 1863(6), 194491. <https://doi.org/10.1016/j.bbagr.2020.194491>
- Grealish, S., Diguët, E., Kirkeby, A., Mattsson, B., Heuer, A., Bramouille, Y., Van Camp, N., Perrier, A. L., Hantraye, P., Björklund, A., & Parmar, M. (2014). Human ESC-derived dopamine neurons show similar preclinical efficacy and potency to fetal neurons when grafted in a rat model of Parkinson's disease. *Cell Stem Cell*, 15(5), 653–665. <https://doi.org/10.1016/j.stem.2014.09.017>
- Grealish, S., Heuer, A., Cardoso, T., Kirkeby, A., Jönsson, M., Johansson, J., Björklund, A., Jakobsson, J., & Parmar, M. (2015). Monosynaptic Tracing using Modified Rabies Virus Reveals Early and Extensive Circuit Integration of Human Embryonic Stem Cell-Derived Neurons. *Stem Cell Reports*, 4(6), 975–983. <https://doi.org/10.1016/j.stemcr.2015.04.011>
- Grigor'eva, E. V., Malankhanova, T. B., Surumbayeva, A., Pavlova, S. V., Minina, J. M., Kizilova, E. A., Suldina, L. A., Morozova, K. N., Kiseleva, E., Sorokoumov, E. D., Lebedev, I. N., Zakian, S. M., & Malakhova, A. A. (2020). Generation of GABAergic striatal neurons by a novel iPSC differentiation protocol enabling scalability and cryopreservation of progenitor cells. *Cytotechnology*, 72(5), 649–663. <https://doi.org/10.1007/s10616-020-00406-7>
- Grimes, D. A., Han, F., Panisset, M., Racacho, L., Xiao, F., Zou, R., Westaff, K., & Bulman, D. E. (2006). Translated mutation in the Nurr1 gene as a cause for Parkinson's disease. *Movement Disorders*, 21(7), 906–909. <https://doi.org/10.1002/mds.20820>
- Gupta, S., & Shukla, S. (2021). Non-motor symptoms in Parkinson's disease: Opening new avenues in treatment. *Current Research in Behavioral Sciences*, 2(May), 100049. <https://doi.org/10.1016/j.crbeha.2021.100049>
- Häbig, K., Gellhaar, S., Heim, B., Djuric, V., Giesert, F., Wurst, W., Walter, C., Hentrich, T., Riess, O., & Bonin, M. (2013). LRRK2 guides the actin cytoskeleton at growth cones together with ARHGEF7 and Tropomyosin 4. *Biochimica et Biophysica Acta - Molecular Basis of Disease*, 1832(12), 2352–2367. <https://doi.org/10.1016/j.bbadis.2013.09.009>
- Harris, J. P., Burrell, J. C., Struzyna, L. A., Chen, H. I., Serruya, M. D., Wolf, J. A., Duda, J. E., & Cullen, D. K. (2020). Emerging regenerative medicine and tissue engineering strategies for Parkinson's disease. *Npj Parkinson's Disease*, 6(1). <https://doi.org/10.1038/s41531-019-0105-5>
- Hartmann, A. (2004). Postmortem studies in Parkinson's disease. *Dialogues in Clinical Neuroscience*, 6(3), 281–293. <https://doi.org/10.31887/dcns.2004.6.3/ahartmann>
- Hasselmann, J., Coburn, M. A., England, W., Figueroa Velez, D. X., Kiani Shabestari, S., Tu, C. H.,

- 
- McQuade, A., Kolahdouzan, M., Echeverria, K., Claes, C., Nakayama, T., Azevedo, R., Coufal, N. G., Han, C. Z., Cummings, B. J., Davtyan, H., Glass, C. K., Healy, L. M., Gandhi, S. P., ... Blurton-Jones, M. (2019). Development of a Chimeric Model to Study and Manipulate Human Microglia In Vivo. *Neuron*, *103*(6), 1016-1033.e10. <https://doi.org/10.1016/j.neuron.2019.07.002>
- Hemby, S. E., Trojanowski, J. Q., & Ginsberg, S. D. (2003). Neuron-specific age-related decreases in dopamine receptor subtype mRNAs. *Journal of Comparative Neurology*, *456*(2), 176–183. <https://doi.org/10.1002/cne.10525>
- Heng, N., Malek, N., Lawton, M. A., Nodehi, A., Pitz, V., Grosset, K. A., Ben-Shlomo, Y., & Grosset, D. G. (2023). Striatal Dopamine Loss in Early Parkinson’s Disease: Systematic Review and Novel Analysis of Dopamine Transporter Imaging. In *Movement Disorders Clinical Practice* (Vol. 10, Issue 4, pp. 539–546). <https://doi.org/10.1002/mdc3.13687>
- Hernandez, C. M., Mcquail, J. A., Schwabe, M. R., Bizon, J. L., Burke, S. N., & Setlow, B. (2018). Age-Related Declines in Prefrontal Cortical Expression of Metabotropic Glutamate Receptors that Support Working Memory. *5*(June).
- Hindle, J. V. (2010). Ageing, neurodegeneration and Parkinson’s disease. *Age and Ageing*, *39*(2), 156–161. <https://doi.org/10.1093/ageing/afp223>
- Hong, Y., Dong, X., Chang, L., Xie, C., Chang, M., Aguilar, J. S., Lin, J., Lin, J., & Li, Q. Q. (2023). Microglia-containing cerebral organoids derived from induced pluripotent stem cells for the study of neurological diseases. *iScience*, *26*(3), 106267. <https://doi.org/10.1016/j.isci.2023.106267>
- Hopperton, K. E., Mohammad, D., Trépanier, M. O., Giuliano, V., & Bazinet, R. P. (2018). Markers of microglia in post-mortem brain samples from patients with Alzheimer’s disease: A systematic review. *Molecular Psychiatry*, *23*(2), 177–198. <https://doi.org/10.1038/mp.2017.246>
- Hou, Y., Dan, X., Babbar, M., Wei, Y., Hasselbalch, S. G., Croteau, D. L., & Bohr, V. A. (2019). Ageing as a risk factor for neurodegenerative disease. *Nature Reviews Neurology*, *15*(10), 565–581. <https://doi.org/10.1038/s41582-019-0244-7>
- Hur, E. M., & Lee, B. D. (2021). Lrrk2 at the crossroad of aging and parkinson’s disease. *Genes*, *12*(4). <https://doi.org/10.3390/genes12040505>
- Ishikawa, S., & Ishikawa, F. (2020). Proteostasis failure and cellular senescence in long-term cultured postmitotic rat neurons. *Aging Cell*, *19*(1), 1–15. <https://doi.org/10.1111/accel.13071>
- Ivkovic, S., & Ehrlich, M. E. (1999). *Expression of the Striatal DARPP-32/ARPP-21 Phenotype in GABAergic Neurons Requires Neurotrophins In Vivo and In Vitro.*
- Jalink, P., & Caiazzo, M. (2021). Brain organoids: Filling the need for a human model of neurological

- 
- disorder. In *Biology* (Vol. 10, Issue 8). <https://doi.org/10.3390/biology10080740>
- Jarazo, J., Barmapa, K., Modamio, J., Saraiva, C., Sabaté-Soler, S., Rosety, I., Griesbeck, A., Skwirblies, F., Zaffaroni, G., Smits, L. M., Su, J., Arias-Fuenzalida, J., Walter, J., Gomez-Giro, G., Monzel, A. S., Qing, X., Vitali, A., Cruciani, G., Boussaad, I., ... Schwamborn, J. C. (2021). Parkinson's Disease Phenotypes in Patient Neuronal Cultures and Brain Organoids Improved by 2-Hydroxypropyl- $\beta$ -Cyclodextrin Treatment. *Movement Disorders*, *May*, 1–16. <https://doi.org/10.1002/mds.28810>
- Jarazo, J., Barmapa, K., Rosety, I., Smits, L. M., Arias-Fuenzalida, J., Walter, J., Gomez-Giro, G., Monzel, A. S., Qing, X., Cruciani, G., Boussaad, I., Jäger, C., Rakovic, A., Berger, E., Bolognin, S., Antony, P. M. A., Klein, C., Krüger, R., Seibler, P., & Schwamborn, J. C. (2019). Parkinson's disease phenotypes in patient specific brain organoids are improved by HP- $\beta$ -CD treatment. *BioRxiv*, 813089. <https://doi.org/10.1101/813089>
- Jia, F., Fellner, A., & Kumar, K. R. (2022). *Monogenic Parkinson's Disease: Genotype, Phenotype, Pathophysiology, and Genetic Testing*.
- Jiang, P., Scarpa, J. R., Gao, V. D., Vitaterna, M. H., Kasarskis, A., & Turek, F. W. (2019). Parkinson's Disease is Associated with Dysregulations of a Dopamine-Modulated Gene Network Relevant to Sleep and Affective Neurobehaviors in the Striatum. *Scientific Reports*, *9*(1), 1–14. <https://doi.org/10.1038/s41598-019-41248-4>
- Jo, J., Xiao, Y., Sun, A. X., Cukuroglu, E., Tran, H. D., Göke, J., Tan, Z. Y., Saw, T. Y., Tan, C. P., Lokman, H., Lee, Y., Kim, D., Ko, H. S., Kim, S. O., Park, J. H., Cho, N. J., Hyde, T. M., Kleinman, J. E., Shin, J. H., ... Ng, H. H. (2016a). Midbrain-like Organoids from Human Pluripotent Stem Cells Contain Functional Dopaminergic and Neuromelanin-Producing Neurons. *Cell Stem Cell*, *19*(2), 248–257. <https://doi.org/10.1016/j.stem.2016.07.005>
- Jo, J., Xiao, Y., Sun, A. X., Cukuroglu, E., Tran, H. D., Göke, J., Tan, Z. Y., Saw, T. Y., Tan, C. P., Lokman, H., Lee, Y., Kim, D., Ko, H. S., Kim, S. O., Park, J. H., Cho, N. J., Hyde, T. M., Kleinman, J. E., Shin, J. H., ... Ng, H. H. (2016b). Midbrain-like Organoids from Human Pluripotent Stem Cells Contain Functional Dopaminergic and Neuromelanin-Producing Neurons. *Cell Stem Cell*, *19*(2), 248–257. <https://doi.org/10.1016/j.stem.2016.07.005>
- Jo, J., Yang, L., Tran, H.-D., Yu, W., Xuyang Sun, A., Yin Chang, Y., Chul Jung, B., Lee, S.-J., Yih Saw, T., Xiao, B., Tze Ting Khoo, A., Yaw, L.-P., Jiixin Xie, J., Lokman, H., Ong, W.-Y., Gui Yin Lim, G., Lim, K.-L., Tan, E.-K., Ng, H.-H., & Shawn Je, H. (2021). *Lewy Body-like Inclusions in Human Midbrain Organoids Carrying Glucocerebrosidase and  $\alpha$ -Synuclein Mutations*. <https://doi.org/10.1002/ana.26166>

- 
- Jones, K. L., Zhou, M., & Jhaveri, D. J. (2022). Dissecting the role of adult hippocampal neurogenesis towards resilience versus susceptibility to stress-related mood disorders. In *npj Science of Learning* (Vol. 7, Issue 1). <https://doi.org/10.1038/s41539-022-00133-y>
- Juopperi, T. A., Kim, W. R., Chiang, C. H., Yu, H., Margolis, R. L., Ross, C. A., Ming, G. L., & Song, H. (2012). Astrocytes generated from patient induced pluripotent stem cells recapitulate features of Huntingtons disease patient cells. *Molecular Brain*, *5*(1), 1–14. <https://doi.org/10.1186/1756-6606-5-17>
- Jurk, D., Wang, C., Miwa, S., Maddick, M., Korolchuk, V., Tsolou, A., Gonos, E. S., Thrasivoulou, C., Jill Saffrey, M., Cameron, K., & von Zglinicki, T. (2012). Postmitotic neurons develop a p21-dependent senescence-like phenotype driven by a DNA damage response. *Aging Cell*, *11*(6), 996–1004. <https://doi.org/10.1111/j.1474-9726.2012.00870.x>
- Kamath, T., Abdurouf, A., Burris, S. J., Langlieb, J., Gazestani, V., Nadaf, N. M., Balderrama, K., Vanderburg, C., & Macosko, E. Z. (2022). Single-cell genomic profiling of human dopamine neurons identifies a population that selectively degenerates in Parkinson’s disease. *Nature Neuroscience*, *25*(5), 588–595. <https://doi.org/10.1038/s41593-022-01061-1>
- Kastner, A., Hirsch, E. C., Agid, Y., & Javoy-Agid, F. (1993). Tyrosine hydroxylase protein and messenger RNA in the dopaminergic nigral neurons of patients with Parkinson’s disease. *Brain Research*, *606*(2), 341–345. [https://doi.org/10.1016/0006-8993\(93\)91005-D](https://doi.org/10.1016/0006-8993(93)91005-D)
- Kee, T. R., Gonzalez, P. E., Wehinger, J. L., Bukhari, M. Z., Ermekbaeva, A., Sista, A., & Kotsiviras, P. (2021). *Mitochondrial CHCHD2: Disease-Associated Mutations, Physiological Functions, and Current Animal Models*. *13*(April), 1–15. <https://doi.org/10.3389/fnagi.2021.660843>
- Khan, T., Seetharam, A. S., Zhou, J., Bivens, N. J., Schust, D. J., Ezashi, T., Tuteja, G., & Roberts, R. M. (2021). Single Nucleus RNA Sequence (snRNAseq) Analysis of the Spectrum of Trophoblast Lineages Generated From Human Pluripotent Stem Cells in vitro. *Frontiers in Cell and Developmental Biology*, *9*(July). <https://doi.org/10.3389/fcell.2021.695248>
- Kim, H., Park, H. J., Choi, H., Chang, Y., Park, H., Shin, J., Kim, J., Lengner, C. J., Lee, Y. K., & Kim, J. (2019). Modeling G2019S-LRRK2 Sporadic Parkinson’s Disease in 3D Midbrain Organoids. *Stem Cell Reports*, *12*(3), 518–531. <https://doi.org/10.1016/j.stemcr.2019.01.020>
- Kim, J., Koo, B. K., & Knoblich, J. A. (2020). Human organoids: model systems for human biology and medicine. In *Nature Reviews Molecular Cell Biology* (Vol. 21, Issue 10, pp. 571–584). <https://doi.org/10.1038/s41580-020-0259-3>
- Kim, J., Su, S. C., Wang, H., Cheng, A. W., Cassady, J. P., Lodato, M. A., Lengner, C. J., Chung, C. Y.,



- 
- Dawlaty, M. M., Tsai, L. H., & Jaenisch, R. (2011). Functional integration of dopaminergic neurons directly converted from mouse fibroblasts. *Cell Stem Cell*, 9(5), 413–419. <https://doi.org/10.1016/j.stem.2011.09.011>
- Kim, S., Min, S., Choi, Y. S., Jo, S. H., Jung, J. H., Han, K., Kim, J., An, S., Ji, Y. W., Kim, Y. G., & Cho, S. W. (2022). Tissue extracellular matrix hydrogels as alternatives to Matrigel for culturing gastrointestinal organoids. *Nature Communications*, 13(1). <https://doi.org/10.1038/s41467-022-29279-4>
- Kim, S. W., Woo, H. J., Kim, E. H., Kim, H. S., Suh, H. N., Kim, S. hyun, Song, J. J., Wulansari, N., Kang, M., Choi, S. Y., Choi, S. J., Jang, W. H., Lee, J., Kim, K. H., Lee, W., Kim, S. H., Yang, J., Kyung, J., Lee, H. S., ... Lee, S. H. (2021). Neural stem cells derived from human midbrain organoids as a stable source for treating Parkinson's disease: Midbrain organoid-NSCs (Og-NSC) as a stable source for PD treatment. *Progress in Neurobiology*, 204(May), 102086. <https://doi.org/10.1016/j.pneurobio.2021.102086>
- Kin, K., Yasuhara, T., Kameda, M., & Date, I. (2019). Animal models for Parkinson's disease research: Trends in the 2000s. In *International Journal of Molecular Sciences* (Vol. 20, Issue 21). <https://doi.org/10.3390/ijms20215402>
- Kong, W., Mou, X., Liu, Q., Chen, Z., Vanderburg, C. R., Rogers, J. T., & Huang, X. (2009). *Molecular Neurodegeneration Independent component analysis of Alzheimer's DNA microarray gene expression data*. <https://doi.org/10.1186/1750-1326-4-5>
- Kouli, A., Torsney, K. M., Kuan, W.-L., Van Geest Centre, J., & Repair, B. (2018). Parkinson's Disease: Pathogenesis and Clinical Aspects. In *Parkinson's Disease: Pathogenesis and Clinical Aspects*. <https://doi.org/10.15586/codonpublications.parkinsonsdisease.2018>
- Kouroupi, G., Taoufik, E., Vlachos, I. S., Tsiaras, K., Antoniou, N., Papastefanaki, F., Chroni-Tzartou, D., Wrasidlo, W., Bohl, D., Stellas, D., Politis, P. K., Vekrellis, K., Papadimitriou, D., Stefanis, L., Bregestovski, P., Hatzigeorgiou, A. G., Masliah, E., & Matsas, R. (2017). Defective synaptic connectivity and axonal neuropathology in a human iPSC-based model of familial Parkinson's disease. *Proceedings of the National Academy of Sciences of the United States of America*, 114(18), E3679–E3688. <https://doi.org/10.1073/pnas.1617259114>
- Kumari, R., & Jat, P. (2021). Mechanisms of Cellular Senescence: Cell Cycle Arrest and Senescence Associated Secretory Phenotype. *Frontiers in Cell and Developmental Biology*, 9(March), 1–24. <https://doi.org/10.3389/fcell.2021.645593>
- Kutner, R. H., Zhang, X. Y., & Reiser, J. (2009). Production, concentration and titration of pseudotyped

- 
- HIV-1-based lentiviral vectors. *Nature Protocols*, 4(4), 495–505.  
<https://doi.org/10.1038/nprot.2009.22>
- Kwak, T. H., Kang, J. H., Hali, S., Kim, J., Kim, K. P., Park, C., Lee, J. H., Ryu, H. K., Na, J. E., Jo, J., Je, H. S., Ng, H. H., Kwon, J., Kim, N. H., Hong, K. H., Sun, W., Chung, C. H., Rhyu, I. J., & Han, D. W. (2020). Generation of homogeneous midbrain organoids with in vivo-like cellular composition facilitates neurotoxin-based Parkinson's disease modeling. *Stem Cells*, 38(6), 727–740.  
<https://doi.org/10.1002/stem.3163>
- La Manno, G., Gyllborg, D., Codeluppi, S., Nishimura, K., Salto, C., Zeisel, A., Borm, L. E., Stott, S. R. W., Toledo, E. M., Villaescusa, J. C., Lönnerberg, P., Ryge, J., Barker, R. A., Arenas, E., & Linnarsson, S. (2016). Molecular Diversity of Midbrain Development in Mouse, Human, and Stem Cells. *Cell*, 167(2), 566–580.e19. <https://doi.org/10.1016/j.cell.2016.09.027>
- Lama, J., Buhidma, Y., Fletcher, E. J. R., & Duty, S. (2021). Animal models of Parkinson's disease: a guide to selecting the optimal model for your research. *Neuronal Signaling*, 5(4), 1–24.  
<https://doi.org/10.1042/ns20210026>
- Lamprey, R. N. L., Chaulagain, B., Trivedi, R., Gothwal, A., Layek, B., & Singh, J. (2022). A Review of the Common Neurodegenerative Disorders: Current Therapeutic Approaches and the Potential Role of Nanotherapeutics. In *International Journal of Molecular Sciences* (Vol. 23, Issue 3).  
<https://doi.org/10.3390/ijms23031851>
- Lancaster, M. A., Renner, M., Martin, C. A., Wenzel, D., Bicknell, L. S., Hurles, M. E., Homfray, T., Penninger, J. M., Jackson, A. P., & Knoblich, J. A. (2013). Cerebral organoids model human brain development and microcephaly. *Nature*, 501(7467), 373–379.  
<https://doi.org/10.1038/nature12517>
- Lanfer, J., Kaindl, J., Krumm, L., Acera, M. G., Neurath, M., Regensburger, M., Krach, F., & Winner, B. (2022). Efficient and Easy Conversion of Human iPSCs into Functional Induced Microglia-like Cells. *International Journal of Molecular Sciences*, 23(9). <https://doi.org/10.3390/ijms23094526>
- Lapasset, L., Milhavet, O., Prieur, A., Besnard, E., Babled, A., Ät-Hamou, N., Leschik, J., Pellestor, F., Ramirez, J. M., De Vos, J., Lehmann, S., & Lemaitre, J. M. (2011). Rejuvenating senescent and centenarian human cells by reprogramming through the pluripotent state. *Genes and Development*, 25(21), 2248–2253. <https://doi.org/10.1101/gad.173922.111>
- Lardenoije, R., Iatrou, A., Kenis, G., Kompotis, K., Steinbusch, H. W. M., Mastroeni, D., Coleman, P., Lemere, C. A., Hof, P. R., van den Hove, D. L. A., & Rutten, B. P. F. (2015). The epigenetics of aging and neurodegeneration. *Progress in Neurobiology*, 131, 21–64.

---

<https://doi.org/10.1016/j.pneurobio.2015.05.002>

- Le Grand, J. N., Gonzalez-Cano, L., Pavlou, M. A., & Schwamborn, J. C. (2015). Neural stem cells in Parkinson's disease: A role for neurogenesis defects in onset and progression. *Cellular and Molecular Life Sciences*, 72(4), 773–797. <https://doi.org/10.1007/s00018-014-1774-1>
- Le, W. D., Conneely, O. M., He, Y., Jankovic, J., & Appel, S. H. (1999). Reduced Nurr1 expression increases the vulnerability of mesencephalic dopamine neurons to MPTP-induced injury. *Journal of Neurochemistry*, 73(5), 2218–2221. <https://doi.org/10.1046/j.1471-4159.1999.02218.x>
- Lebedeva, O. S., Sharova, E. I., Grekhnev, D. A., Skorodumova, L. O., Kopylova, I. V, Vassina, E. M., Oshkolova, A., Novikova, I. V, Krisanova, A. V, Olekhnovich, E. I., Vigont, V. A., Kaznacheyeva, E. V, Bogomazova, A. N., & Lagarkova, M. A. (2023). An Efficient 2D Protocol for Differentiation of iPSCs into Mature Postmitotic Dopaminergic Neurons: Application for Modeling Parkinson's Disease. *International Journal of Molecular Sciences*, 24(8). <https://doi.org/10.3390/ijms24087297>
- Leventoux, N., Morimoto, S., Imaizumi, K., Sato, Y., Takahashi, S., Mashima, K., Ishikawa, M., Sonn, I., Kondo, T., Watanabe, H., & Okano, H. (2020). Human Astrocytes Model Derived from Induced Pluripotent Stem Cells. *Cells*, 9(12). <https://doi.org/10.3390/cells9122680>
- Li, H., Jiang, H., Li, H., Li, L., Yan, Z., & Feng, J. (2022). Generation of human A9 dopaminergic pacemakers from induced pluripotent stem cells. *Molecular Psychiatry*, 27(11), 4407–4418. <https://doi.org/10.1038/s41380-022-01628-1>
- Li, J., Dani, J. A., & Le, W. (2009). The role of transcription factor Pitx3 in dopamine neuron development and Parkinson's disease. *Current Topics in Medicinal Chemistry*, 9(10), 855–859. <http://www.pubmedcentral.nih.gov/articlerender.fcgi?artid=2872921&tool=pmcentrez&render type=abstract>
- Li, J., Pan, L., Pembroke, W. G., Rexach, J. E., Godoy, M. I., Condro, M. C., Alvarado, A. G., Harteni, M., Chen, Y. W., Stiles, L., Chen, A. Y., Wanner, I. B., Yang, X., Goldman, S. A., Geschwind, D. H., Kornblum, H. I., & Zhang, Y. (2021). Conservation and divergence of vulnerability and responses to stressors between human and mouse astrocytes. *Nature Communications*, 12(1). <https://doi.org/10.1038/s41467-021-24232-3>
- Li, L. H., Qin, H. Z., Wang, J. L., Wang, J., Wang, X. L., & Gao, G. D. (2009). Axonal degeneration of nigro-striatum dopaminergic neurons induced by 1-methyl-4-phenyl-1,2,3,6-tetrahydropyridine in mice. *Journal of International Medical Research*, 37(2), 455–463. <https://doi.org/10.1177/147323000903700221>
- Li, P., & Elowitz, M. B. (2019). Communication codes in developmental signaling pathways.

- 
- Development (Cambridge)*, 146(12), 1–12. <https://doi.org/10.1242/dev.170977>
- Li, Q., & Barres, B. A. (2018). Microglia and macrophages in brain homeostasis and disease. In *Nature Reviews Immunology* (Vol. 18, Issue 4, pp. 225–242). <https://doi.org/10.1038/nri.2017.125>
- Li, X., & Wang, C. Y. (2021). From bulk, single-cell to spatial RNA sequencing. *International Journal of Oral Science*, 13(1), 1–6. <https://doi.org/10.1038/s41368-021-00146-0>
- Li, Z., Yue, M., Liu, Y., Zhang, P., Qing, J., Liu, H., & Zhou, Y. (2022). Advances of Engineered Hydrogel Organoids within the Stem Cell Field: A Systematic Review. In *Gels* (Vol. 8, Issue 6). <https://doi.org/10.3390/gels8060379>
- Lim, K. L. (2010). Non-mammalian animal models of Parkinson's disease for drug discovery. *Expert Opinion on Drug Discovery*, 5(2), 165–176. <https://doi.org/10.1517/17460440903527675>
- Lin, L., Göke, J., Cukuroglu, E., Dranias, M. R., VanDongen, A. M. J., & Stanton, L. W. (2016). Molecular Features Underlying Neurodegeneration Identified through In Vitro Modeling of Genetically Diverse Parkinson's Disease Patients. *Cell Reports*, 15(11), 2411–2426. <https://doi.org/10.1016/j.celrep.2016.05.022>
- Lin, T., Liu, G. A., Perez, E., Rainer, R. D., Febo, M., Cruz-Almeida, Y., & Ebner, N. C. (2018). Systemic inflammation mediates age-related cognitive deficits. *Frontiers in Aging Neuroscience*, 10(AUG), 1–9. <https://doi.org/10.3389/fnagi.2018.00236>
- Liu, X., Wang, Q., Yang, Y., Stewart, T., Shi, M., Soltys, D., Liu, G., Thorland, E., Cilento, E. M., Hou, Y., Liu, Z., Feng, T., & Zhang, J. (2021). Reduced erythrocytic CHCHD2 mRNA is associated with brain pathology of Parkinson's disease. *Acta Neuropathologica Communications*, 1–16. <https://doi.org/10.1186/s40478-021-01133-6>
- Loerch, P. M., Lu, T., Dakin, K. A., Vann, J. M., Isaacs, A., Geula, C., Wang, J., Pan, Y., Gabuzda, D. H., Li, C., Prolla, T. A., & Yankner, B. A. (2008). Evolution of the aging brain transcriptome and synaptic regulation. *PLoS ONE*, 3(10). <https://doi.org/10.1371/journal.pone.0003329>
- Lombares, C. De, Heude, E., Alfama, G., Fontaine, A., Hassouna, R., Vernochet, C., Chaumont, F. De, Olivo-marin, C., Ey, E., Tronche, F., Bourgeron, T., Luquet, S., & Levi, G. (2019). *Dlx5 and Dlx6 expression in GABAergic neurons controls behavior, metabolism, healthy aging and lifespan*. 11(17), 6638–6656.
- López-Otín, C., Blasco, M. A., Partridge, L., Serrano, M., & Kroemer, G. (2013). The hallmarks of aging. *Cell*, 153(6), 1194. <https://doi.org/10.1016/j.cell.2013.05.039>
- López-Otín, C., Blasco, M. A., Partridge, L., Serrano, M., & Kroemer, G. (2023). Hallmarks of aging: An expanding universe. *Cell*, 186(2), 243–278. <https://doi.org/10.1016/j.cell.2022.11.001>

- 
- Lubec, J., Kalaba, P., Hussein, A. M., Feyissa, D. D., Kotob, M. H., Mahmoud, R. R., Wieder, O., Garon, A., Sagheddu, C., Ilic, M., Dragačević, V., Cybulska-Klosowicz, A., Zehl, M., Wackerlig, J., Sartori, S. B., Ebner, K., Kouhnavardi, S., Roller, A., Gajic, N., ... Lubec, G. (2021). Reinstatement of synaptic plasticity in the aging brain through specific dopamine transporter inhibition. *Molecular Psychiatry*, 26(12), 7076–7090. <https://doi.org/10.1038/s41380-021-01214-x>
- Mahajani, S., Raina, A., Fokken, C., Kügler, S., & Bähr, M. (2019). Homogenous generation of dopaminergic neurons from multiple hiPSC lines by transient expression of transcription factors. *Cell Death and Disease*, 10(12). <https://doi.org/10.1038/s41419-019-2133-9>
- Makrygianni, E. A., & Chrousos, G. P. (2021). From Brain Organoids to Networking Assembloids: Implications for Neuroendocrinology and Stress Medicine. *Frontiers in Physiology*, 12(June). <https://doi.org/10.3389/fphys.2021.621970>
- Marchionini, D. M., Lehrmann, E., Chu, Y., He, B., Sortwell, C. E., Becker, K. G., Freed, W. J., Kordower, J. H., & Collier, T. J. (2007). Role of heparin binding growth factors in nigrostriatal dopamine system development and Parkinson's disease. *Brain Research*, 1147(1), 77–88. <https://doi.org/10.1016/j.brainres.2007.02.028>
- Matias, I., Pereira, L., Isabella, D., Damico, V., Paula, A., Araujo, B., Neves, S., Vargas, G., Leite, R. E. P., Suemoto, C. K., Jacob, R. N. W., Grinberg, L. T., Hol, E. M., Middeldorp, J., Carvalho, F., & Gomes, A. (2022). Loss of lamin- B1 and defective nuclear morphology are hallmarks of astrocyte senescence in vitro and in the aging human hippocampus. *February 2021*, 1–18. <https://doi.org/10.1111/accel.13521>
- McHugh, D., & Gil, J. (2018). Senescence and aging: Causes, consequences, and therapeutic avenues. *Journal of Cell Biology*, 217(1), 65–77. <https://doi.org/10.1083/jcb.201708092>
- Meng, H., Yamashita, C., Shiba-fukushima, K., Inoshita, T., Funayama, M., Sato, S., Hatta, T., Natsume, T., Umitsu, M., Takagi, J., & Imai, Y. (2017). Loss of Parkinson's disease-associated protein CHCHD2 affects mitochondrial crista structure and destabilizes cytochrome c. *Nature Communications*, 8, 1–18. <https://doi.org/10.1038/ncomms15500>
- Miller, J. D., Ganat, Y. M., Kishinevsky, S., Bowman, R. L., Liu, B., Tu, E. Y., Mandal, P. K., Vera, E., Shim, J. W., Kriks, S., Taldone, T., Fusaki, N., Tomishima, M. J., Krainc, D., Milner, T. A., Rossi, D. J., & Studer, L. (2013). Human iPSC-based modeling of late-onset disease via progerin-induced aging. *Cell Stem Cell*, 13(6), 691–705. <https://doi.org/10.1016/j.stem.2013.11.006>
- Mišić, B., Sporns, O., & McIntosh, A. R. (2014). Communication Efficiency and Congestion of Signal Traffic in Large-Scale Brain Networks. *PLoS Computational Biology*, 10(1).

---

<https://doi.org/10.1371/journal.pcbi.1003427>

- Mittelbronn, M., Dietz, K., Schluesener, H. J., & Meyermann, R. (2001). Local distribution of microglia in the normal adult human central nervous system differs by up to one order of magnitude. *Acta Neuropathologica*, *101*(3), 249–255. <https://doi.org/10.1007/s004010000284>
- Miura, Y., Li, M. Y., Birey, F., Ikeda, K., Revah, O., Thete, M. V., Park, J. Y., Puno, A., Lee, S. H., Porteus, M. H., & Pasca, S. P. (2020). Generation of human striatal organoids and cortico-striatal assembloids from human pluripotent stem cells. *Nature Biotechnology*, *38*(12), 1421–1430. <https://doi.org/10.1038/s41587-020-00763-w>
- Miwa, H., Kubo, T., Suzuki, A., Nishi, K., & Kondo, T. (2005). Retrograde dopaminergic neuron degeneration following intrastriatal proteasome inhibition. *Neuroscience Letters*, *380*(1–2), 93–98. <https://doi.org/10.1016/j.neulet.2005.01.024>
- Miyamichi, K., Amat, F., Moussavi, F., Wang, C., Wickersham, I., Wall, N. R., Taniguchi, H., Tasic, B., Huang, Z. J., He, Z., Callaway, E. M., Horowitz, M. A., & Luo, L. (2011). Cortical representations of olfactory input by trans-synaptic tracing. *Nature*. <https://doi.org/10.1038/nature09714>
- Mohamed, N. V., Sirois, J., Ramamurthy, J., Mathur, M., Lépine, P., Deneault, E., Maussion, G., Nicouleau, M., Chen, C. X. Q., Abdian, N., Soubannier, V., Cai, E., Nami, H., Thomas, R. A., Wen, D., Tabatabaei, M., Beitel, L. K., Dolt, K. S., Karamchandani, J., ... Durcan, T. M. (2021). Midbrain organoids with an SNCA gene triplication model key features of synucleinopathy. *Brain Communications*, *3*(4), 1–21. <https://doi.org/10.1093/braincomms/fcab223>
- Moisoi, N., Fedele, V., Edwards, J., & Martins, L. M. (2014). Loss of PINK1 enhances neurodegeneration in a mouse model of Parkinson’s disease triggered by mitochondrial stress. *Neuropharmacology*, *77*, 350–357. <https://doi.org/10.1016/j.neuropharm.2013.10.009>
- Monzel, A. S., Hemmer, K., Kaoma, T., Smits, L. M., Bolognin, S., Lucarelli, P., Rosety, I., Zagare, A., Antony, P., Nickels, S. L., Krueger, R., Azuaje, F., & Schwamborn, J. C. (2020). Machine learning-assisted neurotoxicity prediction in human midbrain organoids. *Parkinsonism and Related Disorders*, *75*(May), 105–109. <https://doi.org/10.1016/j.parkreldis.2020.05.011>
- Monzel, A. S., Smits, L. M., Hemmer, K., Hachi, S., Moreno, E. L., van Wuellen, T., Jarazo, J., Walter, J., Brüggemann, I., Boussaad, I., Berger, E., Fleming, R. M. T., Bolognin, S., & Schwamborn, J. C. (2017). Derivation of Human Midbrain-Specific Organoids from Neuroepithelial Stem Cells. *Stem Cell Reports*, *8*(5), 1144–1154. <https://doi.org/10.1016/j.stemcr.2017.03.010>
- Moreno-Blas, D., Gorostieta-Salas, E., Pommer-Alba, A., Muciño, G., Gerónimo-Olvera, C., Maciel-Barón, L. A., Königsberg, M., & Castro-Obregón, S. (2019). Cortical neurons develop a senescence-

- 
- like phenotype promoted by dysfunctional autophagy. *Aging*, 11(16).
- Moreno-Rodriguez, M., Perez, S. E., Nadeem, M., Malek-Ahmadi, M., & Mufson, E. J. (2020). Frontal cortex chitinase and pentraxin neuroinflammatory alterations during the progression of Alzheimer's disease. *Journal of Neuroinflammation*, 17(1), 1–15. <https://doi.org/10.1186/s12974-020-1723-x>
- Mosevitsky, M. I. (2022). Progerin and Its Role in Accelerated and Natural Aging. In *Molecular Biology* (Vol. 56, Issue 2, pp. 125–146). © Pleiades Publishing, Inc. <https://doi.org/10.1134/S0026893322020091>
- Moysidou, C. M., Barberio, C., & Owens, R. M. (2021). Advances in Engineering Human Tissue Models. In *Frontiers in Bioengineering and Biotechnology* (Vol. 8, p. 620962). <https://doi.org/10.3389/fbioe.2020.620962>
- Muzio, L., Viotti, A., & Martino, G. (2021). Microglia in Neuroinflammation and Neurodegeneration: From Understanding to Therapy. In *Frontiers in Neuroscience* (Vol. 15). <https://doi.org/10.3389/fnins.2021.742065>
- Nagatsu, T., & Sawada, M. (2007). Biochemistry of postmortem brains in Parkinson's disease: Historical overview and future prospects. In *Journal of Neural Transmission, Supplementa* (Issue 72, pp. 113–120). Springer-Verlag. [https://doi.org/10.1007/978-3-211-73574-9\\_14](https://doi.org/10.1007/978-3-211-73574-9_14)
- Nair, A. G., Bhalla, U. S., & Hellgren Kotaleski, J. (2016). Role of DARPP-32 and ARPP-21 in the Emergence of Temporal Constraints on Striatal Calcium and Dopamine Integration. *PLoS Computational Biology*, 12(9), 1–28. <https://doi.org/10.1371/journal.pcbi.1005080>
- Nguyen, K. V. (2019).  $\beta$ -Amyloid precursor protein (APP) and the human diseases. In *AIMS Neuroscience* (Vol. 6, Issue 4, pp. 273–281). <https://doi.org/10.3934/Neuroscience.2019.4.273>
- Nguyen, V., Chavali, M., Larphaveesarp, A., Kodali, S., Gonzalez, G., Franklin, R. J. M., Rowitch, D. H., & Gonzalez, F. (2021). Neuroprotective effects of Sonic hedgehog agonist SAG in a rat model of neonatal stroke. *Pediatric Research*, 90(6), 1161–1170. <https://doi.org/10.1038/s41390-021-01408-7>
- Nickels, S. L., Modamio, J., Mendes-Pinheiro, B., Monzel, A. S., Betsou, F., & Schwamborn, J. C. (2020). Reproducible generation of human midbrain organoids for in vitro modeling of Parkinson's disease. *Stem Cell Research*, 46(June), 101870. <https://doi.org/10.1016/j.scr.2020.101870>
- Noda, M., & Suzumura, A. (2012). Sweepers in the CNS: Microglial migration and phagocytosis in the Alzheimer disease pathogenesis. *International Journal of Alzheimer's Disease*, 2012. <https://doi.org/10.1155/2012/891087>

- 
- Nunes, I., Tovmasian, L. T., Silva, R. M., Burke, R. E., & Goff, S. P. (2003). Pitx3 is required for development of substantia nigra dopaminergic neurons. *Proceedings of the National Academy of Sciences of the United States of America*, *100*(7), 4245–4250. <https://doi.org/10.1073/pnas.0230529100>
- Oh, H., Lewis, D. A., & Sibille, E. (2016). *The Role of BDNF in Age-Dependent Changes of Excitatory and Inhibitory Synaptic Markers in the Human Prefrontal Cortex*. *2*, 3080–3091. <https://doi.org/10.1038/npp.2016.126>
- Orav, E., Atanasova, T., Shintyapina, A., Kesaf, S., Kokko, M., Partanen, J., Taira, T., & Lauri, S. E. (2017). NETO1 guides development of glutamatergic connectivity in the hippocampus by regulating axonal kainate receptors. *ENeuro*, *4*(3). <https://doi.org/10.1523/ENEURO.0048-17.2017>
- Ormel, P. R., Vieira de Sá, R., van Bodegraven, E. J., Karst, H., Harschnitz, O., Sneeboer, M. A. M., Johansen, L. E., van Dijk, R. E., Scheefhals, N., Berdenis van Berlekom, A., Ribes Martínez, E., Kling, S., MacGillavry, H. D., van den Berg, L. H., Kahn, R. S., Hol, E. M., de Witte, L. D., & Pasterkamp, R. J. (2018). Microglia innately develop within cerebral organoids. *Nature Communications*, *9*(1). <https://doi.org/10.1038/s41467-018-06684-2>
- Osakada, F., & Callaway, E. M. (2013). Design and generation of recombinant rabies virus vectors. *Nature Protocols*, *8*(8), 1583–1601. <https://doi.org/10.1038/nprot.2013.094>
- Pang, S. Y. Y., Ho, P. W. L., Liu, H. F., Leung, C. T., Li, L., Chang, E. E. S., Ramsden, D. B., & Ho, S. L. (2019). The interplay of aging, genetics and environmental factors in the pathogenesis of Parkinson's disease. *Translational Neurodegeneration*, *8*(1), 1–11. <https://doi.org/10.1186/s40035-019-0165-9>
- Panoutsopoulos, A. A. (2020). Organoids, Assembloids, and Novel Biotechnology: Steps Forward in Developmental and Disease-Related Neuroscience. *Neuroscientist*. <https://doi.org/10.1177/1073858420960112>
- Papaspyropoulos, A., Tsolaki, M., Foroglou, N., & Pantazaki, A. A. (2020). Modeling and Targeting Alzheimer's Disease With Organoids. In *Frontiers in Pharmacology* (Vol. 11). <https://doi.org/10.3389/fphar.2020.00396>
- Parisiadou, L., & Cai, H. (2010). LRRK2 function on actin and microtubule dynamics in Parkinson disease. *Communicative and Integrative Biology*, *3*(5), 396–400. <https://doi.org/10.4161/cib.3.5.12286>
- Park, H., Kim, H., Yoo, J., Lee, J., Choi, H., Baek, S., Lee, C. J., Kim, J., Lengner, C. J., Sung, J. S., & Kim, J. (2015). Homogeneous generation of iDA neurons with high similarity to bona fide DA neurons using a drug inducible system. *Biomaterials*, *72*, 152–162.



---

<https://doi.org/10.1016/j.biomaterials.2015.09.002>

- Pasca, A. M., Sloan, S. A., Clarke, L. E., Tian, Y., Makinson, C. D., Huber, N., Kim, C. H., Park, J. Y., O'Rourke, N. A., Nguyen, K. D., Smith, S. J., Huguenard, J. R., Geschwind, D. H., Barres, B. A., & Pasca, S. P. (2015). Functional cortical neurons and astrocytes from human pluripotent stem cells in 3D culture. *Nature Methods*, *12*(7), 671–678. <https://doi.org/10.1038/nmeth.3415>
- Paşca, S. P. (2018). The rise of three-dimensional human brain cultures. *Nature*, *553*(7689), 437–445. <https://doi.org/10.1038/nature25032>
- Patthey, C., & Gunhaga, L. (2014). Signaling pathways regulating ectodermal cell fate choices. In *Experimental Cell Research* (Vol. 321, Issue 1, pp. 11–16). Elsevier. <https://doi.org/10.1016/j.yexcr.2013.08.002>
- Peng, S., Zeng, L., Haure-Mirande, J. V., Wang, M., Huffman, D. M., Haroutunian, V., Ehrlich, M. E., Zhang, B., & Tu, Z. (2021). Transcriptomic Changes Highly Similar to Alzheimer's Disease Are Observed in a Subpopulation of Individuals During Normal Brain Aging. *Frontiers in Aging Neuroscience*, *13*(December), 1–16. <https://doi.org/10.3389/fnagi.2021.711524>
- Plowey, E. D., Johnson, J. W., Steer, E., Zhu, W., Eisenberg, D. A., Valentino, N. M., Liu, Y. J., & Chu, C. T. (2014). Mutant LRRK2 enhances glutamatergic synapse activity and evokes excitotoxic dendrite degeneration. *Biochimica et Biophysica Acta - Molecular Basis of Disease*, *1842*(9), 1596–1603. <https://doi.org/10.1016/j.bbadis.2014.05.016>
- Potashkin, J. A., Blume, S. R., & Runkle, N. K. (2011). Limitations of animal models of Parkinson's disease. In *Parkinson's Disease* (Vol. 658083). <https://doi.org/10.4061/2011/658083>
- Poulin, J. F., Zou, J., Drouin-Ouellet, J., Kim, K. Y. A., Cicchetti, F., & Awatramani, R. B. (2014). Defining midbrain dopaminergic neuron diversity by single-cell gene expression profiling. *Cell Reports*, *9*(3), 930–943. <https://doi.org/10.1016/j.celrep.2014.10.008>
- Preibisch, S., Saalfeld, S., & Tomancak, P. (2009). Globally optimal stitching of tiled 3D microscopic image acquisitions. *Bioinformatics*, *25*(11), 1463–1465. <https://doi.org/10.1093/bioinformatics/btp184>
- Prensa, L., Giménez-Amaya, J. M., Parent, A., Bernácer, J., & Cebrián, C. (2009). The nigrostriatal pathway: Axonal collateralization and compartmental specificity. In *Journal of Neural Transmission, Supplementa* (Issue 73, pp. 49–58). [https://doi.org/10.1007/978-3-211-92660-4\\_4](https://doi.org/10.1007/978-3-211-92660-4_4)
- Prieto, G. A., & Cotman, C. W. (2017). Cytokines and cytokine networks target neurons to modulate long-term potentiation. *Cytokine and Growth Factor Reviews*, *34*(2016), 27–33. <https://doi.org/10.1016/j.cytogfr.2017.03.005>

- 
- Qian, X., Song, H., & Ming, G. L. (2019). Brain organoids: Advances, applications and challenges. *Development (Cambridge)*, 146(8). <https://doi.org/10.1242/dev.166074>
- Qin, J., Chen, S. G., Hu, D., Zeng, L. L., Fan, Y. M., Chen, X. P., & Shen, H. (2015). Predicting individual brain maturity using dynamic functional connectivity. *Frontiers in Human Neuroscience*, 9(JULY). <https://doi.org/10.3389/fnhum.2015.00418>
- Rademakers, T., Horvath, J. M., van Blitterswijk, C. A., & LaPointe, V. L. S. (2019). Oxygen and nutrient delivery in tissue engineering: Approaches to graft vascularization. *Journal of Tissue Engineering and Regenerative Medicine*, 13(10), 1815–1829. <https://doi.org/10.1002/term.2932>
- Raffa, R. B., Danah, J., Tallarida, C. S., Zimmerman, C., Gill, G., Baron, S. J., & Rawls, S. M. (2013). Potential of a planarian model to study certain aspects of anti-Parkinsonism drugs. *Advances in Parkinson's Disease*, 02(03), 70–74. <https://doi.org/10.4236/apd.2013.23014>
- Raz, N., Lindenberger, U., Rodrigue, K. M., Kennedy, K. M., Head, D., Williamson, A., Dahle, C., Gerstorff, D., & Acker, J. D. (2005). Regional brain changes in aging healthy adults: General trends, individual differences and modifiers. *Cerebral Cortex*, 15(11), 1676–1689. <https://doi.org/10.1093/cercor/bhi044>
- Reinhardt, P., Glatza, M., Hemmer, K., Tsytsyura, Y., Thiel, C. S., Höing, S., Moritz, S., Parga, J. A., Wagner, L., Bruder, J. M., Wu, G., Schmid, B., Röpke, A., Klingauf, J., Schwamborn, J. C., Gasser, T., Schöler, H. R., & Sternecker, J. (2013). Derivation and Expansion Using Only Small Molecules of Human Neural Progenitors for Neurodegenerative Disease Modeling. *PLoS ONE*, 8(3). <https://doi.org/10.1371/journal.pone.0059252>
- Reinius, B., Blunder, M., Brett, F. M., Eriksson, A., Patra, K., Jonsson, J., Jazin, E., & Kullander, K. (2015). Conditional targeting of medium spiny neurons in the striatal matrix. *Frontiers in Behavioral Neuroscience*, 9, 71. <https://doi.org/10.3389/fnbeh.2015.00071>
- Ren, C., Ding, Y., Wei, S., Guan, L., Zhang, C., Ji, Y., Wang, F., Yin, S., & Yin, P. (2019). G2019S Variation in LRRK2: An Ideal Model for the Study of Parkinson's Disease? *Frontiers in Human Neuroscience*, 13(September), 1–6. <https://doi.org/10.3389/fnhum.2019.00306>
- Rodriguez-Gatica, J. E., Iefremova, V., Sokhranyaeva, L., Yeung, S. W. C. A., Breitzkreuz, Y., Brüstle, O., Schwarz, M. K., & Kubitscheck, U. (2022). Imaging three-dimensional brain organoid architecture from meso- to nanoscale across development. *Development*, 149(20). <https://doi.org/10.1242/dev.200439>
- Rossiello, F., Jurk, D., Passos, J. F., & d'Adda di Fagagna, F. (2022). Telomere dysfunction in ageing and age-related diseases. *Nature Cell Biology*, 24(2), 135–147. <https://doi.org/10.1038/s41556-022->

- Roychoudhury, K., Salomone, J., Qin, S., Cain, B., Adam, M., Steven Potter, S., Nakafuku, M., Gebelein, B., & Campbell, K. (2020). Physical interactions between Gsx2 and Ascl1 balance progenitor expansion versus neurogenesis in the mouse lateral ganglionic eminence. *Development (Cambridge)*, *147*(7). <https://doi.org/10.1242/dev.185348>
- Ryan, S. K., Jordan-Sciutto, K. L., & Anderson, S. A. (2020). Protocol for Tri-culture of hiPSC-Derived Neurons, Astrocytes, and Microglia. *STAR Protocols*, *1*(3), 100190. <https://doi.org/10.1016/j.xpro.2020.100190>
- Sandberg, M., Taher, L., Hu, J., Black, B. L., Nord, A. S., & Rubenstein, J. L. R. (2018). Genomic analysis of transcriptional networks directing progression of cell states during MGE development 06 Biological Sciences 0604 Genetics. *Neural Development*, *13*(1), 1–12. <https://doi.org/10.1186/s13064-018-0119-4>
- Sanfilippo, C., Castrogiovanni, P., Imbesi, R., Kazakowa, M., Musumeci, G., Blennow, K., Zetterberg, H., & Di Rosa, M. (2019). Sex difference in CHI3L1 expression levels in human brain aging and in Alzheimer's disease. *Brain Research*, *1720*(June), 146305. <https://doi.org/10.1016/j.brainres.2019.146305>
- Saorin, G., Caligiuri, I., & Rizzolio, F. (2023). Microfluidic organoids-on-a-chip: The future of human models. *Seminars in Cell and Developmental Biology*, *144*(May 2022), 41–54. <https://doi.org/10.1016/j.semcdb.2022.10.001>
- Schindelin, J., Arganda-Carreras, I., Frise, E., Kaynig, V., Longair, M., Pietzsch, T., Preibisch, S., Rueden, C., Saalfeld, S., Schmid, B., Tinevez, J. Y., White, D. J., Hartenstein, V., Eliceiri, K., Tomancak, P., & Cardona, A. (2012). Fiji: An open-source platform for biological-image analysis. *Nature Methods*, *9*(7), 676–682. <https://doi.org/10.1038/nmeth.2019>
- Schmidt, S. I., Bogetofte, H., Ritter, L., Agergaard, J. B., Hammerich, D., Kabiljagic, A. A., Wlodarczyk, A., Lopez, S. G., Sørensen, M. D., Jørgensen, M. L., Okarmus, J., Serrano, A. M., Kristensen, B. W., Freude, K., Owens, T., & Meyer, M. (2021). Microglia-Secreted Factors Enhance Dopaminergic Differentiation of Tissue- and iPSC-Derived Human Neural Stem Cells. *Stem Cell Reports*, *16*(2), 281–294. <https://doi.org/10.1016/j.stemcr.2020.12.011>
- Schwamborn, J. C. (2018). Is Parkinson's disease a neurodevelopmental disorder and will brain organoids help us to understand it? *Stem Cells and Development*, *27*(14), 968–975. <https://doi.org/10.1089/scd.2017.0289>
- Seegobin, S. P., Heaton, G. R., Liang, D., Choi, I., Blanca Ramirez, M., Tang, B., & Yue, Z. (2020). Progress

- 
- in LRRK2-Associated Parkinson's Disease Animal Models. *Frontiers in Neuroscience*, 14(July). <https://doi.org/10.3389/fnins.2020.00674>
- Shadrina, M., & Slominsky, P. (2021). Modeling Parkinson's Disease: Not Only Rodents? In *Frontiers in Aging Neuroscience* (Vol. 13). <https://doi.org/10.3389/fnagi.2021.695718>
- Shibata, A., & Jeggo, P. A. (2020). Roles for 53BP1 in the repair of radiation-induced DNA double strand breaks. *DNA Repair*, 93, 102915. <https://doi.org/10.1016/j.dnarep.2020.102915>
- Simmnacher, K., Lanfer, J., Rizo, T., Kaindl, J., & Winner, B. (2020). Modeling Cell-Cell Interactions in Parkinson's Disease Using Human Stem Cell-Based Models. In *Frontiers in Cellular Neuroscience* (Vol. 13). <https://doi.org/10.3389/fncel.2019.00571>
- Simpson, D. J., Olova, N. N., & Chandra, T. (2021). Cellular reprogramming and epigenetic rejuvenation. *Clinical Epigenetics*, 13(1), 1–10. <https://doi.org/10.1186/s13148-021-01158-7>
- Singh, A., Liang, L., Kaneoke, Y., Cao, X., & Papa, S. M. (2015). Dopamine regulates distinctively the activity patterns of striatal output neurons in advanced parkinsonian primates. *Journal of Neurophysiology*, 113(5), 1533–1544. <https://doi.org/10.1152/jn.00910.2014>
- Skelton, P. D., Stan, R. V., & Luikart, B. W. (2019). The Role of PTEN in Neurodevelopment. *Complex Psychiatry*, 5(Suppl. 1), 60–71. <https://doi.org/10.1159/000504782>
- Sloan, S. A., Andersen, J., Paşca, A. M., Birey, F., & Paşca, S. P. (2018). Generation and assembly of human brain region-specific three-dimensional cultures. *Nature Protocols*, 13(9), 2062–2085. <https://doi.org/10.1038/s41596-018-0032-7>
- Smits, L. M., Magni, S., Kinugawa, K., Grzyb, K., Luginbühl, J., Sabate-Soler, S., Bolognin, S., Shin, J. W., Mori, E., Skupin, A., & Schwamborn, J. C. (2020). Single-cell transcriptomics reveals multiple neuronal cell types in human midbrain-specific organoids. *Cell and Tissue Research*, 382(3), 463–476. <https://doi.org/10.1007/s00441-020-03249-y>
- Smits, L. M., Reinhardt, L., Reinhardt, P., Glatza, M., Monzel, A. S., Stanslowsky, N., Rosato-Siri, M. D., Zanon, A., Antony, P. M., Bellmann, J., Nicklas, S. M., Hemmer, K., Qing, X., Berger, E., Kalmbach, N., Ehrlich, M., Bolognin, S., Hicks, A. A., Wegner, F., ... Schwamborn, J. C. (2019). Modeling Parkinson's disease in midbrain-like organoids. *Npj Parkinson's Disease*, 5(1). <https://doi.org/10.1038/s41531-019-0078-4>
- Song, L., Yan, Y., Marzano, M., & Li, Y. (2019). Studying heterotypic cell-cell interactions in the human brain using pluripotent stem cell models for neurodegeneration. In *Cells* (Vol. 8, Issue 4). <https://doi.org/10.3390/cells8040299>
- Song, L., Yuan, X., Jones, Z., Vied, C., Miao, Y., Marzano, M., Hua, T., Sang, Q. X. A., Guan, J., Ma, T.,

- 
- Zhou, Y., & Li, Y. (2019). Functionalization of Brain Region-specific Spheroids with Isogenic Microglia-like Cells. *Scientific Reports*, *9*(1). <https://doi.org/10.1038/s41598-019-47444-6>
- Speicher, A. M., Wiendl, H., Meuth, S. G., & Pawlowski, M. (2019). Generating microglia from human pluripotent stem cells: Novel in vitro models for the study of neurodegeneration. *Molecular Neurodegeneration*, *14*(1), 1–16. <https://doi.org/10.1186/s13024-019-0347-z>
- Straccia, M., Barriga, G. G. D., Sanders, P., Bombau, G., Carrere, J., Mairal, P. B., Vinh, N. N., Yung, S., Kelly, C. M., Svendsen, C. N., Kemp, P. J., Arjomand, J., Schoenfeld, R. C., Alberch, J., Allen, N. D., Rosser, A. E., & Canals, J. M. (2015). Quantitative high-throughput gene expression profiling of human striatal development to screen stem cell-derived medium spiny neurons. *Molecular Therapy - Methods and Clinical Development*, *2*(July), 15030. <https://doi.org/10.1038/mtm.2015.30>
- Straniero, L., Guella, I., Cilia, R., Parkkinen, L., Rimoldi, V., Young, A., Asselta, R., Soldà, G., Sossi, V., Stoessl, A. J., Priori, A., Nishioka, K., Hattori, N., Follett, J., Rajput, A., Blau, N., Pezzoli, G., Farrer, M. J., Goldwurm, S., ... Duga, S. (2017). DNAJC12 and dopa-responsive nonprogressive parkinsonism. *Annals of Neurology*, *82*(4), 640–646. <https://doi.org/10.1002/ana.25048>
- Straub, C., Hunt, D. L., Yamasaki, M., Kim, K. S., Watanabe, M., Castillo, P. E., & Tomita, S. (2011). Distinct functions of kainate receptors in the brain are determined by the auxiliary subunit Neto1. *Nature Neuroscience*, *14*(7), 866–873. <https://doi.org/10.1038/nn.2837>
- Sulzer, D., Cragg, S. J., & Rice, M. E. (2016). Striatal dopamine neurotransmission: Regulation of release and uptake. *Basal Ganglia*, *6*(3), 123–148. <https://doi.org/10.1016/j.baga.2016.02.001>
- Sun, X., Sun, F., Zhang, Y., Qu, J., Zhang, W., & Liu, G. H. (2023). A narrative review of organoids for investigating organ aging: opportunities and challenges. *Journal of Bio-X Research*, *6*(1), 3–14. <https://doi.org/10.1097/JBR.000000000000139>
- Sun, X., Zhang, B., Wang, Q., Blennow, K., Zetterberg, H., Yue, Z., Mccarthy, M., Loewenstein, D. A., & Vontell, R. (2021). Association of neurogranin gene expression with Alzheimer ' s disease pathology in the perirhinal cortex. *January*, 1–9. <https://doi.org/10.1002/trc2.12162>
- T. Das, A., Tenenbaum, L., & Berkhout, B. (2016). Tet-On Systems For Doxycycline-inducible Gene Expression. *Current Gene Therapy*, *16*(3), 156–167. <https://doi.org/10.2174/1566523216666160524144041>
- Tabrez, S., R. Jabir, N., Shakil, S., H. Greig, N., Alam, Q., M. Abuzenadah, A., A. Damanhour, G., & A. Kamal, M. (2012). A Synopsis on the Role of Tyrosine Hydroxylase in Parkinson's Disease. *CNS & Neurological Disorders - Drug Targets*, *11*(4), 395–409.

---

<https://doi.org/10.2174/187152712800792785>

- Tagliaferro, P., & Burke, R. E. (2016). Retrograde Axonal Degeneration in Parkinson Disease. *Journal of Parkinson's Disease*, *6*(1), 1–15. <https://doi.org/10.3233/JPD-150769>
- Takahashi, K., Tanabe, K., Ohnuki, M., Narita, M., Ichisaka, T., Tomoda, K., & Yamanaka, S. (2007). Induction of Pluripotent Stem Cells from Adult Human Fibroblasts by Defined Factors. *Cell*, *131*(5), 861–872. <https://doi.org/10.1016/j.cell.2007.11.019>
- Takahashi, K., & Yamanaka, S. (2006). Induction of Pluripotent Stem Cells from Mouse Embryonic and Adult Fibroblast Cultures by Defined Factors. *Cell*, *126*(4), 663–676. <https://doi.org/10.1016/j.cell.2006.07.024>
- Talyansky, S., & Brinkman, B. A. W. (2021). Dysregulation of excitatory neural firing replicates physiological and functional changes in aging visual cortex. *PLoS Computational Biology*, *17*(1), 1–29. <https://doi.org/10.1371/JOURNAL.PCBI.1008620>
- Tanaka, Y., Cakir, B., Xiang, Y., Sullivan, G. J., & Park, I. H. (2020). Synthetic Analyses of Single-Cell Transcriptomes from Multiple Brain Organoids and Fetal Brain. *Cell Reports*, *30*(6), 1682–1689.e3. <https://doi.org/10.1016/j.celrep.2020.01.038>
- Tao, Y., & Zhang, S. C. (2016). Neural Subtype Specification from Human Pluripotent Stem Cells. *Cell Stem Cell*, *19*(5), 573–586. <https://doi.org/10.1016/j.stem.2016.10.015>
- Terzioglu, M., & Galter, D. (2008). Parkinson's disease: Genetic versus toxin-induced rodent models. In *FEBS Journal* (Vol. 275, Issue 7, pp. 1384–1391). <https://doi.org/10.1111/j.1742-4658.2008.06302.x>
- Tolosa, E., Vila, M., Klein, C., & Rascol, O. (2020). LRRK2 in Parkinson disease: challenges of clinical trials. In *Nature Reviews Neurology* (Vol. 16, Issue 2, pp. 97–107). <https://doi.org/10.1038/s41582-019-0301-2>
- Torres-Platas, S. G., Comeau, S., Rachalski, A., Bo, G. D., Cruceanu, C., Turecki, G., Giros, B., & Mechawar, N. (2014). Morphometric characterization of microglial phenotypes in human cerebral cortex. *Journal of Neuroinflammation*, *11*(1), 1–13. <https://doi.org/10.1186/1742-2094-11-12>
- Tran, J., Anastacio, H., & Bardy, C. (2020). Genetic predispositions of Parkinson's disease revealed in patient-derived brain cells. *Npj Parkinson's Disease*, *6*(1). <https://doi.org/10.1038/s41531-020-0110-8>
- Tsarovina, K., Reiff, T., Stubbusch, J., Kurek, D., Grosveld, F. G., Parlato, R., Schütz, G., & Rohrer, H. (2010). The Gata3 transcription factor is required for the survival of embryonic and adult sympathetic neurons. *Journal of Neuroscience*, *30*(32), 10833–10843.

---

<https://doi.org/10.1523/JNEUROSCI.0175-10.2010>

- Ugolini, G. (1995). Specificity of rabies virus as a transneuronal tracer of motor networks: Transfer from hypoglossal motoneurons to connected second-order and higher order central nervous system cell groups. *Journal of Comparative Neurology*, 356(3), 457–480. <https://doi.org/10.1002/cne.903560312>
- Vaiserman, A., & Krasnienkov, D. (2021). Telomere Length as a Marker of Biological Age: State-of-the-Art, Open Issues, and Future Perspectives. *Frontiers in Genetics*, 11(January). <https://doi.org/10.3389/fgene.2020.630186>
- Valiulahi, P., Vidyawan, V., Puspita, L., Oh, Y., Juwono, V. B., Sittipo, P., Friedlander, G., Yahalomi, D., Sohn, J. W., Lee, Y. K., Yoon, J. K., & Shim, J. won. (2021). Generation of caudal-type serotonin neurons and hindbrain-fate organoids from hPSCs. *Stem Cell Reports*, 16(8), 1938–1952. <https://doi.org/10.1016/j.stemcr.2021.06.006>
- van Doorninck, J. H., van Der Wees, J., Karis, A., Goedknecht, E., Engel, J. D., Coesmans, M., Rutteman, M., Grosveld, F., & De Zeeuw, C. I. (1999). GATA-3 is involved in the development of serotonergic neurons in the caudal raphe nuclei. *The Journal of Neuroscience : The Official Journal of the Society for Neuroscience*, 19(12), 2–9. <https://doi.org/10.1523/jneurosci.19-12-j0002.1999>
- Vasudevan, A., & Bhide, P. G. (2008). Angiogenesis in the embryonic CNS: a new twist on an old tale. *Cell Adhesion & Migration*, 2(3), 167–169. <https://doi.org/10.4161/cam.2.3.6485>
- Vera, E., Bosco, N., & Studer, L. (2016). Generating Late-Onset Human iPSC-Based Disease Models by Inducing Neuronal Age-Related Phenotypes through Telomerase Manipulation. *Cell Reports*, 17(4), 1184–1192. <https://doi.org/10.1016/j.celrep.2016.09.062>
- Vizziello, M., Borellini, L., Franco, G., & Ardolino, G. (2021). Disruption of mitochondrial homeostasis: The role of pink1 in parkinson's disease. In *Cells* (Vol. 10, Issue 11). <https://doi.org/10.3390/cells10113022>
- Voytek, B., & Knight, R. T. (2015). Dynamic network communication as a unifying neural basis for cognition, development, aging, and disease. *Biological Psychiatry*, 77(12), 1089–1097. <https://doi.org/10.1016/j.biopsych.2015.04.016>
- Wagner, K. D., & Wagner, N. (2022). The Senescence Markers p16INK4A, p14ARF/p19ARF, and p21 in Organ Development and Homeostasis. *Cells*, 11(12). <https://doi.org/10.3390/cells11121966>
- Walter, J., Bolognin, S., Poovathingal, S. K., Magni, S., Gérard, D., Antony, P. M. A., Nickels, S. L., Salamanca, L., Berger, E., Smits, L. M., Grzyb, K., Perfeito, R., Hoel, F., Qing, X., Ohnmacht, J., Bertacchi, M., Jarazo, J., Ignac, T., Monzel, A. S., ... Schwamborn, J. C. (2021). The Parkinson's-

- 
- disease-associated mutation LRRK2-G2019S alters dopaminergic differentiation dynamics via NR2F1. *Cell Reports*, 37(3). <https://doi.org/10.1016/j.celrep.2021.109864>
- Wang, B., Wang, Z., Sun, L., Yang, L., Li, H., Cole, A. L., Rodriguez-Rivera, J., Lu, H. C., & Zheng, H. (2014). The amyloid precursor protein controls adult hippocampal neurogenesis through GABAergic interneurons. *Journal of Neuroscience*, 34(40), 13314–13325. <https://doi.org/10.1523/JNEUROSCI.2848-14.2014>
- Wang, X., Zhou, X., Li, G., Zhang, Y., Wu, Y., & Song, W. (2017). Modifications and trafficking of APP in the pathogenesis of alzheimer's disease. *Frontiers in Molecular Neuroscience*, 10(September), 1–15. <https://doi.org/10.3389/fnmol.2017.00294>
- Weinhard, L., Di Bartolomei, G., Bolasco, G., Machado, P., Schieber, N. L., Neniskyte, U., Exiga, M., Vadišute, A., Raggioli, A., Schertel, A., Schwab, Y., & Gross, C. T. (2018). Microglia remodel synapses by presynaptic trogocytosis and spine head filopodia induction. *Nature Communications*, 9(1). <https://doi.org/10.1038/s41467-018-03566-5>
- Wilson, D. M., Cookson, M. R., Van Den Bosch, L., Zetterberg, H., Holtzman, D. M., & Dewachter, I. (2023). Hallmarks of neurodegenerative diseases. *Cell*, 186(4), 693–714. <https://doi.org/10.1016/j.cell.2022.12.032>
- Winner, B., Kohl, Z., & Gage, F. H. (2011). Neurodegenerative disease and adult neurogenesis. *European Journal of Neuroscience*, 33(6), 1139–1151. <https://doi.org/10.1111/j.1460-9568.2011.07613.x>
- Winner, B., Melrose, H. L., Zhao, C., Hinkle, K. M., Yue, M., Kent, C., Braithwaite, A. T., Ogholikhan, S., Aigner, R., Winkler, J., Farrer, M. J., & Gage, F. H. (2011). Adult neurogenesis and neurite outgrowth are impaired in LRRK2 G2019S mice. *Neurobiology of Disease*, 41(3), 706–716. <https://doi.org/10.1016/j.nbd.2010.12.008>
- Wong, R. S. H., Mohammad, S., Parayil Sankaran, B., Junek, R., Kim, W. T., Wotton, T., Bandodkar, S., & Balasubramaniam, S. (2023). Developmental delay and non-phenylketonuria (PKU) hyperphenylalaninemia in DNAJC12 deficiency: Case and approach. *Brain and Development*. <https://doi.org/10.1016/j.braindev.2023.04.004>
- Xia, D., Lianoglou, S., Sandmann, T., Calvert, M., Suh, J. H., Thomsen, E., Dugas, J., Pizzo, M. E., DeVos, S. L., Earr, T. K., Lin, C. C., Davis, S., Ha, C., Leung, A. W. S., Nguyen, H., Chau, R., Yulyaningsih, E., Lopez, I., Solanoy, H., ... Sanchez, P. E. (2022). Novel App knock-in mouse model shows key features of amyloid pathology and reveals profound metabolic dysregulation of microglia. *Molecular Neurodegeneration*, 17(1), 1–29. <https://doi.org/10.1186/s13024-022-00547-7>
- Xiang, Y., Tanaka, Y., Cakir, B., Patterson, B., Kim, K. Y., Sun, P., Kang, Y. J., Zhong, M., Liu, X., Patra, P.,



- 
- Lee, S. H., Weissman, S. M., & Park, I. H. (2019). hESC-Derived Thalamic Organoids Form Reciprocal Projections When Fused with Cortical Organoids. *Cell Stem Cell*, 24(3), 487-497.e7. <https://doi.org/10.1016/j.stem.2018.12.015>
- Xu, R., Boreland, A. J., Li, X., Erickson, C., Jin, M., Atkins, C., Pang, Z. P., Daniels, B. P., & Jiang, P. (2021). Developing human pluripotent stem cell-based cerebral organoids with a controllable microglia ratio for modeling brain development and pathology. *Stem Cell Reports*, 16(8), 1923–1937. <https://doi.org/10.1016/j.stemcr.2021.06.011>
- Yamatoya, K., Nagai, Y., Teramoto, N., Kang, W., Miyado, K., Nakata, K., Yagi, T., & Miyamoto, Y. (2022). Cryopreservation of undifferentiated and differentiated human neuronal cells. *Regenerative Therapy*, 19, 58–68. <https://doi.org/10.1016/j.reth.2021.12.007>
- Yan, C., Jiang, J., Yang, Y., Geng, X., & Dong, W. (2022). The function of VAMP2 in mediating membrane fusion: An overview. *Frontiers in Molecular Neuroscience*, 15(December), 1–15. <https://doi.org/10.3389/fnmol.2022.948160>
- Yeh, F. C. (2022). Population-based tract-to-region connectome of the human brain and its hierarchical topology. *Nature Communications*, 13(1). <https://doi.org/10.1038/s41467-022-32595-4>
- Zagare, A., Barmpha, K., Smajic, S., Smits, L. M., Grzyb, K., Grünewald, A., Skupin, A., Nickels, S. L., & Schwamborn, J. C. (2022). Midbrain organoids mimic early embryonic neurodevelopment and recapitulate LRRK2-p.Gly2019Ser-associated gene expression. *American Journal of Human Genetics*, 109(2), 311–327. <https://doi.org/10.1016/j.ajhg.2021.12.009>
- Zanetti, C., Spitz, S., Berger, E., Bolognin, S., Smits, L. M., Crepaz, P., Rothbauer, M., Rosser, J. M., Marchetti-Deschmann, M., Schwamborn, J. C., & Ertl, P. (2021). Monitoring the neurotransmitter release of human midbrain organoids using a redox cycling microsensor as a novel tool for personalized Parkinson’s disease modelling and drug screening †. *Cite This: Analyst*, 146, 2358. <https://doi.org/10.1039/d0an02206c>
- Zeng, X. S., Geng, W. S., & Jia, J. J. (2018). Neurotoxin-Induced Animal Models of Parkinson Disease: Pathogenic Mechanism and Assessment. In *ASN Neuro* (Vol. 10). <https://doi.org/10.1177/1759091418777438>
- Zhai, S., Tanimura, A., Graves, S. M., Shen, W., & Surmeier, D. J. (2018). Striatal synapses, circuits, and Parkinson’s disease. *Current Opinion in Neurobiology*, 48, 9–16. <https://doi.org/10.1016/j.conb.2017.08.004>
- Zhang, W., Jiang, J., Xu, Z., Yan, H., Tang, B., Liu, C., Chen, C., & Meng, Q. (2023). Microglia-containing human brain organoids for the study of brain development and pathology. *Molecular Psychiatry*,

---

28(1), 96–107. <https://doi.org/10.1038/s41380-022-01892-1>

- Zhang, W., Xiao, D., Mao, Q., & Xia, H. (2023). Role of neuroinflammation in neurodegeneration development. *Signal Transduction and Targeted Therapy*, 8(1), 267. <https://doi.org/10.1038/s41392-023-01486-5>
- Zhang, Y., Xie, X., Hu, J., Afreen, K. S., Zhang, C. L., Zhuge, Q., & Yang, J. (2020). Prospects of Directly Reprogrammed Adult Human Neurons for Neurodegenerative Disease Modeling and Drug Discovery: iN vs. iPSCs Models. In *Frontiers in Neuroscience* (Vol. 14). <https://doi.org/10.3389/fnins.2020.546484>
- Zhong, S., Zhang, S., Fan, X., Wu, Q., Yan, L., Dong, J., Zhang, H., Li, L., Sun, L., Pan, N., Xu, X., Tang, F., Zhang, J., Qiao, J., & Wang, X. (2018). A single-cell RNA-seq survey of the developmental landscape of the human prefrontal cortex. *Nature*, 555(7697), 524–528. <https://doi.org/10.1038/nature25980>
- Zhou, Z. D., Chan, C. H. S., Ma, Q. H., Xu, X. H., Xiao, Z. C., & Tan, E. K. (2011). The roles of amyloid precursor protein (APP) in neurogenesis, implications to pathogenesis and therapy of Alzheimer Disease (AD). *Cell Adhesion and Migration*, 5(4). <https://doi.org/10.4161/cam.5.4.16986>
- Zhu, L., Sun, C., Ren, J., Wang, G., Ma, R., Sun, L., Yang, D., Gao, S., Ning, K., Wang, Z., Chen, X., Chen, S., Zhu, H., Gao, Z., & Xu, J. (2019). Stress-induced precocious aging in PD-patient iPSC-derived NSCs may underlie the pathophysiology of Parkinson's disease. *Cell Death and Disease*, 10(2). <https://doi.org/10.1038/s41419-019-1313-y>